Data Fusion of Relative Movement in Fast, Repetitive-Action Sports using Body Wireless Area Networks

Siân Armstrong

Thesis submitted to Cardiff University for the degree of

Doctor of Philosophy

Institute of Medical Engineering and Medical Physics

Department of Electrical and Electronic Engineering

Cardiff University

2013

Declaration

This work has not previously been accepted in substance for any degree and is not concurrently submitted in candidature for any degree.

Signed……(candidate) Date……

Statement 1

This thesis is being submitted in partial fulfilment of the requirements for the degree of PhD

Signed……(candidate) Date……

Statement 2

This thesis is the result of my own independent work/investigation, except where otherwise stated.

Signed……(candidate) Date……

Statement 3

I hereby give consent for my thesis, if accepted, to be available for photocopying and for interlibrary loan, and for the title and summary to be made available to outside organisations.

Signed……(candidate) Date……

Abstract

Rowing is an intensive, all-body sport, where bad technique can lead to injury. Crew cohesion, particularly timing, is vital to the performance of the boat. The coaching process, and injury prevention, could be enhanced if data relating to the movement of the oarsmen could be collected, without hindrance to the oarsmen, during on-water training.

Literature until recently has concentrated upon boat-centric measurement. Advances in wireless technology have made feasible the collection of data from multiple physically separate sites, including on-body.

After analysis of candidate radio standards, a Zigbee wireless Body Sensor Network (BSN) was designed and developed to synchronously collect data from several sensors across the wireless BSN. By synchronising sensor nodes via scheduled synchronising messages from the central coordinating node, synchronisation within 0.79msec ±0.39ms was achieved. Minimisation of the on-time of the sensor node radios currently extends the battery life by a factor of 5.

Acceleration and muscle activity data collected using the wireless BSN was compared to data synchronously collected using proven motion analysis techniques to validate the system. Synchronous muscle activity data was collected via the wireless BSN from several muscles during both land-based and on-water rowing and the results compared. The system was proven to facilitate the identification of bad rowing technique, as well as differences in muscle recruitment between land- and water-based rowing. Data collection from a rowing

crew was also demonstrated, and their muscle activity and inter-crew timing analysed. With an additional sensor node upon the boat, it is possible to correlate acceleration and muscle activity from the oarsman with acceleration of the boat itself.

A novel, power-optimised wireless sensor network has been designed and demonstrated to facilitate on-water rowing monitoring that can be extended beyond single oarsman measurements to analyse the interaction and cohesion of a crew and their impact upon boat performance.

Acknowledgement

There are so many people to whom I owe a huge debt of gratitude in the completion of this thesis.

In particular I would like to thank my supervisor Prof Len Nokes for his support and direction throughout this time, for his patience, and his trust in my ability.

Huge thanks to my small band of hardy rowers, for giving their time to help, and for braving the cold weather.

Most of all, I need to thank my family: the love and ever-constant support of my mother, and the uncharacteristically quiet support of my father – I hope he realises how much I appreciate that he refrained from quizzing me about my work.

And finally, all my love and thanks to my husband and children, without whose help, support, understanding and love I could not have survived the journey.

This thesis is for Wrigglebottom, Squigglebottom and Smashing.

And in memory of Gerald, the original engineer.

Aims, Objectives and Thesis Structure

Aims and Objectives

Monitoring of the rowing stroke, including body-segment sequencing, force-time profiles, and inter-crew timing and rowing variation, can, when analysed in conjunction with boat acceleration, lead to optimisation of boat performance.

The aim of this research project was to design and implement a wireless body sensor network to facilitate the analysis of the rowing stroke on-land and in-boat. To this end, a number of objectives were considered:

- The system should allow unencumbered monitoring of various metrics, such that body segment timing can be analysed, along with the impact of variations in the rowing stroke upon boat performance.
- It should be possible to collect at least one hour of rowing data for post-training de-briefing with a view ultimately to allow remote monitoring by a coach or physician.
- Such a wireless system should be extendable, without added infrastructure, to allow crews to be monitored, such that inter-crew variation can be identified.
- Data should be synchronously collected from all sensor nodes.
- Throughout the design process, emphasis should be made to the optimisation of the network hardware and firmware to minimise the processing overhead and thus allow smaller, less obtrusive nodes with greater longevity of power.

Chapter Organisation

The thesis is organised into 6 chapters as follows:

1: Introduction

Following a description of the boat and the rowing stroke, the key determinants of successful rowing are considered, with reference to literature.

Rowing Literature is reviewed giving both the current understanding of the rowing stroke and indicating how technology has been exploited in the advancement of rowing monitoring. The wider literature is also surveyed where sensors and measurement techniques, and wireless network advances, could be utilised in rowing monitoring.

2: Wireless Networks: Possibilities and Challenges

Several candidate wireless standards are reviewed to determine their suitability for the application of Wireless Body Sensor Network for rowing monitoring, and Zigbee chosen as the most suitable market-ready standard. The challenges to wireless BSN are discussed in more detail, in particular factors affecting power consumption, data integrity, and time synchronisation.

3: Sensors, and System Design

The diversity of measurements that might be made to an oarsman and boat are considered, with reference to the key determinants of successful rowing, and a subset of sensors are reviewed which can maximise the relevant information regarding the performance of an oarsman or crew. Linear accelerometry and surface electromyography are chosen to best demonstrate the benefits of a wireless data collection system to analysing boat performance through body-segment, and inter-crew timing.

4: System Development and Testing

The system design and functional testing of both hardware and firmware is described. Optimisations of the system, particularly the memory design, node synchronisation, data transfer and related power considerations are discussed.

5: Experimental results and Discussion

Land-based (ergometer) and on-water experimentation is detailed. Data collected with the wireless BSN is compared and validated with laboratory measurements using Qualisys landmark measurement motion capture and Delsys sEMG. Ergometer measurements are compared to on-water data, and analysed in conjunction with boat acceleration data. Comparison is made between athletes of similar build and rowing skill, on-water and ergometers, demonstrating

simultaneous measurement upon two athletes, and allowing their timing and muscle activity to be compared. Results are discussed with reference to previous literature.

6: Conclusions and further work

Achievements in the design and implementation a novel, power-optimised Wireless Body Sensor network are summarised, most notably the un-encumbered and synchronous collection of sensor data across a rowing crew and boat, on-water, allowing the analysis of the effect of rowing technique and timing of multiple oarsmen upon boat performance.

Areas for further work are identified, and split into two areas: technical development and further research study.

Contents

List of Figures

Tables

Abbreviations

802.11	WLAN working group
802.15	WPAN working group
802.15.1	Bluetooth standard
802.15.3a	Ultra-Wideband standard
802.15.4	Standard upon which Zigbee is based
802.15.6	Body Area Network standard
ac	Alternating Current
ACK	Acknowledgement
ADC	Analogue to Digital Converter
APL	Application Layer
BAN	Body Area Network
Bluetooth LE	Bluetooth Low Energy
BSN	Body Sensor Network
CCA	Clear Channel Assessment
CCK	Complementary Code Keying
CMRR	Common Mode Rejection Ratio
CSMA/CA	Carrier Sense Multiple Access with Collision Avoidance
dc	Direct Current
DSSS	Direct Sequence Spread Spectrum
EDR	Enhanced Data Rate
ECG	Electrocardiogram
EMG	Electromyography
ETSI	European Telecommunications Standards Institute
FCC	Federal Communications Commission
FFD	Full-Function Device
FHSS	Frequency-Hopping Spread Spectrum
FM-UWB	Wideband FM Modulation
FSK	Frequency Shift Keying
FTSP	Flooding Time Synchronisation Protocol
GDSK	Gaussian Frequency Shift Keying
GHz	Gigahertz
HBC	Human Body Communications
IC	Integrated Circuit
IEEE	Institute of Electrical and Electronics Engineers
IDE	Integrated Development Environment
IMU	Inertial Measurement Unit
IR-UWB	Impulse Radio Ultra-Wideband
ISM	Industrial, Scientific and Medical frequency band
Kbps	Kilobits per Second
KHz	Kilohertz
LAN	Local Area Network
MAC	Medium Access Layer
Mbps	Megabits per Second
MEMS	Micro-Electro-Mechanical System
MHz	Megahertz
MICS	Medical Implant Communications Service
MMC	Multimedia Card
MUAP	Motor Unit Action Potential
NWK	Network Layer
OFDM	Orthogonal Frequency Division Multiplexing
OOK	On-Off Keying
O-QPSK	Offset Quadrature Phase Shift Keying
PAN	Personal Area Network

PCB	Printed Circuit Board
PHY	Physical Layer
QPSK	Quadrature Phase Shift Keying
RBS	Reference Broadcast Synchronisation
RFD	Reduced Function Device
RMS	Root Mean Square
SD	Secure Digital memory card
sEMG	Surface Electromyography
SPI	Serial Peripheral Interface
TDD	Time Division Duplex
TDMA	Time-Division Multiple Access
TPSN	Timing-Sync Protocol for Sensor Networks
TQFP	Thin Quad Flat-Pack
UWB	Ultra-Wideband
WLAN	Wireless Local Area Network (Wi-Fi)
WMTS	Wireless Medical Telemetry Services
WPAN	Wireless Personal Area Network
WSN	Wireless Sensor Network
ZDO	Zigbee Device Object
π/2-DBPSK	π/2-Differential Binary Phase Shift Keying

1 Introduction

In many sports it would be highly beneficial to monitor multiple variables including body kinematics and biometrics such that they might be scrutinised to determine their effect upon performance. In addition to contribution to performance, this could be used both to monitor the fitness and potential for injury of the athlete.

The ability to record a breadth of data pertaining to body position, velocity or acceleration, force, muscle activity, respiration, heart rate, etc. and to correlate that information to actual performance would facilitate the coaching process, possibly removing some of the subjectivity from the task and enable fast or otherwise obscured movement to be studied. It would also enable the coach to more easily illustrate to the athlete where particular problems exist and where they need to work on a particular part of their technique. The capacity to simultaneously monitor both the sporting action and medical factors would help in the prevention or identification of injury or health issues. In sports where the performance of a team is crucial to success, the ability to simultaneously collect data from multiple athletes might yield information pertaining to the cohesion of the team unit.

The environment under which the sport is practised might not facilitate the use of high-speed video capture, whilst laboratory-based analysis might not fully-replicate the conditions that the athlete would experience in the sport's natural environment. Additionally, wired systems might encumber the natural movement

of the athlete. This could lead to false information regarding the true performance of the athlete or hide potential injury until the condition becomes more severe.

Rowing is a sport which encompasses many of the issues described above, being practiced on lakes or rivers in narrow racing shells which do not facilitate detailed video capture. An intensive all-body sport, it places extreme demands upon the body, where bad technique can induce injury, and where the cohesion of the crew is vital to the performance of the boat.

1.1 Chapter Organisation

This chapter is divided into two main sections: a description of the boat, the rowing stroke, and the key determinants of successful rowing, such that further description of the research into rowing technique can be better understood, and a critique of the research into boat movement and kinetics, the rowing stroke, and body kinematics of the oarsman. Where relevant, a study of the research has been extended into kinematic or biometric measurement of other sports or health applications, and pertinent research utilising wireless data collection has also been reviewed, although wireless technology is covered in more detail in chapter 2.

1.2 Background

The first reference to a boat propelled with oars can be found in an ancient stone relief dating between 3300 and 3000 BC. Initially used as a form of transport, it was adopted as a form of sport in the 19th century, the Cambridge-Oxford University boat race first taking place in 1829, and its introduction as an Olympic event was in 1900 (Redgrave 1995).

In 1870 the first riggers were fitted, such that the oarlocks could be mounted at a distance from the hull, enabling the hull to be narrower without loss of leverage. Early boats had fixed seats and were thus largely powered by arms only, progressing in 1870 to greased leather pants to enable some introduction of leg power into the stroke, and a year later to a sliding seat. (Redgrave 1995). Since this time the basic form of the boat has remained largely unchanged.

Rowing can be sub-divided into two categories: Sculling, where each oarsman holds an oar in each hand on each side of the boat, and Sweep-oar rowing, where each oarsman holds just one oar (an even number of oarsmen are required for sweep-oar rowing). Sculling boats can be rowed by one, two, four or eight oarsmen (single-, double-, quadruple- or octuple-sculls respectively), whilst Sweep-oar rowing can be rowed by two, four or eight oarsmen (pair, four or eight respectively). Both sculling and rowing boats can be coxless or coxed, with the coxswain (cox) either facing the stroke-person in the stern of the boat, or sitting behind the bow-person at the bow of the boat. The physics of rowing, whether each oarsman holds a single oar or two, is essentially the same.

1.2.1 The boat and the rowing stroke

Figure 1-1 depicts a typical single scull boat. The essential components are labelled as follows: the bow (the front of the boat), the stern (the rear of the boat), stroke-side (the left side of the boat, but to the right of the oarsman who face the stern) and bow-side (the right of the boat, but to the left of the oarsman), the foot-stretcher, the rigger to which is attached the gate and pin, and the seat which slides freely on runners. The main components of an oar are the spoon or blade (most spoons used competitively are “cleaver” blades), the loom, the collar and button that swivel within the boat’s gate, and the handle.

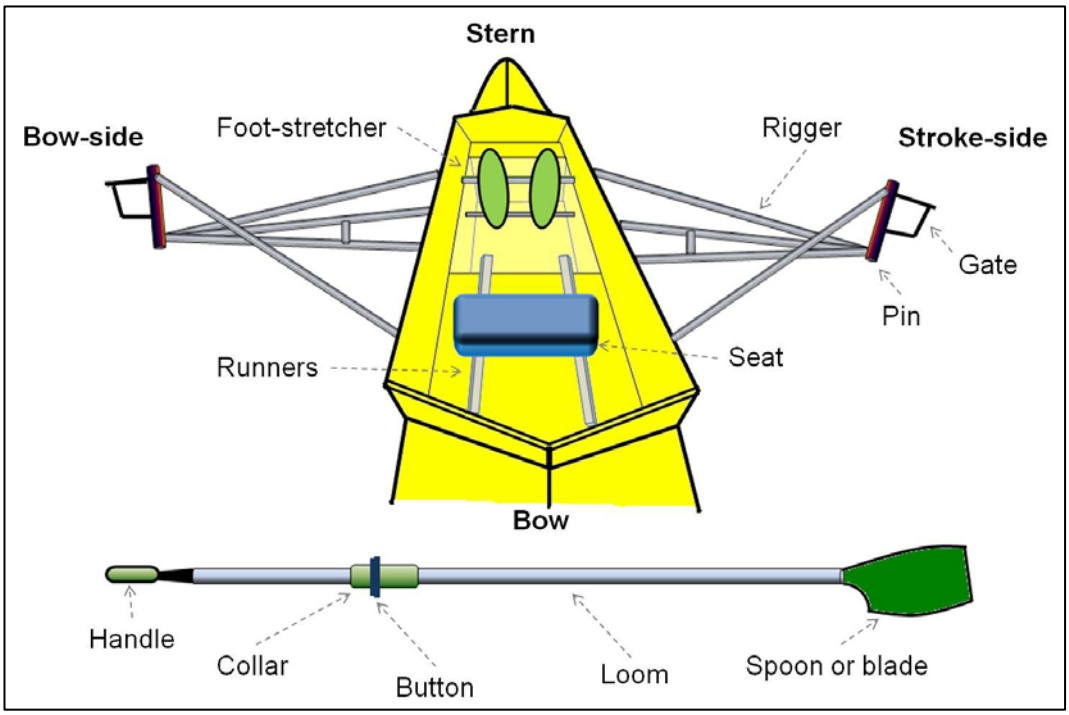

Figure 1-1: *Typical single scull boat*

Main components of boat and oars

In order to consider the forces, energy, and body segments involved in the rowing action, and therefore how it might be monitored, the stroke cycle itself needs to be understood.

The stroke cycle can be divided into two phases: the drive, and the recovery. The drive phase is the period when the spoon of the oar is in the water and force is being applied to propel the boat through the water. It begins when the spoon of the oar is squared (vertical) and placed in the water at the catch position. At this point the oarsman is at front-stops, knees bent, and arms extended such that the handle of the oar is at its closest position to the stern of the boat. The drive phase is the period when the spoon is being driven through the water by force applied by pushing with the feet on the footplate. This force is translated to the oar from the leg drive upon the foot-stretcher through the rigid connection of the oarsman's back and arms (Tonks 2005).

The seat slides forward towards the bow of the boat (backwards in relation to the oarsman). When the legs are fully extended, the body follows by levering open from the hips, some work is applied with the arms to control the oar handle as it travels towards the oarsman's chest (Spracklen 2005). When the work has been done in the water the oar is at the finish position, and the oarsman is at backstops. The oar is tapped down by the outside hand of the oarsman (on the end of the handle), the spoon extracted cleanly and square (vertically) from the water, then feathered (turned such that the spoon is parallel to the water).

The recovery phase is the period when the oar is not in the water, and the oarsman is returning up the slide to the catch position to take the next stroke. From backstops, the oarsman "sends his hands away" – essentially straightening

his arms to the locked position and pivots his body forward at the hips (rock-over) ready for the next stroke (Spracklen 2005). He then allows the boat to travel beneath him by raising his knees and the seat slides back towards front-stops. The recovery must be done in a controlled manner or the combined weight of the oarsmen travelling towards the stern of the boat will cause the boat to decelerate (Tonks 2005). As the oarsman approaches front-stops, he squares his oar (returning the spoon to a vertical position ready to take the next stroke) and raises his hands slightly so that the spoon drops into the water. Figure 1-2 summarises the main parts of the rowing cycle.

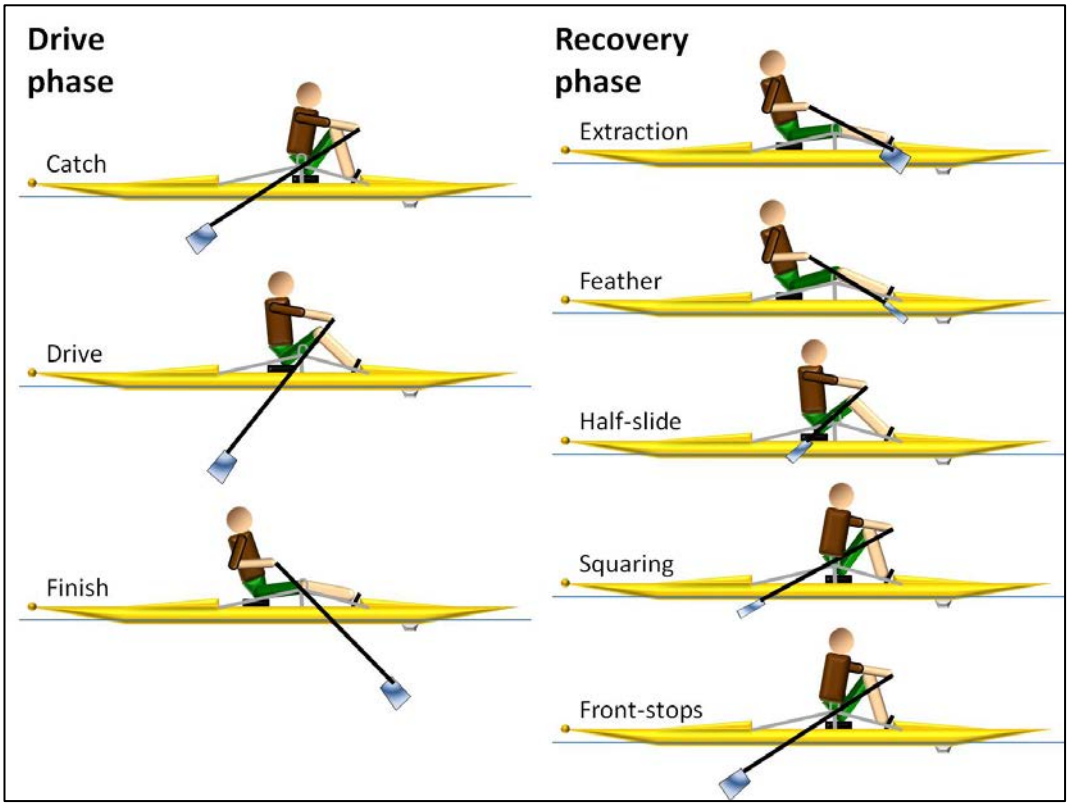

Figure 1-2: The rowing cycle[1]

Drive phase and recovery phase of the rowing stroke cycle

[1] Figure 1-1 and Figure 1-2 artwork: A. Hollins

It is a common misconception that the pivot point of the oar is at the gate where the oar rotates relative to the boat hull. In reality, whilst the oar acts as a class 1 lever (Load–Fulcrum–Effort) within the frame of the boat, with the fulcrum at the gate, an observer outside the boat views the oar as a class 2 lever (Fulcrum–Load–Effort), with the fulcrum point at the spoon (Pulman 2005). The boat is levered along the river by the stationary spoon pushing against the body of water. This again is a simplification, as in reality as the water is a fluid, and the force upon it causes it to move. Thus the spoon, and so the fulcrum slips a little in the water (McBride 2005).

The aim of the rowing stroke is to maintain an overall constant shell velocity (Soper and Hume 2004b). The cyclical nature of the rowing stroke (and because the propulsive force accelerating the boat can only be applied during the drive phase when the spoon of the oar is in the water), means this is not possible, and so the aim is to minimise the variation of velocity over the stroke. The idealised acceleration curve described by Young and Muirhead (Young and Muirhead 1991) is given in Figure 1-3.

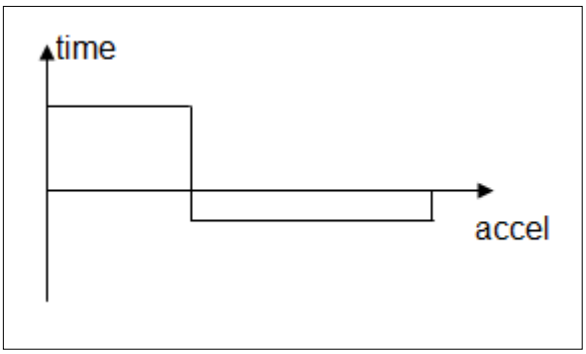

Figure 1-3: *Idealised acceleration curve (Young and Muirhead 1991)*

During the drive the boat would ideally have a constant positive acceleration, and during the recovery a constant but negative deceleration. There are some assumptions made to create this model however: there is no weight shift within the shell, and the catch and release are performed cleanly with all oarsmen in perfect synchrony.

The reality is somewhat different. Analysing a typical boat velocity-time graph generated by Soper and Hume (Soper and Hume 2004b), from data measured on a single scull by Martin and Bernfield (Martin and Bernfield 1980), it can be seen (in Figure 1-4) that the boat experiences a decrease in velocity at the catch. This is due to the blade entering the water and energy being absorbed through the oar by the oarsman. Martin and Bernfield postulate that this is in part because the oar is at an inefficient angle at the catch position, with a large proportion of the applied force being directed away rather than along the boat. Additionally they conclude that the movement of the oarsmen towards the bow of the boat during the drive causes the boat to move towards the stern, decelerating the boat further. If the drive upon the footplate is made before the spoon is in the water, this effect is obvious. Partway through the drive, the force exerted by the oarsman causes the boat velocity to increase, reaching a maximum partway through the recovery (McBride 2005). During the recovery, the combined weight of the oarsmen travelling towards the stern of the boat causes the boat to surge forward (to obey the conservation of linear momentum). If however the oarsman were to “rush the slide” (a common error whereby the oarsman attempts to reach front-stops at a rate faster than the boat is travelling in the opposite direction) then the boat would rapidly decelerate.

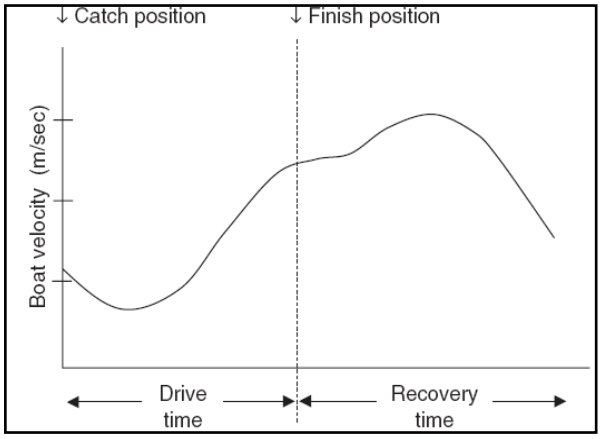

Figure 1-4: *Velocity-Time curve of the stroke cycle, data from Martin and Bernfield*

(Soper and Hume 2004b)

This is explained well by Chris Pullman (Pulman 2005) through illustration (Figure 1-5). When the oarsman is at backstops, the drive is complete (along with any transfer of momentum between blade and water), and the blade has just been extracted from the water. At this point, before he begins to slide towards the stern during the recovery, the combined centre of mass (CM) of both the oarsman and the boat are travelling at equal velocity, V_t.

As the blade is not in the water, momentum cannot be transferred through it to the water, and momentum must be maintained within the boat (assuming no other losses). By raising his knees slowly and travelling towards the stern at a velocity of V_c, the boat must surge forward in the opposite direction to the oarsman in order to conserve momentum.

$$m_c v_t + m_b v_t = m_c (v_t - v_c) + m_b (v_t + v_b) \Rightarrow v_b = \frac{m_c}{m_b} v_c \qquad 1\text{-}1$$

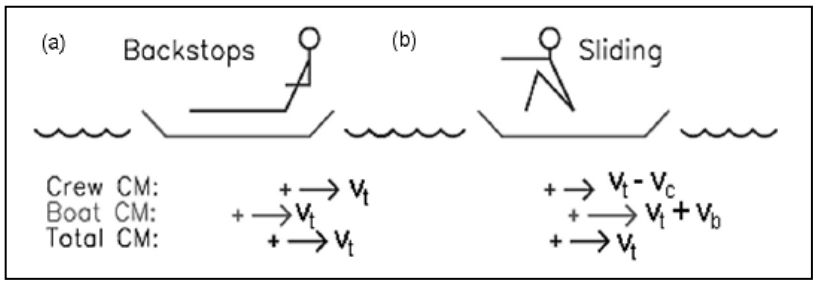

Figure 1-5: *Velocities of component centres of mass of boat and crew (Pulman 2005)*

Thus whilst the crew cannot propel the boat during the recovery phase, they can greatly influence the velocity of the boat during this part of the stroke.

There are however forces which oppose the movement of the boat through the water. This resistance takes the form of drag, both by water (form, skin and wave) and air (aerodynamic).

Wave drag is caused by energy lost in the creation of waves. At certain hull velocities, depending upon the length of the boat, wave drag will reach a maximum (Pulman 2005).

Form drag consists of both water and air resistance due to the shape and profile of the boat and crew. However, since air density is several hundred times less than that of water at a similar temperature, it generally only causes a significant detrimental factor in strong headwinds, as the area exposed to the wind is relatively small. Form drag due to the shape of the hull below the water level

causing turbulence (hull drag) attributes 8% of the total resistance, though this is minimised by the narrow profile of the racing shell (Soper and Hume 2004b).

Skin drag, where the formation of a shear boundary layer of water along the hull, which is dragged along by the boat (increasing its overall effective mass and thus decreasing the boat's momentum), provides by far the largest contribution, at 88% (Soper and Hume 2004a). Skin drag, like form drag, follows the standard drag equation for objects moving through fluids.

Drag equation: $$\boldsymbol{R = \frac{1}{2}\rho v^2 A C_d \Rightarrow R = Dv^2} \quad \text{1-2}$$

This fluid resistance increases proportionally with the squared velocity of the boat. The proportionality constant, D, consists of the density of the fluid, ρ, the surface area exposed to the flow, A, and the drag coefficient of the boat, C_d.

For a given boat and crew, the power required to overcome this resistance in order to maintain a constant velocity is thus:

$$\boldsymbol{P = v.R = Dv^3} \quad \text{1-3}$$

Thus to double the velocity of the boat, the power must increase by a factor of 2^3=8. By the same relationship, it can also be shown that it is more energy-efficient to maintain a constant velocity over a set time period, than to vary the velocity (even if the overall average velocity is the same). The same applies to each stroke – it is more efficient to maintain the shell velocity of the boat over a stroke than to allow the shell velocity to vary too much. This substantiates the

idealised acceleration curve proposed by Young and Muirhead and reproduced in Figure 1-3.

Whilst this helps to explain the forces required to maintain a constant velocity or to accelerate a perfectly sat (balanced) boat, it does not yet explain the complex interactions of boat and crew with the boat balance.

A boat has a centre of gravity and a centre of buoyancy – this latter is derived from the centre of gravity of the water it displaces. While a rowing boat has a geometric centre close to the waterline, due to the mass of the crew its centre of gravity is generally above this. This makes the boat inherently unstable.

Boats often have a “dynamic stability”, becoming easier to balance when moving (water displaced by the moving hull produce turning moments which help the boat return to an upright position). However, whilst this means that only small correctional movements in the hand-heights of the crew are required to correct an imbalance, it also means that just small errors in the stroke technique (hand-heights or timing) can unbalance the boat.

Boat velocity is largely dictated by three factors: stroke rate (the number of strokes per minute), power (force applied x speed of travel of oar), and oar angle (which dictates the distance which the oars move the boat during the drive phase) (Spracklen 2005). Whilst increasing the stroke rate will increase the velocity of the boat, Nolte (Nolte 2005) discusses how upon increasing the stroke rate, the drive time of the stroke cycle changes only little. It is the recovery time which decreases significantly with increasing stroke rate. This can be seen in Figure 1-6.

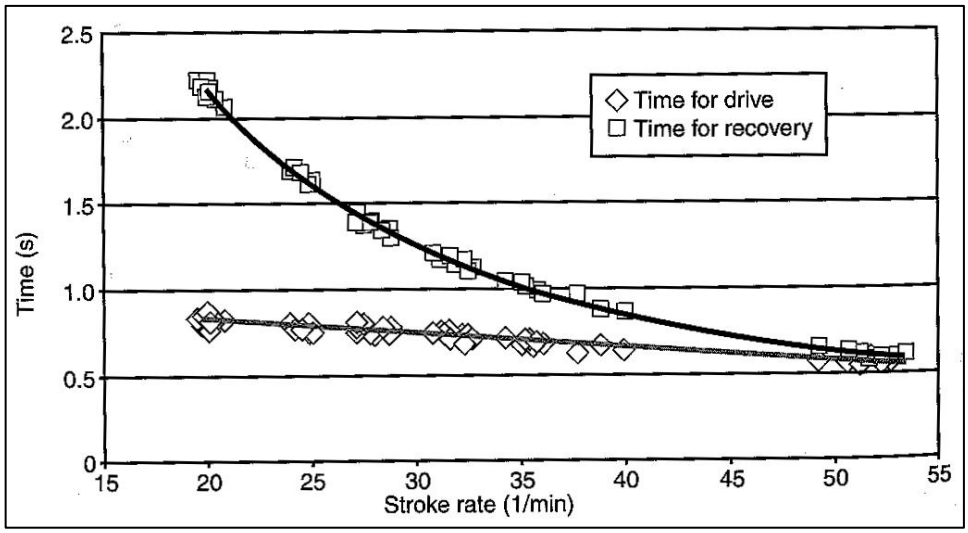

Figure 1-6: Recovery and drive times for different stroke-rates

Demonstrates correlation between decreased recovery time and increased stroke-rate (Nolte 2005)

Thus, crew technique during the recovery has a huge impact upon the performance of the boat.

1.3 Key determinants of successful rowing

Biomechanics of rowing show how the rower can best translate physiological capacity into boat velocity (Nolte 1991). Ultimately, the key determinant of successful rowing is the time taken to row a set distance. Thus boat velocity, for a given boat type, termed the Gold Standard (Kleshnev 1998), determines the success of a crew. However, monitoring boat velocity alone does not inform the oarsman or coach about where technique can be improved in order to achieve a better result. It is necessary therefore, to look at other parameters that affect boat velocity.

1.3.1 Boat Velocity and intra-stroke velocity fluctuations

Boat velocity should not be mistaken for instantaneous velocity, as the nature of the rowing stroke (propulsive drive phase, and recovery phase) means that boat velocity varies over the course of a stroke (Martin and Bernfield 1980). Variation in boat velocity should be kept to a minimum in order to minimise the effect of drag upon the boat hull (Soper and Hume 2004b). It can be shown that a boat with an average velocity of $5ms^{-1}$, where the velocity varies between 4 and $6ms^{-1}$, has 4% greater drag resistance than a boat with a constant velocity of $5ms^{-1}$ (Nolte 1991). Minimising variation in boat velocity is achieved through economy of movement, and a controlled recovery that is relative to the speed of the boat (McArthur 2002). Nolte also comments that vertical movement of the centre of gravity of the rower (for example through straightening up too early in the drive phase or too excessive a lay-back at the finish) or large and fast changes in horizontal movement of body weight, increases the drag resistance and impacts

upon boat velocity (Nolte 1991). A balanced boat (roll, pitch, yaw) also minimises water drag, allowing for more efficient rowing (Loschner et al. 2000), and whilst there is a direct correlation between stroke-rate and boat velocity, this is usually at the expense of a degree of boat stability, and in increased fluctuations in intra-stroke boat velocity (Martin and Bernfield 1980). Thus increased fluctuations in boat velocity over the course of a stroke are associated with less successful technique (McBride 2005). A deterministic biomechanical model showing the basic mechanical factors of rowing that influence performance, namely average boat velocity, is shown in Figure 1-7 (Soper and Hume 2004b). A similar model has been reported by Smith and Loschner (Smith and Loschner 2002).

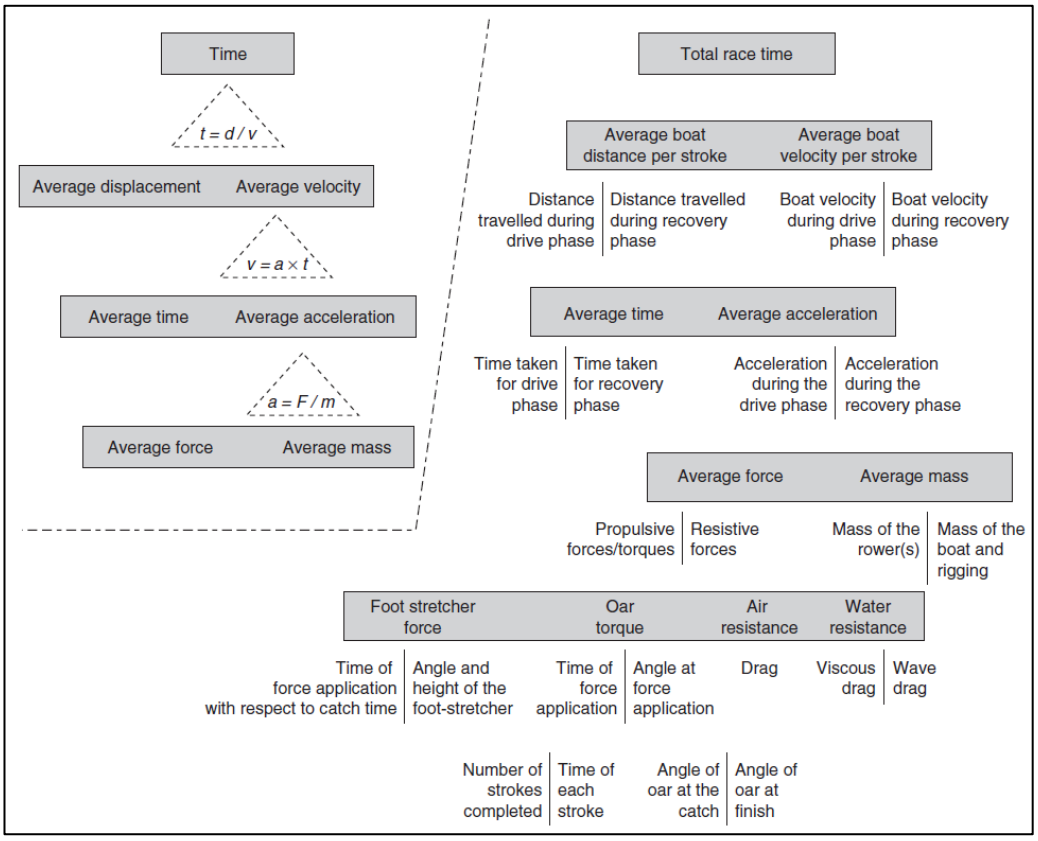

Figure 1-7: A deterministic biomechanical model showing the basic mechanical factors of rowing that influence performance

(Soper and Hume 2004b).

1.3.2 Force application

From the laws of physics, maximum power is generated through the application of a large force over a long distance in a short time; thus force applied, stroke length, and drive time are significant contributors to achieving maximum performance.

Maximum force application is achieved through appropriate timing and sequencing of power application to overcome the drag forces upon the boat (Soper and Hume 2004b). Many researchers have measured oar force (pin and handle) and foot stretcher force application (Kleshnev 2000; Smith and Draper 2002), and others have attempted to try to analyse blade (oar spoon) forces and efficiencies as the blade travels through the water, in order to determine when the oarsman can best maximise his power delivery. A blade experiences maximum drag force when perpendicular to the boat (it is this force that the oarsman levers against to propel the boat), and hydrodynamic lift forces at sharp oar angles (the catch and finish) (McBride 2005). Many researchers have identified drag forces as the dominant propulsive force (McBride 2005), however Kleshnev reports that blade lift and drag forces contribute 56% and 44% respectively to the propulsive force of the blade (Kleshnev 2011). That stroke length has a significant correlation to average boat velocity (Soper and Hume 2004b) further cooborates the notion that oar force at the catch and finish are significant to successful rowing (McBride 2005). However, as stated in section 1.3.1, yaw has an effect upon boat velocity, and transverse forces are greatest at the catch and finish (Smith and Draper 2002). Kleshnev (Kleshnev 2011) states that a front-loaded drive gives 47% higher average velocity and distance travelled during the drive,

provides better utilization of the most powerful muscle groups, and allows the hydrodynamic lift forces on the blade to be exploited.

Maximising the application of power when the spoon of the oar is in the water is also vital; when the spoon is in the water, it acts as a brake, thus strong acceleration of power, derived from the leg muscles, must be applied the moment the spoon is buried (McArthur 2002). The ability of an oarsman to limit the reduction in velocity at the catch and initial drive phase can be viewed as an indicator of performance (Soper and Hume 2004b). There is high correlation (r=0.95) between interval from catch and the point of minimum velocity and the average velocity over the stroke cycle (Aujouannet and Rouard 2001, cited in (Soper and Hume 2004b)).

1.3.3 Limb segment coordination

Coordination of limb segment contribution towards the rowing stroke needs also to be considered as a performance indicator for rowing. Several papers including Lamb (Lamb 1989) have reported upon the importance of lower limb contribution towards initiating the drive phase, followed by trunk contribution. This is known as the Rosenberg style (Rosenberg was the American national team coach in 1975). However, there is no consensus as to the ideal sequencing. Kleshnev (Kleshnev 2006) analyses results from four accepted rowing styles (Rosenberg, Grinko, DDR and Adam) the former two being of sequential style, and the latter two simultaneous approach. He reports that sequential style results in greater power, but that the simultaneous approach was more biomechanically efficient. This last point is important when considering the contribution of individual physiology (see

section 1.3.4). Kleshnev also discusses the percentage contributions of the main body segments – legs, trunk, arms (Kleshnev and Kleshneva 1992) and upon the emphasis of the leg drive due to the biarticulate muscles of the thigh (Kleshnev 2011).

1.3.4 Rower Physiology and injury free rowing

Key determinants of successful rowing technique are not limited to skill. Soper and Hume (Soper and Hume 2004b) summarise a breadth of research to determine physiological and anthropometrical attributes of successful oarsmen, listing mass, standing and sitting height, body segments lengths and girths and total skinfolds as significant parameters. Literature was in agreement that successful oarsmen were taller and heavier, with greater limb length and girths.

Effectiveness of training towards best preparing the body for effective and successful rowing is also an important factor. Schwanitz (Schwanitz 1991) discusses the importance of not depending solely upon mechanical findings, but also to consider biomechanical/energetic and biological/energetic interactions of the oarsman, with a view to achieving the fastest time over a given distance for a particular oarsman's individual available biological energy potential.

Hagerman (Hagerman et al. 1978) states that maximal aerobic capacities of competitive oarsman are among the highest recorded. Hartmann and Mader (Hartmann and Mader 2005), with reference to the extensive studies of Hagerman, and other researchers, discuss energy requirements of intensive rowing and the deficit that exists between energy requirement and available

aerobic energy, the deficit supplied through anaerobic lactic and alactic metabolic systems, and compare these to relationships between power output, heart-rate, oxygen uptake (VO_2) and lactate levels during simulated rowing. Blood lactic acid concentrations are often blamed for the decline of muscle force and impared performance, and certainly blood lactate concentration can be used as a useful marker of exercise intensity and adaptation to training (Cairns 2006). Cairns, however, suggests that the link might not be quite as simplistic, and that greater understanding of the links is required.

There is evidence to show the different physiological effects of different rowing styles. Roth (Roth 1991) analysed the blood lactic acid concentration in oarsmen with different force/time curves and observed a higher concentration in those rowers with a steaper power increase at the beginning of the stroke. He also observed a higher VO_2 for strokes with an emphasis on drive early in the stroke.

Success must however be analysed in conjunction with preserving health. An optimised rowing stroke, yielding the fastest boat velocity, does not result in successful rowing if it significantly increases the chance of injury. Biomechanical research in rowing can now be applied to analysis to preserve health (Nolte 1991). Much of the research performed by Bull and McGregor (Bull and McGregor 2000) analyses spinal motion with a view to studying and increasing understanding back injury in rowing.

1.3.5 Efficiency, Equipment and Equipment set-up

Rowing efficiency can be improved through many different factors covered in the previous sections. Correct equipment and rigging for a particular oarsman or crew will allow their power to be most efficiently translated into boat velocity.

Optimising equipment through research, design and evolution can lead to more efficient power delivery. For example, different hull shapes or materials can help reduce hull drag (Soper and Hume 2004b); New spoon design (e.g. larger spoons) can aid delivery of power from the oar into propulsive forces (Kleshnev 2011); optimising the pitch, height and rake of the foot-stretcher to suit an individual (Redgrave 1995; McArthur 2002).

1.3.6 The Crew Unit

Synchronisation between the movements of a rowing crew is understood to be paramount to the successful rowing of a multi-oarsman boat (Bernstein et al. 2002; Hill 2002; Baudouin and Hawkins 2004). Experienced rowers can more easily adapt their movement kinematics to suit a particular crew dynamic than their actual force pattern (Hill 2002). However, research shows that successful crews who have been rowing together for a long time develop similar rowing styles; moreover that successfully paired crews have adapted their force application according to their seat in the boat, such to minimise the effect of transverse forces upon the yaw of the boat (Hill 2002; Smith and Loschner 2002).

A controversial idea is that of anti-phase crew coordination. An ergometer study (upon coupled ergometers) seems to indicate that velocity fluctuations within a boat can be reduced by rowers rowing in anti-phase coordination (de Brouwer et al. 2013), whilst acknowledging that synchronous rowing ultimately delivers a more stable boat. It does, however, demonstrate that optimal performance does not always equate to practicable methods.

Thus, monitoring synchronisation between oarsmen movement kinematics and force application, in conjunction with boat movement should gain valuable information regarding crew rowing performance, and might ultimately yield a tangible measure for the “swing” effect, described by US Rowing Nomenclature as “a hard-to-define feeling when near-perfect synchronisation of movement occurs in a shell, enhancing the performance and speed of the crew” (Cornett et al. 2008).

1.3.7 Monitoring and feedback on Key determinants

In summary, boat movement (velocity, acceleration, balance) and force application and limb coordination (profiles, timing and sequencing) are primary key determinants for successful rowing. Other biometrics such as $V0_2$ and lactate levels could also yield important information regarding a rower’s physiological state during training.

Knowledge of the key determinants of successful rowing is only one step towards achieving this goal. Measuring and collecting data that can be usefully fed back to oarsmen and coaches, or to further understanding of the rowing stroke and the

most efficient method of rowing for rowing success is the next step. The literature study in the remainder of this chapter contains some of the key research into rowing technique and rowing measurement. Ultimately, achieving an unobtrusive method of monitoring key metrics that can feedback upon these key determinants can allow a crew and coach to analyse their own rowing stroke with a view to maximising their rowing potential. Choices of sensor, and decisions regarding system design to achieve this aim, are discussed in chapters 3 and 4.

1.4 Ergometer

Since monitoring of rower kinematics and rowing kinetics is difficult within the narrow hull of a rowing boat, much of the research has taken place upon rowing simulators or ergometers. The majority of rowing ergometers employ air resistance flywheels – the rowing handle is connected via a chain to a flywheel, and air-fins on the flywheel provide the resistance. An adjustable vent can be moved to increase or decrease the resistance. The power applied is calculated using tachometer readings to measure flywheel speed during the stroke and deceleration over the recovery. Using the flywheel moment of inertia and tachometer reading, speed, distance, and other parameters can be calculated also. The basic components of a rowing ergometer are indicated in Figure 1-8.

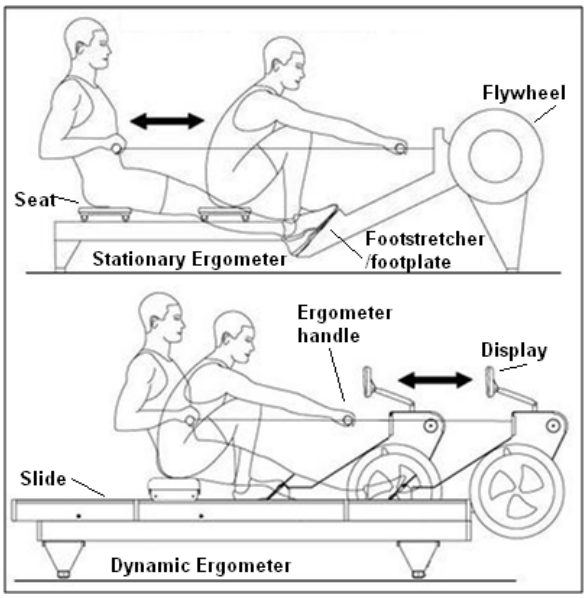

Figure 1-8: Rowing ergometer: stationary and dynamic
(Adapted from Oartec (Oartec 2011)

There are two basic forms of rowing ergometer – stationary and dynamic. A stationary ergometer has a fixed flywheel and foot-stretcher, and a sliding seat.

As the foot-stretcher is fixed, any force applied by the rower upon the foot-plate produces an equal reactive force upon the rower himself (Elliot et al. 2003). This is not representative of the conditions within a boat. A dynamic ergometer has both seat and feet free to slide, though with good technique the seat actually stays largely stationary. Concept 2, Rowperfect and Oartec are popular manufacturers of rowing ergometers.

In addition to being used as a tool for training or to facilitate research into rowing biomechanics, research has taken place to compare the performance of these two different ergometers, to compare ergometers of different manufacturers and also to compare land rowing to on water rowing.

Early research by Lamb (Lamb 1989) generated X-Y coordinates of body joint locations by digitizing video of on-river and ergometer rowing which allowed him to describe the contributions of five body segments to oar or handle velocity. He was able to determine that whilst the kinematics of the upper arm and forearm were significantly different between ergometer and on-river rowing both at the catch and the finish, the effect of these differences was of minor importance because of the small contributions of the arm to the power in the stroke at these points.

Later Dawson (Dawson et al. 1998) undertook similar research, but going further than Lamb to look at the timing of the complete rowing cycle, specifically the variance of individual movement durations over different stroke rates. He found that variance reduced with increasing stroke rates, and was similar for both on-water and ergometer rowing.

Elliot *et al* (Elliot et al. 2003) compared shapes of force-length curves of the RowPerfect dynamic ergometer and on-water rowing at three different stroke rates. On-water measurements were made of blade force and oar angle using linear proximity sensors and potentiometers respectively, whilst handle force and stroke length on the RowPerfect ergometer were calculated by the RowPerfect software itself from flywheel momentum and predetermined moment of inertia of the flywheel and other known variables. Stroke length on the ergometer was calculated from the rotation of the flywheel. Body position at the catch and finish were also digitized from video footage of both on-river and ergometer tests. They found that force-angle curves and body angles were similar between on-river and RowPerfect ergometer rowing.

Further comparisons were made by Kleshnev (Kleshnev 2005a) both to contrast on-water rowing with ergometer rowing, and stationary ergometers (Concept 2) with dynamic ergometers (RowPerfect). Kleshnev measured handle force in the boat and upon the ergometers with force transducers. Oar angles in the boat were measured using conductive-plastic potentiometers, thus allowing handle position to be determined. Seat and trunk positions were measured using custom-made transducers using spring-loaded potentiometers and low-stretchable lines connected to the points of measurement. His results include comparisons of handle force, handle speed, legs, trunk and arms velocity, and acceleration over the stroke cycle (Figure 1-9). He found there to be differences in the biomechanical structure of the rowing technique between ergometer and on-water rowing, most obvious in the handle force. Upon both stationary and dynamic ergometers similar force is applied to the handle as to the foot-stretcher, whilst on-water the handle force is 30-40% less. He also found that ergometer drive lengths were shorter than on-water rowing. Overall he determined that

whilst there were differences between stationary and dynamic ergometers, that these differences were not significant.

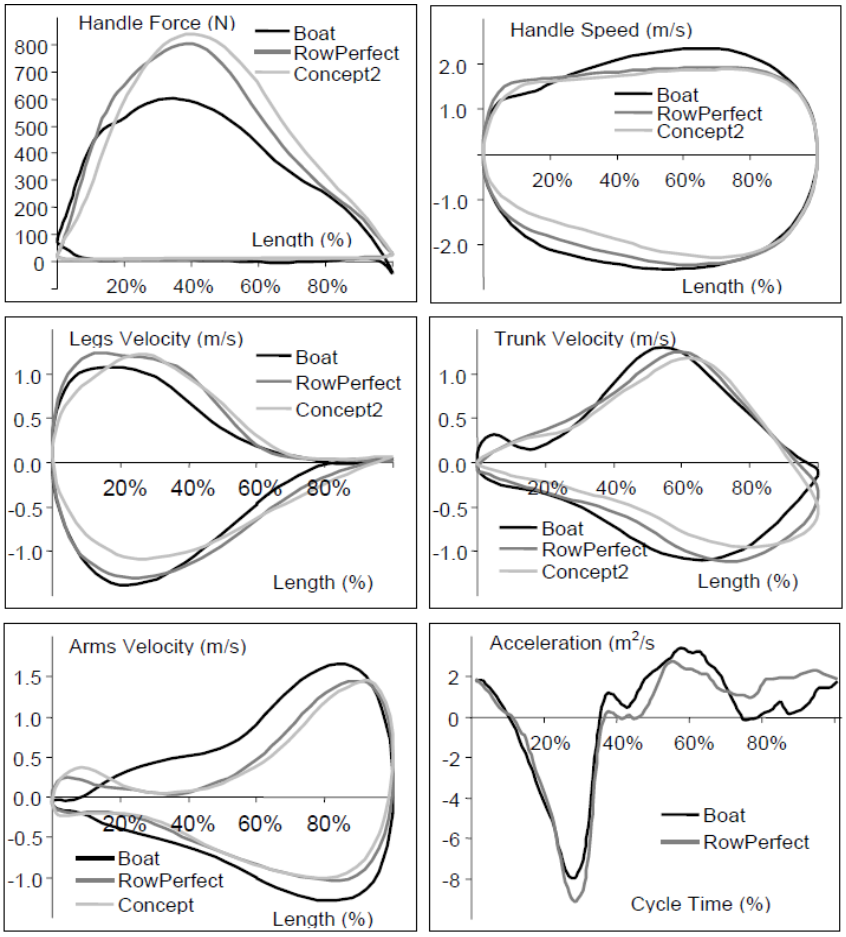

Figure 1-9: Patterns of biomechanical parameters

Averaged Patterns of biomechanical parameters, comparing single scull and ergometer rowing: handle force and speed and body segment velocity measured with respect to percentage stroke length. (Kleshnev 2005a)

Further comparisons between ergometer designs have been made by four groups: Bernstein *et al* (Bernstein et al. 2002), Colloud *et al* (Colloud et al. 2002; Colloud et al. 2006), Benson *et al* (Benson et al. 2011), and (Nowicky et al. 2005).

1. Bernstein *et al* used the CODA motion analysis system with infra-red markers on handle and foot-stretcher to measure displacements and correlated these with force data from the Rowperfect software. They found that stroke length was 53mm longer and the mean forces were higher for a stationary ergometer than for a dynamic ergometer. They speculate that the increased kinetic energy is being absorbed by muscles working eccentrically and that this might have the impact of increased injury rates.
2. Colloud *et al* also employed markers and a motion analysis system to compare flexion/extension angles of upper and lower limbs upon stationary and dynamic RowPerfect ergometers, and also determined that forces were greater for the stationary ergometer, and that inertial forces were higher during the transition between drive and recovery phases, concluding that muscular coordination might differ between the two types of ergometer.
3. More recently, Benson *et al* compared stationary and dynamic ergometers made by Concept 2. Due to the design differences between the dynamic ergometers of RowPerfect and Concept 2, the dynamic mass of the Concept 2 ergometer is more than twice as large as the RowPerfect equivalent. Load cells mounted between the handle and chain of the ergometer were used to measure handle force, and parameters such as stroke rate, stroke ratio, rate of force development etc were calculated from this raw data. They found that higher stroke rates and lower stroke forces were used to achieve a similar power output on the dynamic Concept 2 ergometer when compared to the stationary.
4. The Concept 2 and Rowperfect ergometers were analysed from an electromyographic point of view by Nowicky *et al* (Nowicky et al. 2005). Monitoring erector spinae, rectus abdominus and rectus femoris muscles, with a pressure switch under the foot to identify the beginning of the stroke cycle,

he found no significant differences between the two designs of ergometer, but commented upon the need to extend the study to on-water rowing. Further Electromyographic study of rowing is covered in section 1.7.

Throughout these comparisons between on-water rowing and ergometer rowing and between ergometer designs, most researchers agree that whilst there are differences between rowing on the different platforms, measurements performed upon an ergometer are a good initial basis for analysis of both rowing kinetics and kinematics.

1.5 Review of relevant on-water and ergometer studies

It can be seen from the explanations above that the velocity of the shell and the efficiency of the stroke are affected by a number of factors, some more thoroughly understood than others by researchers and sportsmen alike. Attempts have been made to gather more information about the sequencing, force production and kinematics of rowing using a wide variety of sensors and techniques.

Prior to the 1980's the size of sensors and electronics instrumentation systems limited the measurements that could be made in or upon a rowing boat. A review by McBride (McBride 2005) describes early research by Baird and Soroka (Baird and Soroka 1951) which utilised strain gauges to measure force at the oarlock, but were forced to connect these sensors to bulky data collection equipment carried on a following motorboat. She goes on to say that additional measurements made by Schneider, Angst and Bradt (Schneider et al. 1978) allowed the oar force to be analysed in conjunction with oar angle and overall boat acceleration. As integrated electronics reduced the size of measurement systems, an increasing number of research projects looked into instrumenting the rowing boat. Early examples of these are Gerber *et al* (Gerber et al. 1987) and Smith, Spinks and Moncrieff (Smith et al. 1988) who used linear proximity sensors and electrogoniometers on the oars to measure handle force and angle respectively. Commonly turbines and impellers were used to monitor hull velocity such that force at the oar could be compared to boat performance.

Since the late 1980's a few research groups stand out for their continued research in mechanics and biomechanics of on-water rowing: Smith, working initially with Spinks and later with Loschner (later called Draper) and Kleshnev. Because of the breadth of work by these two groups, these will be reviewed first before a broader look at the research and measurement techniques of rowing kinetics and kinematics of other groups.

1.5.1 Smith and Loschner/Draper

Smith, Spinks and Moncrieff (Smith et al. 1988) developed a measurement system (ROWSYS) to monitor several parameters within the rowing boat. Initially this was to enable monitoring of the rowing force curve so that compatibility of this force curve could lead to improved performance of a crew. These measurements initially included oar force data using linear proximity strain gauge transducers, oar angle using rubber band electrogoniometers (essentially a rotary potentiometer), and boat velocity via an impellor. Although this equipment would have required quite involved modifications/additions to the boat, it did benefit from the use of radio telemetry to transmit data to another boat or to the shore.

Subsequent research by Smith and Loschner (later Smith and Draper) employed this measurement system or improved upon it to make a number of conclusions regarding force production and timing of the rowing stroke. In one example, they used the ROWSYS system, measuring also seat velocity using a cable and drum potentiometer, and an accelerometer to measure boat acceleration in order to look at the relationship between seat velocity and boat acceleration (Loschner and Smith 1999). They postulated that seat position could be used as an

approximation of the centre of mass of the trunk and thighs which compose the greater part of the rower's mass, and that since seat velocity would need to increase for increased stroke rates, that this might have an impact upon boat acceleration. They plotted seat velocity and boat acceleration against oar angle for a number of stroke rates and concluded that whilst the pattern was remarkably similar over the differing stroke rates, that boat acceleration was more sensitive to changes in the seat velocity (and hence to changes in large body segment acceleration changes) during the recovery phase.

In later research, they updated their measurement system to the Rowsys2, using 3D piezoelectric transducers to measure both propulsive and transverse forces at the oar pin, and shear beam load cells to measure the stretcher force. Oar angle was measured as previously, and accelerometers and gyroscopes were used to sense acceleration and orientation of the boat (Smith and Loschner 2002).

Smith had previously presented data (Smith and Spinks 1995) showing the relationship between oar force and boat velocity (Figure 1-10). The complex variations of boat velocity cannot be related solely to this oar force, and as such, other parameters needed to be monitored to attempt to explain these variations.

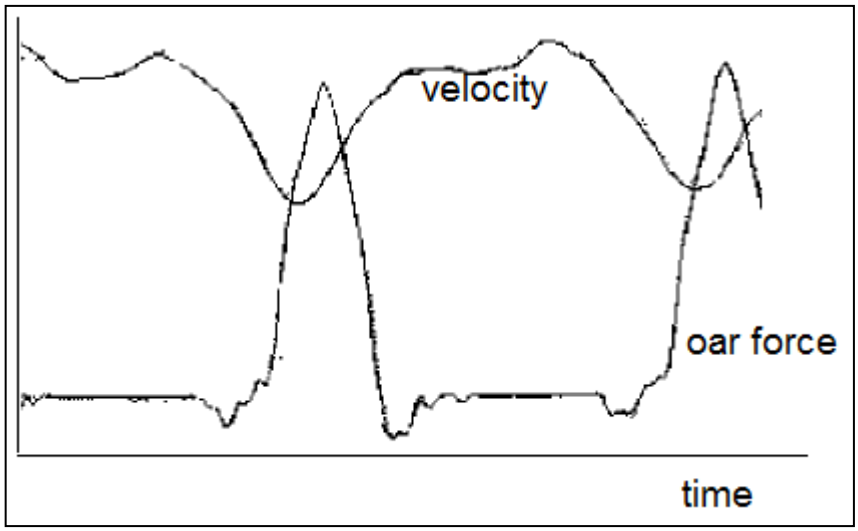

Figure 1-10: Oar force and boat velocity over the rowing stroke
(Smith and Spinks 1995)

Since the stretcher forces are in part reaction to the production of pin forces by the rower during the drive phase and in part reaction to the rower's acceleration during both drive and recovery phases, they believed that measuring stretcher force should yield more information about the propulsive forces within the boat.

By plotting total pin propulsive force and total stretcher propulsive force as a function of oar angle, they were able to show that they have a similar shape, but that pin forces exceed stretcher forces over the majority of the stroke (Figure 1-11 b). It is also clear that whilst the pin force is zero over the recovery, the stretcher force has significant magnitude during the recovery, which, if equal or greater to the drag forces maintain boat speed or accelerate the boat. Combining the pin and stretcher forces they show that this combined force reflects the overall boat acceleration (Figure 1-11 c).

Due to the application points of the oar pin forces on a pair boat, equal propulsive forces on each oar would produce equal but opposite moments about the centre

of mass of the boat (Smith and Draper 2002). However, the transverse pin forces cause a net anticlockwise moment upon the boat (Figure 1-11 d). They were also able to show that in order to ensure the boat travels in a straight line pair rowers compensate for this net anticlockwise moment by optimizing their force application; the (stroke-side) stroke rower leads the bow rower by about 1% of the stroke, this earlier application helping to counteract the net anticlockwise moment of the boat (Smith and Draper 2002) (Figure 1-11 d). Additionally they were able to show the asymmetry of force application at the stretcher (Figure 1-11 e).

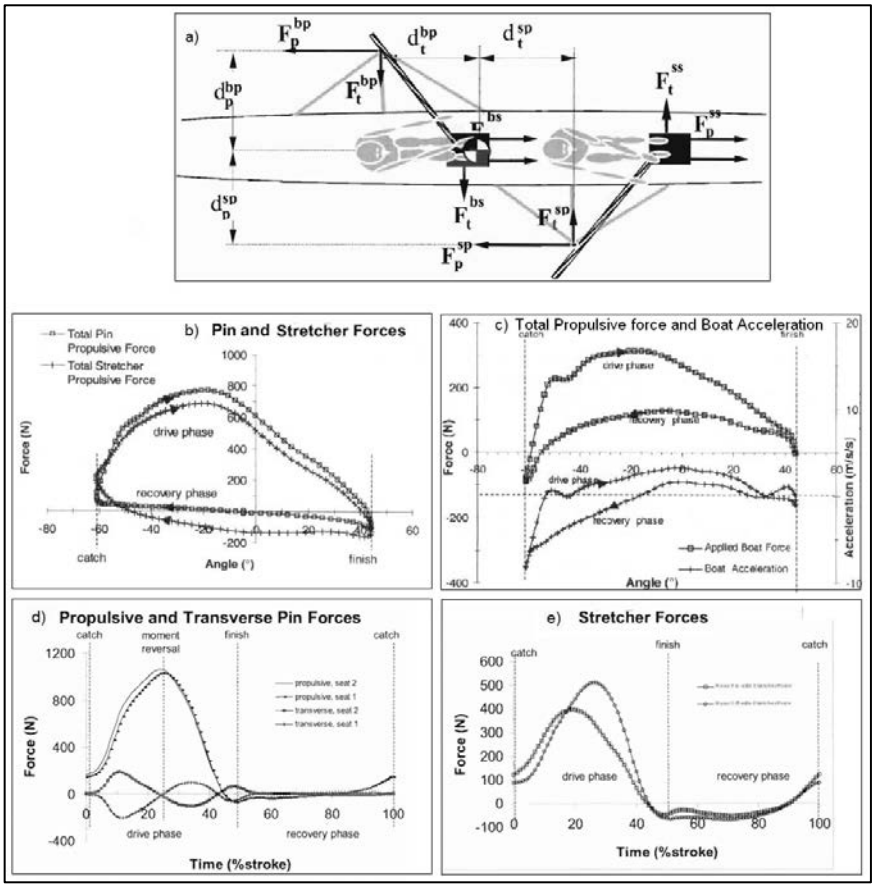

Figure 1-11: Forces about the stretcher and pin

a) Net Moment in Pair boat, b) Pin and Stretcher propulsive forces, c) Combined pin and stretcher force and boat acceleration, d) Optimised force application, e) asymmetric stretcher force application (adapted from (Smith and Draper 2002; Smith and Loschner 2002).

Later experimentation by Smith and Draper were able to show the ability to use their measurement system to discriminate between elite and sub-elite pair rowing, including showing increased stroke length of elite rowers, but reduced vertical oar deviation (Smith and Draper 2006).

1.5.2 Kleshnev

Kleshnev published a number of papers in the 1990s discussing propulsive efficiency of rowing (Kleshnev et al. 1996; Kleshnev 1998, 1999) by performing on-water experiments measuring oar angle, handle force, boat acceleration and boat velocity with equipment similar in description to that of Smith and Loschner. He calculated efficiency of boat propulsion using total propulsive power and boat velocity fluctuations for a number of different boat types and stroke rates. He concluded that since increasing the stroke rate increased velocity variation over the stroke there was a loss of efficiency in every crew. Other important factors he highlighted included ratio of drive time to overall stroke time.

In 2000 Kelshnev too added stretcher force to his on-water measurements using strain gauges, concluding that 52.8% of total rowing power was applied at the oar handle, and 47.2% at the foot-stretcher (Kleshnev 2000). Figure 1-12 shows the comparison between the traditional calculation of total power from handle force alone, and the new calculation which included the foot stretcher force. He also includes plots of body component power contributions over the stroke cycle calculated from measurements of velocities obtained using custom-made transducers using spring-loaded potentiometers and low-stretchable lines connected to the points of measurement.

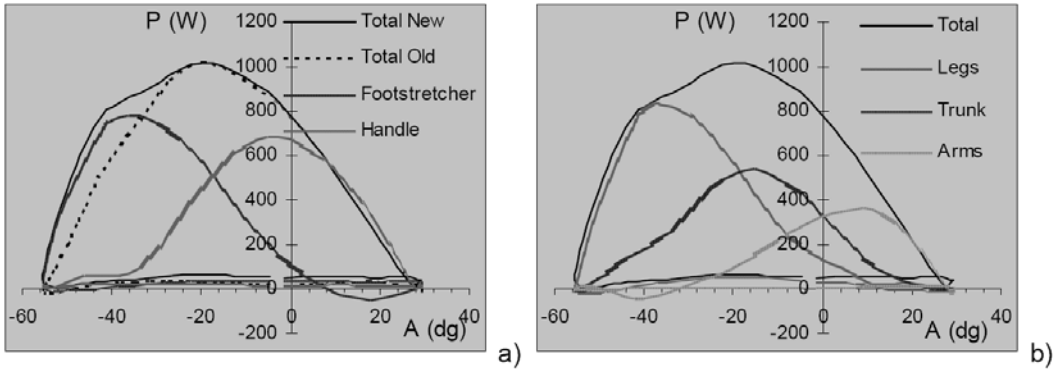

Figure 1-12: Powers applied and component power contributions

a) instantaneous power at handle and footstetcher, and b) segmental powers (for sequential style rowing), measured relative to oar angle.(Kleshnev 2000)

In an earlier ergometer-based experiment (Kleshnev and Kleshneva 1992) he also reported his findings of relative (%) contributions of the body segments. These varied depending upon the experience of the rower, but his elite rower measurements gave leg, trunk and arm contributions as 43.9%, 36% and 20% respectively. As stroke rates increase the legs increase their percentage contribution.

In his 2006 paper on Rowing Biomechanics (Kleshnev 2006), Kleshnev divides the stroke up into micro-phases (6 in the drive and 3 in the recovery) in order to better understand the kinematics and kinetics involved. These are shown in Figure 1-13, where D1-D6 are blade immersion, initial rower acceleration, initial boat acceleration, rower acceleration, boat acceleration and blade removal, and R1-R3 are arms and trunks return, legs return and catch preparation respectively.

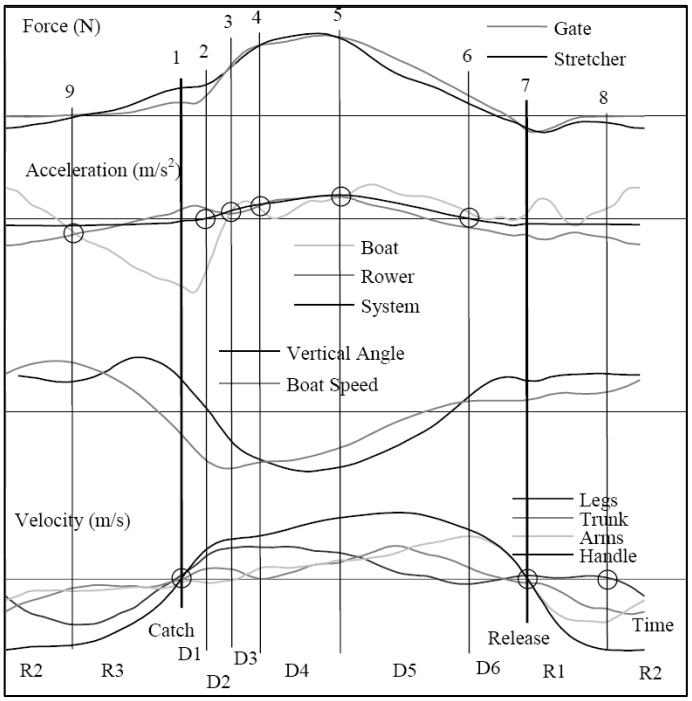

Figure 1-13: Micro-phases of the rowing stroke

Biomechanical parameters and micro-phases of the stroke cycle (M1x, 32spm). (Kleshnev 2006)

D1-D6 - Drive Phase: Blade immersion, initial rower acceleration, initial boat acceleration, rower acceleration, boat acceleration, blade removal

R1-R3 – recovery phase: arms and trunk return, legs return, catch preparation

He also highlights the effect of rowing style upon the shape of the force curve, showing how sequenced application of work by legs, trunk, and arms produces a different shape to a simultaneous application of work approach (Figure 1-14).

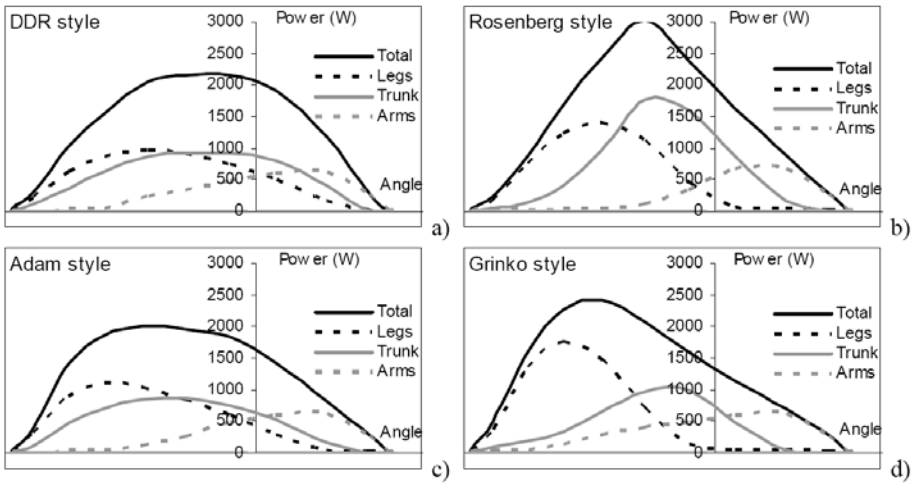

Figure 1-14: Force curves for different rowing styles

Effect of the segments sequencing, and emphasis on the shape of power curve, given for four different rowing styles (DDR and Adam are simultaneous, Rosenberg and Grinko are sequential). (Kleshnev 2006)

In a 2010 article Kleshnev made a departure from discussion of boat kinetics and kinematics of rowing to consider electromyography (EMG) as a biomechanical method of analysis (Kleshnev 2010). He published data from a pilot ergometer study which aimed to look at the sequencing of muscle activation during the rowing stroke (Figure 1-15). The results of measurements upon Quads (rectus femoris), Hamstrings (biceps femoris) and Gluts (gluteus medius) are compared to the body segments velocity discussed earlier, showing good correlation.

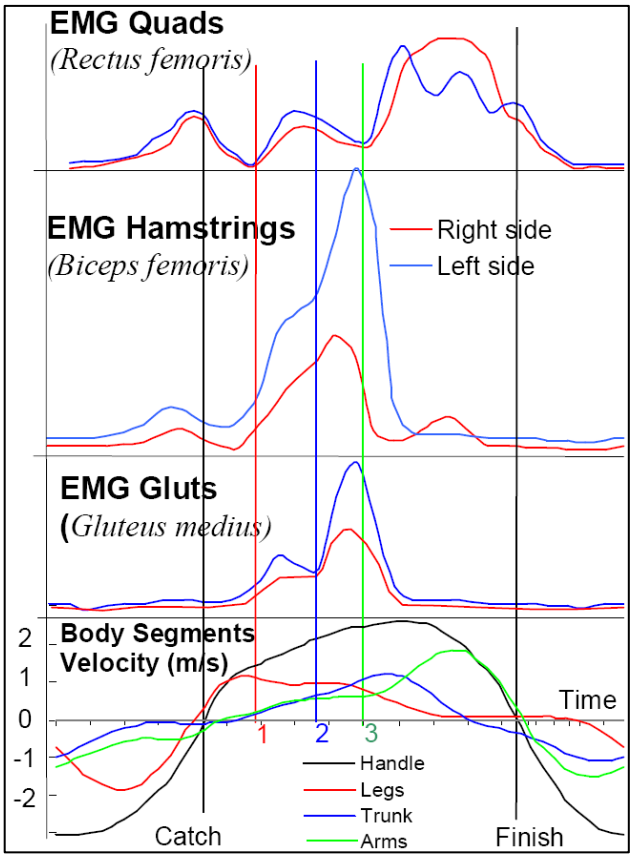

Figure 1-15: Electromyography of the rowing stroke

Pilot study on ergometer to evaluate the sequence of muscles activation during the stroke cycle. quads (Rectus femoris), hamstrings (Biceps femoris and Semimembranosus) and gluts (Gluteus medius), compared to body segments velocity. (Kleshnev 2010)

He concludes that such measurements might be used to evaluate rower technical effectiveness. This will be revisited later in section 1.7.

1.5.3 Other notable in-boat and ergometer research studies

Strain gauges and potentiometers were also employed by Hill (Hill 2002) to measure handle force and oar angle. He used this data to look at the synchronisation of rowers within the boat, concluding that synchronisation was better at the catch than at the finish of the drive. He demonstrated that there was a systematic change in the centre of force pattern in the coxless pair that was not

evident in a larger boat, agreeing with the observations seen by Smith and Loschner (Smith and Draper 2002) the same year. He was also able to show that this asymmetry of force disappeared within 40 strokes of the rowers rowing in an eight.

A number of researchers have used video and landmark measurement as a method of analysis. Both these techniques have the benefit of no-contact data collection, but both suffer the difficulties of obtaining useful information for on-water rowing. In particular, landmark measurement systems employing infra-red markers are exclusively used in-laboratory experiments upon ergometers.

Young and Muirhead (Young and Muirhead 1991) comment how force measurements are measured in an ystem (the boat) and thus cannot be applied directly. Preferring to look at velocity and acceleration of the boat directly, they compared boat acceleration results of intermediate and experienced rowers, and also the results of acceleration determined from video footage with that measured with the hull-mounted accelerometer, noting that some features would likely be missed with the video technique. Interestingly they also note that by placing an accelerometer upon the seat, thus measuring the acceleration of the combined centre of mass of boat and shell, an acceleration plot adhering more closely to the idealised acceleration curve (Figure 1-16) is produced.

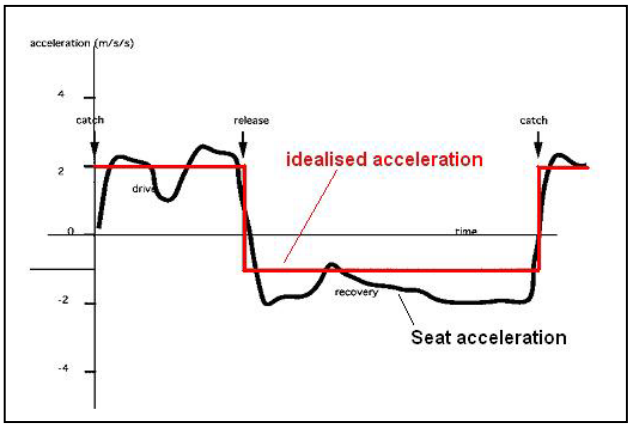

Figure 1-16: Measured seat acceleration compared to the idealised acceleration curve

(Young and Muirhead 1991)

This is the earliest reference found to the use of accelerometers mounted within the boat.

Data derived from video footage has been a popular technique because of the non-invasive nature of the data collection. This approach is also employed by Haglin and Sztul (Haglin and Sztul 2000) who digitised video footage, both on ergometer and on-river. Using VideoPoint software they logged data-points of handle, shoulder and seat coordinates upon the ergometer, and rower's head and boat bow ball coordinates on-river. No correlation to power output was made in either environment, but the research did yield some interesting analysis techniques, specifically using phase diagrams to compare velocities to positions, or accelerations to velocities. In this way, characteristics of stroke-length and rating was analysed. From the results it appears possible to compare the strokes of two different oarsmen and to compare stroke-length and speed of the catch (Figure 1-17). Further analysis might yield other subtleties of the stroke that can be identified in this way. Interestingly, this paper also analyses weightlifting using

a similar method – the rowing drive is often described as “standing on your catches” as the leg drive is similar to that employed in weightlifting.

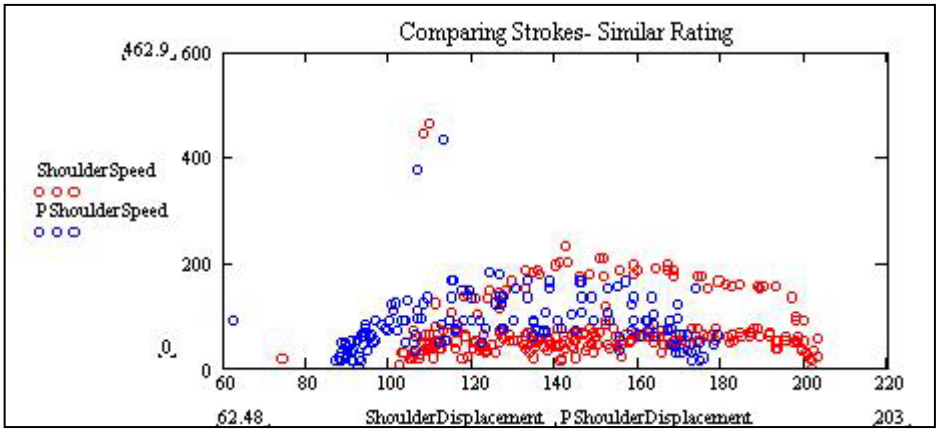

Figure 1-17: Speed–Displacement phasor diagram

Using a shoulder phase diagram to compare strokes with similar stroke ratings – indicates red rower has more stroke length and a more controlled recovery speed (Haglin and Sztul 2000)

In addition to Bernetein *et al* and Collaud *et al* mentioned earlier in the analysis of ergometer performance, other research groups have used landmark measurement techniques. Kaya *et al* (Kaya et al. 1995) developed a biomechanical model consisting of eight rigid segments and 31 muscles. It allowed them to calculate the knee and trunk angles, rowing power and muscle power using 3D landmark measurement and force sensor (ergometer handle and foot-stretcher force) data, along with multiple EMG measurements. This was achieved through the use of several different measurement and data collection methods rather than one integrated system. They were able to compare output power and knee and trunk angles of a number of rowers. Landmark measurement and video monitoring techniques are frequently used to validate other techniques.

A different 3D positioning technique is used prolifically by the human performance research group at Imperial College London. Between them Bull and McGregor have published a number of papers of their kinesiological investigations of movement of the lumbar spine of rowers to research mechanisms of injury in rowing. This originated from an interest in the significant lumbar spine injury rate of rowers (Bull and McGregor 2000). They use a system called “Flock of Birds”. Like infrared marker landmark measurement it is a lab-based technique and their experiments are exclusively ergometer based. Initially their method was developed to monitor rowing technique (specifically lower spine and pelvis position and angle) by means of Ascension Technology’s “Flock of Birds” equipment and a load cell to measure ergometer handle force. “Flock of birds” is an electromagnetic motion capture system which provides fast and accurate magnetic position and orientation tracking of a number of wired receivers giving position and orientation relative to the transmitter. With three receivers placed at the sacrum, thoraco-lumbar junction and femur, they analysed the thoraco-lumbar angle, lumbo-sacral angle, and femoral flexion angle for different common rowing techniques (Figure 1-18).

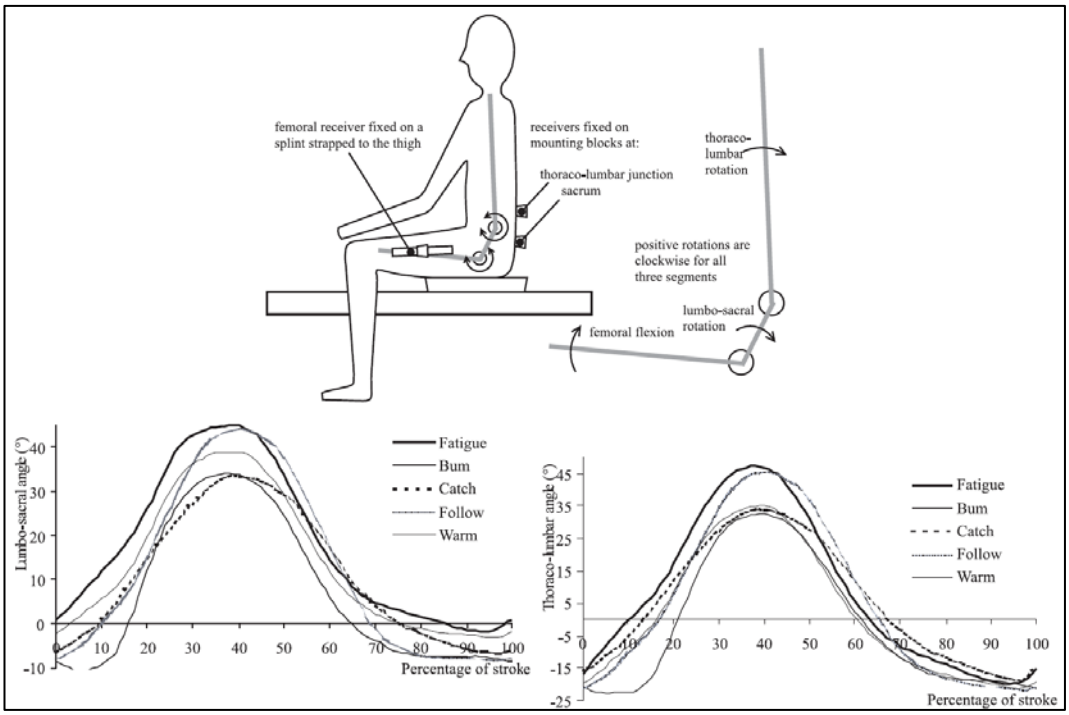

Figure 1-18: Sensor placement and joint angles measured

Mounting block fixation points to determine body segment angle. Lumbo-sacral flexion and Thoraco-lumbar flexion. Comparing different rowing styles. (Bull and McGregor 2000)

They have also used this technique to look at kinematics of rowing technique over prolonged rowing (Holt et al. 2003), revealing marked increases in the amount of spinal motion during the hour exercise, and also to analyse rowing technique at different stroke rates (McGregor 2003). Here they saw marked changes in the force output curve, a shift in the peak torque, and changes in the lumbo-pelvic kinematics depending upon the intensity of the rowing.

The same group added a four uni-axial load cells to the ergometer slide rail to which the rowing seat was attached in order to measure the force magnitude and centre of pressure on the rowing seat during indoor rowing (Murphy et al. 2010). Typical results are shown in Figure 1-19.

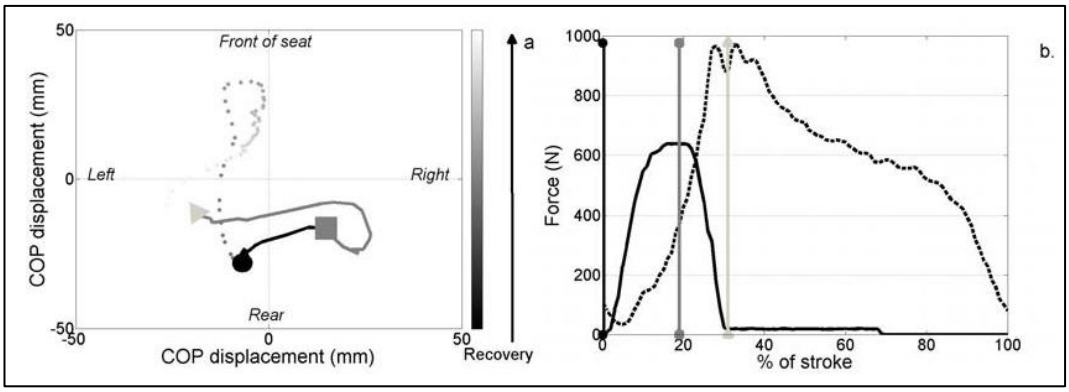

Figure 1-19: Centre of pressure (COP) displacement (seat), handle, and seat force.

Seat force and COP measured using uniaxial load cells upon a modified ergometer seat, monitored relative to handle force over the rowing stroke. Tensile handle force – solid line, vertical seat force – dashed. (Murphy et al. 2010)

This seat force addition to the measurement system was further utilised by the group (Buckeridge et al. 2012) to look at kinematic asymmetries of the lower limbs. They found that all groups demonstrated lower limb asymmetries, with hip asymmetries significantly greater than knee asymmetries, concluding that whilst ergometer rowing is symmetrical with respect to lower limb motion, these deviations from symmetry result from rowing experience of sweep oar rowers.

Direct measurement of joint angles has been made by a number of groups employing electrogoniometers. Hawkins (Hawkins 2000) developed an ergometer-based measurement system which used four electrogoniometers attached to the rower to measure joint angles at the ankle, knee, hip and elbow, and potentiometers and force transducers on the ergometer to measure force. His system was able to show a stick-man playback animation alongside plots of the handle force, handle velocity and joint angles. Whilst this was a measurement system designed for laboratory use, unlike other joint angle measurement approaches described above it could be used in on-river measurement, though

the author notes possible limitations due to encumbered motion to the rowers and slippage of the electrogoniometer attachment to the limbs.

1.6 Accelerometry and Rower Kinematics

Up to this point, accelerometers and gyroscopes have been considered for measurement of boat or seat acceleration only. However, with the reduction in size and cost of integrated MEMS (micro-electro-mechanical systems) sensors, there has been an increased interest (in sporting and health applications) in using these devices to monitor movement upon the body. Research has been undertaken using multiple accelerometers, multiple gyroscopes, a combination of both, or inertial measurement units (IMUs). IMUs are devices usually containing tri-axial accelerometers, dual- or tri-axial gyroscopes, and often magnetometers (earth magnetic field sensors), allowing linear and rotational accelerations to be measured. These are not wholly fabricated on the same silicon chip, but are often packaged in the same housing or module, allowing good alignment of axes of the different sensors). Whilst the individual integrated circuits are small, the modules themselves are still a little bulky and very expensive (Starting price $320: Analog Devices ASIS16400 dims:23x23x23mm).

The possibility of using IMUs to quantify and visualise on-water rowing technique was recently investigated by Tessendorf *et al* (Tessendorf et al. 2011). Their system is wired, and uses two IMUs placed upon the boat and oars. Their ultimate aim is to implement the system wirelessly, and as such the algorithms used are computationally light, their aim being to ultimately transmit calculated features rather than raw data to reduce bandwidth requirements. They were able to extract stroke rate, length drive/recovery ratio and feather/square ratio, and

also to monitor oar rotation angle and boat acceleration against horizontal oar angle, enabling some analysis of technique to be made of particular rowers.

Two years previously, Llosa *et al* (Llosa et al. 2009) also concentrated upon monitoring boat movement and oar movements. Their system however, used only tri-axial accelerometers mounted in a cube arrangement in the oar handles, their orientation allowing rotation and translation data to be derived by algorithm. They too looked at boat acceleration and velocity (through integration of acceleration) and compared stroke angles of two rowers. Figure 1-20 shows how they compared oar acceleration and boat acceleration and velocity allowing the conclusion that oar acceleration shape gave a good indication of good rowing technique. Notably, this system is wireless, and will be considered again in section 1.9.

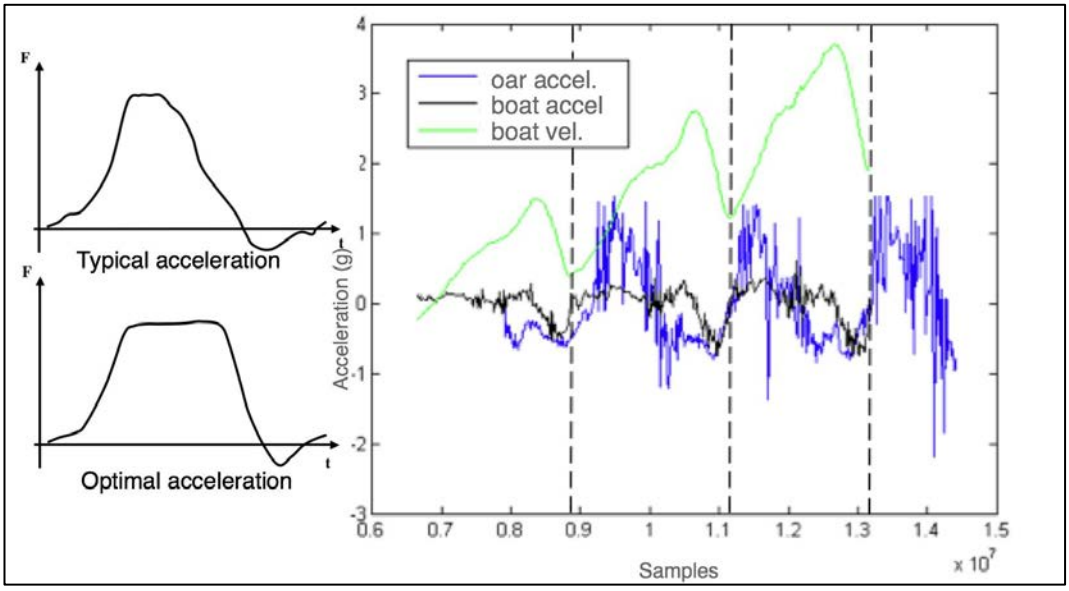

Figure 1-20: Comparison of boat acceleration and velocity with oar acceleration for technique analysis

Measurement technique using tri-axial accelerometers only, in a cube arrangement to derive rotation and translation (Llosa et al. 2009)

Tessendorf *et al* and Llosa *et al* both exploit the use of inertial measurement systems to monitor more than just boat acceleration on-river. However, King *et al* (King et al. 2009) goes one step further to place acceleration sensors on the rower's body to determine joint angle. Working with Bull and McGregor within the aforementioned human performance research group at Imperial College London, they monitored rotation and in the lower back and femur employing a IMU that comprises tri-axial accelerometer and dual-axis gyroscope. They determined joint rotation angle by integrating gyroscope data, and compensated for integration drift that takes place in these types of sensors through the fusion of this data with accelerometer data measured during the pauses in the stroke where angular velocity is zero (the accelerometers would then just read a component of gravitational acceleration indicating joint inclination). They verified their system by comparing their joint angle measurements with that determined using passive infra-red landmark measurement system(Figure 1-21 a), and showed (Figure 1-21 b) that using their system they could identify particular technique traits (over-leaning and slide-shooting). This again is a wireless measurement system and will be revisited in section 1.9.

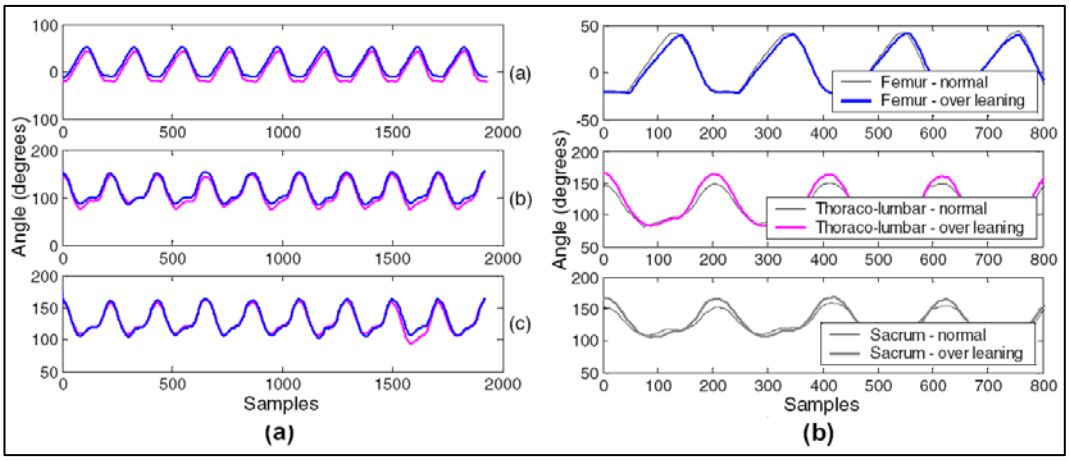

Figure 1-21: Joint angle measurements

(King et al. 2009)

An example of the rotation of the femur, thoraco-lumbar junction and sacrum.

(a) Comparison of measured rotation (magenta) against infra-red landmark measurement (cyan)

(b) Comparison of femur, thoraco-lumbar and sacrum data during poor technique (over-leaning) and good technique

1.6.1 Wider research of accelerometry in kinematics

It is useful to not limit the study of research into inertial measurement upon the body to that concerned with rowing. As MEMs acceleration sensors have become smaller and cheaper they have pervaded personal gadgetry. However, this has largely been limited to pedometer or orientation (with respect to gravity) applications. Their feasibility to recognise other positions, gestures or motions is still widely researched. Literature in this much broader field encompassing pervasive health monitoring, context awareness and activity recognition using accelerometry, IMUs or similar sensors were surveyed, though not exhaustively. These reveal a number of different techniques employed to extract useful information from the raw data.

As early as 1993, Veltink *et al* (Veltink et al. 1993) considered the feasibility of accelerometry for posture and movement detection. They used 2 accelerometers mounted on upper leg and trunk, and by plotting these on x and y axes they were able to show clustering of data denoting postures such as sitting, lying and standing (Figure 1-22 a).

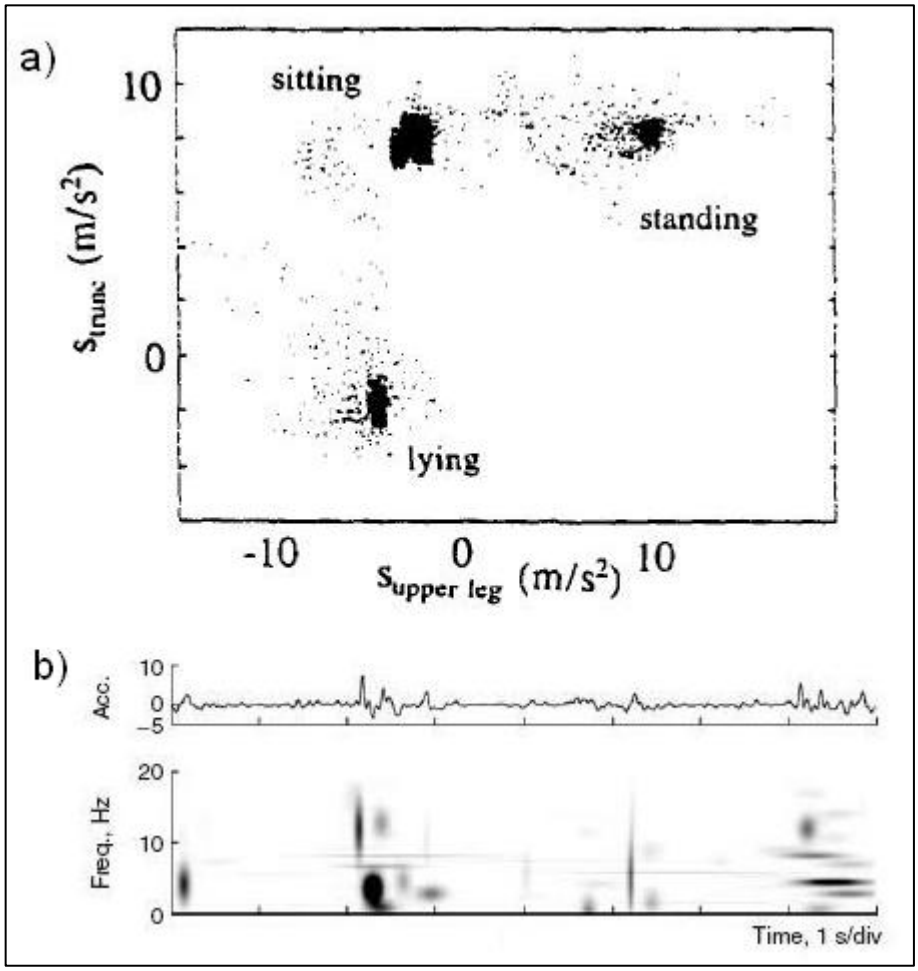

Figure 1-22: Other uses of accelerometry upon the body for health applications

(a) Posture recognition using accelerometry by combining data from multiple accelerometers (Veltink et al. 1993)

(b) Frequency-time energy distribution of accelerometer signals in post-stroke hemiplegic patients (Akay et al. 2003)

Mantyjarvi *et al* (Mantyjarvi et al. 2002) similarly mounted tri-axial accelerometers about the body (at the hips) to recognise different human motion, and using

principal component analysis and independent component analysis to achieve feature extraction from the raw acceleration signals.

A single waist-mounted accelerometer was used by Akay *et al* (Akay et al. 2003) to monitor post-stroke hemiplegic patients. They were able to show using frequency-time energy distribution graphs of acceleration signals that severe post-stroke hemiplegic patients displayed significantly increased circular burst patterns when compared to healthy elderly subjects (Figure 1-22 b).

A number of groups, like King *et al* (King et al. 2009), have exploited the different features of linear accelerometers and gyroscopes for orientation and angle calculation, compensating for the integration drift in the calculation of orientation from gyros with measurements made using linear accelerometers, and using this information in Kalman filters to improve upon the calculation. It is acknowledged by most of these groups that some further assumptions or restrictions need to be made to the measurement system if magnetometers are to be avoided; magnetometers allow absolute rotation in the horizontal direction (azimuth) to be determined. Magnetometers are problematic due to non-uniformity of the earth's field in buildings and interference due to proximity of ferromagnetic materials.

A number of papers were published by Luinge and Veltink (Luinge et al. 1999; Luinge and Veltink 2005) investigating the estimation of limb orientation. Employing gyroscopes and accelerometers they first split the gyroscope measurement into tilt and rotation about a global Z-axis, and then fed the difference between the tilt measurements of both gyroscope and linear accelerometer into a Kalman filter to obtain a better estimation of the tilt. Recombining this improved tilt estimation with the rotation about the Z-axis they

were able to gain much improved results fusing these two sensors compared to using gyroscope information alone.

Favre *et al* (Favre et al. 2006; Favre et al. 2008) similarly looked at how linear accelerometer data could be fused with gyroscope measurements within a Kalman filter to provide a better estimation of knee joint angle. To improve upon the estimation still further, they used known anatomical constraints of the knee, and an initial alignment calibration routine to align the IMUs to a common reference frame (thus the orientations of the two IMUs are calculated within a fixed reference frame). They saw a 7 times reduction in error of tilt angle using this method.

Anatomical constraints were also exploited by Cooper *et al* (Cooper et al. 2010), but this time as an input to the measurement process rather than just for an initial alignment/calibration process. Comparing their results with validation from reflective marker landmark measurement, they showed RMS errors of 0.7 degrees for walking and 3.4 degrees for running.

Liu *et al* (Liu et al. 2009) also developed a method of determining rotation of the thigh body segment in a 2D frame, though unlike the above, they used only linear accelerometers. An accelerometer at the hip monitored translational acceleration, whilst two further tri-axial accelerometers are used to give acceleration data at two points upon the thigh body segment attached to the same rigid plate. These two accelerometers would experience the same translational and gravitational acceleration, but different rotational acceleration. With the hip at the local origin of a body coordinate system, they calculated thigh angular displacement by their double-sensor difference algorithm, knowing the overall translational acceleration

of the system and the distances of the thigh accelerometers from the local origin. The results were compared to measurements using an optical (retro-reflective marker) motion analysis system. They found that whilst errors increased with increasing rotational velocity of the body segment, it was indeed possible with their method to determine angular displacement without the integration errors of gyroscopic techniques.

The integration drift was reduced by Vlasic *et al* (Vlasic et al. 2007) in their practical motion capture system by the addition of another sensor. They employed ultrasonic measurements to determine distances between multiple accelerometer/gyroscope sensor nodes in addition to an extended Kalman filter to combine the measurements from the three different sensor inputs. This Kalman filter uses information about the system from a model to perform pose estimation until these estimates can be updated from actual measurements. Again the performance of this system was evaluated against an optical motion capture system, and the combination of all three sensors provided the best correlation to the optical system rather than accelerometers, gyroscopes or ultrasonic alone.

1.7 Muscle activity analysis in rowing literature

An early and often cited paper looks at the rowing stroke from an entirely physiological point of view. Mazzone, a medical doctor, describes the catch, drive, finish and recovery, explaining how the muscles in the rower are recruited for each part of the rowing stroke, and noting when muscles are in flexion or extension (Mazzone 1988). He also accompanies this description with a number of figures (Figure 1-23 is given as an example) highlighting the muscles involved in a particular part of the rowing stroke.

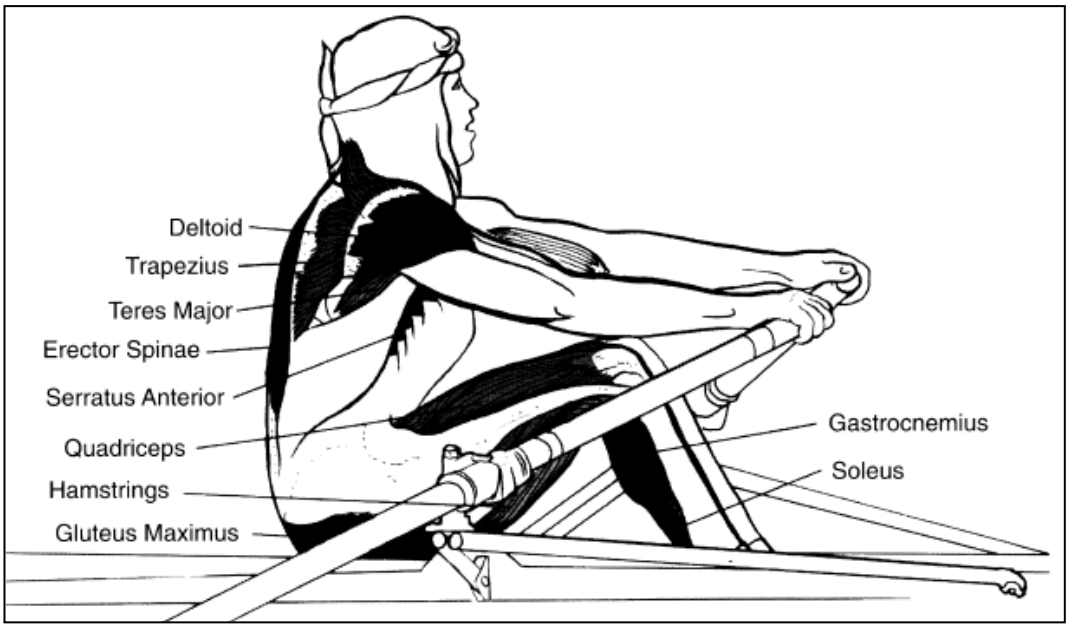

Figure 1-23: An example of the illustrations accompanying Mazzone's kinesiology of the rowing stroke

Indicates the recruitment of muscles at different points of the rowing cycle (Mazzone 1988)

Byford employed the use of electromyography (EMG) using surface electrodes (Byford 1992) to compare three rowing styles upon a Concept 2 ergometer. Monitoring the rectus abdominis and erector spinae muscles of the trunk, he

observed that peak force and shape of EMG profiles varied between the three styles of rowing even though they generated the same power output at the ergometer handle. He reported that one style (DDR style, which originated in East Germany Olympic rowing of the 1970s) had consistently and significantly lower metabolic cost over the other two observed styles, and concluded that different styles recruited different motor units within the same muscle. He further surmised that sequence and force of contraction differed between styles of rowing. He proposed using EMG as a biofeedback tool to rowers such that what they 'feel' their muscles are doing can be compared with what is actually occurring, but stated that challenges of wireless data capture and miniaturisation of measurement electronics needed to be overcome.

Another ergometer-based study that employed surface electromyography (sEMG) was conducted in conjunction with the previously mentioned McGregor at Imperial College London. Parkin et al (Parkin et al. 2001) monitored the erector spinae muscles of rowers and control subjects to determine if there were asymmetries in the muscles of rowers that rowed traditionally bow-side or stroke-side. They observed that whilst there was little difference in isometric strength of the observed muscles between the two measurement groups, rowers exhibited markedly greater sEMG signals in extension and flexion compared to the control group. They also confirmed that there was a trend towards left-right asymmetry in rowers, related to rowing side. A co-author to this paper is Nowicky, whose later paper (Nowicky et al. 2005) was previously discussed in the ergometer performance studies (section 1.4). A similar study to that of Parkin, looking at asymmetries of the leg muscles, was conducted by Janshen et al (Janshen et al. 2009). They monitored 6 muscles on each leg, along with pressure distribution under each foot, to monitor asymmetries in the leg drive of sweep-oar rowers

during symmetrical ergometer rowing, showing a 20-45% higher intensity in the muscle activity of the oarside leg correlated with 56-91% higher mean pressure under the ball of the inside foot.

A follow up to the ergometer-based study of Nowicky is a recent Congress paper presented in 2012 by Fleming and Donne (Fleming and Donne 2012). They assessed recruitment patterns of the rectus femoris, vastus medialis, biceps femoris and erector spinae during rowing upon a dynamic ergometer and on-water with a view to validating the task specificity of rowing ergometry. Whilst they observed little difference in overall muscle activity of the biceps femoris and erector spinae muscles with increasing intensity of rowing, they did find an increase for the rectus femoris. They also reported increased muscle activity throughout their measurements for on-water rowing compared to rowing upon an ergometer, concluding that significant differences existed in the recruitment patterns, possibly due to the altered acceleration and deceleration of moving masses which are not perfectly replicated by the ergometer. This study was performed using a mobile data-logger (Mega ME6000) that allows a number of muscles to be simultaneously monitored and their signals logged in a portable, wearable unit – the measurement channels are connected via wires to the data-logger worn upon the body. Fleming employed a similar system earlier in 2012 to conduct a study into kayak rowing (Fleming et al. 2012). This time monitoring different muscles more relevant to kayaking, he observed that activity was higher (particularly in the anterior deltoid) in some muscles and lower in others when comparing on-ergometer and on-water kayaking, and concluded that this was likely due to additional forces associated with the ergometer loading mechanism.

Similar use of a portable data-logger (wired connections to data-logger, wireless facility to transfer data to a PC after the logging session) to monitor on-water

sEMG was made by a couple of other groups. Sommer et al (Sommer et al. 2008) used a Biovision-EMG data logger to monitor nine muscles, also monitoring oar angle and oar force, and analysed the relative duration the drive and recovery phases of the rowing stroke in conjunction with the on-time of each muscle expressed as a percentage of the rowing cycle. Comparing ergometer rowing to on-water rowing, they observed, amongst other observations, that the biceps brachii had a longer on-time in the boat compared to on-ergometer, whilst the trapezius had a longer on-time upon the ergometer.

Guevel et al (Guevel et al. 2011) used a similar data logger (Myodata compact) to monitor sEMG of several thigh muscles (including quadriceps: rectus femoris and vastus lateralis, and biceps femoris) on water rowing. Also monitored were oar angle (potentiometer), torque (strain gauge) and knee angle (electrogoniometer). They found that pace sessions of different intensities produced highly correlated muscle activity patterns, but showed only moderate correlation to maximal intensity rowing. Additionally maximum intensity rowing showed the quadriceps muscles' intensity to remain constant, but the hamstring muscles' intensity to decrease over the 500m piece, along with a decrease in output power intensity. They proposed a number of different hypotheses as to why this might be.

1.8 e-Textiles

Wearable sensors, that can be integrated into fabric of clothing rather than just worn upon the body or retro-fitted to existing garments is a growing area of research that could greatly benefit measurement in sports environments.

Piezo-resistive sensors have been used by Tesconi *et al* (Tesconi et al. 2007) for kinematic measurement of lower limbs during ergometer rowing. An electrically conductive elastomer was integrated into a leotard to form 6 piezo-resistive sensors that allow measurement of flexion-extension of the knee and hip (Figure 1-24). This conductive elastomer can be printed onto the fabric using an adhesive mask process. Acquisition was via a body-worn unit which transmitted via Bluetooth to a nearby PC. By linear mapping of raw signals to limb kinematic variables they show good correlation with those captured using a camera measurement system (SMART-e).

One of the other authors of this research is de Rossi who has published widely in the field of e-Textiles. He has also produced an upper limb kinetics garment using the same conductive elastomer for post stroke patient rehabilitation (Paradiso and De Rossi 2006).

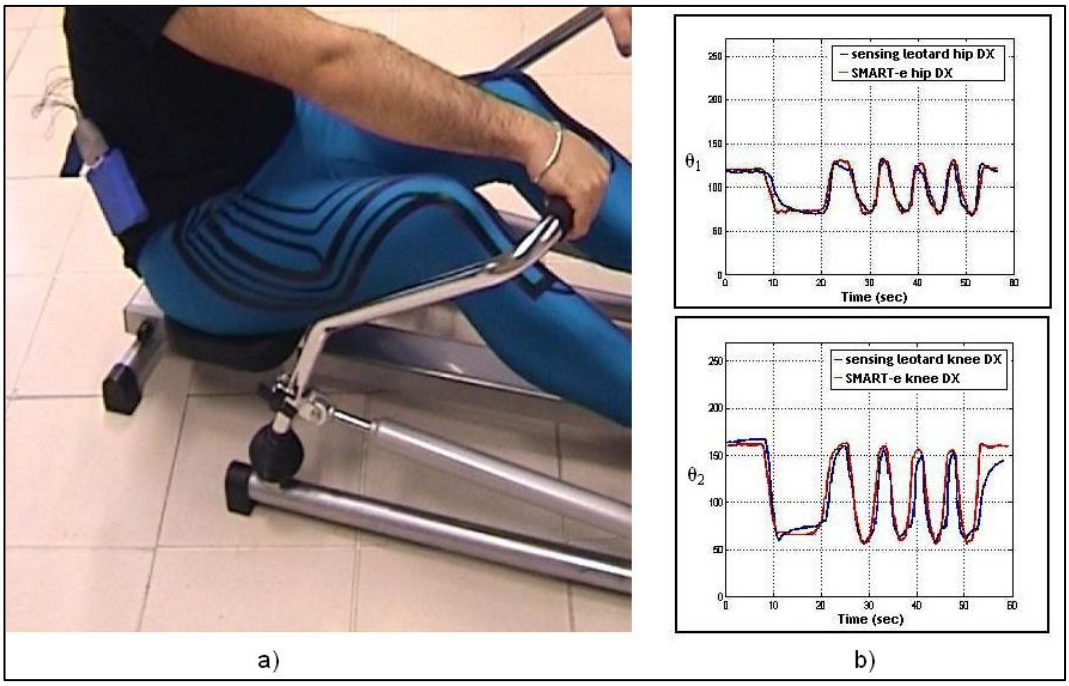

Figure 1-24: Piezo-resistive material incorporated into a leotard

a) Piezo-resistive leotard for measurement of hip and knee flexion-extension, and b) results compared to camera measurement system (Tesconi et al. 2007)

Paradiso (Paradiso et al. 2005) has worked upon the WEALTHY wearable healthcare system which also uses piezo-resistive strain sensors, but additionally includes electrodes for Electrocardiogram (ECG) and EMG measurement. The piezo-resistive sensors are fabricated using carbon-loaded rubber printed onto Lycra®, and weaving electro-conductive yarn into the piezo-resistive patch. The electrodes are knitted with metal-based yarns. Inter-garment connections were made with conductive yarns to a portable unit for signal processing and wireless transmission to a PC. She measured ECG, EMG, respiration, movement of shoulder, elbow and gluteus, and also EMG of the right quadriceps, showing how a diverse range of measurements can be made in one garment.

Other publications of particular interest in this growing field include Rothmaier *et al* (Rothmaier et al. 2008) and Coyle *et al* (Coyle et al. 2009). Rothmaier

employed photonic textiles for pulse oximetry by weaving plastic optical fibres into the fabric of a cotton glove. Coyle tested a sweat pH analysis system during indoor cycling where a textile-based wearable patch is dyed with a pH sensitive indicator which is optically analysed and shows sensitivity to change of 0.2 units of pH.

1.9 Wireless Systems

Body sensor networks (BSN) with small integrated sensors can facilitate kinematic and biometric data to be exploited to look at rowing technique. Collecting data across a wider geography rather than from just one specific data collection point can also clearly allow more information for interpretation. However, collecting data from multiple nodes across the body and/or boat without hindering movement or requiring a significant amount of modification to the boat becomes a limiting factor. Here, wireless data transmission can hugely reduce the infrastructure required for measurement and data collection.

A number of wireless standards have been introduced within the last decade which facilitate the creation of wireless networks, including Bluetooth and Zigbee, but without specifying a particular wireless standard, the concepts of Wireless Sensor Networks (WSN), Body Area Networks (BAN) and Body Sensor Networks (BSN) have been explored for the facilitation of data collection and system control across a number of sensor nodes. These technologies will be explored further in chapter 2 but research implementing them within sports and health monitoring are considered here.

Wireless data transmission from a traditional wired system to a PC or laptop at a remote location has been used by a number of groups before the advent of recent wireless network standards. Smith and Loschner (Smith and Loschner 2002) and Kleshnev (Kleshnev 2005a), both discussed previously, for example, employed a wireless link to transmit from rowing boat to a motor boat or the

shore. Here though the wireless link is largely just a cable replacement, rather than a means to remove wired connections between sensors or to play a greater role in system control.

A combination of wired and wireless data collection was used by Fok *et al* (Fok et al. 2004) in his analysis of rowing, measuring boat balance and seat acceleration with accelerometry, and boat speed using an impellor. The sensor nodes upon the seats were part of a WSN, but other measurements were wired. He discusses the problem of packet collisions (a packet is the transmission of a portion of data wirelessly) as he scheduled the nodes to transmit at front-stops, and of course a well-synchronised crew should reach front-stops at the same time.

Zigbee WSNs were employed by both Llosa (Llosa et al. 2009) and King (King et al. 2009), again previously discussed, to collect data across the boat (Llosa) or rower (King), both therefore showing the possibilities of wireless networking rowing measurement. One of the other authors of King *et al* is Guang-Zhong Yang, one of the pioneering researchers in the field of BAN and BSN, who has developed his own BSN nodes for use in his research which spans a range of applications, most notably in pervasive health monitoring. Another of his papers (Zhang et al. 2011) looks at human back movement analysis using BSN. Where King's rowing research was limited to back and femur in the sagittal plane, this extends the use of BSN to analyse 3D bending and twisting using 5 IMUs placed strategically across the back, yielding estimation of human back movement with good accuracy.

Continuing a study of the literature beyond rowing, WSNs have often been used as just part of a larger system. An example of this is Zijlstra *et al* (Zijlstra et al.

2010) who used BSN for the analysis of power during sit to stand movements. Three wireless inertial sensor nodes upon the body (at the hips and sternum) were combined with force-plates beneath the chair and feet, and an optical motion analysis system. An additional wireless inertial sensor node mounted with an optical marker was used to effectively synchronise these three systems; this 4th node was subjected to a sharp lifting action at the start of a trial such that this peak in acceleration could be matched to optical position data.

WSNs are used to analyse swimming technique by Le Sage (Le Sage et al. 2010; Le Sage et al. 2011), extending the network to look at multiple swimmers. Using an inertial WSN placed upon the swimmer's back as part of a larger system including force and pressure sensors at the pool edge, and high speed video, Le Sage looked at lap count, stroke count, stroke rate, velocity and distance, synchronising the elements of the system with a trigger from the force plate at the pool edge. Because of the large amount of potential raw data that needs to be processed by the system, Le Sage pays consideration to the benefits of transmitting processed information rather than raw data to reduce transmission overheads, and includes significant data buffering in a individual node such that transmissions can be periodic.

Likewise Martin *et al* (Martin et al. 2011) combines different Bluetooth-connected systems – a Bio-harness measuring heart rate, respiration rate, skin temperature and posture, a Bluetooth enabled pulse oximeter, and a set of *Shimmer* inertial wireless sensors, also using Bluetooth – to study the enhancement of activity recognition through the fusing of inertial and biometric information. The method of time synchronisation between these systems is not given. Similarly, Wang *et al* (Wang et al. 2010) also considers fusing inertial and biometric sensors using a

combination of wireless (inertial) and wired (sEMG) systems for the evaluation of patient recovery post operation based upon daily activity and abdominal muscle activity, though details of how these two systems were integrated together is sketchy.

Jovanov *et al* (Jovanov et al. 2009) proposes Avatar, a hybrid system encompassing “of-the-shelf” components including Nintendo Wii Remotes as optical position sensors, and *iSense* inertial sensor nodes (both employing Bluetooth to send data to a laptop) to achieve a multi-sensory system for body position monitoring, fusing these two approaches to reduce drift of absolute position.

Jovanov, however, is actually well-published in the field of full WSNs. One example is a BAN for computer assisted physical rehabilitation (Jovanov et al. 2005) which uses a Telos WSN and a custom-designed sensor board incorporating accelerometers and ECG circuitry. Interestingly, the nodes in this system include two processors – one cited on the Telos WSN board tasked with controlling the wireless communications, and one upon the sensor module. Many of his publications are directed more towards the challenges imposed by WSNs – for example power consumption of radio transmission, time synchronisation between wireless nodes, etc. Some of these challenges will be revisited in chapter 2.

Further notable examples of applications using WSNs or BSNs include Chelius *et al* (Chelius et al. 2011), and Braysy *et al* (Briiysy et al. 2010). Chelius designed a wearable sensor network for gait analysis incorporating inertial sensing nodes upon runner’s limbs, insole pressure sensors in the shoes, and a central

coordinating node. This was trialled in the harsh conditions of the “Sultan Marathon des Sables” desert race. This system is notable not just because of the harsh conditions and long duration of the experiment (which did cause problems with node ruggedness), but also due to the choice of a distributed approach – the individual nodes stored their own data for the duration of the race, leaving the wireless network for synchronisation messaging only. That time synchronisation effectively took place post-race – transmitted and local timestamps were saved with the data and the offsets corrected upon post-processing.

Braysy utilised a WSN for the movement tracking of sports team members. Accelerometer data was fused with RSSI (received signal strength indicator) data in order to determine player location, the RSSI data reducing acceleration data drift. Players wore wireless ‘tag’ nodes, and the sports field was surrounded by anchor nodes from which the ‘tag’ nodes could effectively triangulate their position using the RSSI signals.

1.10 Chapter summary

Rowing Literature has been reviewed which indicates the current understanding of the rowing stroke through the monitoring of different sensor parameters, both upon the boat, ergometer or rower. Relevant literature has been included to show how technology has been exploited in the advancement of rowing monitoring, and in the wider fields of sports and health monitoring. Finally the advance of wireless technologies, specifically wireless sensor networks, has been considered through recent publications, both rowing- and health-related, to determine how wireless systems can benefit the monitoring of human activity.

2 Wireless Networks: Possibilities and Challenges

To allow simultaneous data collection across the boat and multiple rowers without encumbering movement of either athlete or boat mechanisms requires a minimisation of wired connection. The choice of wireless system is thus a fundamental consideration. The method of wireless transmission is in part set by the constraints of a body-worn system: size, placement, power requirements, data volume, and extent of the network both in terms of range and number of wireless elements (nodes).

2.1 Chapter Organisation

The definition and scope of the terms Wireless sensor networks (WSN), Body Sensor Networks (BSN) and Body area networks (BAN) are considered. Candidate wireless standards will be summarised and reviewed to determine their suitability for the application of Wireless Body Sensor Network for sports applications. The challenges of WSN and BSN will be considered in more detail.

2.2 Wireless Sensor Networks and Body Area Networks

In recent years there has been a proliferation of names to describe networks of sensors, both wired and wireless, leading to a confusion of different acronyms describing the same thing, and similar acronyms for systems which are actually quite different. Three such acronyms have crossed the threshold into accepted use: WSN, BSN and BAN.

Wireless Sensor Networks (WSN) describes systems of sensor nodes which connect and communicate wirelessly to form a distributed sensor network, allowing ubiquitous, pervasive sensing and data collection. Applications of WSNs are varied, with uses seen in personal networking, healthcare, sporting connectivity, and industrial and environmental monitoring; in fact, anywhere where wired systems would prove problematic or impractical. The scale of WSNs can be from a few nodes to hundreds, and extending from just a metre to hundreds of metres.

Body Sensor Networks (BSN) again describes systems of sensor nodes, but specifically for applications within or upon the body. As such the inter-node distance is small, and depending upon the node sites and function, wireless connectivity might not be essential. As such BSN describes a wired or wireless sensor network.

The different requirements and challenges that dictate the nature of WSN and BSN is detailed concisely in the book Body Sensor Networks (Yang 2006),

contributed to, and edited by Guang-Zhong Yang, a pioneer in BSN technology (Table 2-1).

Challenges	WSN	BSN
Scale	As large as the environment being monitored (metres/kilometres)	As large as human body parts (millimetres/centimetres)
Node Number	Greater number of nodes required for accurate, wide area coverage	Fewer, more accurate sensors nodes required (limited by space)
Node Function	Multiple sensors, each perform dedicated tasks	Single sensors, each perform multiple tasks
Node Accuracy	Large node number compensates for accuracy and allows result validation	Limited node number with each required to be robust and accurate
Node Size	Small size preferable but not a major limitation in many cases	Pervasive monitoring and need for miniaturisation
Dynamics	Exposed to extremes in weather, noise, and asynchrony	Exposed to more predictable environment but motion artefacts is a challenge
Event Detection	Early adverse event detection desirable; failure often reversible	Early adverse events detection vital; human tissue failure irreversible
Variability	Much more likely to have a fixed or static structure	Biological variation and complexity means a more variable structure
Data Protection	Lower level wireless data transfer security required	High level wireless data transfer security required to protect patient information
Power Supply	Accessible and likely to be changed more easily and frequently	Inaccessible and difficult to replace in implantable setting
Power Demand	Likely to be greater as power is more easily supplied	Likely to be lower as energy is more difficult to supply
Energy Scavenging	Solar, and wind power are most likely candidates	Motion (vibration) and thermal (body heat) most likely candidates
Access	Sensors more easily replaceable or even disposable	Implantable sensor replacement difficult and requires biodegradability
Biocompatibility	Not a consideration in most applications	A must for implantable and some external sensors. Likely to increase cost
Context Awareness	Not so important with static sensors where environments are well defined	Very important because body physiology is very sensitive to context change
Wireless Technology	Bluetooth, Zigbee, GPRS, and wireless LAN, and RF already offer solutions	Low power wireless required, with signal detection more challenging
Data Transfer	Loss of data during wireless transfer is likely to be compensated by number of sensors used	Loss of data more significant, and may require additional measures to ensure QoS and real-time data interrogation capabilities

Table 2-1: Different challenges faced by WSN and BSN

(Aziz et al. 2006)

Finally, Body Area Networks (BAN) represents wireless communications in, on or near the body. As such it is not specifically used to describe the use of sensors. The term was adopted in 2007 by a task group of The Institute of Electrical and Electronics Engineers (IEEE) (IEEE TG6 2007) to produce a short-range BAN standard specifically tailored for body-based applications. This will be discussed later in section 2.3.6.

It can be seen from the brief descriptions above that the nature and applications of these three networks overlap. It is useful to consider them from the point of view of a Venn diagram (Figure 2-1). On their own, each network differs from one of the others by one aspect of the application. However, if any two of these types of networks overlap, the same system results. The shaded overlapping regions essentially describe the same system: a wireless network of sensors that are mounted upon the body.

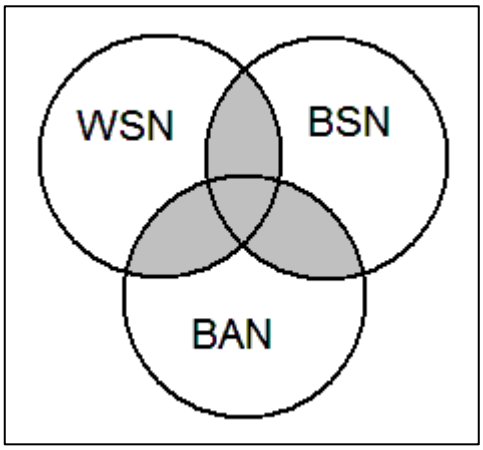

Figure 2-1: Venn diagram describing the overlap of WSN, BSN and BAN

The first challenge to designing a wireless body sensor network for sporting applications is therefore to find a suitable wireless platform upon which the

system can be based. In considering the candidate wireless standards, a number of elements need to be considered. In judging the suitability of a wireless standard for the application, the amount of data that needs to be transmitted, and over what time period is a fundamental consideration; data rate and duty cycle of a wireless standard are thus important factors. Reliability and interference mitigation need also to be considered as BAN does not have the luxury often afforded to larger WSNs of node redundancy; each node has one or more particular parameters to measure, and node failure or data loss would result in that information not being available to the system. Node size, number and power consumption are also essential factors for a body-centric network. Power consumption itself impacts upon node size and battery life, limiting the available power choices for a node. Finally, for a wireless data collection system, time synchronisation between nodes is essential such that data can be collected from across the network at simultaneous points in time. Typical requirements for a wireless BSN (Table 2-2) are nicely summarised by Patel (Patel and Wang 2010) from technical requirements for BAN technology discussed by the IEEE BAN Task Group 6, and give an indication of the impact of application upon requirements.

Application	Target data rate	No. of nodes	Topology	Setup time	P2P latency	BER	Duty cycle	Desired battery lifetime
Deep brain stimulation	1 Mb/s	2	P2P	< 3 s	< 250 ms	$< 10^{-3}$	< 50%	>3 years
Hearing aid	200 kb/s	3	Star	< 3 s	< 250 ms	$< 10^{-10}$	< 10%	>40 hours
Capsule endoscope	1 Mb/s	2	P2P	< 3 s	< 250 ms	$< 10^{-10}$	< 50%	>24 hours
Drug dosage	< 1 kb/s	2	P2P	< 3 s	< 250 ms	$< 10^{-10}$	< 1%	>24 hours
ECG	72 kb/s (500 Hz sample, 12-bit ADC, 12 channels)	< 6	Star	< 3 s	< 250 ms	$< 10^{-10}$	< 10%	>1 week
EEG	86.4 kb/s (300 Hz sample, 12-bit ADC, 24 channels)	< 6	Star	< 3 s	< 250 ms	$< 10^{-10}$	< 10%	>1 week
EMG	1.536 Mb/s (8 kHz sample, 16-bit ADC, 12 channels)	< 6	Star	< 3 s	< 250 ms	$< 10^{-10}$	< 10%	>1 week
O2/CO2/BP/ temp/respiration/ glucose monitoring, accelerometer	< 10 kb/s	< 12	Star	< 3 s	< 250 ms	$< 10^{-10}$	< 1%	>1 week
Audio	1 Mb/s	3	Star	< 3 s	< 100 ms	$< 10^{-5}$	< 50%	>24 hours
Video/med imaging	< 10 Mb/s	2	P2P	< 3 s	< 100 ms	$< 10^{-3}$	< 50%	>12 hours

Table 2-2: Technical requirements for BAN technology for different applications *(Patel and Wang 2010)*

Potential candidate wireless standards are therefore summarised in section 2.3 and considered in turn for their suitability. When the most suitable wireless standard has been identified, the challenges confronting the wireless BSN will be considered in more detail in section 2.5.

2.3 Licence-Free radio and IEEE 802

Radio waves have been employed for information transmission for over a century (since Marconi in 1896) and yet it has only been in the last couple of decades that wireless technology has begun to permeate everyday life to the point where it can take on the tasks of wired equipment. Mobile phones, wireless Internet and wireless data transfer between electronic devices have now become commonplace.

The radio spectrum is a crowded medium where there are strict regulations (governed by the Federal Communications Commission (FCC) in North America and the European Telecommunications Standards Institute (ETSI) in Europe) over how, and at what frequency and power level you can transmit. There are segments of bandwidth within the radio spectrum that are allocated to licence-free use. These are called Industrial, Scientific and Medical (ISM) frequency bands, and the band's name indicates the original intended use of these reserved frequencies. More recently, however, they have been used for applications in consumer devices such as remote-controlled vehicle operation, garage door actuation or keyless car-fobs, cordless telephone, and cable replacement. Provided the user conforms to the rules for these frequency bands (e.g. the maximum power that can be transmitted in the band and the power levels that are allowed to leak into adjacent bands) they are free to use.

There are several ISM bands in use in Europe and the USA, and across the world, predominantly used for low data rate communications in consumer

devices. However, until recently, none were common across all countries, making global sale or roaming with devices impossible. The emergence of the *global* ISM band at centre frequency 2.45GHz has brought about several radio standards that might be exploited for health and sports monitoring. However, their subtle differences dictate the application for which they are used (Fuhr March 2002).

A number of these new wireless standards occupying the 2.45GHz ISM frequency band might at first glance provide the wireless platform for sensor networks: Wireless LAN (Wi-Fi), Bluetooth, Zigbee, Ultra-Wideband (UWB) and BAN. These radio standards are all members of the IEEE 802 family of standards which deals with Local Area Networks (LANs) and Metropolitan Area Networks (the city 'hotspot' equivalent of LANs), and Personal Area Networks (PANs). These different standards cannot interoperate, and yet must co-exist in the same frequency band. The interference immunity they need must be obtained either by suppressing the noise or by avoiding it.

Within this family exist a number of working groups; 802.11 is the working group given the responsibility of Wireless LAN, also called Wi-Fi, the working group 802.15 is responsible for Wireless PANs. Working groups are also subdivided into task groups, and task groups 802.15.1, 802.15.3a, 802.15.4, and 802.15.6 are the task groups set up by the IEEE to develop Bluetooth, Ultra-Wideband, Zigbee and BAN respectively. Other task groups are given other roles, such as 802.15.2 which deals not with a particular radio standard, but with coexistence of these standards. Whilst Wireless PAN technologies are the focus of this technology comparison, other radio standards which share frequency bands (or other similarities) such as Wi-Fi will be covered, as will other proprietary wireless technologies which might be of interest to wireless sensor and wireless data

acquisition applications. The description of these wireless standards necessitates the mention of their modulation schemes, as these impact upon the range, power consumption, and complexity (and therefore size) of the radio hardware. For clarity, explanations of these modulation schemes have been kept to a minimum, but further details are given in appendix A.1.

2.3.1 Wireless LAN – 802.11

The most familiar of the standards mentioned above is Wireless Local Area Networks (WLAN) which has reached global acceptance and use in corporate, private and public environments over a relatively short period of time. First defined in 1990 with the initial standard finalised in mid 1997 (Geier August 2002) the 802.11 working group described a radio standard which operated at 2.4GHz and offered a data rate of 1 and 2Mbps. The WLAN standard (IEEE 1997) allowed for three different physical layer methods to be adopted: infrared, Frequency-Hopping spread spectrum (FHSS) and Direct Sequence spread spectrum (DSSS) (Carney 2002). This was just the first step in an ongoing evolution of the standard which has seen a number of milestones up to the present day.

The evolution of the standard initially took two parallel paths, dictated by two task groups 802.11a and 802.11b. Both standards were approved at the same time, but it was the 802.11b standard that reached the market first in 1999. Its single-carrier 2.4GHz DSSS radios enhanced the original 802.11 standard by using Complementary code Keying (CCK) modulation techniques to increase the data rate to 11Mbps. The DSSS modulation scheme of the 802.11b standard is simpler than the Orthogonal Frequency Division Multiplexing (OFDM) of 802.11a, and its 2.4GHz frequency is global, unlike the 5GHz band of 802.11a (Kapp 2002), further aiding its adoption worldwide.

Further evolutions have followed, the principal ones being 802.11g (which gained working group approval in 2003) and 802.11n (approved in 2009). 802.11g

combines the best of both 802.11a and 802.11b, increases the data rates to 54Mbps, operates in the 2.4GHz ISM band, and has been designed to be backwardly compatible with the 802.11b standard such that there are no operating conflicts in compliant devices. 802.11n allows data rates of up to 600Mbps using spatial multiplexing (using multiple antennas) and spatial diversity to achieve the increased data rate and range (IEEE 2012a).

The driving factor in the adoption of 802.11g is the worldwide availability of the 2.4GHz ISM frequency band. In order to be compatible with the 802.11b standard already occupying this band, the 802.11g standard also uses DSSS modulation, to achieve its lower data rates (5.5 and 11Mbps); for higher data rates up to 54Mbps it uses OFDM. The coded signal can be distinguished at the receiver even in the presence of substantial interference (IEEE 2012a).

The biggest benefit of WLAN over the other standards is the data rates it can achieve. At 54Mbps 801.22g has data rates fifty times greater than the best of the other standards considered here. However, for a sensor network, data throughput is not the paramount consideration. WLAN is not designed to be used in applications where power consumption must be kept at a minimum (typical consumption might be as much as 1Watt) (MuRata 2012a). Its primary application is in wireless connection of mobile PCs to a wired Ethernet infrastructure (via fixed base stations or access points).

However, whilst not suitable for wireless BSN, it has been used for sensor networks within the industrial environment. For example, Paola Ferrari et al (Ferrari et al. 2006) describes such a network, set up in a master-slave configuration, which allows several sensors to be connected via laptop PC’s to

take transducer measurements in an industrial plant where 802.11 wireless networks might already be implemented to extend the wired Ethernet-based environment. He suggests two different implementations, the first a wireless-transducer network with an access point to the wired network, and a second where the wireless transducer nodes can communicate between themselves in an ad-hoc network. He does acknowledge the unsuitability of the prototype for battery operation, but states that in an industrial environment where measurements are required on machines with rotating parts it could be powered by the means of brushes where data cables would be problematic.

Ultimately, WLAN consumes too much power to be used within a BSN and would thus be unsuitable in the formation of a system to take measurements from an athlete. However, it is important not to reject it out right, as it remains a consideration for a mixed radio standard system where the network is implemented by a more suitable standard might be connected via WLAN to the internet.

2.3.2 Bluetooth– 802.15.2

Of the 802.15 wireless PAN standards, Bluetooth is the one which has had the deepest penetration into everyday life. Its impact has much to do with the low cost and small size of the radio modules, and the work that was done to make ISM 2.4GHz band available globally.

The idea for Bluetooth was developed in the late 1990s as a number of telecom companies and PC companies realised the need for connections between electronic devices – either between mobile devices and PCs or between these electronic equipment and peripheral devices. As such, in February 1998 five of these companies formed a special interest group (SIG). These founding companies – Ericsson, Nokia, Toshiba, Intel and IBM collaborated to draw up a radio standard to fulfil this need, and named it Bluetooth after the tenth century Viking King, Harald Blatand (Bluetooth) who united Norway and Denmark (Haartsen and Mattisson 2000). This initiative was soon supported by many other companies, and the Bluetooth 1.0 standard (IEEE 2002) was ratified as 802.15.1 in 1999.

The major difference in Bluetooth compared with the other radio standards sharing the 2.4GHz band is that rather than connect users via a wireless connection to a fixed wired backbone (like WLAN or mobile (cellular) telephones), Bluetooth-enabled devices form personal connections. In other systems, the mobile radio and the base-station connecting it to the wired backbone have fixed and well-determined roles, but with Bluetooth, there is essentially no difference between the radio modules. A Bluetooth module might establish a connection or

network between one or more other radio modules, it becoming the master radio to the others' slaves, but if that connection or network is terminated, another module might become a master and the original master might this time be a slave. These ad-hoc connections lend the name of ad-hoc radio to Bluetooth.

An ad-hoc Bluetooth radio network consisting of two or more radio modules is called a Piconet. A piconet consists of one master node, and up to 7 slave nodes. More than one piconet can share the same physical space, and it is possible for a Bluetooth radio to be a slave in more than one piconet, or a master in one and a slave in another. Such scenarios are called scatternets (IEEE 2002) (Figure 2-2). Clearly involvement in more than one piconet requires the Bluetooth node to perform time-division multiplexing (TDMA).

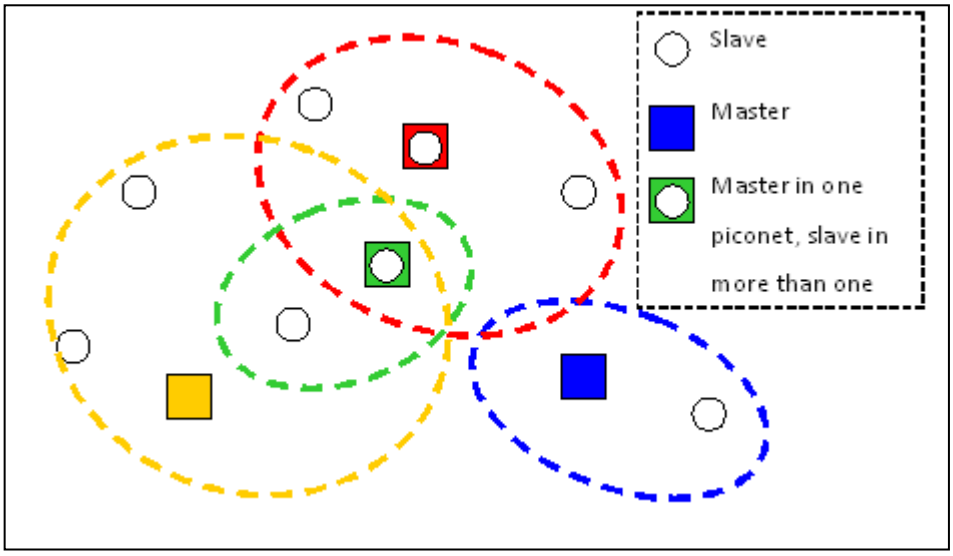

Figure 2-2: An example of Bluetooth Scatternets

Indicates piconets sharing the same physical space, and potential dual role of nodes in more than one piconet

As with the development of all new radio standards located in the 2.4GHz ISM band, the paramount consideration, beyond ensuring that it met its aspirations for

“ad-hoc networking” and “personal cable replacement” applications, was that Bluetooth would be robust enough to share the increasingly crowded license-free spectrum.

As such, the modulation technique employed was carefully considered before settling upon Frequency-Hopping Spread-Spectrum (FHSS) (IEEE 2002). FHSS exploits interference avoidance rather than interference suppression, and does this by hopping around the available spectrum. Averaged over time, the signal is spread across a broad range of frequencies, yet instantaneously the signal possesses a narrow bandwidth. The signal might encounter interference at one hop frequency, but since the radio only dwells at this frequency for a short period of time, the amount of corrupted data is small, and can be retrieved through error correction techniques.

The available spectrum in the 2.4GHz ISM band is divided up into 79 hop channels set at 1MHz spacing, and the nominal dwell time at a particular frequency is 625µs (IEEE 2002). The hopping sequence is pseudo random, and is dictated by the master node in the network. This master node also dictates the phase of the frequency hopping and as such, all slave nodes in the network need to know not only the hopping sequence, but the offset of its own clock with respect to the master’s. By adding an offset to their own clocks, the slaves can remain synchronous with the master node. If a node is a slave in two networks, it will need to switch between two different hopping sequences and apply different time offsets to its clock depending on whether it is interacting with one network or the other.

Communication between nodes occurs according to a time division duplexing method (TDD) – a unit alternatively transmits and receives. This not only simplifies the implementation of communication between nodes, it also further minimises the possible interference, and simplifies radio design.

Maximum data rate for Bluetooth 1.0 communication is 1Mbps (IEEE 2002). However, as the number of nodes in a piconet increases, so the data throughput drops significantly. This is because within the same piconet, radios are sharing the same 1MHz hop channel. This is the primary reason for restricting the number of nodes in a piconet to eight (1 master, 7 slaves).

Bluetooth radios have a range of between 10 and 100m depending upon the power class of the radio. Power consumption of a single radio can be reduced through its mode of operation. The Bluetooth 1.0 standard describes a number of reduced power modes (IEEE 2002):

Standby mode where the radio is not connected in a network, but listens to the hop channels for activity, hopping with a low duty cycle (<1%) over a subset of 32 of the total of 79 frequencies, thus reducing the power consumption of a node, but also greatly increasing the time in which a connection can be made.

Hold mode – if transmissions are to be halted for a period of time, a radio can enter a hold mode. During this fixed period of time, no communication takes place.

Park mode – here, like in standby mode, the Bluetooth radio listens on a low duty cycle. However, as it is still slave to a master node, it retains the information concerning the hop sequence and so knows upon which frequency to listen.

Sniff mode – in sniff mode the slave radio does not listen to its master on every receive slot, but listens to a reduced number of slots agreed upon with the master node.

An advantage of Bluetooth radios is their small form factor, dictated by a number of factors: TDD means that separate transmit/receive oscillators are not required, and neither is filtering to avoid crosstalk between transmitter and receiver. The modulation scheme chosen for Bluetooth also reduces the overall transceiver size – Gaussian FSK modulation produces a constant envelope further simplifying radio design.

The Bluetooth standard has undergone a number of revisions over the last decade. Bluetooth 1.2 introduced, amongst other improvements, adaptive frequency hopping, where crowded frequencies in the hopping sequence can be avoided to improve immunity to interference. Bluetooth 2.0 introduced in 2004 increased maximum raw data-rates (greater than the actual achievable information rate) to 3Mbps referred to as Bluetooth Enhanced Data rate (EDR), and achieved actual information rates of 2.1Mbps. (Gold Jan/Feb 2005).

The primary advantages that a Bluetooth radio system might bring to a sports or health monitoring application therefore are low power, small size and low cost, and its ad-hoc topology. Clearly the ability to add and remove nodes from the network ad-hoc would be greatly beneficial for a PAN that was configured for use

in a sports or health monitoring application where it might be desirable to increase the number of sensors located upon the athlete or patient or to alter the configuration of the nodes. This and the small size of the chipsets required to set-up a fully functioning Bluetooth radio make Bluetooth worthy of close consideration. However, the limit of 8 nodes in one piconet, a power consumption still a little high to facilitate the use of small, light batteries (MuRata 2012b), and a latency – the time from sleep-to-active – of 3 seconds could prove challenging for its implementation in a wireless BSN.

2.3.3 Bluetooth Low Energy

A recent evolution of the Bluetooth standard is Bluetooth Low Energy (Bluetooth LE). This is part of the Bluetooth 4.0 evolution of the 802.15.1 standard, adopted in June 2010. This recent development of the standard comes too late for consideration in this piece of research, but nevertheless is discussed now to allow consideration in further work.

Nokia began to investigate adapting the Bluetooth standard for low power applications in 2001, releasing the then-named Wibree in 2006 (BBC News 2006). In 2007 it was agreed to incorporate Wibree into Bluetooth Low Energy (Bluetooth LE).

The Bluetooth 4.0 Standard (Bluetooth Special Interest Group 2010) describes two forms of Bluetooth: classic Bluetooth (basic rate and enhanced rate) and Bluetooth LE. Whilst the classic system can achieve up to 3Mbps on the enhanced data rate, Bluetooth LE has an over the air data rate of 1Mbps but an actual application throughput of only 0.26Mbps due to short packets and the periodic nature of transmissions. As such, like Zigbee (section 2.3.4), it targets applications requiring low power consumption at the expense of data rate (Bluetooth Special Interest Group 2010).

Bluetooth LE operates in the same ISM frequency band as classic Bluetooth, again employing FHSS to mitigate interference, and uses the same GFSK modulation scheme. However, it has a higher modulation index than classic

Bluetooth (0.5 compared to 0.35) leading to better range (Heydon and Hunn 2011).

Another difference is in the channels allocation. Bluetooth LE uses 40 2MHz channels contrary to the classic Bluetooth's 79 1MHz channels. Of these 40 channels, 3 are advertising channels used to initiate connections between nodes (forming a piconet), and the remaining 37 are data channels. A time division scheme is then used to divide a physical channel into time units. The master of a piconet dictates the specific frequency hopping pattern in a pseudo-random fashion across the 37 data channels (Bluetooth Special Interest Group 2010). Once again adaptive frequency hopping is employed to avoid specific interference from other (non-Bluetooth) radio systems sharing the ISM band. Bluetooth LE currently only supports a star network topology, with links only between a master and slave. Slaves cannot have physical links to more than one master. However, Bluetooth LE is not limited to 7 slave nodes in a piconet like classic Bluetooth. The number of nodes is limited only by available memory.

Bluetooth LE achieves its low power consumption by ensuring fast connection (through simplified connection schemes between nodes) and maximising standby time. To make a connection, Bluetooth LE only has to scan its 3 advertising channels, whilst classic Bluetooth uses 32 channels for connection detection. Scanning for a connection thus takes Bluetooth LE a fraction of the time it takes classic Bluetooth – up to 1.2ms compared to 22.5ms. This time saving equates to significant power saving. Bluetooth LE can complete a scan--link--send data--authenticate—terminate in around 3ms. It might take classic Bluetooth 100 times longer (Nordic Semiconductor 2011).

To summarise, Bluetooth LE is tailored towards different applications than classic Bluetooth. Optimised for short packet transmissions at intervals, with long periods in standby, if used for applications more suited to classic Bluetooth it loses the power benefits for which it is intended. In many respects there are more comparisons to Zigbee, and certainly it will be competing for a similar market. Despite the differences to classic Bluetooth however, it gains from the market dominance of classic Bluetooth. When it becomes a mature technology, it should be a good contender for wireless sensor applications, depending upon the frequency with which data packets need to be transmitted.

2.3.4 Zigbee – based upon 802.15.4

The origin of the Zigbee standard can be traced back to 1999 from the failed Firefly working group. The name Zigbee is derived from the zig-zag path of bees that form mesh networks between flowers (Frank March 2004). In 2003 they built Zigbee around the IEEE 802.15.4 PAN standard for low-rate wireless PANs, and ratified the standard late in 2004. At that time the Zigbee Alliance had just 70 members, but just a year later this had increased to 200 (Geer 2005). Specifically designed for low data-rate sensor networks where battery life is a priority, Zigbee has to be a strong contender for wireless sports and health monitoring.

The Zigbee standard (Zigbee Alliance 2006) can actually be used in three different ISM frequency bands – 868MHz, 915MHz, and the global 2.4GHz. The maximum data rate that Zigbee can realise is achieved in the highest frequency band, and is still only 250Kbps. This is only the raw data rate, so when header data is taken into account, the actual information rate is far lower. Data is sent in small packets up to 128bytes in size, and the maximum payload (after removing headers) is only 104bytes (Poole 2004). Clearly then, Zigbee is not a high data rate standard, but it is not designed to be. It cannot achieve the higher data rates of WLAN or Bluetooth, and cannot therefore be used for applications such as transmitting real-time video, but in setting its sights a little lower, it gains its own niche in a crowded market – battery-powered sensor networks.

Zigbee can be considered a superset of the IEEE 802.15.4 standard. The IEEE standard contributes the physical (PHY) and medium access control (MAC) layers of the radio, and Zigbee adds the network layer and the application layer.

The PHY layer defines the number of channels – 16 in the 2.4GHz band – and also the activation and deactivation of the radio transceiver, the channel selection, the clear channel assessment (CCA) and the transmitting and receiving of packets of data between radio nodes (Gang et al. 2005). The modulation technique employed by Zigbee in the 2.4GHz band is Direct Sequence Spread spectrum (DSSS), where the data is spread over a wide bandwidth (5MHz for Zigbee). Unlike the FHSS utilised by Bluetooth, which achieves interference immunity by hopping around the spectrum, DSSS minimises interference by spreading the signal over a broader spectrum of frequencies than its data rate would suggest. This is achieved by taking each 4-bit nibble of raw data, and substituting each with one of 16 different symbols. Employing a look-up table defined within 802.15.4, each symbol is represented by a 32-bit sequence called a chipping code, each bit of this code is called a chip (Descleves March 2006). A chip interval is thus much shorter than a bit interval, spreading the energy of the signal in the frequency domain. The total power of the signal is therefore spread over a wide range of frequencies, making the instantaneous power spectral density lower. This also results in a noise-like appearance to the signal. The chipping rate of a Zigbee signal in the 2.4GHz band is $2x10^6$chips/s (symbol rate of 62Ksymbols/s), where 32 chips represent 4-bits of original data pre-spreading, yielding the 250kbps data rate (Zigbee Alliance 2006). The spread data is then modulated and transmitted using offset quadrature phase shift keying (O-QPSK), a constant envelope modulation scheme, which means that Zigbee, like Bluetooth, achieves simplified hardware requirements, reducing the cost and size of the radio module. (Khanh Tuan 2004).

The 802.15.4 standard does not specify an output power, but most Zigbee devices currently on the market have an output power of 0dBm, giving an

operating range of about 10m in indoor environments and up to 200m for outdoors.

The PHY layer also defines two types of node – the full function device (FFD) which can be a network coordinator or just a fully functioning regular node which can communicate with any other node, or a reduced function device (RFD) which can communicate only with an FFD.

The MAC layer defined by the IEEE 802.15.4 standard controls access to the radio channel using Carrier Sense Multiple Access with Collision Avoidance (CSMA/CA). This is where the device monitors the channel, and only transmits if the channel is idle. This technique avoids collisions between transmissions from different radios by using package acknowledgement (ACK) to confirm that data was successfully received (the transmitter has no other way of knowing if a collision occurred or not). If a collision occurs, the transmitter performs a back-off – waiting a random amount of time - and if the channel is idle, trying again.

The network layer defined by Zigbee takes responsibility for nodes to join or leave the network, for security, routing of data between nodes, and storing information about node neighbours. Theoretically a network can have 2^{16} = 65535 nodes. The network can be arranged in three different configurations – star, tree and mesh (Figure 2-3).

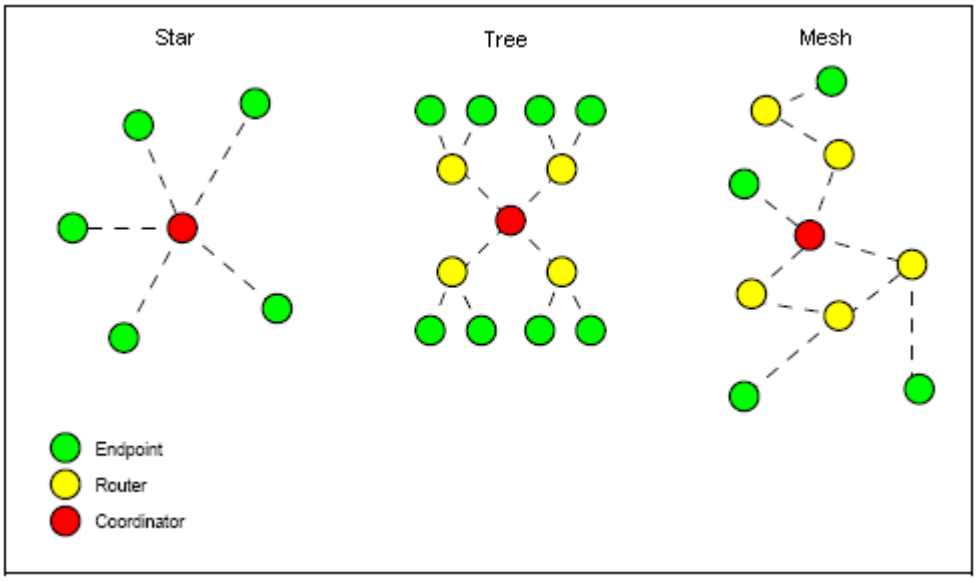

Figure 2-3: Different network configurations for a Zigbee network

Star networks are single-hop networks where one coordinating node at the centre of the star is surrounded by end devices. These end devices can be RFD or FFD nodes, but they are only allowed to communicate with each other via the coordinator. Performance of star topologies is high since it has a maximum of two hops from source to destination (always via the coordinator). In a cluster tree topology, RFD end nodes in a star network are replaced by FFDs which can themselves act as parent nodes to other FFD or RFD devices, the primary goal being to extend the geographical reach of a network. Whilst star networks are the simplest to implement and maintain, mesh networks offer increased reliability in the presence of interference or node malfunction. Such a topology is called a self-healing network because messages can be routed a different way across the network to avoid a malfunctioning node or interference in a particular section of the network. This is achieved in the Zigbee network layer using router-capable FFD nodes which allow data to take a multi-hop path across the network from source node to destination. This also means that whilst the transmission range of

a node might be restricted to 10m in an indoor environment, by employing multi-hopping, ranges much in excess of this can be achieved. Associations (links) between nodes are limited by parameters within the routing or coordinating node which dictate the number of children it can have and the maximum depth of a network. For example, a star network is created if the maximum depth of the network set in the coordinator is equal to 1. Likewise, if the number of children of FFD nodes within a network is limited to one, then a linear structure is created.

The application layer (APL) defines the custom application of the individual network and the function of the devices within the network. In the Zigbee specification this involves the use of a device profile. When a device joins the network, it informs its parent node (the coordinator in a star network) of its profile. This will dictate its function, and the messages and parameters it can share with other nodes.

One of the primary benefits of Zigbee over other standards like Bluetooth is in its low latency. Latency is the time that the device can go from an idle sleeping state with the transceiver off, to a fully active state where it can exchange data with another node. Whilst Bluetooth and WLAN have latencies of the order of 3 and 10 seconds respectively (Arcom Control Systems 2005), Zigbee's latency can be less than 15ms (Baker 2005). This makes it ideal for applications where time is critical, and also impacts the power consumption of the nodes. If a node can wake from sleep in a very short time, then that node can be placed into a low-power sleep mode more frequently between active periods and thus save power.

Low power consumption is thus optimised through the use of low duty cycle transmissions. RFD nodes need only switch on to listen to messages from other

nodes or to transmit data according to the application requirements. The Zigbee specification was designed specifically for the end device nodes to have a duty cycle of ideally less than 1% (Zigbee Alliance 2006), although this can be altered to meet the needs of the application. In this way the RFD nodes can be battery powered and have a battery life measured in months or even years. The coordinator needs to remain active to receive messages from other nodes upon the network, and requires more memory and processing power to both maintain a neighbour table of other devices in the network and to buffer messages for RFD nodes which power down for long periods of time and wake only periodically to receive any messages destined for them. Thus the coordinator is usually a mains-powered device.

Much of the saving in power is gained therefore by minimising the time in which the node is transmitting. Taking into account the three main modes of a device: idle, receive and transmit, and the percentages of time a node is in each mode, it is possible therefore to calculate approximately the power consumption of a node dependent upon its function as RFD, FFD or coordinator (Streeton and Stanfield 2005).

Another power-saving characteristic of Zigbee is its small protocol stack. Because Zigbee networks are designed to perform relatively simple control or measurement tasks, the protocol stack is less than 30Kbytes. The less memory required by the microprocessor controlling the network, the less power is required.

Zigbee is therefore designed to be simple, and through judicious design can also be implemented on the simplest of hardware. The radio module has been

simplified through choice of modulation scheme such that it can be implemented in a single chip solution with minimal peripheral passive components. The additional components required include a microprocessor or microcontroller with a modest amount of memory to contain the protocol stack and to control the network functionality, and power supply components. The only other circuitry required is specific to the application. Table A-2 in Appendix A.2 compares the power consumption of WLAN, Bluetooth and Zigbee ICs from the same manufacturer (Texas Instruments) thus demonstrating the low power advantage of Zigbee.

2.3.5 UWB – 802.15.3a

Historically, the main goal of telecommunications was to transmit radio as far as possible, and narrowband, sinusoidal signals travel a far greater distance than broadband ones. However, with interest today in wireless connectivity in the workplace or home, or even between devices upon the person, ultra-wideband signals which can carry a great deal of data over a short distance are increasingly more attractive. The term UWB is used to describe many different wireless technologies that display a wide bandwidth approach to data transmission.

One of the main uses of UWB until recently has been military Radar (e.g. for target identification) and commercial ground penetrating radar (e.g. for archaeological exploration), neither application requiring the radios to be fitted into a particularly small form-factor, or to have low power consumption or low cost. By the 1990's however, a number of technology advancements in processing and fast-switching technologies, and the inherently simpler transceiver architecture required for carrier-less UWB transmission has increased the possibility of the single chip UWB front-end solution, bringing with it the potential for small, cheap, low-power systems more suitable for consumer electronic devices.

The reason why UWB has garnered increased interest is because of its reputation for high-data rate capacity, low power spectral density, and high immunity to interference. The Shannon Channel Capacity Limit Equation gives the following relationship between channel capacity, bandwidth and signal-to-noise ratio.

$$Channel\ Capacity\ \left(bits/s\right) = BW.\log_2\left(1+SNR\right)$$

BW = Channel bandwidth (Hz), SNR = Signal-to-Noise ratio

Thus it can be noted that whilst there is a linear relationship between the channel capacity and bandwidth, an exponential increase in signal power is required to produce comparative changes in the channel capacity to those achieved through increasing the bandwidth. A Gigahertz bandwidth UWB signal might therefore achieve data-rates of gigabits/second. The logarithmic relationship between the Channel Capacity and the signal-to-noise ratio also means that the SNR can deteriorate greatly before any significant reduction in the channel capacity leading to robustness in harsh areas of the radio spectrum.

Answering the increased interest in UWB, FCC proposed a definition in 2002 for UWB that has commonly been accepted – that a UWB device has a fractional bandwidth (that is, its bandwidth to centre frequency ratio) greater than 0.25, or that the absolute bandwidth is greater than 1.5GHz (these two guidelines have since been reduced to 0.2 and 0.5GHz respectively) (Yarovoy and Ligthart 2004). To compare, 802.11b (Wi-Fi) has a bandwidth of 22MHz at a centre frequency of 2.4GHz – a fractional bandwidth of 0.0083 – clearly narrowband transmission.

The essence of a UWB signal is a very short duration pulse, which when analysed in the frequency domain is spread over a very wide bandwidth. A traditional narrowband signal is always present, with a corresponding 100% duty cycle (duty cycle is the ratio between the time a signal is present compared to the total transmission time), but an UWB pulse has a very low duty cycle of less than 0.5%. This means that the average transmitted power is very low. Because the

signal is spread over such a wide frequency range, the overall power spectral density is also very low, enabling it to share spectrum with other standards.

Its immunity to fading can be attributed to its short pulses which prevent the destructive interference caused by multipath reflections received out of phase which results in a reduction of the overall amplitude of the signal. As the pulse duration is generally shorter than a nanosecond, the chance of a reflected pulse colliding with the line-of-sight pulse is low. Pulse UWB methods, where streams of pulses are used enabling high data-rate communication, which form the basis of the 802.15.3a draft standard, have demonstrated a throughput of 1.6 Gbps (Mlinarsky 2008).

It also has the possibility of high-resolution position location and tracking to within a few centimetres because its short impulse, wideband signal allows for accurate delay calculation. This form of location awareness might be highly useful in ad-hoc networks where multi-hop routing could extend the transmission range (Hirt 2003).

UWB transmissions are also believed to have high security – the interception and prediction of such short pulses is difficult, and the low transmission power makes detection difficult. The broad bandwidth also makes it not just resistant to many forms of unintentional interference, but also resilient against hostile jamming of particular frequencies.

Despite these many benefits, there are still many challenges to overcome. The very low power spectral density of UWB signals (one of its major selling-points) might also precipitate problems of increased susceptibility to in-channel

interference or noise within the radio receiver. Pulse-shape distortion can also be a problem – where narrowband signals are largely sinusoidal, the low-power UWB pulse can be distorted during transmission between transmitter and receiver.

Another problem lies in maintaining synchronisation between transmitter and receiver. This is an issue for all radio standards, but the synchronising and sampling of such short pulses used in UWB requires extremely high specification analogue-to-digital converters. For the sampling of UWB pulses analogue-to-digital converters with sampling frequencies of the order of gigahertz would be required, in addition to tight requirements in sampling frequency jitter and drift (Nekoogar 2005).

UWB has also found a new home in a recently legalised frequency spectrum between 3.1 and 10.6GHz, and each UWB radio can transmit signals with bandwidths greater than 500MHz. What this means is that the spectral density of the power can be spread such that UWB signals do not emit enough energy to interfere with nearby narrowband devices whose signal to noise ratio is necessarily far greater; FCC regulations limit UWB signals to power levels of less than -41dBm/MHz (Wilson 2002). The low power of these devices does mean however that they must be in very close proximity to communicate. They are therefore trading high throughput and high immunity to interference for range.

The IEEE working group for Wireless Personal Area Networks submitted a call in late 2001 (Hirt 2003) for "*Applications for Applications and Usage scenarios for a radio system that would, in addition to other requirements, coexist with all IEEE 802 wireless standards (like Bluetooth, Zigbee and Wi-Fi), have a data rate in*

excess of 100MB/s, and robust multipath performance". This call, and subsequent developments, seemed to point towards a commitment to UWB radio technology in some form in the near future. However, UWB is still not yet market-ready – in 2004 the two main groups comprising the IEE 802.15.3a working group striving towards a UWB solution were at a stalemate over the precise technology that UWB would encompass. After protracted discussions, in January 2006, the working group admitted defeat, and voted unanimously to disband. Both groups pledged to continue to develop their own approaches and let the marketplace decide which one will become the de facto standard. (Deffree January 2006), however to date there has been little penetration of UWB into consumer products, in part due to cost of initial implementation and poorer performance than initially forecast (Takahashi 2009).

As a radio technology therefore, UWB, whilst remaining a promising technology on the horizon, has lost momentum, and is not yet at a stage where it might easily be exploited for sport- or health monitoring; data-rate, range of use, power consumption, multi-user scalability are all aspects yet to be decided. That said, its low power, short-range tendencies indicate perhaps that it might be well suited to Wireless Personal Area Networking (WPAN) and low power sensing networks.

2.3.6 BAN – 802.15.6

BAN is a new addition to the 802.15 group of PAN standards. The formation of the working group 802.15.6 was approved in November 2007 tasked with "*developing a communication standard optimized for low power devices and operation on, in or around the human body (but not limited to humans) to serve a variety of applications including medical, consumer electronics / personal entertainment and others*" (IEEE TG6 2007). A draft standard was approved in 2011 and released in May 2012. Like Bluetooth LE it is too new a technology to be exploited in this research, but is again considered here for suitability in future work.

Existing standards are not optimised for use in or around the body. The BAN standard has therefore been developed to specifically target this environment, addressing some of the challenges of close proximity to the body. Its range is designed to be "about human body range", achieving data rates up to 10Mbps – higher than many of the other standards that to date could be exploited for body area networks. This higher data rate makes it attractive not just to healthcare services but to entertainment applications (IEEE 2012b).

BAN networks can consist of up to 64 nodes, with one hub (master or coordinator). Nodes and hubs within a BAN establish a reference time base. This is divided into beacon periods, and a beacon period is subdivided into allocated numbered (0-255) timeslots of equal length. Transmission frames can span more than one timeslot, and do not need to start at the beginning of an allocated

timeslot. Through the transmission of super-frames or timed (T-pol) frames, the BAN hub can communicate the boundaries of the beacon period (IEEE 2012b).

The BAN standard describes three physical layers (PHY): Narrowband PHY, Ultra-wideband (UWB) PHY and Human Body Communications (HBC) PHY. A number of different frequency bands are available for BAN. In addition to the 2.4GHz ISM band used by most of the PAN standards, BAN can use the Medical Implant Communications Service (MICS) frequency band (402-405MHz), Wireless Medical Telemetry Services (WMTS) frequency bands (a range of bands spanning 420-1429.5MHz in Japan and USA), and the UWB frequency band (3100-5800MHz) (Kwak et al. 2010).

Narrowband PHY is an optional PHY responsible for activation/deactivation of the radio transceiver, clear channel assessment and data transmission and reception. This PHY is optimised for medical applications, and has scalable data-rates (100-1000kbps) to allow a trade-off between range and data rate. It supports several frequency bands of operation, which are divided in to a number of channels (from a minimum of 10 in the MICS band, to 79 in the ISM band) (IEEE 2012b). A number of different modulation schemes are employed (depending upon the frequency band) and can achieve different information data rates. These are summarised in Table A-2 appendix A.3.

The initial header information (PLCP) transmitted before the data packet (PSDU) is coded in π/2-DBPSK and allows timing synchronisation and carrier offset information to be conveyed such that the remainder of the data packet can be correctly recovered. This header is compact, minimising overhead to the transmitted packet. The data packet is then transmitted in one of a number of

modulation schemes. The frequency band, modulation scheme and symbol rate dictate the overall information data rate. A BAN node should be able to transmit and receive in at least one of the frequency bands.

The Narrowband PHY's low-complexity modulation schemes and short range achieves low peak power consumption (<3mA), low Signal-to-noise ratio requirements and a robustness to interference (Rabaey 2011).

UWB PHY operates in two frequency bands; the low band has 3 channels, the high band 8 channels. All channels have a bandwidth of 499.2MHz. One channel in each band is considered mandatory. UWB transceivers are low complexity and due to the wide bandwidth can achieve higher data rates (up to 10Mbps) with very low power levels compatible with use in particular for medical implant applications. The low power levels also mean low interference for other devices sharing the same frequency bands.

UWB PHY includes two different types of UWB technology: Impulse radio UWB (IR-UWB) and Wideband frequency modulation (FM-UWB). Complementing these are three possible modulation schemes: on-off keying (OOK), which is mandatory, differential- BPSK or QPSK, and FM-UWB (IEEE 2012b). This latter achieves an ultra-wideband signal through the use of a very high modulation index which spreads the signal.

The third PHY – HBC PHY – exploits electrical field communication to capacitively couple systems to the human body via an electrode. The signal travels along the surface of the skin. It uses two channels at 21MHz and 32MHz

and can achieve data rates up to 2Mbps, employing a frequency-selective coding scheme to spread the signal (IEEE 2012b).

In summary, BAN is still in early stages, having only just released a first standard document. Until it becomes a more mature technology, with chipsets available, it cannot be a candidate for any wireless body area network for sports monitoring, and comes too late to have been considered in this research. However, as a wireless standard explicitly targeting on- or near- body communications, and with data rates up to 10Mbps, it is a strong candidate for consideration in the future.

2.3.7 Proprietary standards

Aside from the IEEE standards, a number of manufacturers have created their own proprietary wireless networking protocol. Notable amongst these are Microchip's MiWi and Dynastream's ANT.

2.3.7.1 MiWi

MiWi is Microchip's own proprietary protocol stack, first introduced in 2007, and like Zigbee builds upon the 802.15.4 standard. Microchip produce an RF IC – MRF24J40 – which can be used by both Zigbee or MiWi. MiWi, like Zigbee, is also intended for low data rate, short distance, low cost networks, but additionally has tried to target smaller applications that have fewer nodes in the network, and fewer hops between nodes (Flowers and Yang 2010). In this way it achieves a smaller protocol stack than Zigbee (between 16 and 32KB depending upon the functionality of the node).

MiWi supports up to 1024 nodes in a network, with a coordinator being able to have up to 127 children (this contrasts with a potential 65535 nodes in a Zigbee network). A transmitted message can only make four hops across a network from source to destination. A collection of MiWi nodes forming a network are called a cluster. A PAN coordinator sets up and manages the network, and end devices perform monitoring functions. Like Zigbee the network can be extended through the use of fully functioning devices (FFD) to form a cluster network. A network with a depth of one is a star network. Mesh networks are also possible, with FFD nodes routing messages.

The modulation scheme is the same as Zigbee because MiWi uses the same MAC and PHY stack layers from the 802.15.4 standard, and as such employs a similar acknowledgment scheme to indicate to the sending node that the receiving node has received a transmitted packet.

In summary, the MiWi protocol stack shares many of the functionalities and features of Zigbee, but with a lower overhead, and depending upon the complexity of the application, might be a suitable platform. Like all proprietary solutions, it lacks interoperability.

2.3.7.2 ANT/ANT+

Ant was developed by Dynastream owned by Garmin, which notably is one of the leading manufacturers of consumer sports monitoring products and targets ultra-low power networking applications (Dynastream 2012).

Like most of the wireless standards described already, ANT uses the 2.4GHz ISM frequency band, and employs GFSK modulation, operating on up to 78 channels on a 1MHz spacing. ANT can be configured into peer-to-peer, star, tree and mesh topologies, with an ANT device supporting up to 8 independent ANT channels. If a channel is shared the network could theoretically be increased to 65533 nodes. It has a information throughput of 20kbps (raw RF data rate is 1Mbps). ANT supports 3 types of messaging: broadcast, acknowledge and burst. Broadcast messaging is one-way, for non-critical messages, whilst the receiving node transmits a receipt message during acknowledge messaging. Burst messaging is used for the transmission of bulk data, and it is this which achieves the 20kbps throughput. ANT employs an adaptive channel synchronization

technique to achieve protection from interference, with channels divided into hundreds of timeslots such that a transmission occurs in an interference-free timeslot allowing effectively up to 100 ANT channels to exist on one frequency. ANT+ is the interoperability function that can be added to the base ANT protocol to facilitate the collection, automatic transfer and tracking of sensor data. Typical peak current consumption is 17mA peak currents, with average currents as low as 11µA utilising burst transmissions.(Nordic Semiconductor 2010).

The closest comparator to ANT is Zigbee, and on raw data-rate alone, ANT can transmit 4 times as much data over a given time period than Zigbee, and requires lower host resources to hold the protocol stack. However as a proprietary protocol, it offers less interoperability than Zigbee.

2.4 Wireless Standard Summary

The wireless standards summarised and considered in the previous pages could all, theoretically, be used in wireless BSNs for sports monitoring. However, in each case there are features which make them good candidates, and others which detract from their use for such an application. The high power consumption of WLAN makes it unsuitable despite its global adoption, mature technology, and high data rates. Classic Bluetooth likewise suffers from having a higher than desirable power consumption, and does not support more than 7 slave nodes attached to a master in a piconet. Several of the other standards discussed are either not market-ready, or have come too late to be considered in this research.

As such, one standard stands out at this time as the focus wireless technology for this research – Zigbee, built upon 802.15.4. Whilst its 250kbps data rate is not high, it does support transmission of long enough packets for the transmission of larger volumes of data. It supports large and flexible networks, and its low latency allows for long periods in standby to conserve power. However, Bluetooth LE and BAN are strong candidates and should be revisited during any future research.

2.5 Challenges in Wireless BSNs

The choice of Zigbee as the wireless platform for this research still requires careful consideration. There are a number of challenges to successfully forming a wireless BSN to collect data for sports monitoring. Some of these were introduced at the beginning of this chapter, and will now be discussed further.

Many of these challenges are intimately linked such that solving one challenge might also solve another, or likewise have a detrimental impact elsewhere. Some attempt has been made to discuss these particular challenges together.

2.5.1 Node size and energy supply

Node size and energy supply are two closely linked challenges. With increased integration of electronics into single integrated circuits (ICs), and increasingly, multiple ICs encapsulated into one package (System In Package -SiP), the limiting factor to node size becomes the power supply. In order to ensure long battery life, the battery capacity becomes a primary concern. Minimising power consumption will clearly aid in node power longevity, but this in itself is a multi-faceted issue and will be discussed under its own heading in section 2.5.2.

Battery technology has progressed in recent years due to the proliferation of handheld devices. Pocket-sized mobile telephones require adequate battery life with a small form factor to make them practical, and the rapid adoption of smart

phones has put greater pressure upon battery life, still requiring a compact size, but also having to power larger screens, multiple wireless standards, high processing capabilities, and frequent use. One of the most popular batteries used in handheld devices is the rechargeable lithium ion battery, which exhibits excellent energy density, and has no memory effect (an issue with nickel-based rechargeable batteries such as NiCd and NiMH technologies) and maintains good charge when not in use; it has a self discharge rate of only 5-10%/month (Winter and Brodd 2004). Washington State University reported of some research by Grant Norton into extending the life of Lithium ion batteries which claims to be able to triple the energy capacity by replacing the traditional carbon-based anode with a tin-based anode (Hilding 2012).

Other battery research is looking towards the use of fuel cells to power consumable electronics. Batteries are closed systems, with the anode and cathode being the charge-transfer medium and taking an active role in the redox reaction. Conversely Fuel cells are open systems where the anode and cathode are just charge-transfer media and the active masses undergoing the redox reaction come from outside the cell (Winter and Brodd 2004). If fuel cells can be practically developed, they could provide much greater capacity for their size compared to batteries. Figure 2-4 compares different types of storage devices.

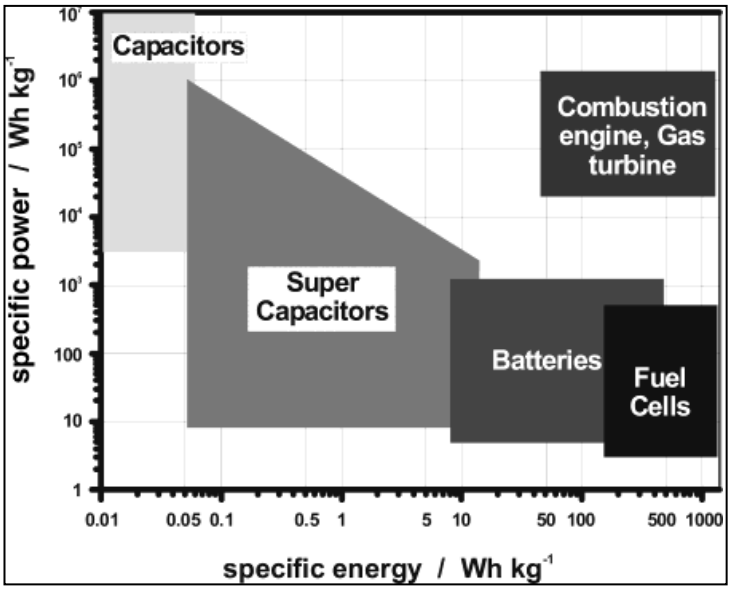

Figure 2-4: Ragone plot comparing energy domains for various electrochemical energy conversion systems

(Winter and Brodd 2004)

An alternate method being explored for powering wireless BSN nodes is energy scavenging. Energy scavenging or harvesting is a growing research area, not just in the area of wireless BSN, with radio frequency, solar, heat, and vibration all methods being investigated. Yeatman and Mitcheson (Yeatman and Mitcheson 2006) discuss the ambient energy sources that can be found in the environment of the body, noting vibration or body motion – or inertial energy scavenging - as having the most potential. They note that research publications of inertial energy scavenging have shown an exponential increase in reported normalised power output over the last 20 years or so, and expect this trend to continue. However, they also make the cautionary note that body-powered applications remain challenging because of the low frequency of movement meaning low power levels. Energy storage is still a requirement with this technique as power availability through scavenging is unlikely to correspond in time with demand.

2.5.2 Node power longevity

This is a complex issue, linking a number of the other challenges confronting wireless BSN. Power storage has been discussed in the previous section. However, maximising the length of time a node will operate on one battery charge is reliant upon minimising the power consumption of the node itself. Optimising the electronic circuit design can only go so far.

The highest power consumption in a wireless BSN is likely to take place during transmission of data, closely followed by reception of data (or being receptive to any data). Thus, assuming the transceiver design is optimised to be as energy efficient as possible, the choice of radio standard discussed earlier plays a large part in minimising the power consumption. Zigbee is a low power radio standard which allows the nodes to be put to sleep for extended periods where the power consumption can be as low as 5µW, switching on to listen for transmissions or to transmit data packets only periodically, as per the application requirements.

Minimising the amount of data that needs to be transmitted will also minimise the on-time of the transmitter. Here a number of factors need to be considered. What information needs to be determined from measurements? What sensor or sensors need to be chosen to complete this task? Careful choice of sensors means that fusion of data could lead to more information being available than the individual sensors could provide. In complementary fusion two sensors might capture different aspects of a physical process, and merge to give a more complete picture. With cooperative sensor fusion, sensors can work together to provide information not available from any one sensor (Yang and Hu 2006). Individual sensors might also be able to provide more than one type of

information. Thus, careful choice of sensor or sensors might minimise the data that needs to be measured to gain particular information.

Another consideration is what is transmitted. Raw data allows maximum processing to be performed at the central data collection point (a mains powered central node or a PC) where maximum processing power is available, and where all sensor data is available. However, raw data transmission can mean transmission of a large amount of data, not all of which is necessarily essential to the end result. As such, performing some processing in the sensor nodes themselves, possibly performing feature extraction from the raw data can greatly reduce the amount of data that needs to be transmitted. This does not come without an overhead however, as increased processing in the nodes will increase the power consumption, and also take processing time away from other tasks. Sampling rate is therefore also an important factor. Sampling at an unnecessarily high rate increases the amount of data collected, and increases the power consumption of the node.

2.5.3 Data Integrity and Synchronisation

Reliability of data transmission is an important consideration in wireless networks. Crowded frequency spectrums can lead to interference which can cause packet loss. Zigbee uses spread spectrum modulation to mitigate interference and also operates dynamic frequency selection for coexistence to other networks. However, methods of ensuring successful reception of data need to be considered; these include the acknowledgement schemes of radio standards such as Zigbee, and the use of resend requests if data is not received. Packet

collision from several nodes attempting to transmit at the same time can also cause delay in transmitting packets (Zigbee operates a collision avoidance scheme, and waits a back-off period before trying again). The longer the node needs to keep its transmitter active, the higher the power consumption. Baronti (Baronti et al 2007) discusses using a TDMA protocol within the network to schedule transmissions such that every node knows when it is allowed to turn on so that no collision can result.

Another vital consideration for wireless BSN is that of synchronisation. Nodes need to be synchronised in time for two reasons: in order to correctly schedule data transmissions, and to ensure that data is sampled from sensors synchronously across the network.

In a wired network, synchronisation can be performed by distribution of a common clock or synchronisation signal. However, in a wireless network, no physical electrical connection exists between the nodes. Nodes can be synchronised through a wired connection prior to establishing the wired network – i.e. at initialisation – but this does not account for clock drift over time. Even precise crystal oscillators have variations (normally measured in parts-per-million) from their specified fabricated frequency. Even when this variation is small, if the network were to run for an extended time, a time drift would appear between nodes. Therefore it is necessary to wirelessly transmit a synchronising signal such that the individual node clocks can be adjusted to match that of a global clock.

One of the problems of time synchronising nodes in a network is the non-determinacy factor (Song et al. 2009). Taking Zigbee as an example, the protocol

stack has a number of levels – the application layer (APL) from where a message originates, then network layer (NWK), Medium access layer (MAC), and physical layer (PHY). The time taken to assemble a packet (essentially the time it takes for a message to pass through the stack from APL to PHY in the transmitting node, the propagation time across the wireless link, and the receive time from PHY to APL within the receiving node is not accurately known. Time-stamping messages higher up the stack (in the MAC or PHY) can help to reduce this non-deterministic element. There are a number of different techniques that have been developed to perform the task of time synchronisation in wireless sensor networks.

The most well-known of these approaches is Reference Broadcast Synchronisation (RBS) (Elson et al. 2002). This assumes that receiving nodes receive a broadcast synchronisation message at the same time from a reference node. Thus, rather than synchronising the sender to the receiver, the receivers are effectively synchronised with each other. The reference beacon does not contain a timestamp, it is the packet time of arrival which is used to compare the clocks (the receiving nodes compare their arrival times and estimate their relative clock offsets).

Another scheme is the Timing-sync protocol for sensor networks (TPSN) developed by Ganeriwal (Ganeriwal et al 2003). This method has two stages. First a hierarchical topology of the network is created, assigning each node a level (in a star network all nodes except the coordinator would be at level 1). In the synchronisation phase a node in level n would synchronise with a node in level n-1. This synchronisation phase is a two way exchange between a pair of nodes which enables the drift between their local clocks to be determined. MAC level time-stamping is employed in this technique.

Another popular method of time synchronisation is that of Flooding Time Synchronisation Protocol (FTSP) (Maroti et al. 2004). Here every node periodically broadcasts time synchronisation messages, with one root node providing a global time. Nodes are synchronised by receiving global time estimates from nodes closer in the network hierarchy to the root synchronising node. MAC level time-stamping is again employed in this technique.

However, many of these methods are either computationally expensive, or require the exchange of multiple messages (increasing transmit time, power consumption and chance of packet collision). Kusy (Kusy et al. 2006) suggests that depending upon the application, many of these efforts are unnecessary. He proposes that whilst WSN requires time synchronisation, the model of synchronisation should be tailored to the application. Synchronising to a global time is often not necessary. Different approaches might be used for applications requiring event time-stamping (single isolated events are observed and time-stamped) compared to data-series time-stamping (periodical sampling which is collected at a central node and correlated). If a global time is not required, nodes do not need a continuous synchronised time, but just need to agree upon single points in time. This can reduce the overhead of time synchronisation upon both the network and the node itself.

2.6 Chapter Summary

The terms Wireless sensor networks (WSN), Body Sensor Networks (BSN) and Body area networks (BAN) have been considered, along with the specific requirements of a wireless BSN. Several candidate wireless standards were reviewed to determine their suitability for the application of Wireless BSN for sports applications and Zigbee chosen as the most suitable market-ready standard. The challenges to wireless BSN have been discussed in more detail, in particular factors affecting power consumption, data integrity, and time synchronisation.

3 Sensors, and System Design

Through the creation of a wireless BSN to collect sensor data, both on and around an athlete's body whilst he is performing his sport, measurements can be more ambitious than might be possible through standard leaded measurements. It should allow increased freedom in both the environment and conditions under which the measurements take place, as well as the number, diversity, frequency and distribution of the measurements that can be taken. It should be possible for the athlete to perform his sport, whilst being monitored, in conditions very close to those under which he ordinarily would, without movement or comfort being unduly hindered. It remains therefore, with reference to the key determinants of successful rowing, to determine what measurements an athlete (the oarsman), his physician, physiotherapist or coach might want to make, what information they might hope to gain, and under what conditions.

3.1 Chapter Organisation

This chapter will briefly consider the diversity of measurements that might be made to an oarsman and boat, building upon discussion of the key determinants of successful rowing in chapter 1, section 1.3. A subset of sensors will be reviewed to determine the optimum number and types of sensors which together could maximise the relevant information available regarding the performance of an oarsman or crew. Sensor choice will also be influenced by system design decisions which will best highlight the benefits of a wireless data collection

system. The chapter will culminate with a broad requirements specification for both hardware and software elements of the system.

3.2 Desirable metrics

Rowing demonstrates many of the issues that make data collection in some sports both vitally useful, and difficult to gather. Rowing is an all-body sport, requiring extreme fitness to be performed well, involving development of all muscle groups from the arms, torso, back, and legs (Mazzone 1988). The rowing stroke also requires the execution of a very precise sequence of actions, some of which are rapid and not adequately visible by eye (Nolte 1991). The rowing stroke is repetitive, and it would be useful to be able to gauge repeatability of the action. Rowing is also a team sport (in the case of multi-oarsman boats) and the cohesion within the boat is vital to the boat's performance (Baudouin and Hawkins 2004). Finally, whilst some observations can be made upon a rowing ergometer, or in specially fabricated dry-land training tanks, true rowing action, coupled with the effect it has on the performance of a boat, is difficult to monitor; the narrow rowing boat hull, and river or lake conditions make wired measurements, or detailed video measurements difficult or impossible.

The key determinants of rowing discussed in chapter 1, section 1.3 facilitate the identification of a number of metrics that would be desirable for the study and optimisation of the rowing stroke.

Thus, with a view to maximising the potential for increasing the average velocity of the boat, and mitigating injury, measurements can largely be categorised into:

1. kinetics and kinematics (body or boat) for the purposes of rowing stroke analysis to maximise boat performance (either individual or crew), or
2. oarsman kinematics or biometrics for the purposes maximising biomechanical/energetic and biological/energetic interactions (Schwanitz 1991) leading to increased efficiency of the rowing stroke or rowing training.

The first category is concerned with studying the interactions of movement of the oarsman, oars and boat, monitoring forces, and the timing of forces applied, and analysing the impact upon the movement of the boat.

Desirable metrics might thus include:

- Boat acceleration, velocity or displacement over time
- Oar angle
- Oar force
- Stretcher force
- Body segment acceleration, velocity or position over time
- Relative body segment movement – e.g. joint angle
- Muscle force profile over time
- Inter-muscle sequencing
- Muscle activation time related to the stroke sequence
- Inter-crew timing
- Action repetition rate
- Action repeatability

Until the miniaturisation of sensors and integrated electronics facilitated increased instrumentation of the oarsman, boat instrumentation, namely oar and stretcher force, oar angle and boat acceleration and velocity have been a staple of rowing stroke analysis (Kleshnev 2005b; McBride 2005), and are thus accepted and meaningful to oarsmen and coaches. Body segment acceleration and velocity has been studied by Kleshnev (Kleshnev 2000), albeit with bulky cable position transducers, and the application of muscles (Mazzone 1988) is well understood, although feedback of muscle data to oarsmen is not extensive due to the difficulty (until recently at least) in monitoring multiple muscle sites simultaneously; multi-channel, wired, personal data-loggers have recently been utilised by a number of research groups to facilitate this (Sommer et al. 2008; Guevel et al. 2011; Fleming and Donne 2012). Inter-crew timing, identified as a key determinant of successful rowing in multi-oarsmen boats (Baudouin and Hawkins 2004) is an obvious candidate for benefit from a wireless system.

The second category includes physiological measures related to fitness, exertion, and physiology, but not directly related to force production. Here we might wish to measure:

- Heart-rate
- Skin temperature
- Oxygen Uptake (VO_2)
- Blood oxygenation
- Respiration rate
- Muscle fatigue
- Joint angle / range of motion

- Lactate profile
- Skin humidity (sweat)
- Glucose levels

Heart-rate is commonly measured across all sports, and VO_2, and lactate levels are measured in elite sportspeople. Analysis has been performed into relative levels of these biometrics during simulated rowing and race conditions (Di Prampero et al. 1971; Hartmann and Mader 2005) and also the effect of different rowing styles upon these measures (Roth et al. 1993).

Some of these metrics might be gained through the measurement of another parameter (for example velocity can be determined from the integration of acceleration data). As such, it might be possible to determine more than one metric from a given sensor. Conversely, many of the metrics in the second list above would require sensors particular to that metric. Some measurements might be inferred through linear correlation: Prampero (Di Prampero et al. 1971) indirectly determined VO_2 through accepted relationship between VO_2 and heart-rate.

For the purposes of designing a system that can best exploit the benefits of wireless BSN within the limits of this research project, it would seem prudent to focus upon measurements within the first category.

Table 3-1 correlates the desirable metrics to possible sensors. The sensors considered are not exhaustive, but include those that can be practically implemented and have been utilised in previous research reviewed in chapter 1, and can inform upon metrics that have been highlighted as a key determinant of

successful rowing in section 1.3. The table does not attempt to indicate the ease or suitability with which a given sensor could infer a particular metric. In some cases more than one sensor might be required to determine a metric (particularly in the case of the shaded rows towards the end of the table). The table was refined through discussion with a number of club-level rowers and coaches to ensure that metrics were useful and meaningful.

Most of the metrics in the performance analysis category of measurements could be made with a limited number of sensors. Sensors that could yield or contribute to more than one metric are considered briefly in the next section.

Desired metric	Sensor					
	Accelerometer	gyroscope	Boat impellor	Strain gauge	Goniometer	EMG
Boat acceleration, velocity or displacement	X		X			
Oar angle	X	X			X	
Oar force				X		
Stretcher force				X		
Body segment acceleration, velocity or position	X	X				
Joint angle	X	X			X	
Muscle force over time						X
Inter-muscle sequencing						X
Muscle activation time						X
Inter-crew timing	X	X		X	X	X
Action repetition rate	X	X		X	X	X
Action repeatability	X	X		X	X	X

Table 3-1: Desirable metrics and potential sensors

3.2.1 Accelerometers

Accelerometers are devices that can be used to measure acceleration, where acceleration can take one of three forms: vibration (an a.c. phenomenon), tilt (a d.c. phenomenon, due to Earth's gravity) and inertia (also a d.c. phenomenon). There are many types of accelerometers distinguished by the parameter measured to determine acceleration.

Piezo-electric accelerometers utilise a piezoelectric crystal mounted to a loading mass. When the crystal lattice is subjected to a force, the positive and negative points in the lattice are pushed against each other to produce a dipole moment. The charge generated at the output is proportional to the applied acceleration. The crystal can be cut in 3 different ways, and the piezo-electric effect takes different forms (longitudinal, transverse or shear) dependent upon the orientation of the cut. This determines the precise application for which they are used. The instantaneous nature of the charge makes it only suitable for shock or vibration (a.c.) measurement (Kulwanoski and Schnellinger 2004).

Piezo-resistive accelerometers employ a piezo-resistive material rather than a piezoelectric one. In this case a force exerted by the loading mass in the presence of an acceleration will cause the piezo-resistive material to become strained or deflected. This will cause its internal resistance to change. Unlike the piezo-electric effect, this resistance change remains unless the material is restored to its original position. This makes it suitable for d.c. acceleration phenomenon such as gravity or inertia measurement. The structure of the

accelerometer is often fabricated through bulk micro-machining (a mass is suspended on two sides by piezo-resistive springs etched into silicon) (Liu 2006).

Capacitive accelerometers measure a change in capacitance. In its most basic form, a capacitance is measured between two parallel plates, one fixed, one attached to an inertial mass. In the presence of an acceleration the plate attached to the mass is deflected either towards the fixed plate or further away from it. The change in the inter-plate distance thus changes changing the capacitance according to:

$$C = \frac{\varepsilon A}{D \pm d} \qquad 3\text{-}1$$

C: *capacitance*
ε: *Dielectric constant of air*
A: *plate surface area*
D: *un-deflected plate separation*
d: *change in plate separation due to deflection*

Like the piezo-resistive accelerometer, this approach lends itself to being micro-machined in silicon (both bulk and surface micromachining), and is also able to measure both a.c. and d.c. acceleration phenomena (Doscher 1999).

Of the above methods of measuring acceleration, the ability to micro-machine the structure of the accelerometer in a planar (surface micro-machined) fashion, facilitating integration and miniaturisation drives down cost, and the majority of the low-cost accelerometers available on the market are surface MEMS (Micro Electro Mechanical Systems) Capacitive accelerometers.

The capacitive sensing elements are fabricated from polysilicon using a masking and etching process (the polysilicon is deposited on a sacrificial oxide layer that is subsequently etched away to leave the suspended sensing elements). A simplified structure is shown in Figure 3-1 a, showing a movable central mass to which a set of capacitive plate beams are attached (Doscher 1999). Acceleration causes the central proof mass to be displaced from its rest position, thus changing the distance between the suspended plate and fixed plates. The change in distance is proportional to the change in acceleration, and is manifested in the change in capacitance in the two capacitors.

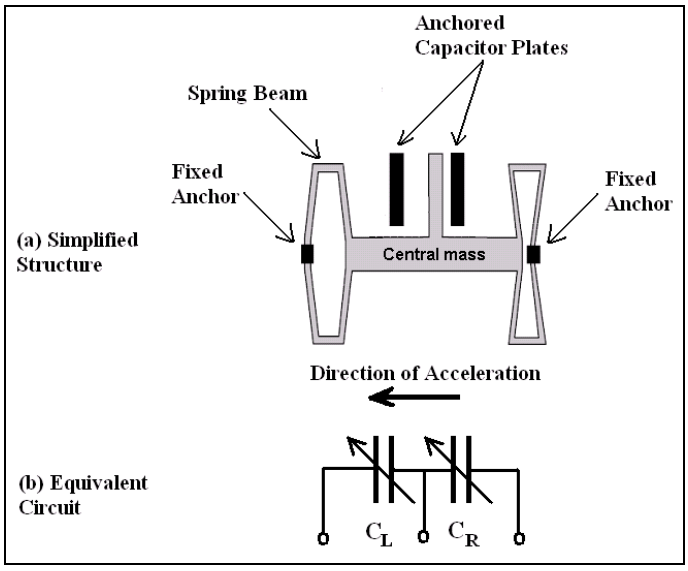

Figure 3-1: Structure and equivalent circuit for MEMS capacitive accelerometer

Variable capacitance formed between anchored and moving capacitor plates, due to change in inter-plate air-gap under acceleration conditions (Doscher 1999)

The equivalent circuit shown in Figure 3-1 b shows the differential capacitive arrangement. In equilibrium, when the structure experiences no acceleration, the total capacitance is:

$$C = \frac{C_L C_R}{C_L + C_R} = \frac{\varepsilon A/D \; \varepsilon A/D}{\varepsilon A/D + \varepsilon A/D} = \frac{\varepsilon A}{2D} \qquad 3\text{-}2$$

However, in the presence of an acceleration, the central plate is deflected, and the separation between the deflected plate and the two anchored plates is such that the increase in separation on one side is mirrored by an equal decrease in separation on the other.

$$C = \frac{C_L C_R}{C_L + C_R} = \frac{\varepsilon A/D+d \; \varepsilon A/D-d}{\varepsilon A/D+d + \varepsilon A/D-d} = \frac{\varepsilon A}{2D} \qquad 3\text{-}3$$

The total capacitance will remain equal, but the plate separation change will result in a capacitance decrease of the capacitor with greater plate separation, and an increase in capacitance of the other. One of the signal processing tasks of the IC housed within the accelerometer package is to convert the difference in capacitance between the two capacitors into an output signal that can be related to acceleration.

Inclination or tilt sensing can be used to determine the orientation of a limb segment with respect to the vertical. Here acceleration due to gravity is projected onto the axes of the accelerometer. Linear accelerations can be used to provide an estimation of force in a given direction. However, both gravity and inertial acceleration are d.c. accelerations, and as such there is no guaranteed way of separating the two parameters. Orientation in the azimuth can also not be determined by accelerometer alone. Tri-axial accelerometers allow measurements of linear acceleration to be measured in three dimensions, and

also allow for more accurate measurement of tilt sensing (the sensitivity of a single axis to acceleration varies with the angle of acceleration relative to the axis, and is at a maximum when perpendicular to the axis – section 3.3.1 describes this in more detail).

3.2.2 Gyroscopes

Gyroscopes measure angular rate. Three axes are used to reference this rotation – yaw, pitch and roll. The output of the gyroscope (usually a voltage) is therefore proportional to the angular rate. MEMS gyros measure angular rate using Coriolis acceleration. The Coriolis effect is where the instantaneous speed of a point on a rotating object is proportional to the radius from the centre of rotation to the measurement point. For a given rotation rate, a point further from the centre of rotation has to cover a greater distance per unit of time than a point closer to the centre of rotation (Analog Devices 2008).

Tangential Velocity = angular rate x radius

MEMS gyroscopes exploit the Coriolis effect by using a resonating mass micro-machined in polysilicon, tethered to the silicon substrate by springs at 90^{o} to the motion of the mass (Analog Devices 2008). This can be seen in Figure 3-2.

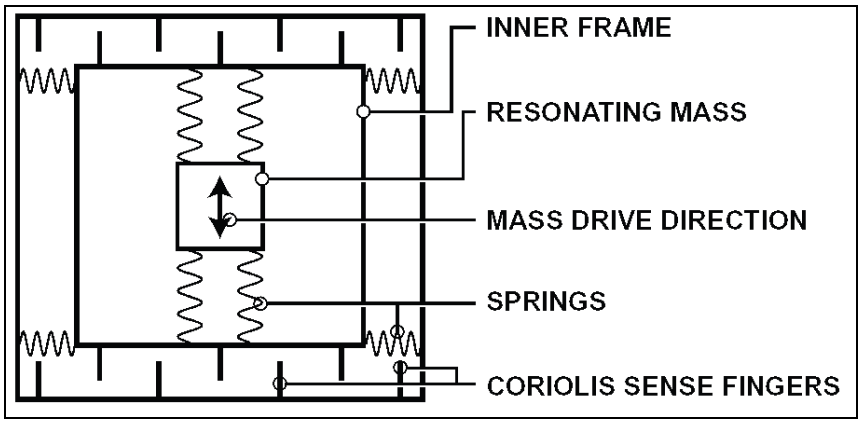

Figure 3-2: Gyroscope mechanical structure

Inter-digitised fingers result differential capacitance in a rotating system (Analog Devices 2008)

Like the linear accelerometer, angular rate is measured in the gyroscope through a variation in capacitance. Inter-digitised fingers comprised of those attached to frame containing the resonating mass, and those attached to the silicon substrate form 2 capacitors of equal capacitance at rest. Displacement of the frame containing the resonating mass induces a differential capacitance (one increases, the other decreases), and this is transformed to a change in output voltage.

Gyroscopes can be used to measure limb segment angles through integration of angular rate with respect to time. However, this method is prone to integration drift due to bias errors. Thus corrective methods have to be employed to ensure an accurate result (e.g. fusing gyroscope measurement with linear acceleration measurements - this has been discussed in chapter 1). Gyroscopes can also be used in conjunction with linear accelerometers to determine 6 degree of freedom of movement.

3.2.3 Goniometers

The goniometer is used to measure single degree of freedom in joint angles. Joint angles can be measured in many ways, but a popular method (shown in Figure 3-3) is the use of a pair of optic fibres.

Figure 3-3: Optic fibre Goniometer

Light transmission along the optic fibre is a function of bend angle (ADInstruments)

The goniometer is fixed to either side of the joint in an exoskeleton manner such that flexing the joint bends the optic fibres. The amount of light travelling through the optic fibres from one end to the other is determined by the angle of bend in the fibres. The amount of light measured is converted to a voltage output which can be dynamically measured. Smaller goniometers are available to monitor smaller joints such as finger joints. Measurement of joints exhibiting more than one degree of freedom would require a much more complex arrangement of these sensors and subsequent processing of data.

Whilst moderately robust and easy to use, these sensors might be unsuitable for the monitoring of some sports due to the nature of their attachment to the body. Some movement might be inhibited, and sensor calibration is altered if the sensor attachments shift, leading to possible errors in angle estimations. It was also reported by Hawkins (Hawkins 2000) that the goniometer encumbered motion to rowers during his experimentation and there was slippage of the goniometer attachment to the limbs.

Other goniometers include those employing a rotary potentiometer whose resistance changes as it is rotated. These were used by several researchers for measuring oar angle (Kleshnev 2000; Hill 2002; Smith and Loschner 2002) as summarised in chapter 1.

3.2.4 Strain Gauges

Strain gauge force transducers are common tools for monitoring force. They exploit the fact that when a force is applied to a material it will deform, causing a change in its resistance. This change in might only be a fraction of a percent of the nominal resistance value. In order to measure this small change accurately, the resistance is placed within a Wheatstone bridge circuit configuration (Figure 3-4).

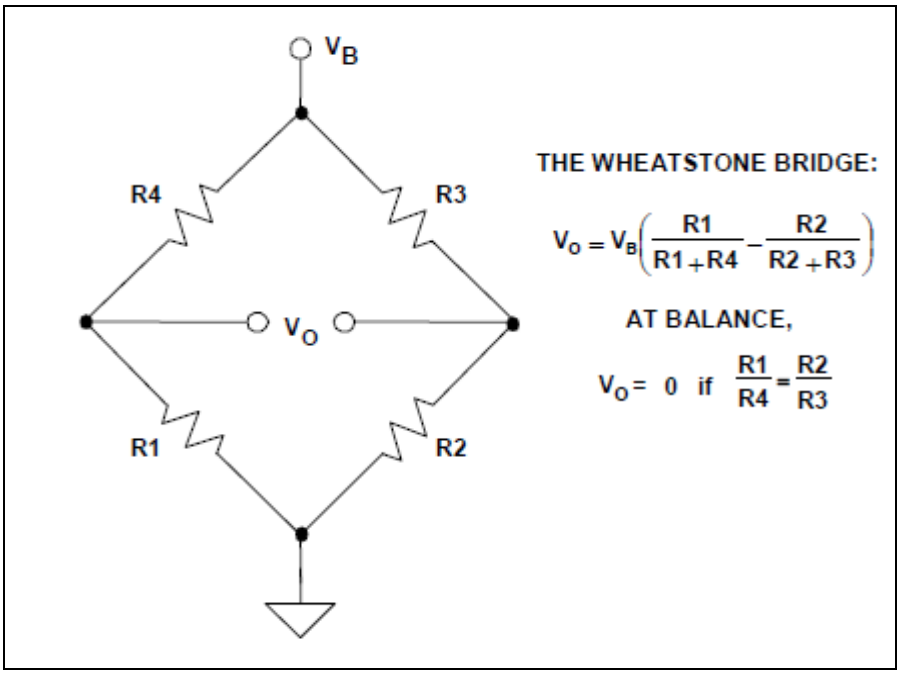

Figure 3-4: Wheatstone bridge configuration

Allows accurate measurement of small changes in resistance of a material due to applied force (Kester 1999)

A Wheatstone bridge circuit works by applying a constant known current through the resistive measurement element such that any variation in voltage measured is due to the resistance change due to the force alone. In a typical setup more than one – often all four – of the resistance elements in the bridge are strain gauges, arranged to maximise the output voltage for a given deflection (Kester 1999).

3.2.5 Surface Electromyography

Electromyography (EMG) is the detection of the electrical signals produced by the contraction of muscles, and Surface Electromyography (sEMG) is a subset of this concerned with the measurement of electrical signals via electrodes on the surface of the skin (rather than needle electrodes inserted into the muscles).

A muscle is made up of many motor units that consist of a number of fibres that are innervated (stimulated) by a motor neuron; the number of muscle fibres in one motor unit can range from a few to several hundred (Joe F Jabre 1983). The motor neuron carries the impulse to contract the muscle to the muscle fibres. The muscle fibres of a motor unit are spread over a small area of muscle tissue and intermingle with the muscle fibres of other motor units (Kamen and Gabriel 2009). The connection between motor neuron and muscle fibre is called the neuromuscular junction. The signal generated by a single motor unit is called the motor unit action potential (MUAP), and an algebraic sum of MUAPs make up the EMG signal that is picked up by surface electrodes.

Surface electrodes cannot pick up a single motor unit action potential (needle electrodes can be more specific than surface electrodes in pinpointing the group of muscle fibres to be monitored but this technique is invasive) – as such, the superposition of a number of motor unit action potentials means that the sEMG signal exhibits Gaussian characteristics (De Luca 2006). If the force of the contraction increases, more motor units and hence more muscle fibres are activated, and the overall amplitude of the sEMG signal appears to increase. Figure 3-5 shows a typical sEMG signal in the time and frequency domain.

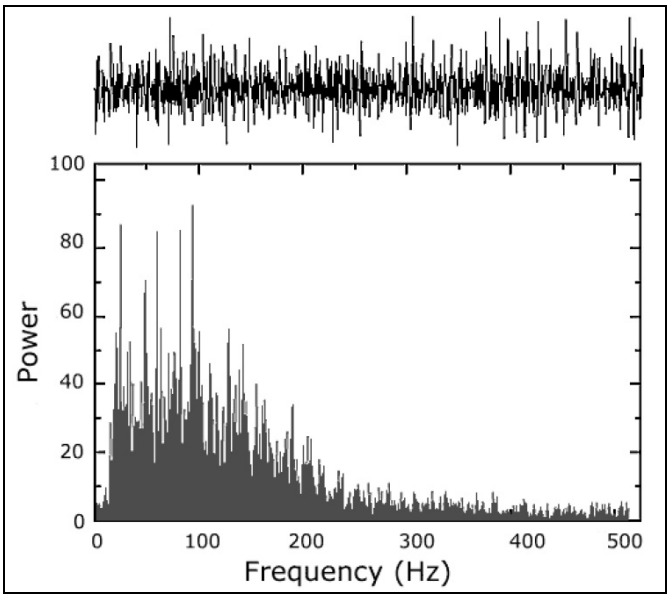

Figure 3-5: Typical sEMG signal

Indicates typical 20-500Hz frequency distribution, measured during constant force isometric contraction of the tibialis anterior muscle (De Luca 2002)

The frequency spectrum over which the sEMG signal is typically spread is dependent upon the shape, configuration and placement of the electrodes. In sEMG, the signal distribution is typically 20-500Hz (De Luca 2006).

The detection and measurement of these noise-like signals is compounded by their amplitude; sEMG signals typically range from a faint 20μV to a more robust 2mV) (De Luca 2001) depending upon the electrode configuration and placement, as well as the force exerted by the muscle. As such, the measurement circuitry must perform substantial amplification of the signal before it is digitised. However, amplification alone of the signal detected at the electrodes is not sufficient to accurately record the sEMG signal; the signal detected will include not only the desired sEMG signal, but also noise from a number of different sources (including ambient noise, motion artefacts and muscle crosstalk). These will be discussed further in section 3.3.2.

The measurement of sEMG can be used not just to show the magnitude and duration of muscle activity. Indeed, caution should be exercised in relating muscle force and amplitude of the sEMG signal because of the many factors that influence the production of the sEMG signal. Relative amounts of muscle activation can however be determined if other variables are kept constant (electrode placement, measurement subject, etc); performing one task might produce more force than the performance of another task) (De Luca 1997).

Muscle activation timing, indicating the time motor units in the detection volume of the electrode begin to fire at a level above the noise floor of the measurement apparatus, is another useful parameter that can be observed (Kamen and Gabriel 2009). Muscle Activation timing is useful for correlation of muscle activation with other measurements or observations.

Extending the analysis of the EMG signal to look at spectral frequency changes allows further insight. An example of this is muscle fatigue. The sEMG signal can be used to determine the point at which a muscle cannot maintain a contraction; this is measured during isometric submaximal contraction (Florimond 2010). This is called the failure point. Analysing the frequency distribution at points during a sustained muscle contraction can help in the identification of muscle fatigue. The bandwidth and range of the frequency spectrum of the signal decreases as the muscle fatigues, and by monitoring either the mean or median frequency, or the ratio of maximum to minimum frequency allows this to be monitored (De Luca 1997). Analysing the frequency spectrum of sEMG however does require a far higher sampling rate in the measurement process than monitoring the overall envelope shape of the muscle activity.

3.3 Sensor Choice

The choice of sensor impacts upon the overall system design. Consideration should be made for what would benefit a performance driven system. Whilst it is possible to combine many sensors to provide precise information – for example 9 sensor inputs from tri-axial accelerometers, gyroscopes and magnetometers to determine 6 degrees of freedom (Tessendorf et al. 2011), or combining accelerometer and gyroscope data to determine limb angle to a high degree of accuracy (King et al. 2009) – does knowing this information provide more value than a simpler system with fewer, carefully chosen sensors, which ultimately allow the system itself to be optimised? Sensor choice and desired output from the system also impacts upon the ease with which measurements can be made. It would be beneficial to have a system that requires minimum set-up and calibration upon placing the nodes in their measurement positions.

It is important to choose a couple of sensors that will reveal the maximum information about the oarsman or crew and boat performance, and as such a sensor that provides great flexibility is the linear accelerometer. This can be used to give an appreciation of force due to the proportionality of force and acceleration from Newton's second law of motion, along with the onset and cessation of force. Accelerometers can also measure acceleration of the boat (Young and Muirhead 1991) from which boat velocity (both instantaneous and average) can be calculated. Acceleration of the seat can be used to derive acceleration of the oarsman centre of mass (Loschner and Smith 1999), and accelerometers placed upon limb segments, can yield information regarding the

acceleration and velocity of limb segments which can help the analysis of stroke sequencing (Lamb 1989). An indication of limb angle, and thus position can be derived depending upon other factors (other sensor inputs, instantaneous inertial acceleration, anatomical constraints (Favre et al. 2008; King et al. 2009)).

Another measurement parameter that can yield much information about the performance of the oarsman is sEMG. This should be able to yield an appreciation of relative force produced by a muscle (not directly the actual force), information about the muscle activation timing and sequencing of the different muscles recruited for the rowing stroke (Kleshnev 2010). It should also be able to provide an accurate indication of muscle activation time amongst the crew. Additionally, unlike accelerometers, it is independent from the acceleration of the boat itself. All body-mounted accelerometers are operating within an accelerated system of the rowing boat (Young and Muirhead 1991). However, accelerations of the boat should have no influence upon the muscle activity.

These two sensors will now be considered in more detail before final system design choices are summarised.

3.3.1 MEMs Capacitive Accelerometers

Accelerometers can be fabricated with different sensitivities, dictated by the amount of displacement of the sensor per g of acceleration. This is determined by the structure's resonant frequency, set by the mass and spring constant of the device (Bernstein Feb 2003).

$$d_g = \frac{g}{\omega_n^2} = g.\frac{M}{k_s} \qquad 3\text{-}4$$

ω_n: *resonant frequency*
d_g: *displacement per g*
M: *mass*
K_s: *spring constant*

Most accelerometers are designed to be ratiometric – meaning that the sensitivity, and any offset voltages are scaled linearly with the supply voltage. If the supply voltage increases, the sensitivity and offsets will increase linearly. This reduces supply-induced errors in the analogue-to-digital conversion (ADC) process (assuming the ADC input range is also scaled to the supply).

Whilst accelerometers are manufactured to a given sensitivity, they still need to be calibrated. There are a number of factors to consider: the precise number of volts per g of acceleration (sensitivity), the output at zero g (zero g offset) and equilibrium axes offset calibration.

Offset errors can be caused by trim errors, mechanical stresses within the package and due to mounting of the accelerometer and shifts due to temperature and aging (Tuck 2007a). The optimum way to calibrate the accelerometer is to rotate the active axis of the accelerometer through 180^o. This will enable to accelerometer to experience both +1g and –1g (passing through 0g where the axis is momentarily perpendicular to gravity). Of the range of values obtained, the maximum value will be +1g and the minimum value –1g, giving the sensitivity of the accelerometer. Assuming linearity of the output, the value for 0g is halfway between the two. The zero g offset is therefore the difference between the

nominal 0g value and this value. This of course would need to be repeated for each active axis.

$$S = \frac{(V_{MAX} - V_{MIN})}{g - (-g)}.g = \tfrac{1}{2}(V_{MAX} - V_{MIN})$$
$$V_{0g} = \tfrac{1}{2}(V_{MAX} + V_{MIN}) \qquad 3\text{-}5$$
$$\Rightarrow A = (V_{OUT} + V_{0g}).S$$

S: *Sensitivity (V/g)*
V_{0g}: *Voltage output at 0g*
A: *Acceleration*

The manner in which the accelerometer is mounted will also contribute to its sensitivity. Consider an accelerometer mounted such that its axis is parallel to the force of gravity – i.e. it is in its +1g position (Figure 3-6 a). A 1^o change in orientation will cause the acceleration along its axis to be:

$$A_{axis} = g.Cos(1^O) = 0.9998.g \qquad 3\text{-}6$$

This corresponds to a 0.0002.g change in value with respect to 1g.

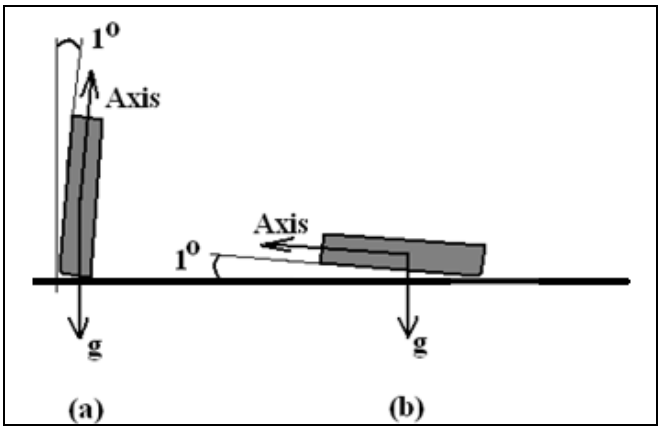

Figure 3-6: Sensitivity of a linear accelerometer depending upon axis orientation with respect to the direction of acceleration

However, mounting the accelerometer such that its axis is perpendicular to the force of gravity – its 0g position (Figure 3-6 b) and then altering its orientation by 1^o will yield a 0.017.g change in value with respect to 0g.

$$A_{axis} = g.Sin(1^O) = 1.7e^{-2}.g \qquad 3\text{-}7$$

This equates to an 85 times larger change in sensor output for a 1^o change in angle from a 0g orientation compared to the same angle change in a ±1g orientation. This can be seen graphically by looking at the voltage output versus tilt (see appendix A.4). Thus a single axis method of determining tilt might yield inaccurate results due to reduced sensitivity when the accelerometer is approaching +1g or -1g. Combining two perpendicular axes measurements (using a dual- or tri-axial accelerometer mitigates this problem (Tuck 2007b). It also solves the problem of not knowing which direction the accelerometer is tilted, not just the degree by which it tilts.

Acceleration data contains information about velocity and displacement. Acceleration is the rate of change of velocity, and velocity is the rate of change of displacement. Equation 3-8 shows the relationship between the three variables.

$$a = \frac{\partial v}{\partial t} = \partial\left(\frac{\partial x}{\partial t}\right) = \frac{\partial^2 x}{\partial t^2}$$
$$as \quad v = \frac{\partial x}{\partial t} \qquad 3\text{-}8$$

Thus, if acceleration can be derived through differentiating velocity or double-differentiating displacement, then velocity and displacement information can be determined through integrating or double-integrating acceleration respectively.

$$x = \int v.dt = \int\left(\int a.dt\right)dt = \iint a.dt^2$$
$$as \quad v = \int a.dt \qquad 3\text{-}9$$

There are, however, some things to consider. Any noise or dc offset in the sampled acceleration will, integrated over time lead to errors in the velocity or displacement information. Some of this noise can be filtered out prior to digitisation, and some can be removed through the introduction of a discrimination window in software.

In real world scenarios, where there is an initial acceleration and finally deceleration until a body comes to rest, the area above zero (positive acceleration) is never precisely equal to the area below zero (deceleration). This, when double integrated to determine displacement will lead to a small continuous drift in position due to a non-zero velocity value. Thus, the acceleration should be

checked to see if it is resting at zero, and the velocity then forced to be equal to zero (Seifert and Camacho 2007).

Depending upon the application, integration drift can be removed through a re-calibration at various intervals – e.g. if monitoring a cyclic motion where the body being monitored is at a known position every s seconds, we can exploit this feature and reset the position of the body periodically thus minimising drift.

It is not possible to differentiate between the gravitational component along the active axis of an accelerometer and inertial acceleration without additional knowledge (this can be done with the use of additional accelerometers or with an additional gyroscope). An accelerometer does not in fact measure gravitational acceleration. What it measures is a deviation from freefall. This can be best explained through two scenarios: an accelerometer sitting flat on a tabletop will measure 1*g* ms^{-2}, but an accelerometer in freefall measures 0 ms^{-2}. The 1*g* measured by the accelerometer on the tabletop is in fact measuring the reactive force of the table against gravity.

This information is important when considering the use of an accelerometer upon an athlete's limb where the angle of the limb to gravity is unknown. This angle can be calculated if it is known that inertial acceleration is zero, but otherwise, the measured acceleration along an axis will be a sum of the component gravitational and inertial accelerations. However, because the accelerometer is experiencing the reactive force to gravity, it will have a directional value contrary to what one might expect. This is best understood by remembering how the accelerometer works; Figure 3-1 in section 3.2.1 shows how the deflection of the central mass alters the capacitance of the sensing elements of the accelerometer, thus

changing the sensor output. Figure 3-7 illustrates the deflection of the central mass in an accelerometer in the two scenarios previously introduced, and in two further scenarios: acceleration and deceleration upon a flat surface (i.e. perpendicular to gravity).

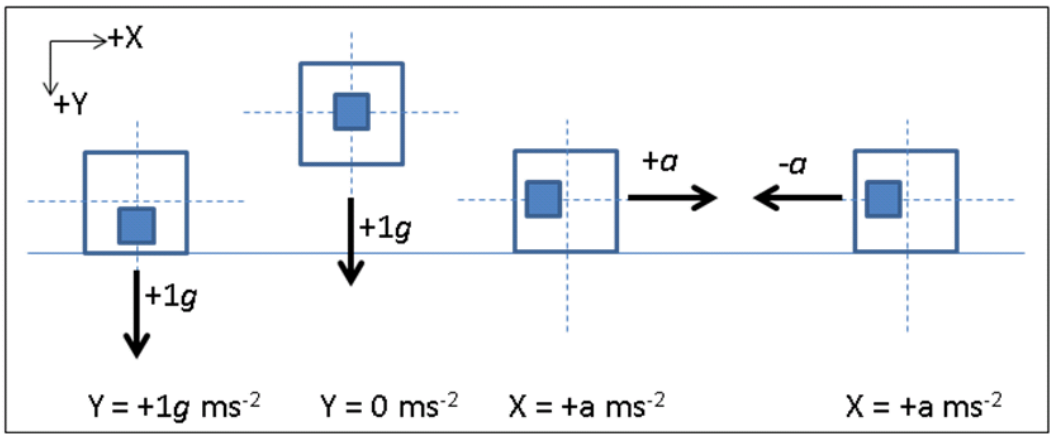

Figure 3-7: Deflection of accelerometer central mass to different accelerations

For clarity, the deflection of the central mass is shown only for a single axis (scenarios (c) and (d) would also exhibit deflection of the mass in the +Y direction)

Thus, an accelerometer attached to a body segment (thus not in freefall), but subjected to an upwards inertia *a* ms^{-2}, would give a reading on the Y axis = 1*g*+*a* ms^{-2}, as the reactive force to gravity, and the inertial acceleration would be acting in the same direction.

Knowledge of this behaviour will be important when the acceleration of nodes upon the athlete's body is considered in chapter 5.

To accurately monitor the acceleration, velocity and displacement of a body, six degrees of freedom is normally required. This needs more than a 3-axis accelerometer (which measures only linear acceleration). A 3-axis gyrometer is

also necessary to determine the 3 axes of rotation. Depending upon the application the full six degrees of freedom might not be required. Alternatively the freedom of the body might be constrained such that the number of acceleration or rotation axes is limited. Other sensors might be utilised to aid in the measurement (e.g. magnetic or light sensors to detect the body at certain points in space).

3.3.2 sEMG

Because of the extremely low level of measured sEMG signals at the electrode, removal of noise or the mitigation of noise in the measurement process becomes a vital consideration.

Ambient noise originates from mains electrical cable emissions (in the UK at 50Hz), but other electromagnetic radiation emanates from radio and television emissions (noise from these sources is not limited solely to their transmission frequencies), computers, and lighting. Any equipment that utilises an alternating frequency, unless properly shielded will radiate unwanted noise at various frequencies. The human body behaves like an antenna, and thus ambient noise is detectable on the surface of the skin and will therefore form a component of the measured sEMG signal. The amplitude of this noise signal might be significantly larger than the desired sEMG signal, and at a frequency within the bandwidth of the sEMG signal; this precludes the use of filtering to remove it. The cables connecting the electrode to the measurement circuitry are also surrounded by this ambient noise, and as the cables move through this electromagnetic noise, they too act as an antenna (since one end is connected to a high impedance source – the electrode – and the other to the high impedance input of the

amplifying circuitry). Out-of-band noise can be filtered out, but in-band noise needs to be avoided through judicious circuit design or differential measurement techniques.

Motion Artefacts are another significant source of interference. This takes two forms: electrode-skin junction motion artefacts, and cable motion artefacts. Electrode-skin junction artefacts are caused by the movement of the electrode during muscle contraction. This causes fluctuations in the skin-electrode impedance which generates an undesirable AC voltage potential between DC and 20Hz. These can be reduced in part through the use of conductive electrolytes to improve contact with the skin or skin abrasion to remove dead skin cells from the upper dermis which would present a higher impedance. Cable motion artefacts are caused again through movement during muscle contraction with a spectral range between DC and 20Hz (De Luca 2002).

Muscle crosstalk is another form of interference. This is caused by the measurement electronics picking up muscle activity from distant muscles. Crosstalk from adjacent muscles is a real problem – as much as 17% of electrical activity from nearby muscles can be picked up by electrodes on the muscle of interest (De Luca 1997).

Finally, there is electrical noise (such as thermal, shot and flicker noise) inherent to the electrical components. As such, any component used in the processing of the signal will add its own noise. This can only be minimised through the use of high quality components and good circuit design (De Luca 2002).

Noise sources such as ambient noise and muscle crosstalk present themselves approximately equally to any electrode placed upon a particular muscle. As such, if the sEMG signal is measured at two electrodes, and those signals subtracted, most of the common noise can be removed and the difference between the two differing sEMG signals amplified. This subtraction of the two signals is performed with a high performance differential amplifier.

The motion artefacts both appear between DC and 20Hz, outside the range of sEMG signal frequencies and can be minimised by electrode design, and removed by high-pass filtering. Unwanted frequencies above the EMG frequency distribution can be removed through low-pass filtering.

A simplified block diagram of the measuring electronics required for sEMG is thus shown in Figure 3-8.

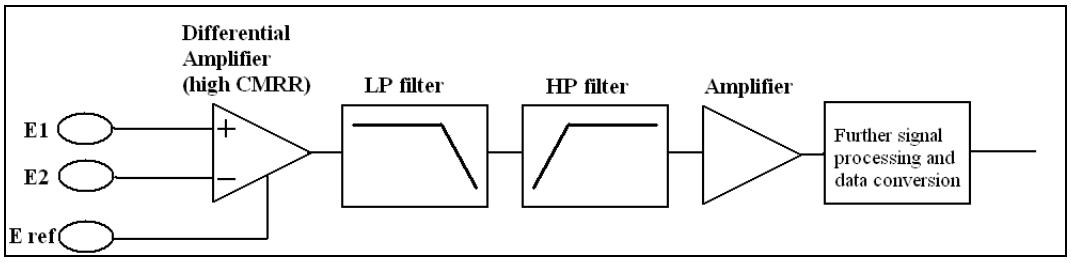

Figure 3-8: Simplified block diagram of front end measurement electronics for sEMG

The shape and area covered by the electrode surfaces determines the number of muscle fibres within the detection volume contributing to the detected signal, and hence the overall amplitude of the sEMG signal (Kamen and Gabriel 2009). The separation of the two measurement surfaces (often housed within the same

electrode casing) determines the frequency distribution (both bandwidth and shape) and also the amplitude of the signals. The minimum distance between the two electrodes is limited due to electrical shunting of the signal through sweating (a real possibility during sports monitoring) (Kamen and Gabriel 2009). This would reduce the amplitude of the signal, thus degrading the signal-to-noise ratio. The amplitude of the signal output from the differential amplifier is directly proportional to the separation between the two measurement surfaces since the differential amplifier will pass and amplify the difference between the two signals presented at its inputs and reject signals that are common to both. Thus increasing the separation might initially seem attractive. However, this will increase the overall surface area of the electrode, and alter the filtering characteristics of the electrode arrangement.

Typical electrode arrangements are either two bar electrodes, 10mm in length (and approximately 1mm wide) with a separation of 10mm, or two circular electrodes 1mm in diameter separated again by 10mm (Figure 3-9) (De Luca 2002). Orientation of the electrode should be along the longitudinal midline of the muscle such that similar muscle fibres intersect both electrodes. This orientation is critical as muscle tissue is anisotropic.

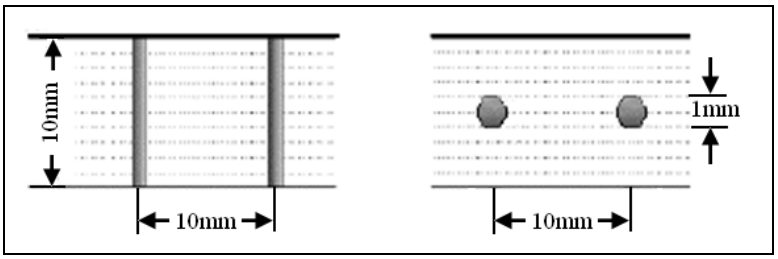

Figure 3-9: Bar and circular configurations for differential electrode arrangement *(De Luca 2002)*

A third electrode is used to provide a reference point on the body. This reference electrode provides the common reference for the differential amplifier. It should be on electrically neutral tissue to minimise contamination of the desired EMG signal, and should therefore be placed on a bony prominence (e.g. the elbow if muscles within the arm are being monitored) (Kamen and Gabriel 2009).

A final consideration regarding the electrodes is that the differential amplifier might be placed as close to the electrodes as possible. Recent advances in printed circuit board techniques and miniaturisation of integrated circuits have lent to the adoption of active electrodes where the differential amplifier is placed upon the electrode itself (De Luca 2006). This eliminates the problem of long cabling between electrode and measurement circuitry where both ends of the cable are at a high impedance that facilitates the pick-up of electromagnetic noise. With the differential amplifier at the electrode, any cabling after this circuit element is at a low impedance (since the output impedance of the differential amplifier is ideally zero) and electromagnetic interference due to pick-up in the cabling is greatly reduced.

The differential amplifier amplifies the difference between the sEMG signals presented at the two electrodes) whilst rejecting the common unwanted noise at each electrode, and is usually implemented in sEMG by a high performance instrumentation amplifier (IA). Where a standard op-amp has its closed-loop gain determined by external resistors between output and inverting input, the IA uses an internal feedback resistor network isolated from the two inputs. One resistor in this resistor network is placed external to the IA for gain selection. The IA is thus designed to have two balanced, high impedance inputs (typically $10^{12}\Omega$ and 5pF) (De Luca 2002) with very low input bias currents of only a few nano-amperes.

Output impedance, like op-amps is typically only a few milli-ohms. The most important quality of the IA is its common-mode-rejection-ratio (CMRR) which gives its ability to amplify any differential signals presented at the inputs whilst rejecting any common signals such as noise. It is defined as the *ratio of the differential gain A_D to the common mode gain A_{CM}.* The CMRR of an IA should be better than 80dB (Kamen and Gabriel 2009).

$$CMRR = \frac{A_D}{A_{CM}} = A_D\left(\frac{V_{CM}}{V_{OUT}}\right) \qquad 3\text{-}10$$

A_{CM}: Common-mode gain

A_D: Differential gain

V_{CM}: Common-mode voltage present at the inputs

V_{OUT}: Output voltage present when only a common-mode voltage is applied to the inputs

After the front end sEMG circuitry has sufficiently amplified and filtered the signal, the remaining signal contains a range of frequencies. Analysing the distribution of these frequencies might be useful for some applications. For example, Constable et al (Constable et al. 1994) looked at the frequency information in the EMG signal in order to analyse muscle action (soleus, vasti, gluteus maximus, hamstrings) during high jumps. However, this requires a high sampling frequency during the digitisation process; for sEMG signals with spectral components up to 500Hz, a sampling frequency of at least 1000Hz is required to perform Nyquist sampling (the Nyquist theorem requires that a sampling frequency of at least twice the highest frequency component of the input signal is used). If Nyquist sampling is not obeyed, then distortion through aliasing occurs (the frequencies of the input signal are not preserved) (De Luca 2001).

If the overall shape of the envelope of the signal is sufficient, then rectification of the signal, either by eliminating negative values (half-wave rectification) or by inverting all negative values such that the entire signal becomes positive (full-wave rectification), and then performing an averaging process will yield useful information.

The averaging process can be performed either prior to digitisation through analogue smoothing of the rectified signal, integration of the signal in the analogue domain, or digitally through digital signal processing. The latter has an advantage over simple analogue integration as a moving window can be employed in the integration, thus obtaining a time-varying average.

$$\left|\overline{s(t)}\right| = 1T \int_{t}^{t+T} \left|s(t)\right| dt \qquad 3\text{-}11$$

If the time, T, over which the integration takes place is sufficiently large, it will result in a smoothly varying measure of the signal as a function of time, similar to choosing the correct capacitor to perform a smoothing of the rectified signal.

The root-mean-squared (rms) value of a signal can provide more information because it measures the energy in the signal (Kamen and Gabriel 2009).

$$rms\{s(t)\} = \left(1T \int_{t}^{t+T} s^2(t)dt \right)^{1/2} \qquad 3\text{-}12$$

Analogue integrated circuits are now available which can perform this rms signal processing.

The benefit of removing the high frequency components to the signal to leave information regarding the force-time relationship prior to digitisation is that a far lower sampling frequency can be employed. This lowers the computational overhead of the system.

Many factors affect the signal monitored at the electrode, and these can be divided into three main groups: Causative, intermediate and deterministic (De Luca 1997).

Causative factors, which affect the signal measured directly, can be further subdivided into extrinsic and intrinsic factors. Extrinsic factors are influenced by the measuring apparatus – the size and configuration of the electrode, and its placement and orientation upon the muscle. Placement will affect the amplitude and the frequency composition of the signal greatly. Intrinsic factors include the number of active motor units, the amount and composition of subcutaneous tissue, variations in the muscle, and blood flow.

The intermediate factors are influenced by the causative factors. For example, the configuration of the electrode will influence the band-pass filtering nature of a differential electrode configuration and the spatial filtering due to the relative

positions of electrode and muscle. The electrode arrangement will also determine the detection volume of the electrode. Other factors here include the superposition of action potentials in the signal from the various motor units, and the possibility of crosstalk from other muscles contaminating the signal.

Deterministic factors, influenced themselves by intermediate factors, directly influence the information contained in the measured signal. These include the number of motor units measured that will contribute to the signal, the motor unit firing rate and the amplitude and duration of the action potentials contributing to the signal.

3.4 System Design

A number of decisions have been made concerning the system design. Some design features were determined through the selection of wireless standard and sensors. Thus nodes wirelessly communicate using Zigbee radios, and all contain tri-axial accelerometers, with two further analogue input channels for sEMG. The following two sections describe the physical and power-related considerations that have been employed at the design stage of the project.

3.4.1 Physical Considerations

Node size has been kept to a minimum to reduce their impact upon the oarsman. However, for prototyping, small size can be problematic from the point of view of debugging. Additionally, whilst printed circuit board manufacture could be outsourced, all components would be soldered by hand, limiting the use of very small package outlines. Ball grid array component packages were avoided, as were components with pin pitches closer than 0.8mm (this is the pin pitch of thin quad flat-pack (TQFP) packages). Double-sided circuit boards were used to reduce size, but multi-layer boards were avoided as they reduce accessibility to all signal paths in the circuit for debugging purposes. As the radio module is by far the largest single component, the main circuit board for a node was designed to follow the approximate dimensions of the chosen radio module. In order to keep the size and weight of the module to a minimum, components required for

the development process only were placed upon an auxiliary board to which the node could be connected for programming, debugging, battery charging, etc.

Batteries were chosen to allow at least an hour lifetime at the estimated power consumption of a node. Power consumption was minimised through use of the standby power modes of the Zigbee radios when not transmitting or listening to the network. Small form-factor batteries were used.

Node placement during experimentation was chosen to maximise the relevant information gained from the fewest number of nodes. Thus all body nodes exploit both acceleration and sEMG data.

e.g.

- acceleration at the hand would yield useful information in rowing, but sEMG data here is less important. However,
- acceleration at the elbow, coupled with sEMG of the biceps brachii would exploit both sensor inputs within one node.

It was decided that it should be possible to collect at least an hour of data at the central coordinating node to allow data from training sessions to be analysed offline.

3.4.2 Power considerations

The power consumption of the nodes was minimised through a number of techniques. All circuitry was designed to operate at the lowest possible supply voltage; suitable components were sourced which operate at 2.5V single supply.

The radio is the single component which consumes the highest power, at its greatest whilst transmitting. Zigbee has been chosen as the most suitable radio standard in part because of its power consumption profile; it can be placed into sleep mode for extended periods to extend battery life, and can be scheduled to wake to listen to transmitted messages or to upload data. The system firmware was thus designed to allow nodes to enter periods of extended sleep, waking for time synchronisation messages and for interrogation and uploading of data.

Data was crudely compressed to reduce the amount of raw data which will be transmitted. For example, where a 10-bit analogue to digital conversion was employed to sample the sensors, the two most significant bits of data from four samples could be combined into one byte, thus reducing the data overhead to five-eighths of the uncompressed data-size. Data was time-stamped by a numerical value corresponding to the number of samples from t=0 rather than a absolute time value in order to further reduce the overhead of data that needs to be transmitted. The timestamp also identifies the node which is transmitting the data.

The sample rate employed by the system is variable and can be set centrally and transmitted to the network. A sample rate of 50 samples per second was selected as this is adequate to capture all data of interest. It is important to keep the sample rate as low as possible to minimise the power consumption. An increased sample rate both directly increases the power consumption of the ADC and processor used by the node, but also significantly increases the amount of data that needs to be processed and transmitted. This single factor influences the hardware of the sEMG circuitry. Prior to digitisation of the sEMG signal, the high frequency components are removed to leave the envelope of the signal.

Prior to experimentation, it is difficult to determine exactly what data processing is required. As such, feature extraction or the transmission of processed data is limited. Raw data is therefore transmitted to the central node. However, all offline processing of data is performed with a view to implementing such processing, where possible, at the individual nodes in future. The data processing is therefore designed to be computationally light. Data processing in the sensor nodes again impacts upon the power consumption of the node. This has to be weighed against the power saving yielded by the transmission of less processed data. Computationally light data processing will also facilitate future implementation of real-time processing of results for instantaneous benefit to the oarsman. A block diagram of the system is shown in Figure 3-10.

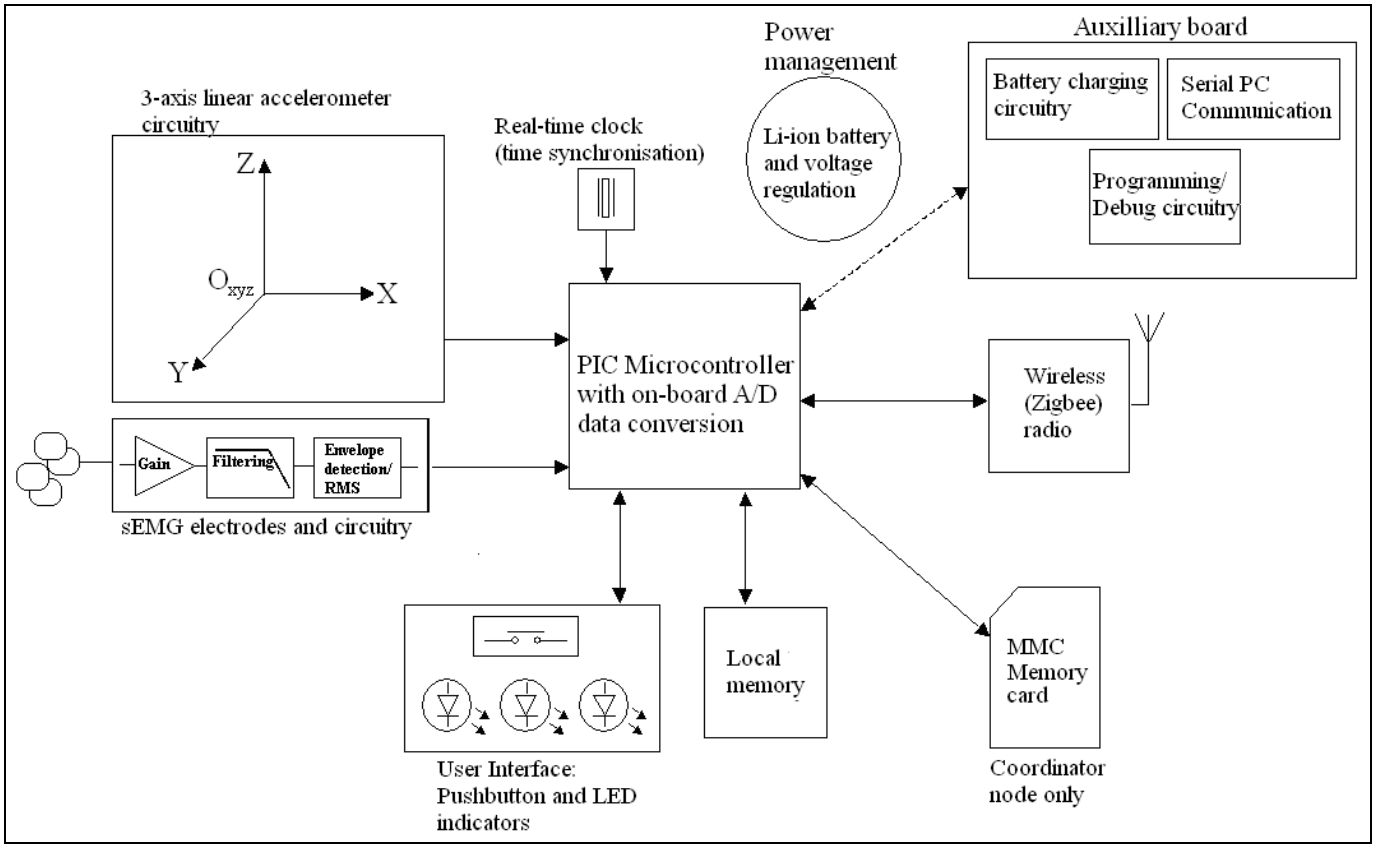

Figure 3-10: Block diagram of Wireless BSN System requirements

3.5 Chapter Summary

Useful information that might be extracted using a wireless BSN with respect to an oarsman, crew and boat has been considered. Accelerometers and sEMG have been chosen from a subset of sensors reviewed which together should maximise the relevant information to be gained from the smallest number of sensors. A number of system design decisions have been made which best highlight the benefits of a wireless data collection system, allowing a broad requirements specification to be made for both hardware and software elements of the system.

4 System Development and Testing

The design and development of the wireless BSN comprises two main areas: hardware and firmware, where firmware describes the software that runs upon the microcontroller controlling the circuit. The main system hardware (excepting sensor circuitry) is predominantly digital in nature, centred around a microcontroller which interfaces all peripheral devices. The peripheral circuitry includes the Zigbee radio, sensor circuitry, and user interface.

4.1 Chapter Organisation

This chapter describes the development of the Wireless BSN system, based upon decisions made in the previous chapters. The system design will be described, and the results of tests upon sub-circuits, firmware and the overall system reported. The chapter is split into two sections: hardware and firmware.

4.2 Hardware Development

The Wireless BSN has one Zigbee coordinator node, which can be mains- or battery-powered, to control the network. This has the facility to interface to a laptop PC, and a memory card for data storage. Five sensor nodes have been fabricated with which to test the system. These are battery-powered, and designed to be small (within the practical limits of prototyping). These 6 nodes are essentially identical; the coordinator has all the hardware functionality of the sensor nodes, with the additional peripheral elements for central data storage and communication with a PC.

4.2.1 Microcontroller and support peripherals

A Microchip PIC18LF4620 microcontroller was chosen to run the developed firmware upon each node. Microcontrollers have the benefit over microprocessors of a range of on-board memory and peripherals which can reduce the number of external devices required by the system.

The PIC18LF4620 (Microchip Technology inc) is a highly flexible micro-controller, with 5 input/output ports which can be configured as a combination of up to 33 digital inputs or outputs, or up to 13 analogue inputs. It has a 13-channel 10-bit on-board analogue-to-digital converter (ADC), 20 interrupt sources to service both hardware and software tasks, and four on-board timers. It can be used in several different oscillator configurations, including an internal oscillator which can generate a clock of up to 32MHz. It supports several different serial communications protocols for interfacing to external peripherals such as the

Zigbee module, external memory, and PC. In addition to 64KB of program memory and 3968bytes of data memory, it has 1024bytes of data flash memory. It also has a hardware multiplier – this allows multiplication operations to be performed in one instruction cycle, greatly improving the efficiency of the code. A more detailed summary of the features of the chosen microcontroller can be found in appendix B.1.

Additionally the 'LF' series of PIC microcontrollers are optimised for low power use and can be operated on supply voltages as low as 2V and use "*nanoWatt*" technology, incorporating a range of features that can significantly reduce power consumption during operation. Microchip microcontrollers are programmed using their MPLAB Integrated Development Environment (IDE), and this also allows flexible simulation of the code prior to in-circuit programming and debugging, allowing the monitoring of registers, program step-through and interaction with circuit inputs/outputs during code development. The Microchip C compiler compiles code efficiently (minimising the number of clock cycles required to execute code) and allows the developer to write in the higher level language of C. Ultimately this also makes the code more portable if an alternative processor was chosen in future.

Another benefit of the Microchip PIC microcontrollers is that Microchip also fabricate a Zigbee module, containing their MRF24J40 Zigbee IC, and supply a licence-free Zigbee protocol stack upon which the system application code can be built.

The use of the PIC18LF4620 means that aside from the sensor circuitry and Zigbee module, the remaining support peripherals are minimal. This includes the power supply circuitry, comprising the battery – a 3.7V 150mAh Lithium ion (Li-

ion) rechargeable battery – and a precision voltage regulator to regulate the supply to 2.5V. All circuitry in the sensor nodes have been designed to operate at 2.5V. The battery measures only 25x20x4mm and weighs only 3.7g. The quoted nominal battery capacity means that a battery-powered node should operate for well over an hour, as 150mA greatly exceeds the maximum power consumption of a sensor node. Further discussion of the power consumption of the node and battery longevity is made in section 4.3.6. A battery charging circuit, comprising a bank of 5 Microchip MCP73831 Charge Management Controller ICs was also designed and fabricated to allow node batteries to be recharged. These provide the necessary power profile for the Li-ion batteries to charge; first a constant current is supplied until the battery voltage reaches the regulation voltage, and then a constant voltage is supplied until average charge current diminishes below a percentage of the programmed charge current. Further details can be found in appendix B.1.

The user interface has been designed to be simple and unobtrusive, as once the nodes are connected to the network they are controlled by the coordinator node via wireless communication and require no user input. Thus the user input comprises a power switch, and one push-button switch. This can be used in conjunction with time-dependant push-to-select input to allow node calibration or function selections to be made. Three surface mount LEDs allow visual output to indicate which function is selected.

Push-button input:

- Press-and release 300ms<duration<2sec)
- Press and hold-short (2secs<duration<5secs)
- Press and hold-long (duration>5sec)

Three LEDs will allow 3^2=8 visual indicators, this range being extended using flashing indication.

Whilst clock generation for the execution of the firmware within the nodes is internal to the microcontroller, a 32.768KHz precision external watch crystal is used in conjunction with one of the on-board timers to generate a real-time clock. This is necessary as the clock frequency used to execute the firmware is high (32MHz) and not conducive to the generation of a real-time clock where seconds (or at most coarse fractions of seconds) are required.

Whilst sensor input for the Wireless BSN is restricted to tri-axial accelerometer and up to two sEMG channel per node, the additional analogue inputs are brought out to external pads so that additional sensors could be added. An additional connector is used to allow programming and debug circuitry to be contained upon an auxiliary board. This means that only circuitry essential to the running of the node within the wireless BSN is required on the main circuit board, and thus the impact upon the size of the node is minimised. The coordinator node which does not have to be minimal size contains this circuitry on the main circuit board. The circuit schematics for the microcontroller and peripheral circuitry are included in appendix B.1.

4.2.2 Zigbee Module

At the time of system design and component selection choice of Zigbee radio module was more restricted than the already established Bluetooth (pre- 4.0 standard) market. Zigbee development was still relatively in its infancy, and

manufacturers were just beginning to release evaluation boards and early modules for purchase.

The chosen Zigbee module needed to be compliant with the IEEE 802.15.4 standard, and the specific functionality of the Zigbee module and its associated protocol stack needed to be evaluated for suitability. Many modules have been developed specifically for the cable-replacement market (although this is the function for which Bluetooth is targeted), and as such do not have complete networking functionality.

As previously stated, the radio module identified for the application is the Microchip Zigbee module based around Microchip's own Zigbee RF IC, the MRF24J40. The MRF24J40 RF transceiver radio is 802.15.4 compatible, operating in the 2.4GHz frequency band. The Zigbee module has an on-board patch antenna (printed into the metal substrate of the circuit board which provides about 200feet (60m) of line-of-sight range (Bible 2008).

The Microchip Zigbee radio module has typically 22mA current consumption in transmit mode, 18mA in receive mode, and typically 2µA in sleep mode (Microchip Technology inc 2010). With a supply voltage of 2.5V, this corresponds to power consumptions in the three considered modes of 55mW, 45mW, and 5µW respectively. Clearly the greater the time the Zigbee module can be placed in Sleep mode, the lower the power consumption and the greater the life of the battery. The ratio between active and idle radio time is thus a vital consideration. This is an important issue as it allows consideration of the power savings that may be made in the sensor node of the wireless BSN, as sensor nodes are usually battery-powered and need to consume as little power as possible in order to lengthen battery life. This is covered in detail in section 4.3.6.

The Zigbee module contains all of the necessary supporting peripheral circuitry for the radio to function, and interfaces to the microcontroller in the host system that runs the application firmware via a 12-pin header connector. This connector allows the hosting system to provide power, reset and wake signals to the MRF24J40 radio, and to receive hardware interrupt from the MRF24J40 radio to indicate the reception of data. Communication between the Zigbee radio and the host system is via Serial Peripheral Interface (SPI) bus.

The SPI bus on the microcontroller is shared between the Zigbee module and external memory ICs. SPI communication is suited to reading and writing streams of data between devices making it ideal for writing and reading large sections of sensor data to and from memory. SPI devices operate using a full-duplex Master-Slave relationship and have three communication lines – serial-in (SDI), serial-out (SDO) and serial-clock (SCK). Where more than one slave device is connected to a Master, then chip-select lines (/CS) are also necessary to enable the slave device with which the master is to communicate.

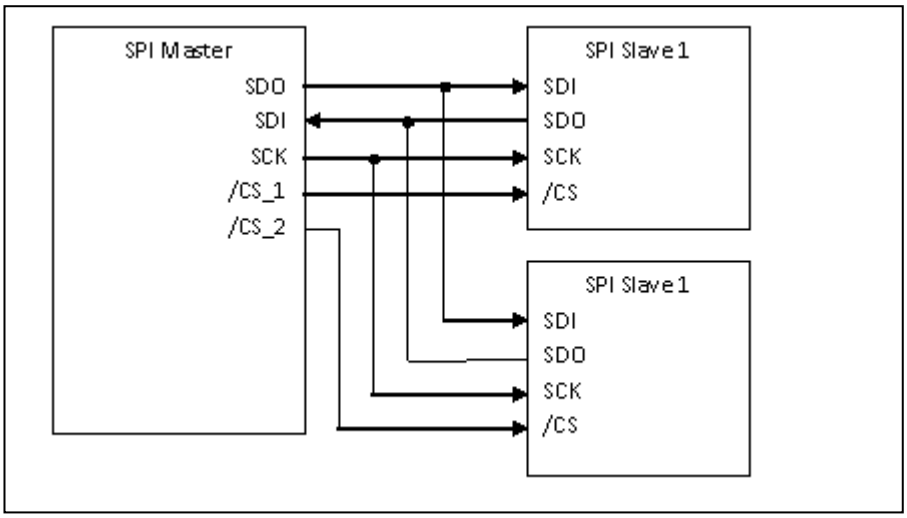

Figure 4-1: Master-Slave SPI communication configuration

Allowing communication between master and several slaves

Local data storage upon sensor nodes is made upon serial flash memory ICs, and central data storage upon the coordinator node is made upon an MMC/SD card. Both of these employ SPI communication for the transfer of data, and share the SPI bus with the Zigbee module. The memory design is discussed further in the next section (section 4.2.3).

4.2.3 Memory design, data transfer and related power considerations

Sensor data is stored locally on the sensor nodes upon serial flash memory ICs, and periodically uploaded in bursts to the coordinator node for central data storage or transfer to a laptop PC. The capacity of the local memory dictates the minimum frequency with which this data needs to be uploaded. By transmitting the data in bursts, the Zigbee radios can be put into low power sleep mode for extended periods, thus conserving power. Because the Zigbee radio standard is designed to keep latency at a minimum, it allows the radio to spend a lot of time in sleep mode, becoming active only when required, without wasting valuable time re-establishing its connection with the network. Once the network of sensor nodes has been established through the node association process, the coordinator conveys to each node an individual upload interval (IUI) so that the sensor node can put its radio to sleep and wake only to listen for interrogation from the central coordinating node with data upload requests, and also periodically for time synchronisation.

Other factors impact upon the ratio between active and sleep of the Zigbee radio. For a given capacity of local memory, the time taken to fill the memory is related to the number of sensors, the resolution with which the sensor data is digitised, and the rate with which these samples are taken. The time taken to transmit the data is determined by the information rate of the radio standard and the processing overhead of the local microcontroller. Whilst the raw data rate for Zigbee is 250kbps, the information rate is about 128kbps due to the header information that is added to the frame payload (the data you wish to transmit) that

is necessary to ensure correct delivery of the data to the correct destination, to identify the source, etc. The actual rate of data transmission is significantly lower again dependent upon the other tasks that the microcontroller of the node has to accomplish, and the instruction cycle time.

It is possible therefore to derive a relationship between these variables to determine how much memory is required locally to a sensor node, how much memory is required to store data centrally at the coordinator, now many nodes and how many sensors per node could be accommodated by the wireless BSN.

The Wireless BSN has been designed to accommodate 5 sensor inputs per sensor node, 10-bit resolution of the on-board ADC, and a chosen sample rate of 50 samples per second (although this is a programmable parameter). The system should be able to store an hour of data centrally upon the coordinator node if data is not also being transferred periodically to a laptop PC.

The first variable to determine is the number of bytes of data that need to be stored every time the sensors are sampled. This is calculated from the resolution of the ADC that digitises the sensor data, the number of sensors, and any bits/bytes pertaining to the timestamp and node identification such that upon arrival at the coordinator, the correct data can be associated with the correct node, and the point in time at which the sample was taken determined.

$$NS = \frac{(NbS)(R)}{8} + (TS) \qquad bytes \tag{4-1}$$

NS: NodeSample
NbS: Number of Sensors
R: Resolution
TS Time stamp and Node identification

In order to time-stamp each *NodeSample* of data with a unique time-code for up to an hour of data, 18bits of data is required as given in [4.2] and [4.3]. A binary number can be used to identify the nodes (thus 3 bits would be required to identify up to 8 nodes)

$$\text{NS/hour} = (SR)(D) = (50NS/\sec).(60).(60) = 180K \qquad 4\text{-}2$$

SR: Sample rate

D: Duration

Thus, to uniquely identify each *NodeSample*:

$$TS = \log_2 180\text{K} + 3 = 21 \ \ \text{bits} \qquad 4\text{-}3$$

This is equivalent to *3bytes*, although 3bits are unused for 1hour of sampling.

Combining the information determined from [4.1] and [4.3], we can determine that 10 bytes of data are stored for every *NodeSample*. This is assuming that the data compression described in section 3.4.2 of chapter 3 is implemented (this is done simply by combining the 9th and 10th bits of four 10-bit samples into a single byte, the reverse process being performed upon processing of the data).

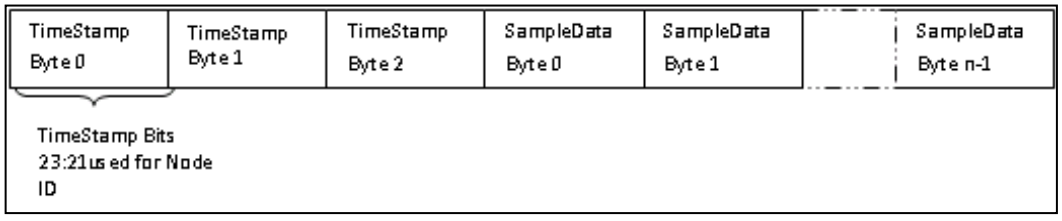

Figure 4-2: Format of a *NodeSample*

First 3 bytes consist of 3-bit Node ID and timestamp information, remaining bytes are one sample of data from all node sensor inputs

Local memory is divided into two partitions: a low and high memory section (Memory_L and Memory_H). The time taken to fill a bank of memory is the Section Storage Time (SST). One memory bank is uploaded to the central coordinator node whilst the other is filled (Figure 4-3).

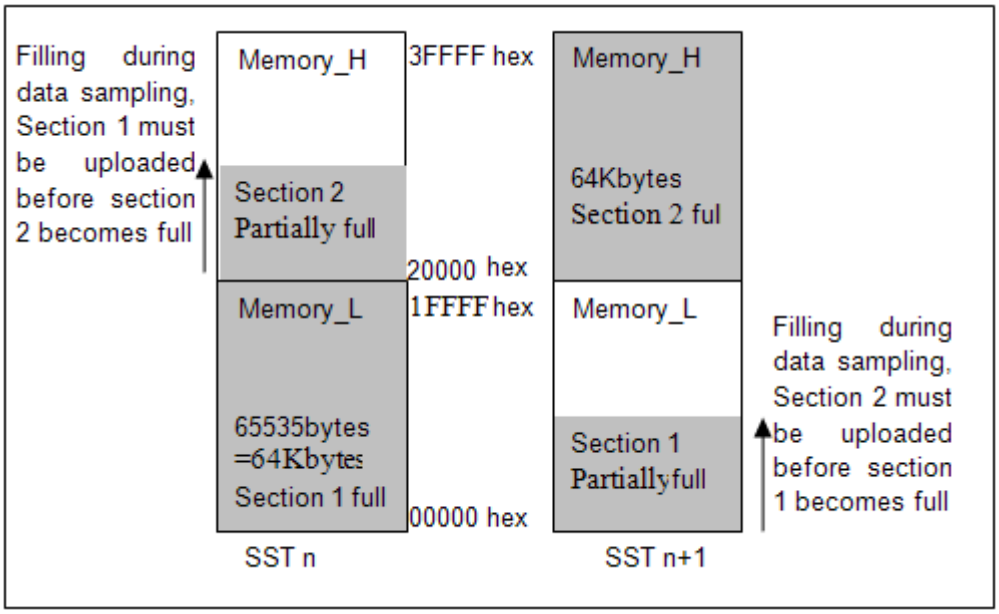

Figure 4-3: Memory Map of Local data storage, and upload

Memory map divided into two sections, one is uploaded whilst the other is being filled

The size of the memory map is dictated by the amount of memory dedicated to data storage upon the sensor nodes. The amount of local memory designed into each sensor node will impact upon how often the data needs to be uploaded to central storage in the coordinator node. A very small amount of memory, perhaps that available on-board the microcontroller, would require a frequent upload of sample data. Serial memory ICs can be written to using only a few input/output and control lines, saving size upon the sensor node (parallel data writing would require more input/output pins, generally increasing the size of the component

package and requiring increased connections to the microcontroller, whose routing would also increase the size of the circuit board).

Two 1Mbits serial EEPROMs (25LC1024) have been used for the local data storage upon each sensor node (1Mbits equates to 131072bytes). These are written to and read using the SPI serial communication standard (detailed in section 4.2.1), and shared with the Zigbee module. As slave device to the micro-controller's master, the 25LC1024 decodes instructions that are sent in exactly the same way as data. These instructions include: read, write, page erase, chip erase and others. The use of instructions, sent in the same manner as data, minimises the number of pins that the device requires. The 25LC1024 can be placed into low power consumption mode when not in use by taking the chip select line /CS HIGH (Standby current consumption <20μA), and into a deep power down mode when the DPD (deep power down) instruction is first written to the device before taking /CS HIGH. In this mode the current consumption is less than 1μA. Current consumption in read or write mode is less than 10mA. The circuit schematic can be found in appendix B.1.

The time taken to fill one memory IC is determined from the memory capacity, the *NodeSample*, and the sample rate.

$$SST = \frac{LM}{(TS + NS)(SR)} = \frac{(131072).}{(10).(50)} = 262\,\text{sec} \qquad 4\text{-}4$$

SST: Section storage time

LM: Local memory

The transmission rate can also be used to determine the upload time (UT) of a section of data, from which the active-to-sleep time can ultimately be determined.

$$UT = \frac{LM}{TR} \quad 4\text{-}5$$

TR: Transmission rate

This will also dictate the maximum number of nodes which can share the Wireless BSN, since all nodes will need to upload their data, in turn, in the time it takes to fill one section of memory.

$$Nodes = \frac{SST}{UT} \quad 4\text{-}6$$

The upload pattern is summarised in Figure 4-4.

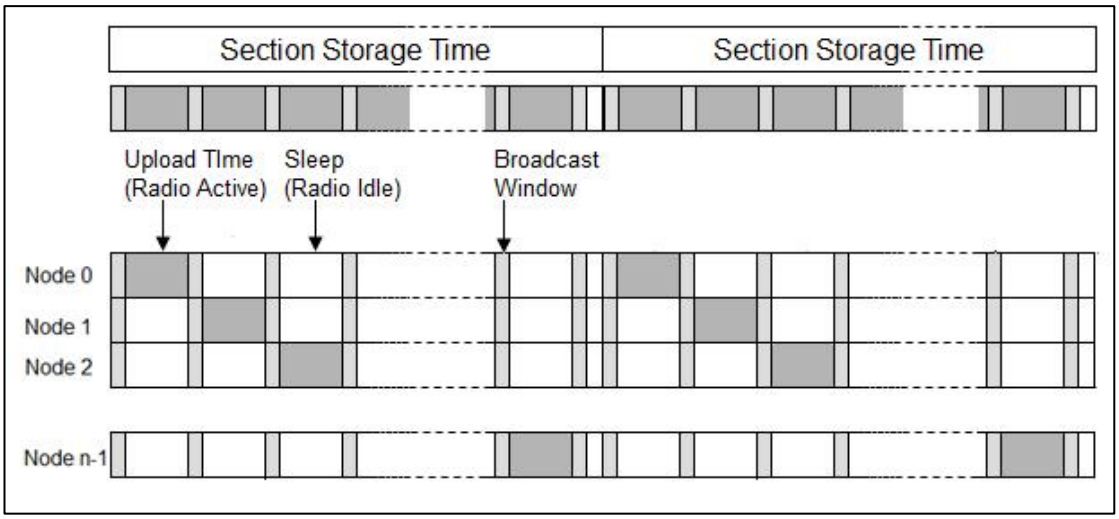

Figure 4-4: System upload pattern

Nodes upload data during their allocated Individual Upload Interval. Nodes wake for their upload interval and for scheduled Broadcast Windows for synchronisation messages and other system control messages

Clearly, whilst doubling the amount of local memory would double the size of a section of memory, and double the length of time available for upload, since there is now double the data to upload, the number of nodes allowable remains

constant without changing other variables such as sample rate, number of sensors/node, or transmission rate.

A further consideration is to ensure that all sampling of the wireless sensor nodes is kept synchronized, and that they also maintain synchronization with the coordinating node so that they wake for their individual upload interval. This can be achieved with periodic time synchronisation messages sent during scheduled Broadcast Windows, from the coordinating node to the rest of the network. This has been discussed previously in chapter 2, section 2.5.3. The sensor nodes in the network thus switch their radios to active listening mode for a brief period (the Broadcast Window) to ensure that they remain in sync. This will be discussed in more detail in section 4.3.4.

Finally, the central storage requirements can be calculated knowing the number of nodes in the system, the size of a node sample and the maximum duration of sampling.

$$CDS = (SR).(D).(NS).(N) \qquad 4\text{-}7$$

CDS: Central Data Storage
N: Number of nodes

Thus, for the system designed, 8789KB is required for one hour of data collection. The central data storage could take many forms. Storage directly upon a laptop PC is one attractive option, making the data readily available for processing. However, given the relatively hostile environment for which this application is intended, and the need for utmost portability, an intermediate option is removable data storage. Flash memory cards provide a flexible solution, allowing the memory capacity to be upgraded to meet application. From a size

standpoint, as well as ease of integration into the hardware and software of the design, an MMC/SD memory card has been chosen for this application. The SD (Secure Digital) card employs a proprietary communication standard that is not freely available, but its predecessor, which uses the same physical form-factor is the MMC card, which employs the SPI communication standard to function. This predecessor has reduced functionality, but serves perfectly as a mass storage device whilst maintaining portability and flexibility of a removable card. The MMC card requires no extra peripheral circuitry aside from the card slot. The connections for this are shown in appendix B.1.

4.2.4 Accelerometer circuitry

MEMS accelerometers are fabricated by a number of manufacturers, including Analog Devices and Freescale Semiconductors. Similar in design and specification, there is little to choose between them. Of more interest is the format of the output. This can take the form of an analogue voltage output proportional to the acceleration experienced along a particular axis or PWM (pulse width modulation) digital output. The micro-controller can accept both analogue or PWM inputs, but for reasons of simplicity (the sEMG input to the microcontroller is also analogue), and the number of available analogue inputs verses limited PWM inputs, the analogue output devices were selected. The MMA7060Q Freescale device was chosen due to the ability to select the sensitivity of the accelerometer (via two programmable inputs) and because it has the option to be powered down into a sleep mode to conserve power when not in use.

The Accelerometer requires very little peripheral circuitry as much of the signal conditioning (conversion from differential capacitance to voltage output, filtering

and amplification) is performed onboard. The selectivity can be altered through the two control lines g-select1 and g-select2, allowing the sensitivity of the accelerometers to be varied such that the achievable range is between 1.5g-6g, A range of 2g was selected.

The internal filtering, limiting the bandwidth to 350Hz means that aliasing of the output is avoided providing the sampling frequency of the A/D converter is greater than 700Hz. As the sample rate of the Wireless BSN system is far less than this, a simple passive R-C low pass filter is added to each output to further restrict the bandwidth to match the sample rate of the ADC. The schematic circuit for the accelerometer circuitry is shown in appendix B.1.

4.2.5 Accelerometer circuit testing

The primary evaluation to make concerning the accelerometer circuitry is the sensitivity. Recall that the output to the accelerometer is ratiometric. The accelerometers are supplied by the Voltage regulator, giving a fixed and reliable reference for both the accelerometer and the ADC conversion of the accelerometer output. With the accelerometers set to a sensitivity of 2g, the sensitivity calibration was made by slowly rotating each accelerometer through 360^{o} about all three of the active axes. This generates a sinusoidal output of 2g peak-to-peak amplitude centred about 0g. Thus the greatest and least accelerometer measurements on each axis correlate to +1g and –1g allowing the sensitivity of each axis, for a particular sensitivity setting and supply voltage, and the zero g value, to be calculated. Table B-1 in appendix B.2 shows the sensitivity results of accelerometer circuitry on all five sensor nodes.

4.2.6 sEMG Circuitry.

Unlike the Accelerometer circuitry, the sEMG requires careful design of several circuit stages: differential amplification, filtering, further amplification, and envelope detection.

The first step of differentially amplifying the difference between the signals received at two electrodes has been discussed previously in chapter 3, section 3.3.2. This allows signals common to both electrodes (including noise, and crosstalk from distant muscles) to be rejected, thus boosting the signal to noise ratio. This technique can be further enhanced through the technique of double-differencing, shown in Figure 4-5. Here two differential amplifiers are used to amplify the differential signal between electrodes E1 and E2 and between electrodes E2 and E3. These two outputs are then further differenced by a third differential amplifier. This double-differencing gain further reduces the common mode signals that might appear at more than one electrode (Kamen and Gabriel 2009). This method has been designed for the wireless BSN. As before, high precision IA's have been used to maximise the CMRR.

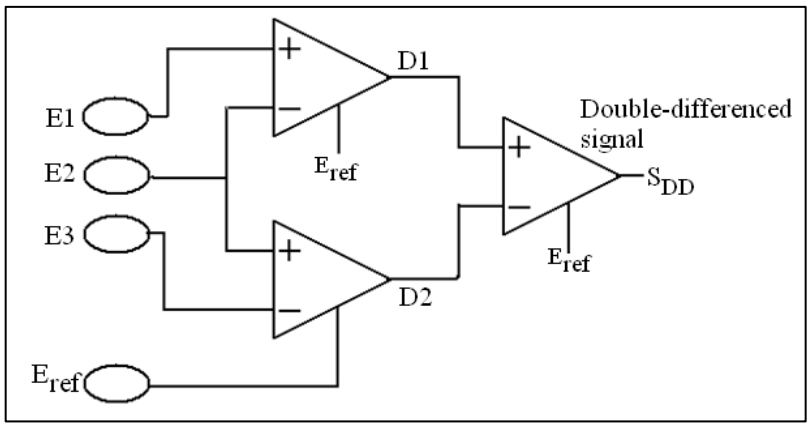

Figure 4-5: Double differencing topology employing 3 Instrumentation amplifiers

Double-differencing technique further improves the rejection of common-mode signals and enhances the signal-to-noise ratio of the system

The two levels of differencing have the effect of filtering out signals from more distant muscles as the signals from the distant muscle at the output of the first level of differencing are approximately equal thus eliminated in the second stage of differencing. Signals from the muscle of interest from the three electrodes are sufficiently different after the first stage of differencing to pass through the second level without attenuation.

Thus the block diagram for the sEMG circuit employed at a sensor node is shown in Figure 4-6.

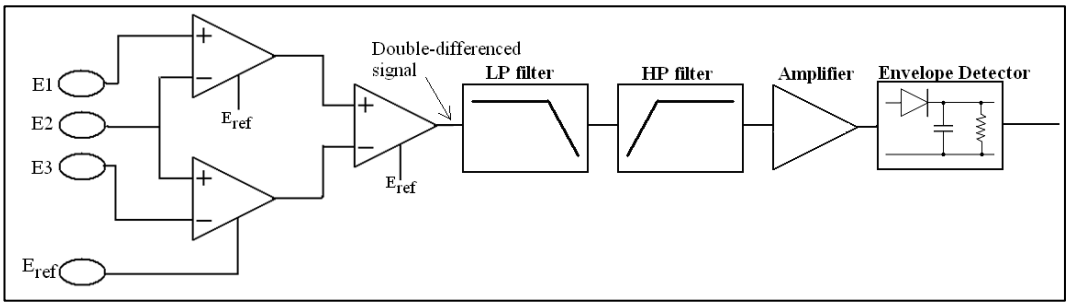

Figure 4-6: sEMG block diagram

Amplification and filtering of sEMG signal, including hardware envelope detection of resultant signal

The block diagram indicates a number of components which needed to be selected and designed: appropriate electrodes, precision instrumentation amplifier, appropriate high pass and low pass filters (active filters will reduce the requirement of additional amplification), and an envelope detector or averaging circuit to remove the high frequency component of the final signal before digitisation. In addition to this, the signal path needed to be considered to determine the overall gain in the system, considering both the expected input

signals at the electrode, the maximum allowable input signals to each stage, and the desired output voltage range of the EMG circuitry presented to the A/D input.

From the study of EMG circuitry in chapter 3, it was determined that EMG signal measurements at the electrodes will likely be of the order of 20µV to 2mV. With a signal supply voltage of 2.5V, which determines the maximum full scale input range of the A/D converter, the required system gain in the signal path of the EMG circuitry from electrode to A/D converter input can be determined. However, limitations in the input voltages allowable for each of the stages in the EMG circuit block diagram need to be considered first.

Analog Devices have an integrated circuit that can be used to determine the root mean square of the EMG signal – the AD736, True RMS to DC converter IC. This has the benefit of retaining more information than simply time-averaging a rectified signal, and by removing the high frequency content of the signal, but retaining the energy of the signal, the force-time information is preserved for analysis. The AD736 performs full wave rectification, conversion to RMS, and then filtering to smooth the output signal.

The IC has two inputs which can be employed. The high impedance input is restricted to only 200mV RMS if the IC is run from a 2.5V supply, although it can accommodate transient inputs of up to 0.9V. However, the low impedance input has similar but more relaxed restrictions: 300mV RMS or 1.7V transient input. Since by nature the EMG signals from muscles will be transient, then this is the limit to which the circuit has been designed. This sets the maximum signal level at the input to the RMS to DC converter, and allows the signal path gain to this point from the electrodes to be calculated. Recall the maximum signal expected at the electrode is 2mV.

$$Gain = \frac{1.7V}{2mV} = 850 \qquad 4\text{-}8$$

The minimum and maximum inputs to the RMS to dc converter IC is therefore:

$$\begin{aligned} V_{MIN} &= (Gain).(V_{EMG_{MIN}}) = (850).(20\mu V) = 17mV \Rightarrow 12mV(RMS) \\ V_{MAX} &= (Gain).(V_{EMG_{MAX}}) = (850).(2mV) = 1.7V \Rightarrow 1.2V(RMS) \end{aligned} \qquad 4\text{-}9$$

This gives an indication of the input to the 10-bit A/D converter, and the resolution that can be achieved.

The gain of 850 has been divided between the gain blocks in the sEMG signal path preceding the RMS to DC converter. There are four gain blocks: the instrumentation amplifiers forming the first stage of differencing of the EMG signals, the instrumentation amplifier conducting the second stage of differencing, the gain in the active low pass filter and the gain in the active high pass filter.

The precise proportioning of the gain to these gain blocks is less important than ensuring that the input stage provides adequate low noise gain. This is crucial because whilst all gain stages will add their own inherent noise to the system, the noise added in any stage will be amplified by any gain stage succeeding it in the signal path. The input stage therefore has the greatest impact on the noise figure of the signal path. As such the ability of the input stage to add gain and little noise, will greatly improve the overall signal to noise ratio of the circuit.

The gain in the EMG signal path has thus been initially proportioned as:

$$Gain = G_{DoubleDiff(1)}.G_{DoubleDiff(2)}.G_{LPfilter}.G_{HPfilter} = (4).(4).(7.3).(7.3) = 852 \qquad 4\text{-}10$$

The double-differencing circuitry consists of three precision instrumentation amplifiers (IA). Instrumentation amplifiers are designed specifically to optimise the CMRR of the input signals. The choice of the instrumentation amplifier should consider not just CMRR and gain, but bandwidth, power consumption, and noise (thermal and otherwise) introduced to the signal path by the amplifier. The chosen instrumentation amplifier is Analog Devices AD8221. This is a Precision Instrumentation Amplifier, with a bandwidth of 560KHz, a CMRR of 100 and max noise (referred to the input) of 8nV/√Hz. The gain of the instrumentation amplifier is set by a single external resistor R_G, and is calculated to be 16466Ω for a gain of 4. The nearest available value is 16KΩ, which, when the gain is recalculated yields a gain of 4.09.

It is important that both the instrumentation amplifiers comprising the first stage of the double differencing are matched. Thus low tolerance resistors (better than 1%) have been used. Both stages of the double differencing employ the same resistors and thus the same gain. The total gain in the double differencing is thus:

$$\boldsymbol{G_{DoubleDiff} = G_{DoubleDiff\,(1)}.G_{DoubleDiff\,(2)} = (4.09).(4.09) = 16.73} \qquad \text{4-11}$$

The new gain required for the active filter stages to maintain a signal path gain of 850 is (assuming the gain in each of the active filters to be equal):

$$\begin{aligned} &Gain = G_{DoubleDiff\,(1)}.G_{DoubleDiff\,(2)}.G_{LPfilter}.G_{HPfilter} \\ &\Rightarrow G_{LPfilter} = G_{HPfilter} = 7.13 \end{aligned} \qquad \text{4-12}$$

The Low pass active filter requires a 3dB cut-off frequency of 500Hz and a gain of 7.13 in the pass band. The high pass filter requires a 3dB cut-off frequency of 20Hz and a gain of 7.13 in the pass band. Two-pole Sallen and key active filters

have been chosen for both of these filters due to its compact topology (one op-amp, two capacitors and two resistors in the filter design and two further resistors forming the feedback circuit that sets the gain). The basic topology for a two-pole Sallen and key filter is given in Figure 4-7.

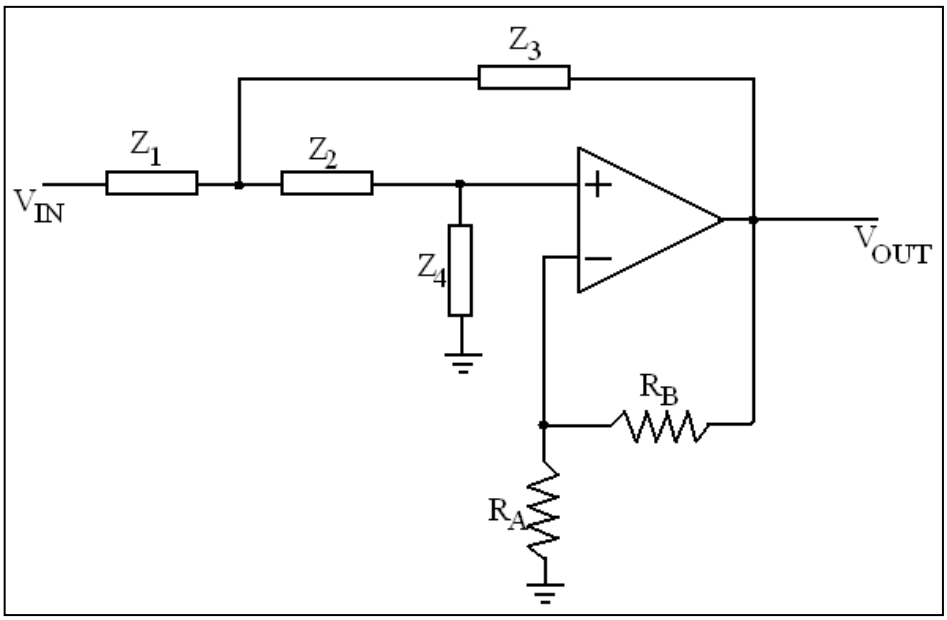

Figure 4-7: Sallen and Key filter topology

Circuit topology can be configured as either low pass or high pass filter through correct placement of calculated capacitors and resistors

The impedances labelled Z_1-Z_4 can be calculated for a generic two pole filter with a given 3dB cut-off frequency, and then substituted with appropriate resistors or capacitors to create either a high pass filter or a low pass filter. Resistors R_B and R_A are used to calculate the required gain. The transfer function of the Sallen Key topology is mapped to a 2nd order Butterworth polynomial (chosen for its flat pass-band response), and the component values calculated. Further details of this design process can be found in appendix B.3.

The accuracy with which the calculated components can be translated into physically available components impacts upon how closely the built circuit matches the specification. There are far fewer capacitor values available than resistors, and their manufactured tolerances are far wider. Thus it is prudent to select capacitors first and then calculate the associated resistors with which to balance the equations and generate the desired result. A simple Excel spreadsheet was generated to allow the choice of capacitor and impact upon resistor values to be compared such that the best match of available components could be used. The circuit diagram for the filtering is shown in appendix B.1.

Using the calculated values, the filters were simulated using Agilent Advanced Design System (ADS) simulation package to verify their expected performance and to compare performance of the calculated and nearest available component values. Simulation results for gain and phase response is given in appendix B.3 for low and high pass filters, and also as inserts to the build measurement results for the filters in Figure 4-8 and Figure 4-9. Simulation results show that there is little change in the simulation between the calculated and the nearest available values.

The operational amplifier chosen as the basis for the active filter is the AD822 (Analog Devices). It is a rail to rail, FET input, dual op-amp with a supply range of ±1.5V to ±18V, unity gain bandwidth of 1.8MHz, maximum noise of 13nV/√Hz and only 800uA quiescent current per amplifier. The dual package means that both low pass and high pass filters can be built using a single integrated circuit and a handful of passive components.

The AD736 True RMS to DC converter IC identified earlier requires only two additional capacitors to function (when using the low impedance input). An

averaging capacitor, C_{AV}, is used to hold the rectified input signal during the root-mean-square computation in the RMS core of the IC. Thus the value chosen directly impacts the accuracy of the RMS conversion. The filtering capacitor, C_F, is optional, but connected across the feedback network of the output buffer amplifier it helps to further reduce any remaining ripple left in the output signal after the RMS process.

Finally, the EMG circuit requires a negative supply input so that the negative voltage range of the EMG signal is preserved and amplified along with the positive range up until the RMS conversion process. A dc to dc converter IC (TC7660) is used for this, requiring only a single external capacitor to operate the charge pump voltage converter. The charge pump capacitor transfers charge from the input source to the output – in the first half a two phase switching cycle the capacitor is charged to the input voltage, and in the second half of the cycle, the capacitor is inverted and the charge transferred to the output, thus producing a negative voltage on the output.

The complete sEMG circuit is shown in appendix B.1. The EMG circuitry is self-contained on its own printed circuit board, allowing it to sit parallel to the main sensor node PCB within the node enclosure, thus minimising overall size of the node. Due to the nature of EMG signals, this PCB should be located as close to the electrodes as possible. Ideally they should be integrated onto the electrodes in the form of active electrodes, but this could be the topic of future work (due to the nature of the wireless BSN, nodes will by design be close to the electrodes). The EMG PCB is essentially a single-sided PCB with all components and track connections on the topside of the PCB. The underside of the PCB is dedicated to an unbroken ground plane to minimise any interference entering the circuit.

4.2.7 sEMG Circuit testing

The Double differencing IA stage exhibited a flat gain response of 16.25 up to 600KHz, in line with the data sheet specification for a two stage design with 16KΩ gain resistors.

The gain and phase response for the low-pass filter is shown in Figure 4-8, the simulation results are shown in inset for comparison.

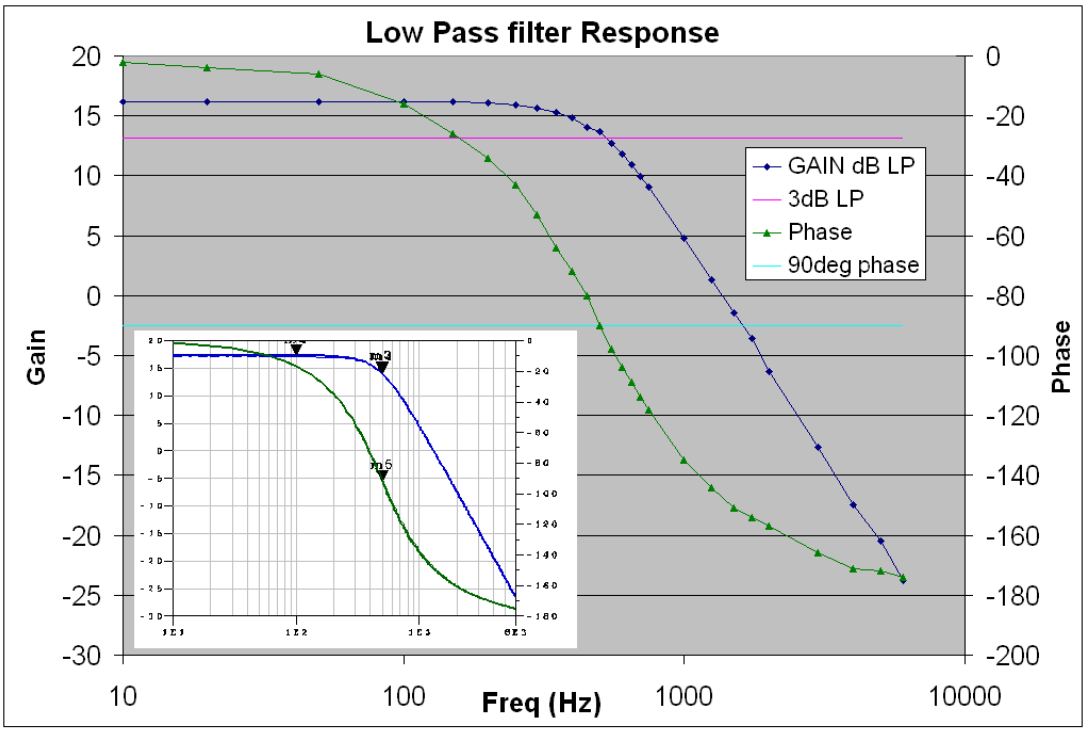

Figure 4-8: Measured low pass filter response and comparison to simulation

Gain and phase response of fabricated low pass filter. Blue – gain response, Green – phase response. 3dB cut-off frequency of filter is indicated in magenta (520Hz)

It can be seen that the built and measured sEMG circuit performs closely to the expected response given by the simulated design. The -3dB point of the built filter is 520Hz and the pass-band gain is 6.44 (16dB).

Likewise the high-pass filter response was measured over an appropriate frequency range and compared to simulation (Figure 4-9). Again, the response is satisfactory; the -3dB point of the filter is 25Hz, and the gain is 6.7 (16.5dB).

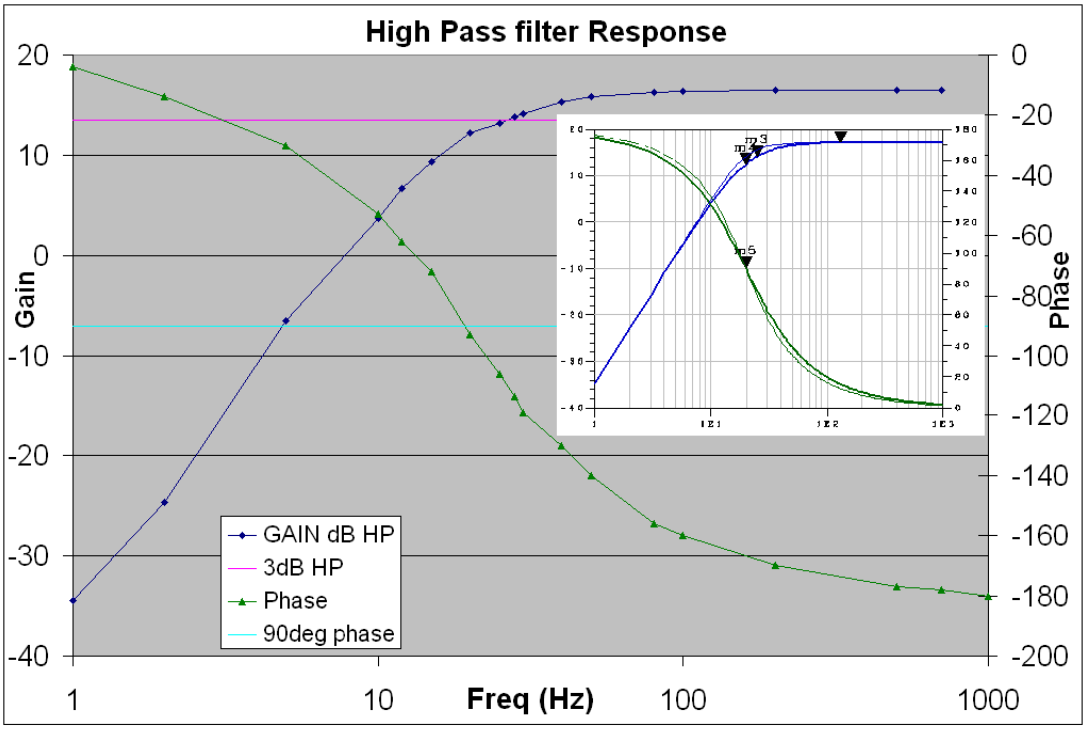

Figure 4-9: Measured high pass filter response and comparison to simulation

Gain and phase response of fabricated high pass filter. Blue – gain response, Green – phase response. 3dB cut-off frequency of filter is indicated in magenta (25Hz)

The filtering stage of a second sEMG circuit was built and tested and the overall filter response (band-pass with a lower 3dB frequency of 20Hz and an upper 3dB frequency of 500Hz) of both circuits measured and plotted for comparison. The two circuits present very similar performance as would be expected of a circuit with low tolerance components, the results of which can be found in Figure B-17 appendix B.3.

When all stages of the sEMG circuits were operating as expected with known signal generator inputs, the outputs of each stage of the sEMG circuits were tested with isometric, and concentric-eccentric muscle contractions of the upper arm biceps brachii muscle. In Concentric Contractions, the muscle actively shortens during the contraction (Figure 4-10 a). Eccentric Contractions cause the muscles to lengthen when they are loaded (Figure 4-10 b). In both these cases, the movement of the electrodes and underlying tissue causes motion artefacts. Conversely, Isometric contractions occur when the muscle is actively contracting but neither lengthening nor shortening in length (Figure 4-10 c).

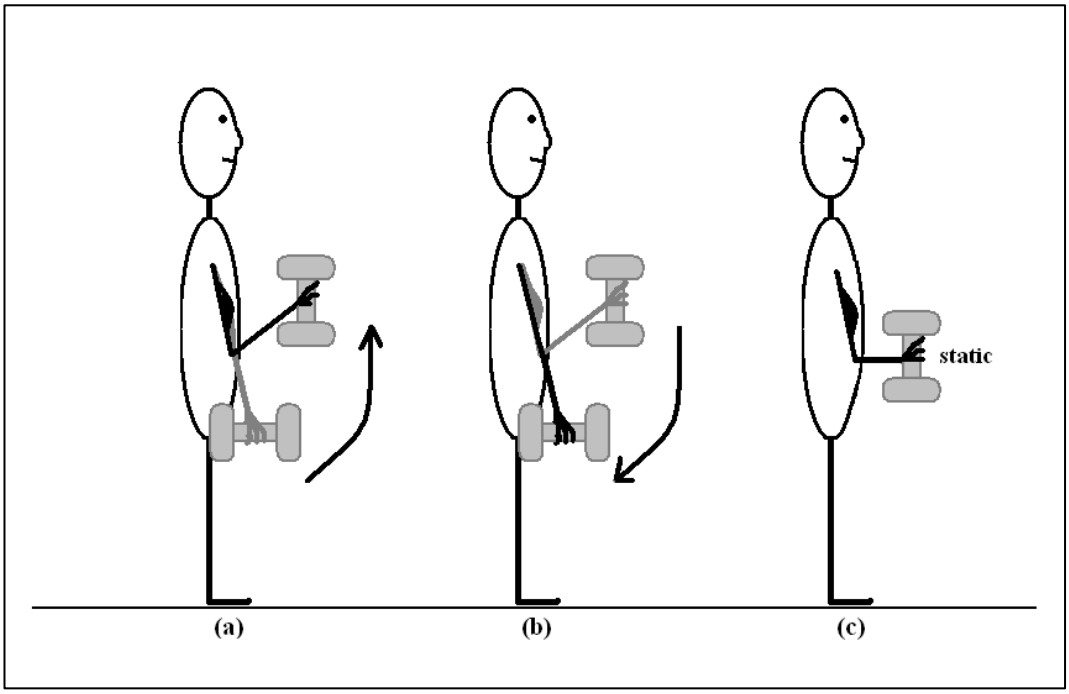

Figure 4-10: Muscle contractions
(a*) Concentric, (b) eccentric, and (c) isometric muscle contractions*

Electrodes used are Ambu Neuroline pre-gelled surface electrodes, placed longitudinally along the muscle with an inter-electrode distance of 20mm. The manufacturer recommends that the same electrodes can be used for reference

electrodes, and this was placed on electrically neutral tissue at a bony prominence near the elbow.

The results of the isometric contractions of the biceps brachii are shown in Figure 4-11. Measurements were made at the input and output of each stage in the sEMG circuitry using a National Instruments' Multi-function Data Acquisition unit (NI USB-6211) sampling at 1000Hz. The NI-DAQ allows data to be captured at several points in the circuit simultaneously. It can be seen that the noise-like signal at the electrodes (double-differential amplifier input) is amplified and noise rejected at each stage in the sEMG circuit, with the final RMS output retaining the energy and shape of the signal without the high frequency components.

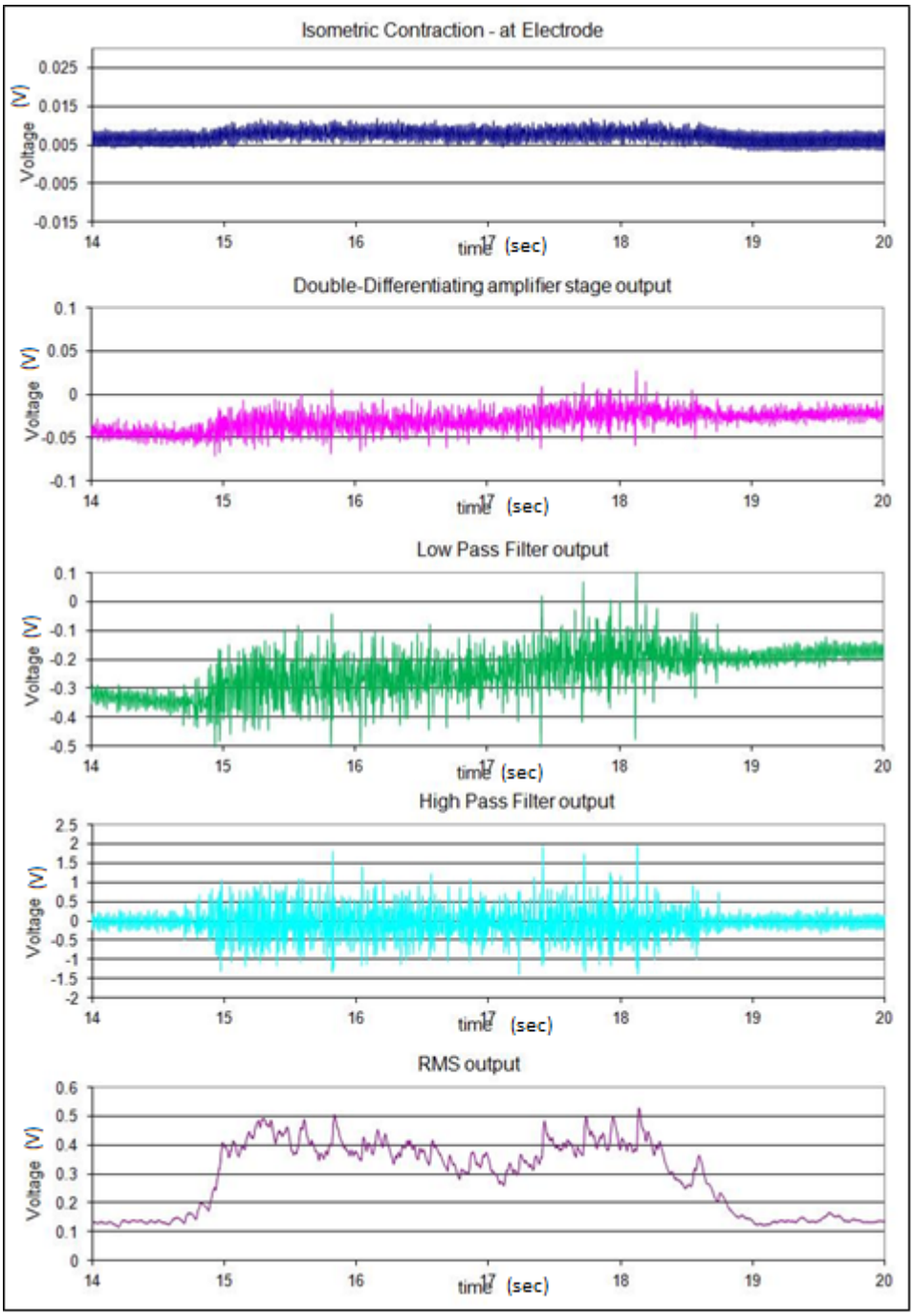

Figure 4-11: Isometric contraction of the bicep brachii

Signals at the output of each stage of the sEMG circuitry

Figure 4-12 likewise shows the results of measurements where the bicep brachii underwent concentric-eccentric contraction twice. Here, the motion artefact is

clearly visible, and when filtered out by the high pass filter, the detail of the muscle contraction is markedly more evident.

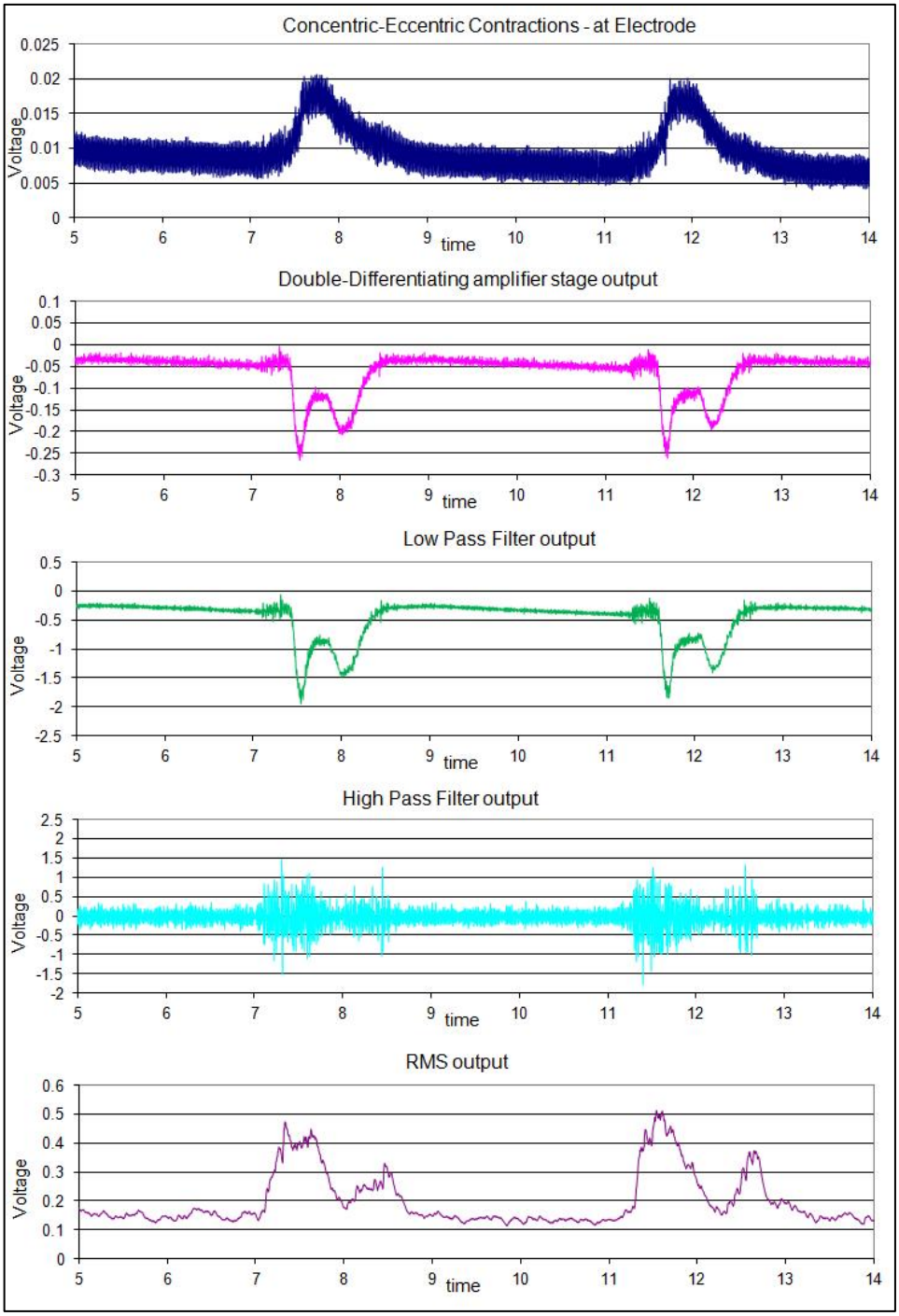

Figure 4-12: Concentric-eccentric contraction of the bicep

Signals at the output of each stage of the sEMG circuitry, motion artefacts clearly visible prior to high pass filtering

4.2.8 Printed Circuit Board (PCB) Design and Fabrication

Schematic capture and Printed Circuit Boards (PCB) design has been achieved using Protel Design Explorer (now integrated into the Altium Designer package). Protel was the first industry standard PCB design tool allowing the schematic capture and PCB layout capabilities. After the schematic capture of the circuit design, PCB footprints are associated with the schematic symbols and a netlist is created which links component connections together in a series of nets. A netlist is a text document which describes all the necessary connections required to enable the printed circuit board to be created. The netlist is then imported into the PCB document, placing all the necessary footprints and a 'rats-nest' of the required connections. Wire links can then be added to the PCB to route the signals to match the schematic document. The rat-nest connections formed by the netlist ensure that the PCB accurately implements the schematic diagram, reducing the chance of routing errors. Design rules can be set up to ensure that fabrication parameters are not violated in the routing process.

The sensor node PCBs were designed to accommodate the largest component – the Zigbee radio module. As such the PCB's measure 44 x 47 mm in size, dictating the size of the nodes and their chosen off-the-shelf box enclosures (64 x 64 x25 mm). The Microchip Zigbee module has subsequently been redesigned and is significantly smaller than the first iteration. As such, the nodes could be redesigned to be smaller in size. Whilst this would be an unnecessary iteration to this research project, one node was subsequently fitted with the smaller radio module such that it could be housed in a smaller box to determine what sort of size could be obtained without a complete redesign. This smaller node measured (49 x 49 x 18 mm).

The PCBs were fabricated off-site by PCB-Pool, a company that provides budget PCB prototyping service for small order multiples with industry quality finish that was not possible with university facilities.

Because five sensor nodes were built, it was important that they were all built and tested to the same standard. Whilst the circuit and PCB design and build was performed with care and attention to detail, it is inevitable that during the building and test process that some small errors in connections, component footprints and circuit design errors would be found. It was also possible that during the testing process a particular sub-circuit would be found to require optimisation or adjustment, either of component values, or a change in the overall design of a sub-circuit. As such, the build and test process was carefully documented, with all PCBs named and build and modification paperwork maintained for each PCB. In this way, it could be ensured that all changes made to one sensor node was also duplicated on the others. Sensor nodes were named #S1-#S5 and sEMG PCBs were named #E1-#E5. Figure 4-13 shows the developed hardware.

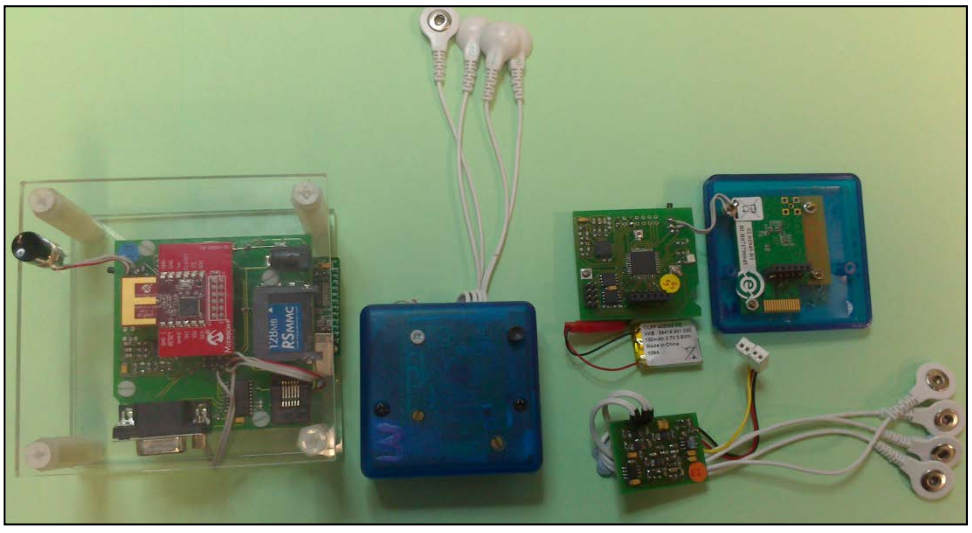

Figure 4-13: Developed Wireless BSN hardware.

Coordinator node, a sensor node and the electronics contained in a sensor node

4.3 Firmware Development

The hardware design gives the physical platform upon which the system will run. However, it is the firmware which runs upon the microcontroller which dictates not just the tasks which the system will perform but also the sequencing and scheduling of those tasks.

Thus, the firmware coding is a fundamental part of the design which must be considered, planned and designed with as much care as the physical circuit design.

A State-Transition Diagram can be used to describe the system flow of the firmware coding. This is a modelling tool described by Ed Yourdon's Modern Structured Analysis (Yourdon 1989), and is similar in style to a flow diagram. Process control systems, including data acquisition systems, which react and capture information about the surrounding environment, are particularly suited to this form of modelling. Such a modelling system describes what happens when, what events trigger a transition from one state to the next, and the action that is performed as a result of the transition. The format of a State-Transition diagram is shown in Figure 4-14.

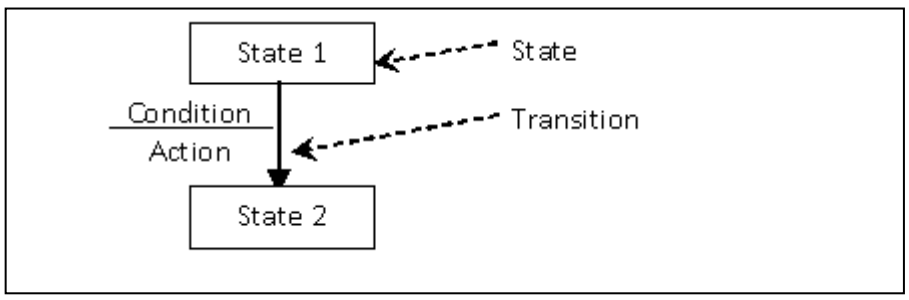

Figure 4-14: Format of a State-Transition diagram for describing system flow

Due to the size and complexity that can result in State-Transition diagrams of large systems, these models can be further subdivided into partitioned diagrams. For example, in Figure 4-14, state 2 might be further subdivided into a sub-diagram consisting of states 2a, 2b, 2c, etc.

A State-Transition Diagram for the basic flow of the firmware coding is shown in Figure 4-15.

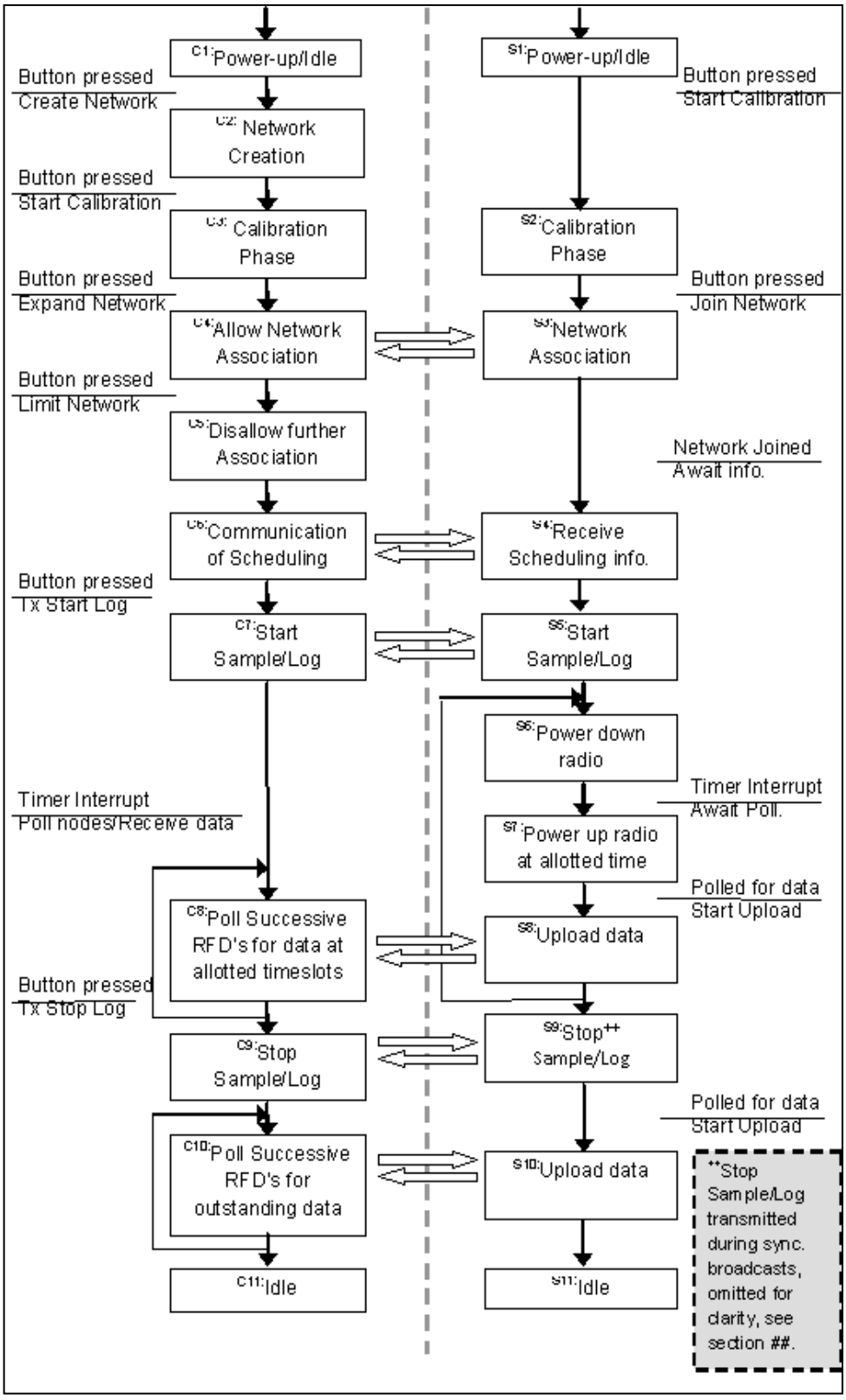

Figure 4-15: Basic State Transition Diagram for Firmware Coding of Wireless BSN

This State Transition diagram describes the basic flow of the system, with the coordinator flow on the left, and the sensor node (Slave) flow on the right. The left/right arrows between the two flows indicate some wireless communication takes place between states in the respective flows. States in the coordinator flow are labelled C#, and in the slave node flow are labelled S#. For clarity, condition/action labels are only included where there is a specific input which causes the transition (for example a button press, or a timer interrupt); if a state transition occurs purely due to completion of the previous state, the condition/action is omitted. At this level, the State Transition diagram does not address some of the specifics of the required scheduling. For example, the Stop Sample/Log state of slave flow state S9 occurs due to the reception of a stop sample/log transmission from the coordinator during a synchronisation broadcast. These are periodic broadcasts from the coordinator for which all slave nodes should simultaneously wake and listen for time synchronisation information and any actionable commands. Details of these broadcasts are covered in section 4.3.4.

The firmware code can be divided into two fundamental parts: the wireless framework, which supports communication between nodes in the system, and the main application, which schedules the main tasks in the system. These two parts are integrated by means of the application framework, part of the Zigbee Stack.

4.3.1 The Zigbee Stack

There are two communication concepts that take place in a functioning Zigbee network, and both need to be understood in order to fully appreciate the implementation of a Zigbee application – the low level communication that takes

place from layer to layer through the Zigbee stack architecture, and the higher level communication that takes place between network nodes. Whilst the inter-node communication is facilitated and ultimately implemented using low level intra-node communication of data and command frames, a number of new concepts need to be introduced to fully understand how nodes interact.

A Zigbee node is a physical electronic object with a radio (specifically an 802.15.4 radio) attached. The device might include a number of different functions, all sharing the same radio. In wireless BSN, the node includes a number of different measurement sensors. The communication between different nodes is supported by the application support sub-layer.

A particular application requires a formal structure describing the method with which it communicates. Three concepts which work together to do this are the application profile, clusters, and endpoints (EP).

4.3.1.1 Application profile

The application profile is an ‘umbrella’ describing the collection of nodes which interact within a given application, and the precise messaging system they use to communicate. The application profile is given a ProfileID – this is the unique name given to the profile, covering all the devices within the application, and all the clusters used by all nodes’ endpoints. This profile can then be used to develop the individual endpoints within the application, by calling upon a subset of clusters that would be required to communicate between endpoints in the application. Individual node types also have a unique DeviceID.

4.3.1.2 Clusters

Clusters are groups of linked information that need to be communicated between devices. The information covered by the clusters are called Cluster Attributes. Clusters can be explicitly written for a particular application profile, or selected from a Zigbee Cluster library. When a cluster is added to a profile, it is allocated a ClusterID unique to that cluster within a particular application.

4.3.1.3 Endpoints

Endpoints of particular nodes have a subset of clusters and their associated cluster attributes, and use the ProfileID and the DeviceID to communicate. They can be considered to be communication entities within a device through which an application is carried. This is similar in concept to a TCP port – for example, internet traffic will be carried by HTTP over a particular port (Daintree Networks inc 2006). 240 endpoints are available for use within a Zigbee device, with Endpoint 0 reserved for the Zigbee Device Object (ZDO).

The Zigbee stack architecture is divided into a number of layers. Each of these layers undertakes a particular function and performs a number of services for the layer above. These services are conducted through a “Service Access Point” (SAP). The structure of the Zigbee Stack architecture is shown in Figure 4-16.

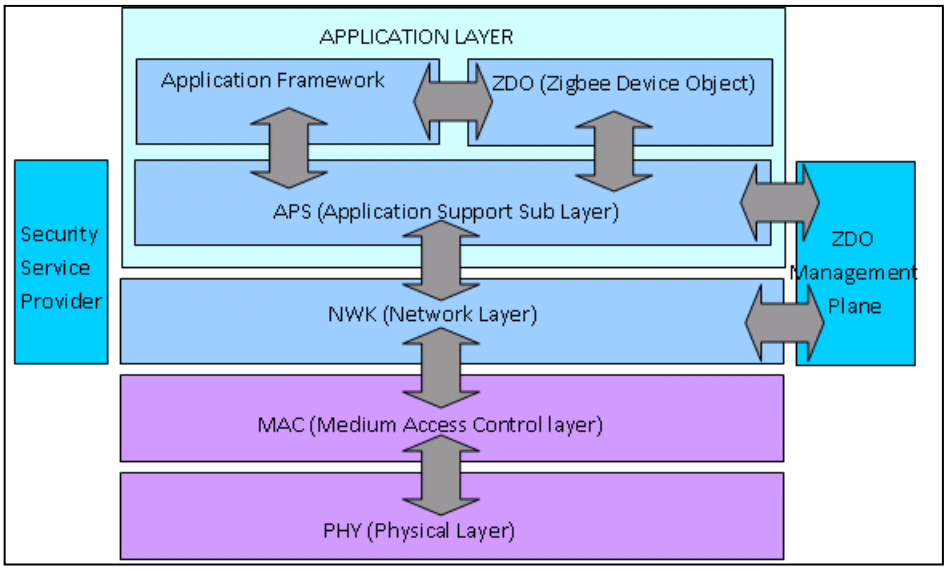

Figure 4-16: Simplified Zigbee Stack architecture

Indicates command and data flow through the Zigbee stack through Service Access Points (SAP)

This architecture follows a standard “Open Systems Interconnection seven layer model” (ISO/IEC 7498-1:1994) implementing only those layers relevant to the Zigbee standard.

The lowermost levels – the physical layer (PHY) and the medium access control layer (MAC), shown in purple in Figure 4-16, implement the requirements of the IEEE 802.15.4 specification upon which Zigbee is based.

This IEEE 802.15.4 Standard details the PHY and MAC for Low rate Wireless Personal Area Networks (LR-WPANs). The Zigbee specification then adds the Network layer (NWK) and the application layer (APL). This topmost layer is application specific, and Zigbee therefore only specifies the framework of this layer and its interface with the layer below. The system developer is left to define and develop the specific application object.

4.3.1.4 Primitives

Primitives are used as a means of passing information between different layers. Layer *n* performs a service to the next layer up, layer *n+1*, by passing a primitive through the relevant SAP. This primitive has a number of parameters that characterise it, the simplest of which is a STATUS parameter, giving a simple True or False status. The naming convention for these primitives is derived from the SAPs through which the service is being performed and the type of primitive. The format takes the general form:

[Layer_SAP]–[Primitive_Descriptor]**.**[Primitive_Type]

There are typically two Layer_SAPs for each layer of the stack. one for data and one for management.

Typical Primitive_Descriptors (a non-exhaustive list), that describe the action being performed, are: DATA, BIND, UNBIND, GET, SET, ASSOCIATE, DISASSOCIATE, RESET, START, SCAN, SYNC.

The Primitive_Types of these primitives can take one of four different forms: Request, Indication, Response, Confirm, depending upon the type of information or service that needs to be conveyed.

For example, upon receipt of a message over the radio, the primitive PD-DATA.indication, generated by the PHY, is sent to the MAC via the PHY Data service access point, PD-SAP, to indicate the transfer of data from the PHY to the MAC. Many of the services performed by the lower layers of the architecture are essentially performed in a manner that is transparent to the main application.

As the data unit is transferred from layer to layer, it acquires headers and footers and adopts a new identification. The PPDU is the total information that is transmitted over the physical radio channel. Starting as raw data further up the layer stack (in the application layer), each layer adds its own overheads to the data that is transmitted.

For example, a MAC service data unit, MSDU, (which itself has headers and footers added from the network and application layers) acquires a MAC header and footer to become a MAC protocol data unit, MPDU. This frame is then transferred via the PD-SAP to the PHY layer where it becomes a PHY service data unit, PSDU. This itself then gets a PHY header (also a synchronisation header), transforming it into the PHY protocol data unit, PPDU for transmission across the physical RF channel. This is summarised in Figure 4-17.

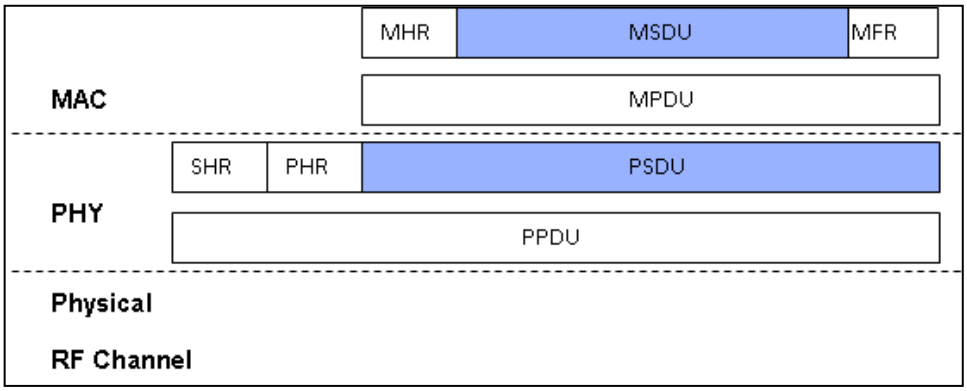

Figure 4-17: Summary of Data Unit naming convention

Data Units accumulate headers from each layer in the stack as they are transferred down the stack towards the PHY layer

These layer-specific overheads are necessary for the successful, robust transmission of the data between layers and individual nodes in a network across a possibly noisy radio channel, but are added such that overall complexity of the transmitted frames is kept to a minimum.

Each layer of the stack has its own specific tasks. The PHY enables the transmission and reception across the physical radio channel, and the MAC sub-layer, whilst one layer removed from the physical RF channel interface, still executes some of the lower level functionality of the radio. Typical tasks of the MAC sub-layer include channel access and maintaining a reliable link between nodes, frame validation and delivery acknowledgement, and node association and disassociation.

The NWK layer controls the MAC layer below, and serves the Application Layer above. Its tasks include starting, joining or leaving a network, assigning addresses to new nodes on the network, discovery of neighbours and routes on the network, and controlling when the receiver is on or off.

The uppermost layer of the Zigbee architecture stack is the application layer. It is left to the developer to define the application as a whole, and as such is not covered within the Zigbee specification. There are three main parts to the application layer that are defined by the specification: the application support layer, the application framework upon which the developer builds the application, and the Zigbee Device Object (ZDO). The application support sub-layer (APS) provides an interface to the next layer down the stack, specifically the NWK layer. The application framework hosts the application objects, of which there can be up to 240. Each of these application objects, has its own APSDE-SAP, called an endpoint. This can be considered the objects' interfaces with the rest of the stack. Endpoint 0 is reserved for the ZDO, which handles the base functionality to interface between the application objects, the device profile and the APS.

The Microchip Zigbee Stack is compliant with version 1.0 of the Zigbee Specification, with a view to being evolved to later releases of the specification as they develop.

The stack is written in C and can be used with the C18 family of 8-bit PIC microcontrollers; a 16-bit version of the stack was under development at the time of this system design. The Microchip stack includes an integrated driver for the supported Zigbee radio modules, which relieves the application from the low level SPI communications with the radio module and manages the RF module functions. Provided the correct SPI connections are made to facilitate the serial communications between microcontroller and radio module, appropriate additional digital control lines are assigned for other functionality (interrupts, chip selection, wake up and reset) and the microcontroller timer TMR0 is made available, the driver should manage the radio functionality transparently to the application.

The Microchip Zigbee Stack is organised into numerous source and header files, located in a number of directories. The two main directories are *Common*, and *ZigBeeStack*. The *ZigBeeStack* directory contains all *Protocol Stack-specific* files common to nodes in a network whilst the *Common* directory contains all *application-specific* files common to all nodes in a network. One notable file is the ZigbeeTasks.c file which contains code which directs the program flow through the layers of the protocol stack. Any additional application files unique to particular types of node (e.g. coordinator, RFD, FFD) are stored in their own directories.

The main application file contains the main code vital to the implementation of the flow of tasks the node must undertake, and this will call subroutines from within

files in the *ZigBeeStack* and *Common* directories. The three remaining files specific to the application of a particular node are:

myzigbee.c
zigbee.def
zlink.lkr

These files tailor the *ZigBeeStack* files for a particular type of node. For example: device type, transceiver power source, Zigbee transceiver chip, etc. (e.g. identifying it as a coordinator, mains-powered, interfacing to the Zigbee radio, etc). It is also here that APS, NWK and MAC layer settings are chosen.

Perhaps most importantly, it is also in these files that the endpoints are set. This is done by linking to a profile header file, and using information from this to select input and output clusters for endpoints. Endpoints can thus be added, allocated to endpoint numbers and given names, and individualised for a given node. These endpoints allow information transmitted from one node to another to be directed to the correct destination.

4.3.2 Zena Network Analyser

The Zena Network analyser is a software tool which graphically displays all 2.4GHz Zigbee wireless network traffic within the range of its own Zigbee radio. Together the hardware and software elements of the Zena Network analyser perform like an oscilloscope for Zigbee radio traffic, allowing the network traffic to be monitored in real-time. Figure 4-18 shows an example of such data traffic as received and displayed by Zena: two different unicast packets sent from an end device (address 0x796F) to coordinator (address 0x0000), along with the acknowledgements (ACKs) from the coordinator and a broadcast message sent

from the coordinator to all nodes in the network. Unicasts are transmissions from one node to another specific node. Broadcasts are transmitted to address 0xFFFF, indicating the message is for all nodes. All broadcasts are retransmitted by any node who receives it. In this way, it is possible to determine which nodes have received the broadcast. The colours indicate the part of the stack from which that part of the packet originated: cyan indicates the data from the application framework, yellow the APS header information, green the NWK layer, White the MAC layer. The time that the packet was received by Zena is indicated also. Zena is thus an invaluable tool for the development of the wireless BSN system.

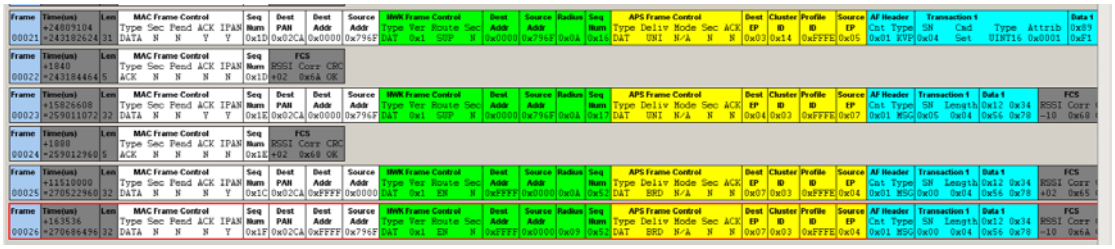

Figure 4-18: Messages intercepted using Zena network analyser

White – MAC layer headers, Green – NWK layer headers, Yellow Application layer headers, Cyan – AF headers and payload. Zena RSSI and packet reception time information also displayed

4.3.3 The application framework.

The application framework allows other non-network related tasks to take place. Situated within the main application file (such as *RowMonitorCoord.c* within the coordinator) it allows the implementation of the various states in the program flow summarised earlier in Figure 4-15. To achieve this aim, the concept of primitives has been extended, with a new set of *StatePrimitives* which indicate the non-ZIgbee related state of the system such as *Idle, Join_Allow, Join_Disallow,*

LogInitialise, Log, Stoplog, SerialUpload. A further example of the use of the State-Transition Diagram to describe the transitioning between these states can be found in appendix B.4.

After all sensor nodes have joined the network created by the coordinator node, the wireless BSN enters a state of information exchange corresponding to C6, *Communication of Scheduling* in the basic state transition diagram of Figure 4-15 (and the corresponding slave state S6). The coordinator calculates the upload schedule for each sensor node, and communicates common information (such as the *Synchronisation Broadcast Interval* (SyncBrI), the Section *Storage Time* (SST), *Sample Rate* (SR), etc by means of broadcasts to all sensor nodes simultaneously, and individual information concerning the *Individual Upload Interval* (IUI) via a unicast to each node in turn. During this state, each sensor node is also interrogated for any calibration variables that might have been determined during node calibration. At this point the slave nodes are also sent a timing broadcast (see section 4.3.4) so that they can synchronise their clocks to the coordinator node's master clock.

4.3.4 System Timing

In order that the Wireless BSN can sample the sensors at a given sample rate and also remain synchronous across the network, timing is an important issue. The microcontrollers running the developed firmware at the centre of each node have 4 on-board timers, timer0-timer3. Whilst timer0 is used by the Zigbee stack to produce the timing for the symbols used in the modulation scheme, the other three timers are free to use by the application. Timer1 is clocked by the external watch crystal timer at 32.768KHz, and is used, along with the relevant interrupt, to produce the local time for each sensor node, given in hours, minutes, seconds, and units (where the unit duration is programmable but is set to ¼ second intervals). By setting the smallest increment of the local time to a coarse fraction of one second, it allows scheduling of tasks within a long experiment without overly burdening the system (every time the interrupt fires to increment the smallest unit of the local time, the program flow is briefly stalled whilst the interrupt is dealt with).

Timer3 is also clocked by the external watch crystal, and set to trigger an interrupt every interval of the sample rate (in this case 50Hz). Upon the timer3 interrupt firing, the sensors are sampled by the on-board ADC, and the sampled value stored locally upon the sensor node until the node's upload interval, when the data is uploaded to the coordinator node.

Whilst it is important that the sensor nodes wake a their allocated timeslot to be interrogated by the coordinator node (allowing them to put the radio into sleep mode for much of the intervening period), it is vital that all sensor nodes sample at the same interval and the same instant across the wireless BSN so that the

collected data can be correlated. As such, the node synchronisation needs to be addressed.

Both the local time and the sample rate of the sensor nodes are set by the external watch crystal. This has a nominal frequency of 32.768kHz (standard for a watch crystal) which means it 'ticks' every 30.518µS. Thus timer1 has to count 8191 cycles of the clock to increment the local time by one ¼ second unit, and Timer3 has to count 655 cycles of the clock to give a time period of 0.02seconds (50Hz). In reality, the watch crystals all have tolerances which mean that they do not operate at precisely 32.768KHz. This will mean that a 'tick' of the watch crystal on one node will not precisely match a 'tick' on another node. This will result in drifts of the sensor nodes away from the coordinator's master clock to which they are initially synchronised, and cause the node to sample at a rate not precisely 50Hz.

However, the watch crystal chosen for the application has an accuracy of ±20ppm (parts per million) at room temperature. This means that it is accurate to $\pm 20.(32.768e^{3}).0.000001 = \pm 0.65536Hz$

This means that the maximum range of values that the watch crystal might exhibit at room temperature (through manufacturing tolerances and reasonable aging) is $32.673.45Hz \leq f_{WC} \leq 32768.655Hz$.

However, in a worst case scenario, one sensor node might have a frequency at one extreme of their tolerance, and another at the other extreme, and thus differ in frequency by as much as 1.31Hz. This would result in a potential worst case drift between sensor nodes of 2.4ms over a minute.

Thus, at regular intervals there is a broadcast window (indicated previously in Figure 4-4). At this time, all sensor nodes should wake to receive any relevant information from the coordinator node. This time slot can be used, for example, to tell the nodes to stop sampling and upload their remaining data in their subsequent upload interval. However, its primary role is to allow the coordinator to send a synchronisation broadcast such that the sensor nodes' local clocks can be adjusted to keep them in sync.

Chapter 2, section 2.5.3 discussed the issue of time synchronisation and the methods which can be employed to keep the nodes of a WSN in sync. In this application it is necessary only to ensure that all nodes begin sampling at precisely the same time, and to adjust their local clocks to remove local drift. This can be achieved by broadcasting the coordinator time at regular intervals when the sensor nodes are listening such that the local clocks of the sensor nodes can be adjusted to match that of the coordinator. Messages are only decoded at the application layer, and the time that the message takes to travel up the stack from reception in the PHY to the application layer is dependent upon the other tasks that the node has to achieve. This non-determinacy factor would mean that the clocks of all sensor nodes would be adjusted at slightly different times and thus not be set to the same value.

The solution is to remove this non-determinacy factor. In the coordinator node, the time synchronisation message is constructed in the application layer, and placed into the transmit buffer (*TXBuffer*), then travelling down the stack (with headers added by each layer) towards the PHY. A flag is set to identify this message as a synchronisation message. At the MAC/PHY interface, if the flag is set, the coordinator time and sample timer values are again read and those

values in the *TXBuffer* updated. This removes the non-determinacy factor within the coordinator.

Upon reception of a message in the PHY of the sensor node, the local time and sample clock values are stored. At this point the message has not been decoded and the sensor node does not know that it is in receipt of a synchronisation message. When a synchronisation message is decoded in the application layer, the local time and sample clock values are again noted, and the time elapsed between receipt of the message in the PHY and its decoding in the application layer is computed and added onto the received coordinator time. In this way, the non-determinacy factor within the sensor node is also removed. The difference in propagation time across the wireless link for a BSN which occupies such a limited space is negligible. As such, the sensor nodes are synchronised to each other.

This can be tested though supplying two nodes with the same input signal (from a waveform generator). By plotting the sampled data against time (determined by $\frac{SampleNumber}{SampleRate}$), any drift becomes apparent, as the same signal, sampled at slightly different moments in time by 2 sensor nodes would appear out of phase. Figure 4-19 (generated through analysis in MATLAB (Mathsworks) of the collected data, shows the results of 2 nodes sampling the same 2Hz sine wave. Figure 4-19(a) shows the sampled inputs of the two nodes at 3, 6, and 9 minutes for the wireless BSN with no synchronisation adjustment. Figure 4-19(b) shows the same two nodes at the same points in time employing synchronisation messages to adjust for drift in the sensor node local clocks. Figure 4-19(c) shows nodes that have been left to drift for an extended period before being synchronised by a synchronising message from the coordinator (at 2008.64secs).

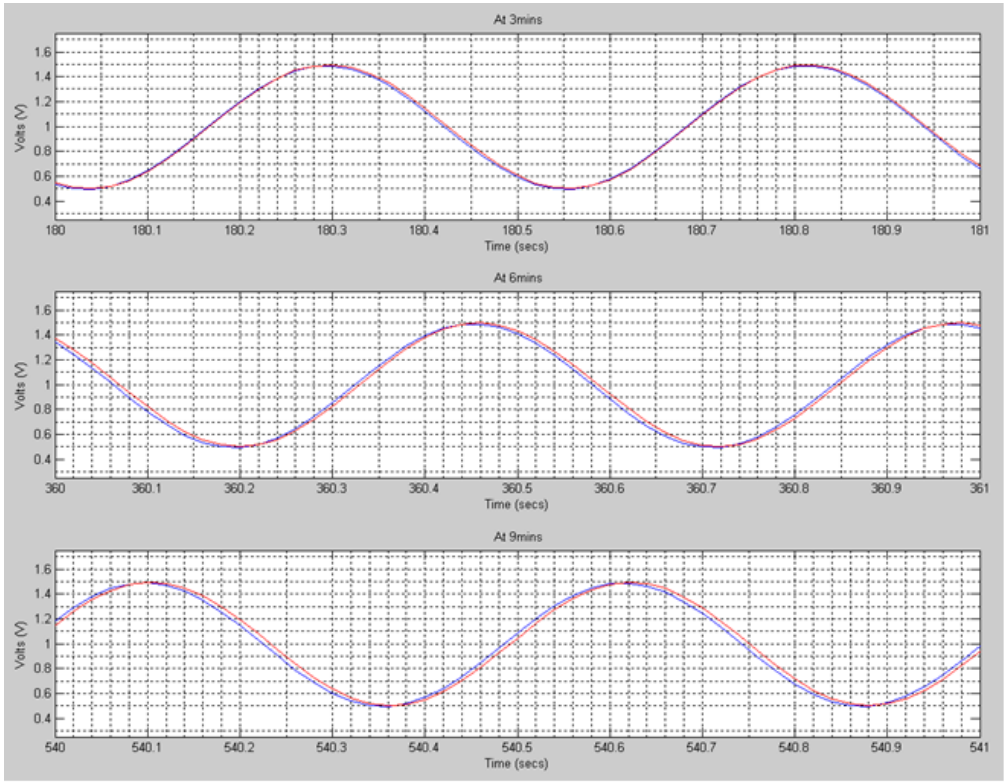

(a) No synchronisation to Sync Broadcasts, shown at 3, 6, and 9mins - Node1=blue, Node2-red

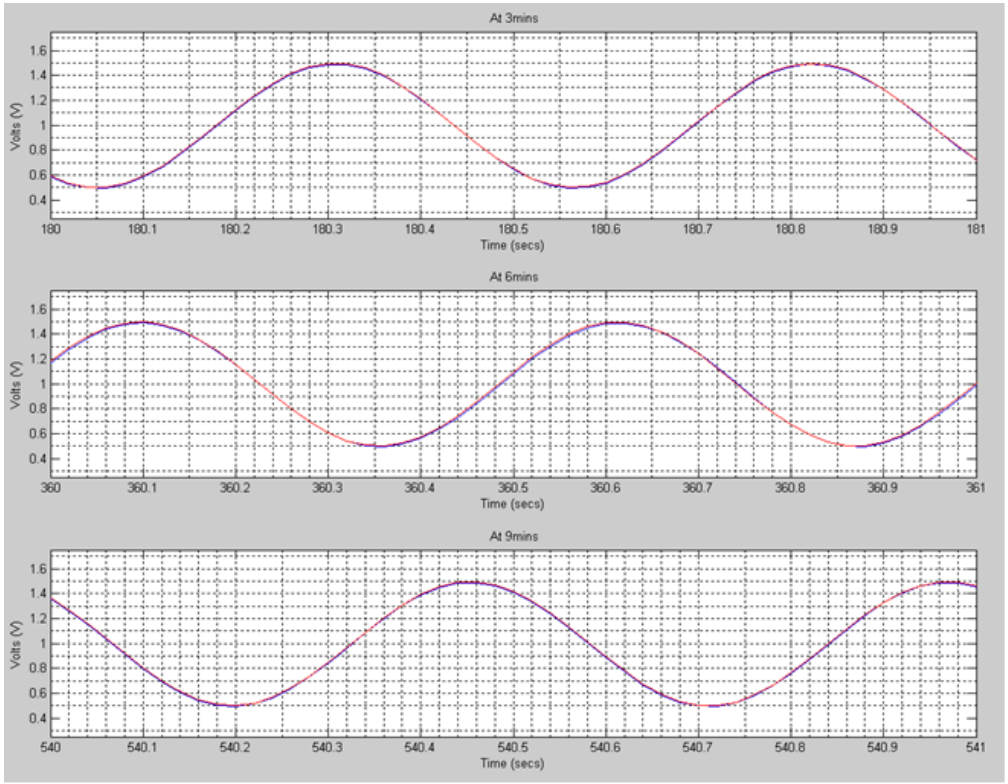

(b) Synchronisation every Sync Broadcast, shown at 3, 6, and 9mins - Node1=blue, Node2=red

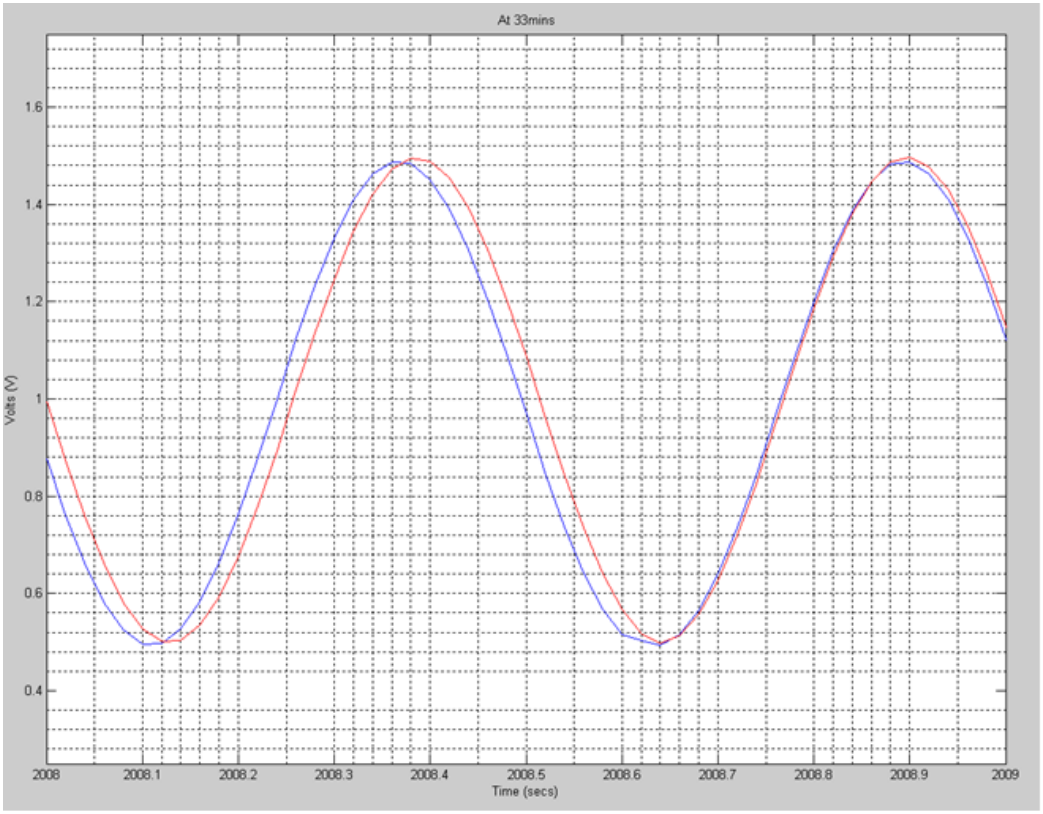

Figure 4-19: Testing of synchronisation between two sensor node

Unsynchronised nodes exhibit 6.28msec drift over 9 minutes, synchronised nodes demonstrate synchronisation to 0.79msec over same period

By taking the sampled voltage for the two unsynchronised nodes at 9 minutes (Figure 4-19 a), the phase difference between the two nodes can be calculated and the drift can be calculated. This was found to be 6.28ms±0.39ms drift over the 9minutes, well within the worst-case tolerance for the watch crystals, but not insignificant. Conversely, the calculated drift for the synchronised nodes (Figure 4-19 b) is 0.79msec ±0.39ms (the accuracy of the measurements is limited to the quantisation of the 10bit ADC). A small difference is to be expected as the resolution of the watch crystals only allows synchronisation to one count of the

crystal clock. A higher frequency clock would allow greater synchronisation, but the results obtained are considered satisfactory.

4.3.5 Data Integrity

The signal generator was also used to generate a known signal so that the firmware code of both sensor nodes and coordinator could be tested to look for discontinuities in the data. Such discontinuities could result from coding errors in the local storage of data, retrieval for upload from sensor node to coordinator node, during transmission of data, or storage at the coordinator (this is a particular concern due to packet collisions or loss).

In order to ensure that all packets of data transmitted from a sensor node are correctly received by the coordinator, a method of hand-shaking was employed. The coordinator requests each batch of 1024bytes of data, transmitted as 10 packets of 95bytes, and one of 74bytes (it was found that 95bytes is the maximum length of a data packet that could be transmitted, excluding the header information). If 11 packets of data is not received within an acceptable time, a resend request is made for the batch of data. This is necessary because MAC level acknowledgements cannot be relied upon by the transmitting node to determine if a packet has been successfully delivered to the application layer. A resend request also causes a *YellowCard* counter to be incremented. If, due to a problem with the sensor node, a predetermined number of *YellowCards* are allocated to the node, it is issued with a *RedCard*. The coordinator will then no longer interrogate the sensor node for data for the duration of its upload interval. The coordinator will cancel the *Yellow*- and *RedCards* at the commencement of the sensor node's next upload interval. If the predetermined number of

YellowCards is not reached, the coordinator will continue to request data until all data stored by the sensor node in the previous *SectionStorageTime* is uploaded.

The application layer has also been written to reject duplicate messages (indicated by messages which carry the same sequence number).. These occur when the receiving node sends an acknowledgement message to say that it has received the packet but the transmitting node misses the acknowledgement. If the acknowledgement is missed, the transmitting note attempts to send the packet again.

4.3.6 Power consumption

By sending the radio in the sensor nodes to sleep when they are not transmitting data to the coordinator node, the power consumption of the nodes can be minimised. The wake-to-sleep pattern can be varied according to the precise requirements of the system. For example, for analysing the data off-line, as implemented at this stage of the research, the sensor nodes fill half the data memory capacity (one of the two memory ICs) with data, and upload this data as a long burst of packets in its upload interval whilst the second memory IC is being filled. Thus the radio is only active for brief periods during the broadcast windows to receive synchronisation messages, and for one Upload Interval per Section Storage Time to upload data.

However, the system can also be implemented to upload one second of data in a short burst every second (by dividing a one second interval into individual upload intervals for each sensor node. This is possible because of the short sleep-to-wake latency of the Zigbee radios. If the coordinator uploads this data

continuously to a laptop, this would allow the system to display sensor data in near-real-time for immediate feedback.

An example of the variation in power consumption of a sensor node when the radio is sleeping, listening or transmitting can be seen in Figure 4-20. Measurements were made of the voltage drop across a 1Ω R_{SENSE} resistor, placed in the positive supply line of the sensor nodes using a current sense amplifier. This outputs a voltage proportional to the current passing through the sense resistor, and the current consumption of the sensor node can be calculated. When the radio is off, the current consumption of the sensor node (including radio, control circuit and peripheral circuitry) is 12.36mA, when the radio is on and listening it is 30.86mA, and when transmitting it draws 33.36mA. Figure 4-20a shows the sensor node radio to be in sleep mode, switching the radio to active listening mode for broadcast windows (to listen for instruction or synchronisation messages from the coordinator node). Data is transmitted in the sensor node's individual upload interval. Figure 4-20 b shows the sensor node radio transmitting 11 packets of data. The actual power profile of the node is complex as there are many factors that influence it. However, in the current configuration, a sensor node has an active radio (either listening or transmitting) approximately 1/5 of the total time, extending the battery life by a factor of 5.

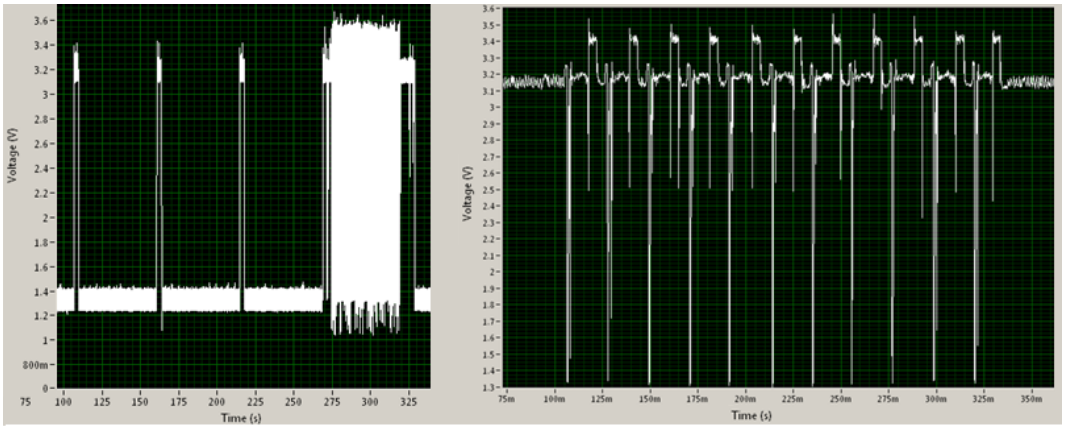

(a) Radio active for broadcast windows, and an individual upload interval

(b) Upload of 1024bytes of data in 11 packets

Figure 4-20: Power profile of the wireless BSN

Complex waveforms of power profile as node performs various functions – most significant variations due to state of Zigbee radio (sleep, receiver active, transmitter active) – highlights importance of minimising radio active time

4.4 Chapter Summary

The hardware and firmware development of the Wireless BSN system has been described. In particular, the Memory design, data transfer and related power considerations were discussed. The design and test of the sensor circuitry is reviewed, and the development of the application framework of the firmware is summarised, including particular consideration to the synchronisation of the sensor nodes.

5 Experimental Results and Discussion

The Wireless BSN has been designed and tested for functionality in a laboratory setting. Through its utilisation in a sporting environment, where either wired measurements would encumber the athlete, or where laboratory-based equipment is impractical, it should be possible to collect information and gain insight into sporting technique with minimal disturbance to the athlete.

5.1 Chapter Organisation

This chapter looks at the synchronous measurement of muscle activity from several muscles across an oarsman during rowing activity, and complements this data with information yielded from accelerometers at multiple sites upon the body. Experimental ergometer data is analysed to determine primary placement of nodes to maximise relevant information pertaining to the rowing stroke with fewest nodes. Data collected with the wireless BSN is compared and validated with laboratory measurements using Qualisys landmark measurement motion capture and Delsys sEMG. Ergometer measurements are compared to on-water data, and analysed in conjunction with accelerometer data from the boat. Comparison is made between athletes of similar build and rowing skill, on river and ergometers, demonstrating simultaneous measurement upon two athletes. Results are discussed with reference to previous literature.

5.2 Wireless BSN experimentation upon Ergometer

Multiple wireless nodes upon the body enable the synchronous measurement at several sites. However, due to practicality, only five nodes were fabricated (excluding the central coordinating node), and as such, decisions needed to be made regarding the most promising sites of interest. In the boat, one node must be used to monitor overall boat acceleration, but upon the ergometer, all 5 nodes can be used for muscle measurement upon the rower and to gain accelerometer data to enhance the information gained by the muscle activity measurement.

Sites were chosen proximal to muscles of interest where accelerometer data might be beneficial: the shank, thigh, upper and lower back, abdominal region and upper arm. Additional sites monitored included the forearm, hip and the ergometer seat. sEMG circuitry upon the nodes was connected to electrodes via 18cm (7inch) cables to allow nodes to be sited a little distant from muscles to benefit from optimal placement for acceleration, and to allow a common node site for both anterior and posterior muscle measurement on rower limbs. Figure 5-1 indicates the sites upon the rower that were monitored over the course of experimentation.

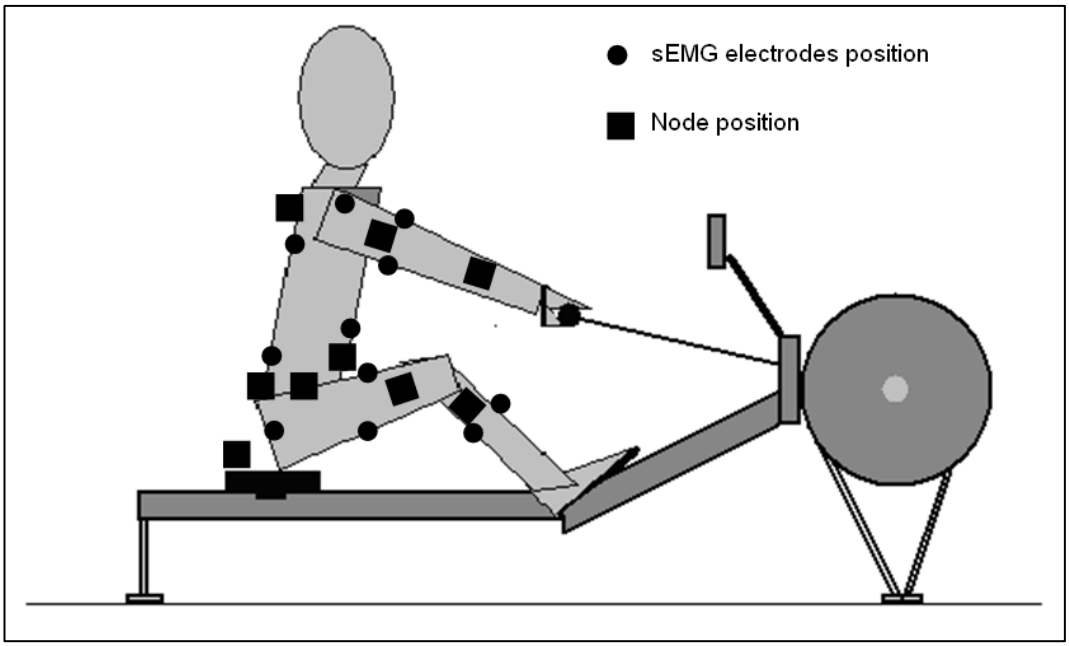

Figure 5-1: Node and sensor placement over all on-land and in-boat experimentation

Experiments were performed to fulfil a number of goals:

- To verify the feasibility of wireless measurement of muscle activity upon a rower (in-boat and on ergometer)
- To monitor multiple muscles simultaneously during the rowing stroke
- To choose optimum node placement for minimum nodes to facilitate demonstration of crew (multi-rower) measurement
- To validate wireless BSN data using motion capture equipment
- To demonstrate crew measurement

5.2.1 Initial measurements and node placement

Before experimentation it was hypothesised that nodes upon the thigh would reveal acceleration information concerning leg drive, as well as progression upon

the slide from increasing or decreasing gravitational component upon the axis of interest, and that nodes upon the back would yield information regarding the catch and body lean. It was theorised that whilst inertial and gravitational acceleration could not be entirely separated, acceleration data at a particular site would demonstrate a signature shape that could be used to gain qualitative information about the rowing stroke. Initial measurements were performed upon a Concept 2 ergometer to analyse acceleration data from the shank, thigh, upper back, lower back and ergometer seat. Figure 5-2 indicates the node sites, and the accelerometer axes of most interest (note the accelerometer axes are not aligned to a global coordinate system but rotate with the rower's body).

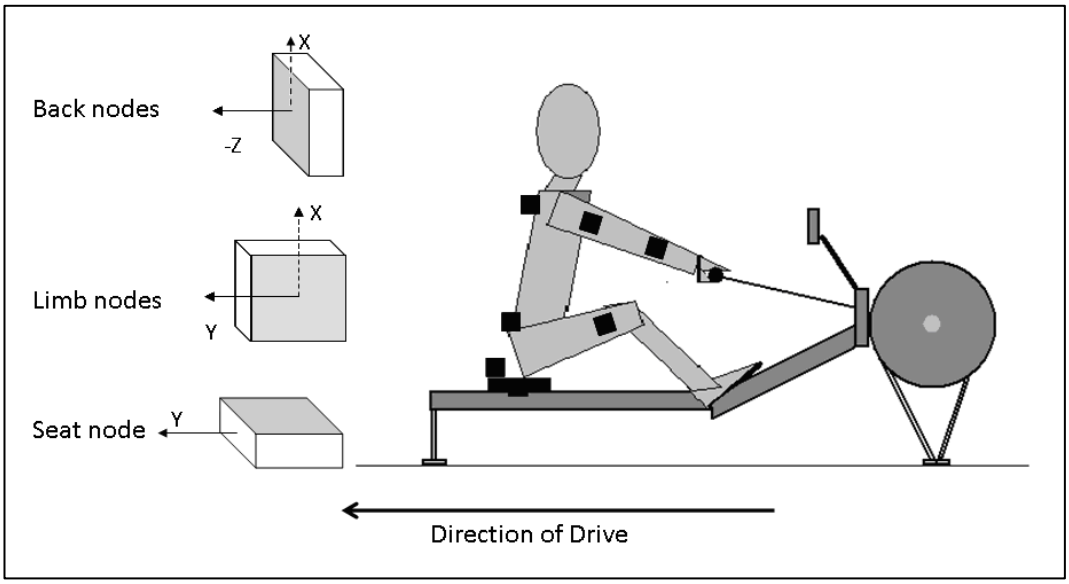

Figure 5-2: Node placement for initial experimentation, and direction of drive

Node orientation is given for backstops position, relative to direction of drive for axes displayed in results

All data was imported into MATLAB (Mathsworks) for processing. Raw ADC digital values were converted to acceleration using zero-g calibration and sensitivity values for each node, and samples converted to time in seconds. Acceleration data was also smoothed using 3-point moving averaging (examples

of 3-and 5-point moving averages compared to raw data can be seen in Figure C-1 of appendix C.1).

Strokes from successive experiments were aligned to demonstrate the repeatability of measurements of the rowing stroke and to gain information regarding the signature shape of acceleration at various sites (Figure 5-3). The catch, drive, finish, recovery are marked. Progression up the slide is evident in the thigh measurement by the decrease in acceleration over the recovery due to the increased gravitational component constituting the acceleration along the axis of interest (recall that the accelerometer measures the reactive force to gravity (upwards) rather than gravity itself). Due to the rotation of the nodes placed upon limb segments, acceleration and deceleration cannot be read as displacement above and below 0g, rather relative acceleration changes must be considered. Thus the apparent increase in acceleration value (measured by an accelerometer axis pointing towards the back of the ergometer) before the catch, evident in all three traces, is due to the deceleration as the rower approaches the catch position. The drive itself is evident in the thigh by the significant deviation of the acceleration contrary to the increase expected by a reduction in gravitational acceleration along the axis of interest. The deceleration towards the catch partially obscures the true 'gravitational' value (~-5.5ms^{-2} according to Figure 5-4) at front-stops, thus the first part of the drive phase is still positive relative to this.

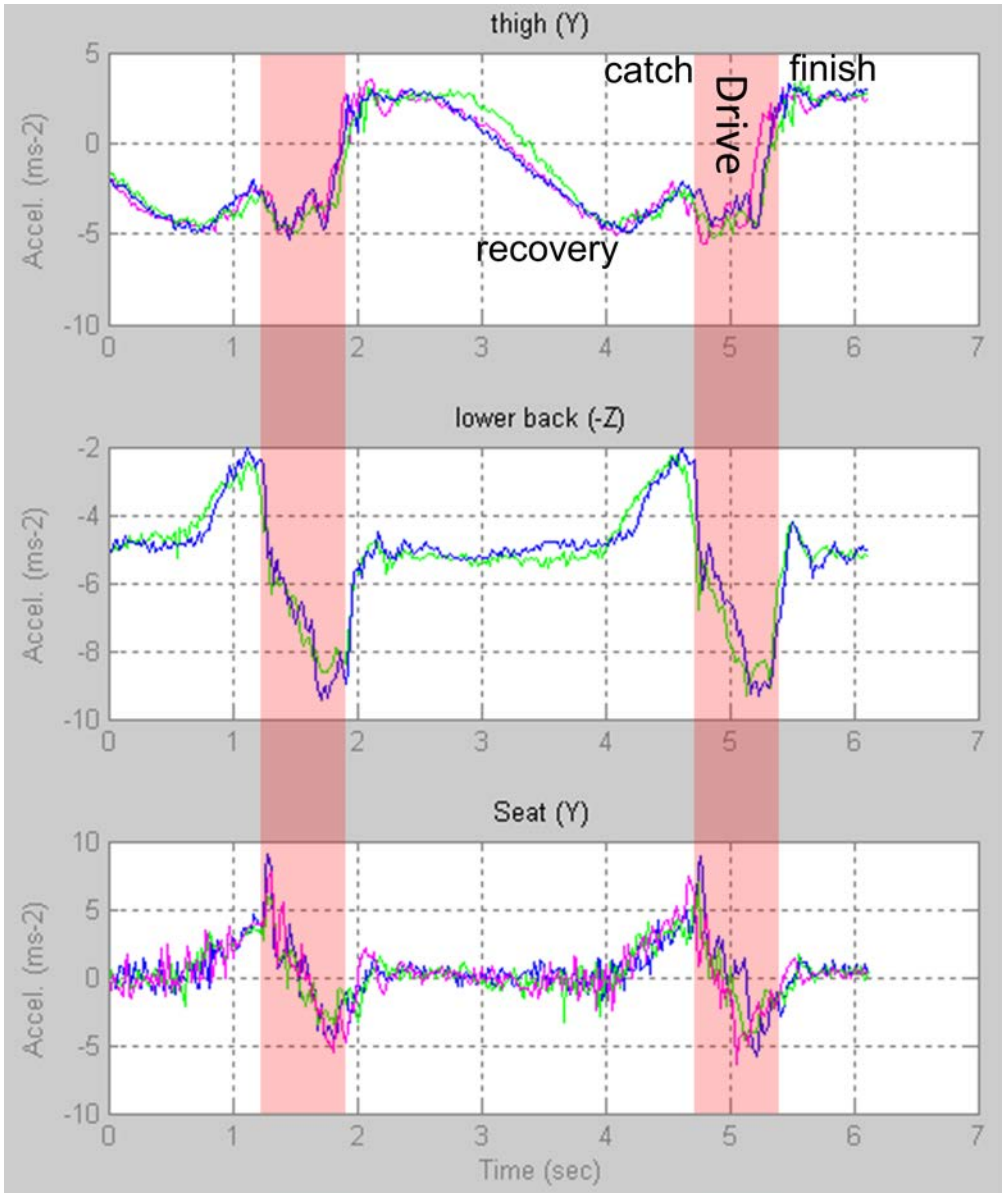

Figure 5-3: Acceleration measurement repeatability over multiple experiments

Accelerometer signature shape at different node positions.

The seat accelerometer (the only one not to experience any change in gravitational contribution (nominally 0g along the axis of interest) clearly shows the deceleration towards the catch, the increase of acceleration at the catch, overall net positive acceleration over the period of the drive where the thigh is exerting force, and a deceleration towards the finish.

Figure 5-4 demonstrates the acceleration measured upon the thigh with gentle progression up and down the ergometer slide with no drive. The step change in acceleration of the drive phase is missing, and the acceleration shows only the contributing gravitational component. The sinusoidal shape of the acceleration is clear. In this case, a good approximation of thigh angle can be made by resolving the gravitational acceleration. In the example given, the angle of the thigh node to the horizontal was 57^{o} at the catch, and 1^{o} at the finish.

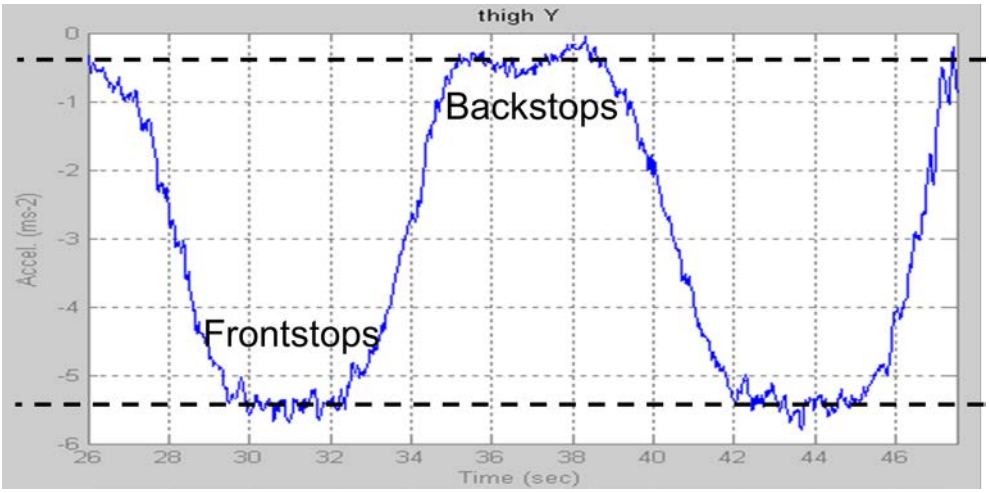

Figure 5-4: Sinusoidal signature of slide progression

Figure 5-5 demonstrates acceleration data for upper back, lower back and seat over the rowing stroke measured simultaneously during one experiment. It can be seen that all three node placements show similar features, with increasing contribution of gravitational acceleration more manifest for upper than lower back, demonstrating body lean.

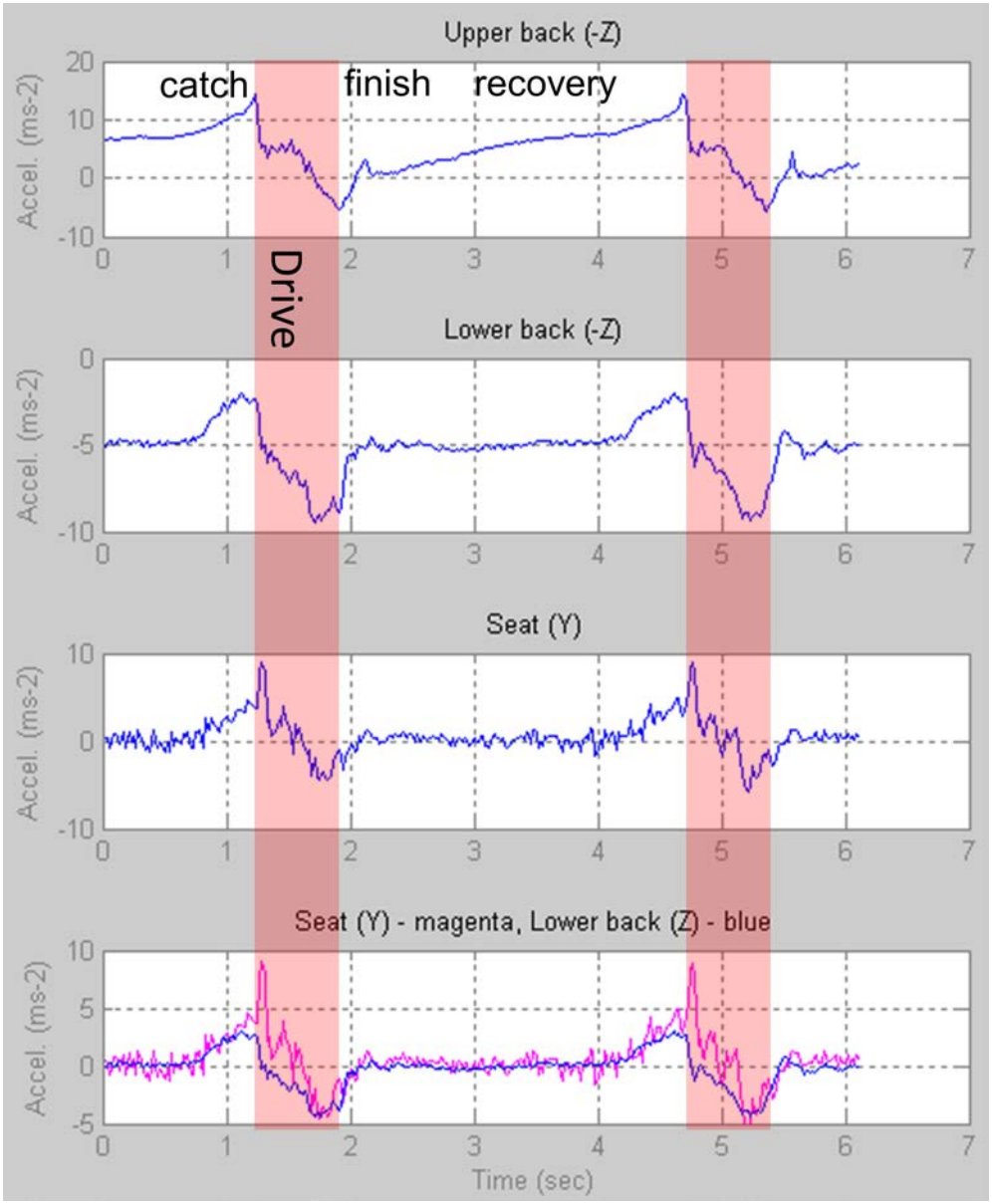

Figure 5-5: Acceleration at different nodes for one experiment

Acceleration at upper and lower back demonstrates effect of body lean. Comparison of seat and lower back acceleration demonstrates vibration noise upon seat accelerometer

Also of note in the bottom trace in Figure 5-5, through superimposing the lower back and seat data (the lower back signal is shifted to remove the offset due to the gravitational component for ease of comparison) is that whilst the traces are similar, the seat data carries a high level of vibration noise from the ergometer itself, which is damped when node placement is upon the body. Additionally,

node placement upon the seat prohibits the simultaneous measurement of muscle activity using the same node. As such, the upper back node placement can facilitate the measurement of muscle activity of the trapezius or deltoid muscles at the same time as revealing information regarding the timing of the catch, rock-over and body lean.

Whilst the accelerometer axes are not aligned to each other, they are aligned in the same plane as the main axis of movement upon the ergometer slide), and as such, the sharp step in acceleration at the catch can be seen on all nodes in Figure 5-5, the magnitude however being dependent upon the angle between the accelerometer axis and the direction of travel, and the displacement of the node in the direction of the axis of interest. This sharp decrease in acceleration, particularly evident in the back nodes is due to a return to zero relative acceleration after the lock-on but before the catch.

Further consideration to node placement upon the arm can be seen in Figure 5-6. Whilst it was felt that the prototype nodes were a little large to place comfortably upon the forearm for extended periods, a single experiment was conducted to analyse the acceleration of the forearm (in the boat the forearm remains largely horizontal and speed of “hands-away” would be an interesting metric to determine). The acceleration measured at the forearm and upper-arm are shown (thigh and upper-back acceleration are also displayed to facilitate understanding of drive and recovery time in relation to the arm movement). The forearm trace clearly shows a small net positive acceleration of the drive phase and pull-through of the arms, followed by the negative transition at hands-away. The upper-arm trace is more complex to interpret as upper arm rotates through $>120^{o}$ during the pull-through, where the gravitational contribution would reach a

minimum partway through the pull-through of the ergometer handle to the chest (when the upper-arm passes through vertical). However, upper-arm acceleration does show the same deceleration towards the catch displayed upon the other nodes, along with a return to zero relative acceleration at the catch. The decrease in acceleration at hands-away is also evident, and synchronous to that of the forearm.

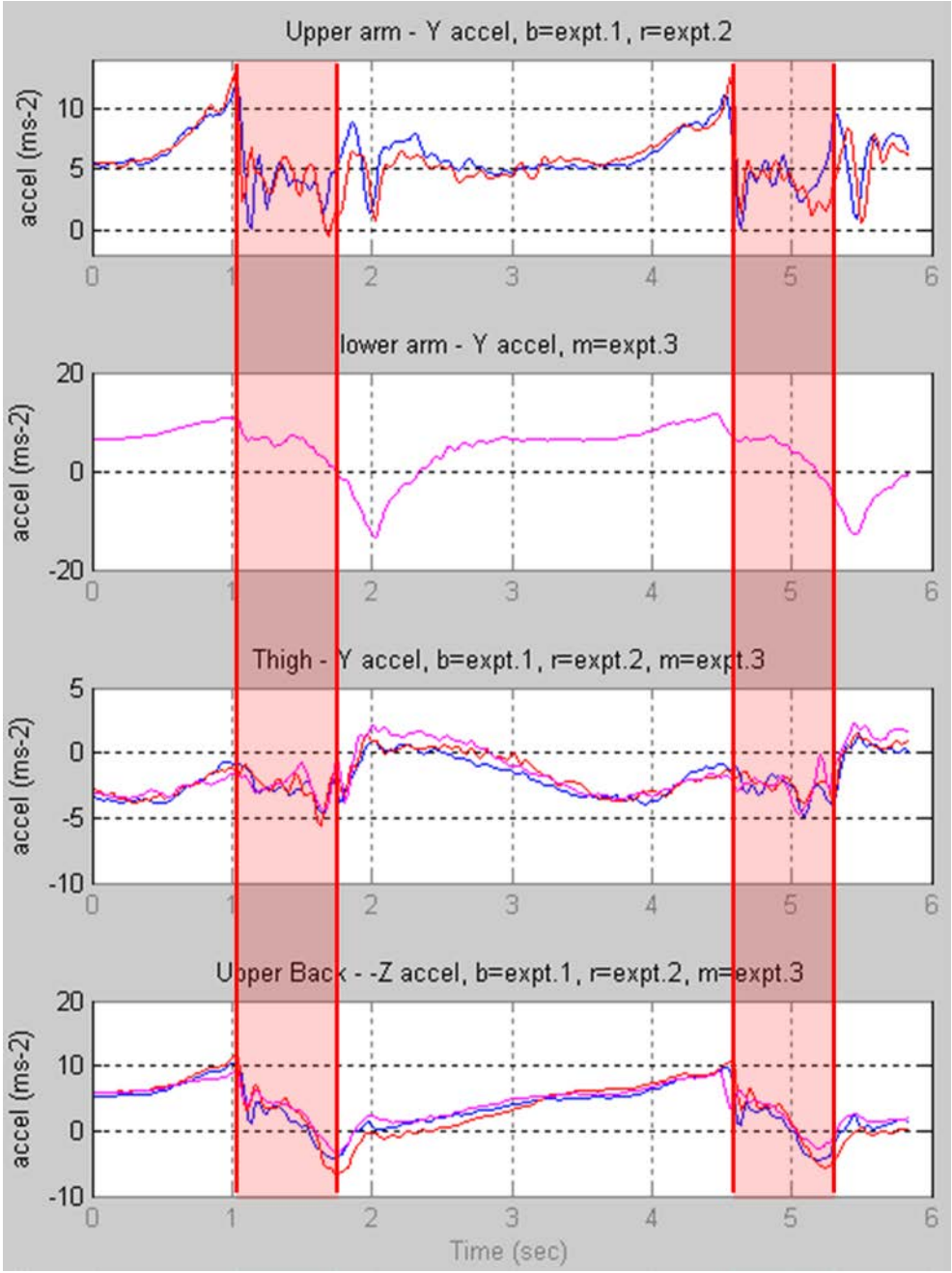

Figure 5-6: Forearm and upper-arm acceleration measurements

b=blue, r=red, m=magenta

In conclusion, nodes placed upon the thigh and upper back yield useful acceleration information to complement muscle activity measurements and are sited in the proximity of muscles of interest. These nodes therefore form the basis

of measurements where minimum nodes are used. A node upon the forearm would be considered after further node minimisation.

5.2.2 Validation of measurements through motion capture.

In order to validate the data measured using the wireless BSN, three nodes were placed upon the right shank, right thigh and central upper back to monitor acceleration and muscle activity (gastrocnemius, biceps femoris and trapezius muscles), and a Qualisys motion capture high speed camera system was used to capture positional and acceleration information from three reflective markers placed upon the nodes to precisely track the node position during the experiment. Figure 5-7 indicates the node placement, and the Qualisys coordinate system. Note the x-axis of the motion capture space is along the main axis of movement upon the ergometer slide. Additionally, two Delsys sEMG sensors were synchronised to the Qualisys motion capture system to monitor muscle activity upon the left shank and thigh. As ergometer rowing is symmetrical, the left and right side of the body can be expected to demonstrate similar (but not identical) activity. Electrode placement was made with reference to Gray's Anatomy (Gray 1998) and the SENIAM-project (SENIAM Project).

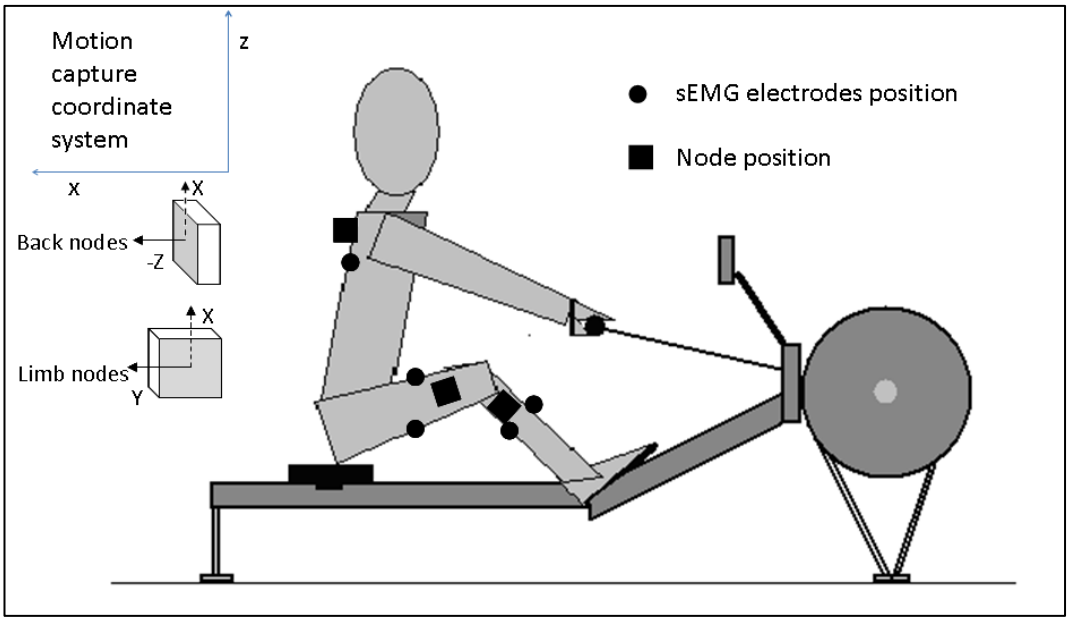

Figure 5-7: Node placement and experiment set-up for motion capture validation

The wireless BSN was programmed to output a trigger signal to start the Qualisys data capture such that the two datasets would begin simultaneously.

Figure 5-8 and Figure 5-9 show, for upper back and thigh, positional and acceleration data for the motion capture x- and z-axes, acceleration data for the wireless BSN accelerometer axes X and Y for the thigh, and Y and Z for the upper back, and muscle activity data. Note, for clarity, lower case letters are used to denote the motion capture coordinate system which is static, and upper case letters are used to denote the accelerometer axes (which rotate with limb movement). Due to the linear action of the rowing stroke upon an ergometer, displacement transversely to the motion along the ergometer slide is minimal and has been omitted here. Muscle activity has been normalised to the largest value in the window displayed. Shank measurements are included in appendix C.1.

Figure 5-10 combines upper back and thigh data, displaying the axes which yield greatest information regarding the position / acceleration of the nodes.

Before comparison of the two sets of data, the rowing stroke shall be analysed and understood through the proven motion capture data.

The motion capture positional data – displaying node travel along the slide (x) and vertical displacement of the node (z) - is clearly cyclical in nature. There are two clear phases – the steep positive x gradient describing the drive portion of the stroke where the entire length of the slide is covered in a short period of time, and the more gradual negative gradient describing the steady travel back up the slide over the recovery.

The accompanying acceleration data indicates when overall acceleration (measured in the direction of the drive – towards the back of the ergometer) is positive or negative. Positive acceleration is measured at the upper back as the rower decelerates towards the catch, and then “locks-on” producing a further brief increase in acceleration of the upper back, and then a sharp return to zero. The deceleration of the back towards the finish is also evident. The rock-over and recovery phases each exhibit small indications of negative acceleration (positive acceleration towards the catch). The thigh acceleration data (in the x direction) displays the same positive acceleration due to deceleration towards the catch, then positive acceleration due to the drive phase, which reduces and becomes deceleration after the initial explosive impulse of the thigh. The thigh acceleration data in the z direction shows a sharp positive spike due to the thigh coming to a sudden stop as the legs lock flat at the finish.

The acceleration data from the wireless BSN is less straightforward to interpret because the accelerometers measure both a changing gravitational acceleration component as the back or thigh rotates with respect to the vertical, and the inertial acceleration due to the rower movement. However, the upper back data displays a similar signature shape to the acceleration data of the motion capture acceleration data, exhibiting the same increases or decreases in relative acceleration, and the sharp transitions of acceleration (indicating a return to zero relative acceleration) are synchronous between the two data measurement systems. Superimposed upon this similar signature shape, evident particularly where the motion capture data reads zero acceleration (constant velocity) is the increasing (during the recovery) or decreasing (during the drive) contribution of gravity due to the body lean.

Likewise the thigh acceleration data visually displays good correlation to the acceleration data of the motion capture measurement system, with the same increases and decreases in relative acceleration, and same sharp transitions but again demonstrating the decreasing gravitational component during the recovery.

The correlation between the two displayed axes of acceleration data for the upper back and thigh nodes were calculated using Pearson's correlation coefficient (Rodgers and Nicewander 1988). The wireless BSN data was first interpolated such that the datasets were of equal size, and then plotted against each other on a scatterplot to check for correlation (Figure C-5 in appendix C.1). It is clear that whilst one axis of each of the back and thigh acceleration measurements shows a strong positive correlation across the whole stroke (subplots (b) and (c)), the other axis shows strong correlation only within *phases* of the stroke (subplots (a) and (d)); the phases are coloured to match the shading

in Figure 5-8 and Figure 5-9 (drive: red, hands-away and rock-over: blue, recovery: green, transitions between phases are noted in cyan). This can be explained by overlaying the motion capture and wireless BSN data upon the same subplots (Figure C-6 in appendix C.1). Clearly whilst they visually display similar shapes, and the sharp transitions in acceleration occur within the resolution dictated by the sample rate of wireless BSN system (20ms), subplots (a) and (d) display a larger gravitational component. As the Motion Capture system measures only inertial acceleration, the changing gravitational contribution to the acceleration measured by the Wireless BSN introduces nonlinearity to the correlation (at different points of the stroke the gravitational component can either add or oppose the inertial component). Nevertheless, good correlation can be demonstrated by calculating the correlation within the phases of the stroke. Thus the thigh acceleration along the Motion Capture x-axis (Wireless BSN Y-axis) is highly correlated with r=0.85, 0.88 and 0.87 for drive, recovery and hands-away/rock-over phases respectively. Indeed, it can be further seen in Figure C-5 that the drive and recovery cover a similar area of the scatterplot (both contain a similar changing gravitational component whilst the hands-away/rock-over has largely static gravitational component) and can thus be combined to achieve a still highly correlated r=0.72. The second axis (motion capture z / Wireless BSN –X) has an overall stroke correlation of r=0.89.

Similarly in the back correlation calculations, whilst the Motion Capture x axis and the Wireless BSN –Z axis acceleration correlation can be calculated over the whole stroke, demonstrating high correlation of r=0.82, the Motion Capture z axis and the Wireless BSN Y axis accelerations need to be correlated for the phases of the stroke due to the increased gravitational contribution along that axis. This time the drive and hands-away/rock-over share the same scatter-plot area

allowing for a combined high correlation of r=0.75 (both r=0.79 individually), and the recovery has moderate correlation of r=0.54.

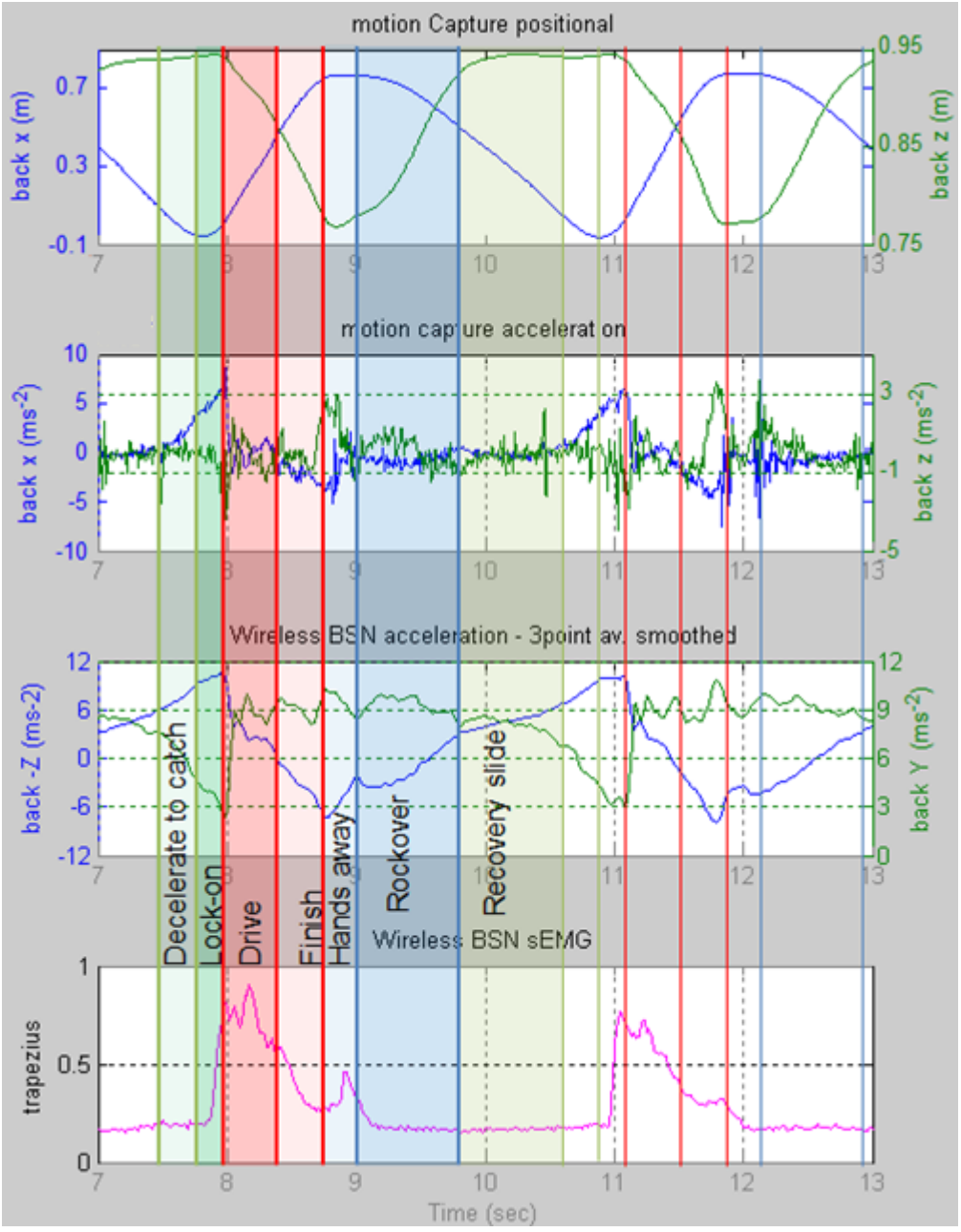

Figure 5-8: Comparison of upper back Motion Capture and Wireless BSN data

Traces from top to bottom: Motion Capture position of back node in x—z plane, Motion Capture acceleration of back node, Wireless BSN acceleration of back node (-Z—Y plane), trapezius sEMG

Motion Capture x / Wireless BSN –Z stroke-phase correlation r=0.87 (hands-away/rock-over) and r=0.72 (recovery)

Motion Capture z / Wireless BSN Y whole-stroke correlation r=0.89.

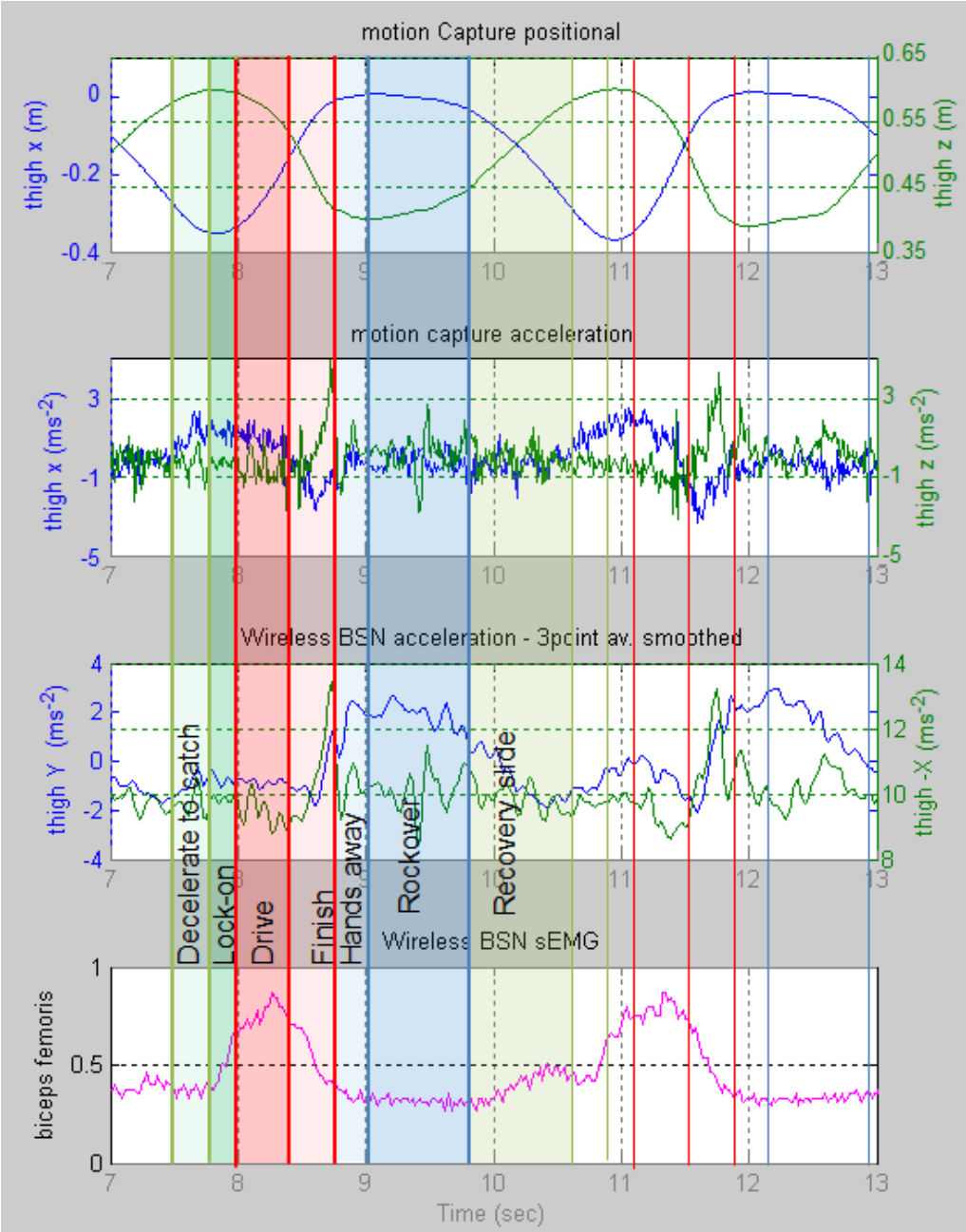

Figure 5-9: Comparison of thigh Motion Capture and Wireless BSN data

Traces from top to bottom: Motion Capture position of thigh node in x—z plane, Motion Capture acceleration of thigh node, Wireless BSN acceleration of back node (Y—-Z plane), biceps femoris sEMG

Motion Capture x / Wireless BSN –Z whole-stroke correlation r=0.82

Motion Capture z / Wireless BSN Y stroke-phase correlation r=0.75 (drive and hands-away/rock-over) and r=0.54 (recovery).

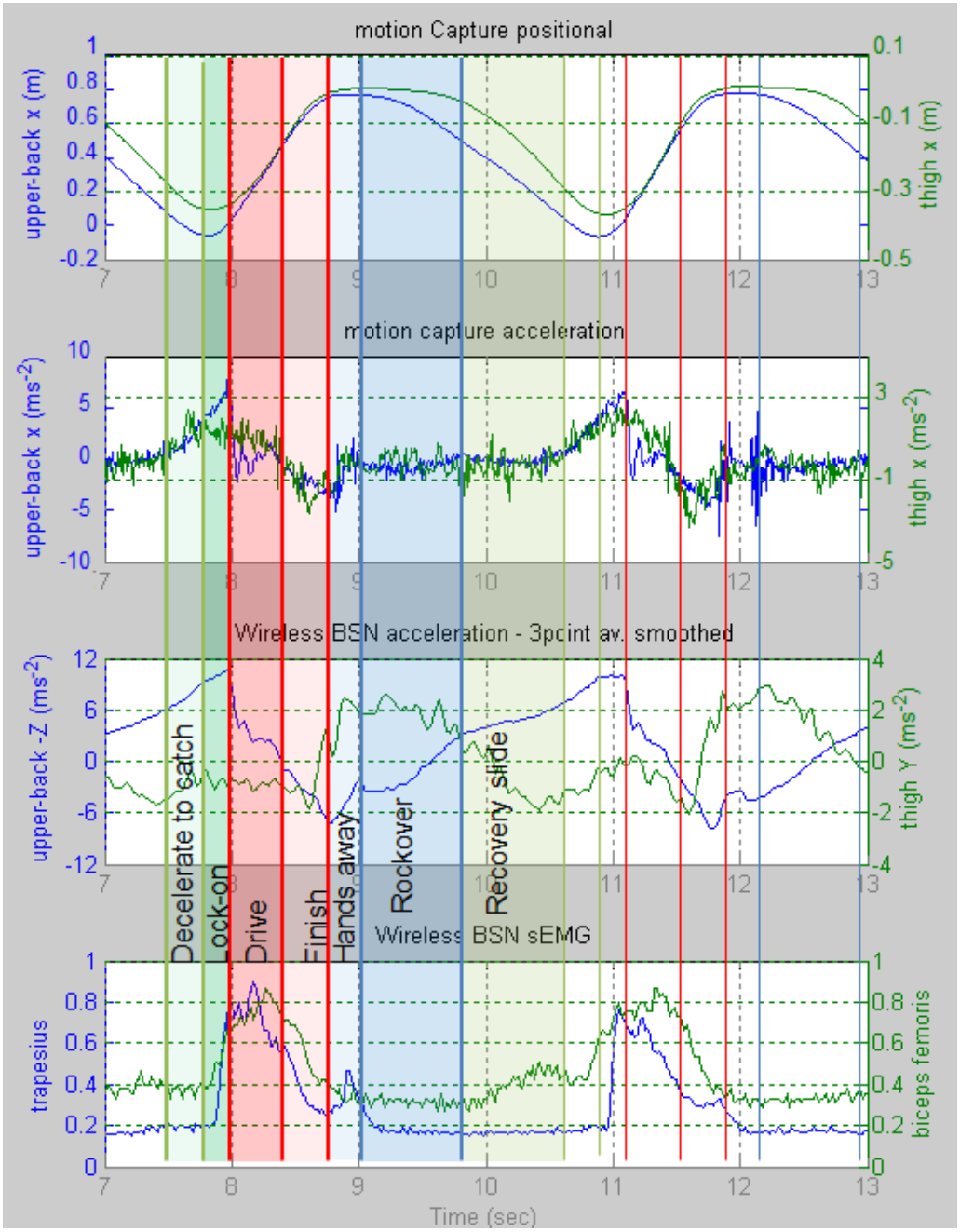

Figure 5-10: Most informative Upper back and thigh data – comparison of Motion Capture and Wireless BSN data using dominant axis only

Traces from top to bottom: Motion Capture position of back and thigh nodes (x-axis), Motion Capture acceleration of back and thigh nodes (x axis), Wireless BSN acceleration of back (-Z axis) and thigh (Y axis) nodes, trapezius and biceps femoris sEMG

Accompanying the wireless BSN acceleration data is the muscle activity. The trapezius muscle is active from the lock-on at the catch, through the drive to the

finish. The biceps femoris of the thigh hamstring muscle group is active over the drive phase of the stroke, has some low activity through the recovery, increasing slightly on the approach to the catch to assist in deceleration towards the catch.

The muscle activity data from the Wireless BSN can be further validated through comparison with the simultaneously captured data from the Delsys sensors. The data from the two measurement systems will not be identical for a number of reasons:

- The two EMG sensing systems could not measure the same site. Left and right biceps femoris and left and right gastrocnemius muscles should show similar but not identical muscle activity over the rowing stroke.
- The electrode shape and number is different. The Wireless BSN sEMG has three circular (10mm dia.) signal electrodes and one reference. The Delsys sEMG has three bar (10mmx1mm) electrodes. The different shape and configuration of the electrodes will mean that the shape of the measured motor unit territory size will be different. Additionally, the electrode spacing is 20mm for the wireless sEMG, and 10mm for the Delsys sEMG; this will alter the amplitude and spectral content of the raw signal.
- The measurement electronics is different meaning that different filtering and amplification will be applied to the signal before digitisation.
- Finally, the extraction of the envelope shape (the force-time profile) of the sEMG signal is performed in hardware in the Wireless BSN. The filtering and envelope extraction is performed in software (within MATLAB) for the Delsys sEMG. The same parameters were used for the software extraction of the Delsys sEMG as in the hardware signal processing of the

Wireless BSN sEMG circuitry such that the signals could be treated as similarly as possible.

Figure 5-11 compares gastrocnemius and bicep femoris muscle data from the Wireless BSN and the Delsys sEMG. A number of strokes are included so that correlation between the two signals can be best ascertained to allow for naturally occurring differences between left and right muscles. The gastrocnemius muscle measurements are highly correlated with r=0.85, and whilst the data from the two systems for the biceps femoris shows greater differences, there is still visual correlation of the peaks during the drive phase, and a moderate correlation of r=0.54 is achieved. It should be noted that the signal level upon the thigh sEMG node for this particular experiment was rather low, which might account for some of the loss of sensitivity of the measurement; perhaps the electrode placement for this node was below optimum.

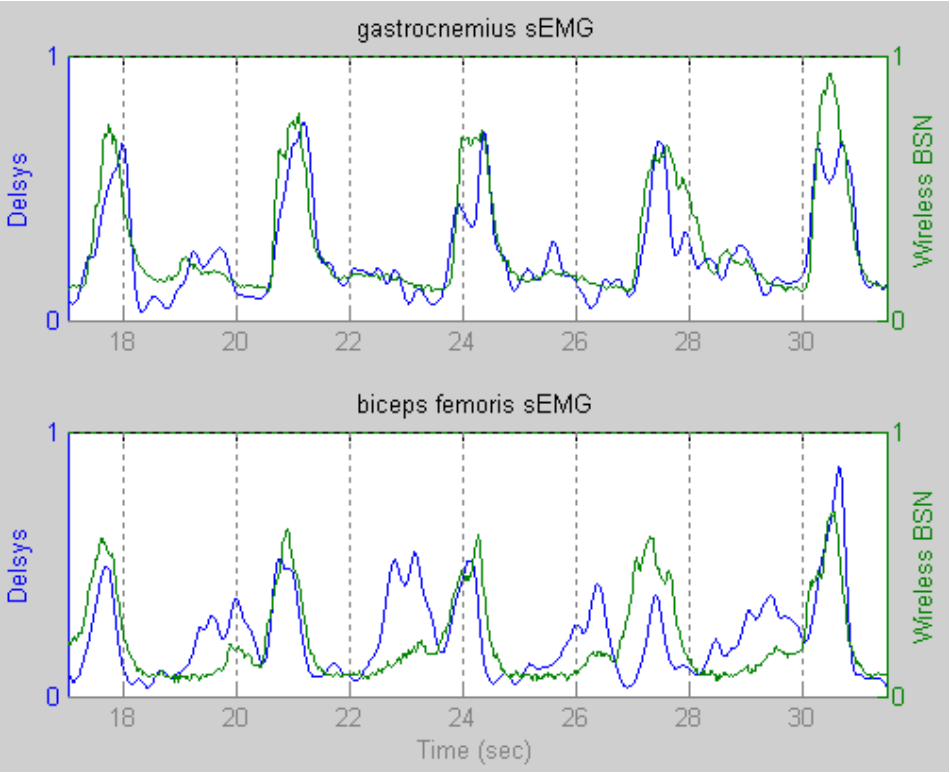

Figure 5-11 Comparison of sEMG data from Delsys sensors and wireless BSN

Wireless BSN nodes upon right leg, Delsys sensors upon left leg

Wireless BSN removal of high frequency components (envelope detection) in hardware, Delsys envelope detection during MATLAB processing.

Correlation between Delsys sEMG system and Wireless BSN: Gastrocnemius muscle r=0.85, Biceps Femoris muscle r=0.54.

In conclusion, the wireless BSN displays synchronous data collection, and demonstrates similar signature acceleration patterns to that observed by the motion capture measurements system, and mostly highly correlated. Where absolute acceleration and deceleration is evident from the motion capture system (acceleration above $0ms^{-2}$ and deceleration below), the gravitational component of the wireless BSN acceleration data means that the “zero-crossing” value drifts with the angle of the nodes. Thus it is the overall trend that needs to be observed rather than absolute values. Comparison of the wireless BSN sEMG data to that of the Delsys sEMG shows high correlation of gastrocnemius, and moderate correlation of the biceps femoris data.

5.2.3 Synchronous measurement of muscle activity

In order to monitor muscle measurement synchronously at multiple sites across the body during ergometer rowing with only 5 sensor nodes fabricated, two experiments were designed such that node placement could remain fixed and anterior and posterior muscles of several body segments monitored. Figure 5-12 indicates the node and electrode placement. Nodes 1-4 remained in fixed positions (at shank, thigh, upper-arm and upper-back), measuring tibias anterior, gastrocnemius, quadriceps femoris – vastus lateralis (VL), biceps femoris, biceps brachii, triceps brachii, and trapezius transversalis. Node 5 was moved from the abdominal region to the hip such that first abdominal muscles, then gluteus maximus muscles could be monitored. A third experiment was later conducted to additionally capture latissimus dorsi (lower back) and deltoid (shoulder) muscle activity. Black indicates where a node or measurement site remained unchanged throughout, blue indicates experiment 1 (posterior muscles), red indicates experiment 2 (anterior muscles), magenta indicates an additional third experiment.

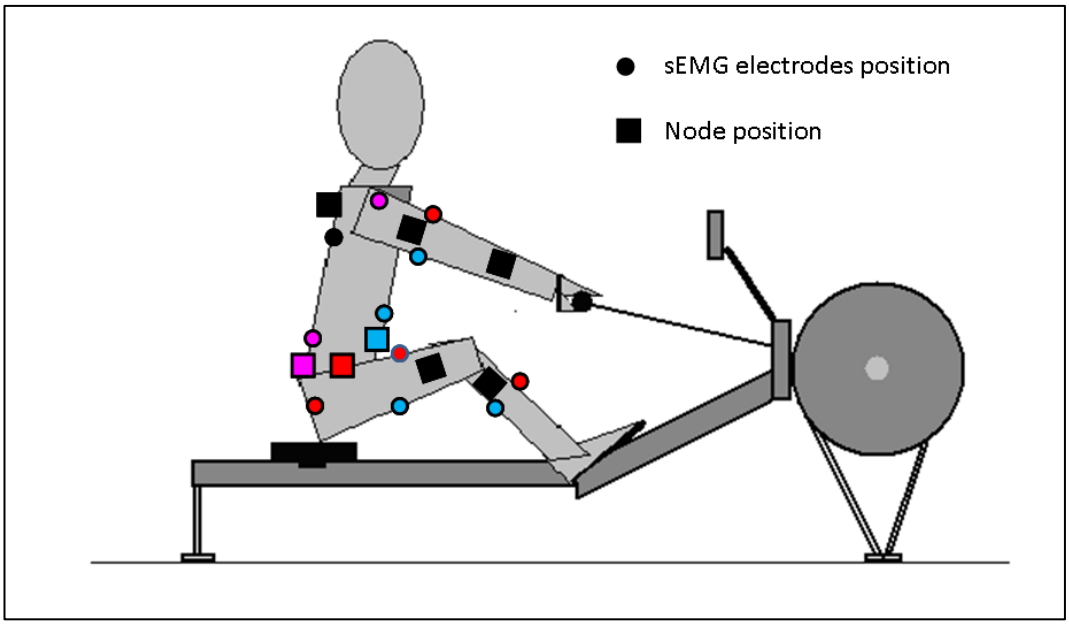

Figure 5-12: Node placement, and sEMG measurement site

Three experiments: black nodes/electrodes position indicates node in common position across the 3 experiments, blue – experiment 1, red – experiment 2, magenta – experiment 3

The sEMG circuitry signal output (and ground reference) was routed to a short connection outside of the node such that good electrode placement could be verified before commencing the experiment through monitoring of the muscle activity upon an oscilloscope.

The athlete was asked to row at a steady rating of 17-18spm with a split-time (a measure of power) of 2-2.10 min/500m.

In order to correlate the two experiments to demonstrate the activity of multiple muscles over the rowing stroke, strokes from both experiments were aligned and overlaid, using the acceleration signals predominantly of upper-back and thigh to ensure that the strokes were synchronised in time.

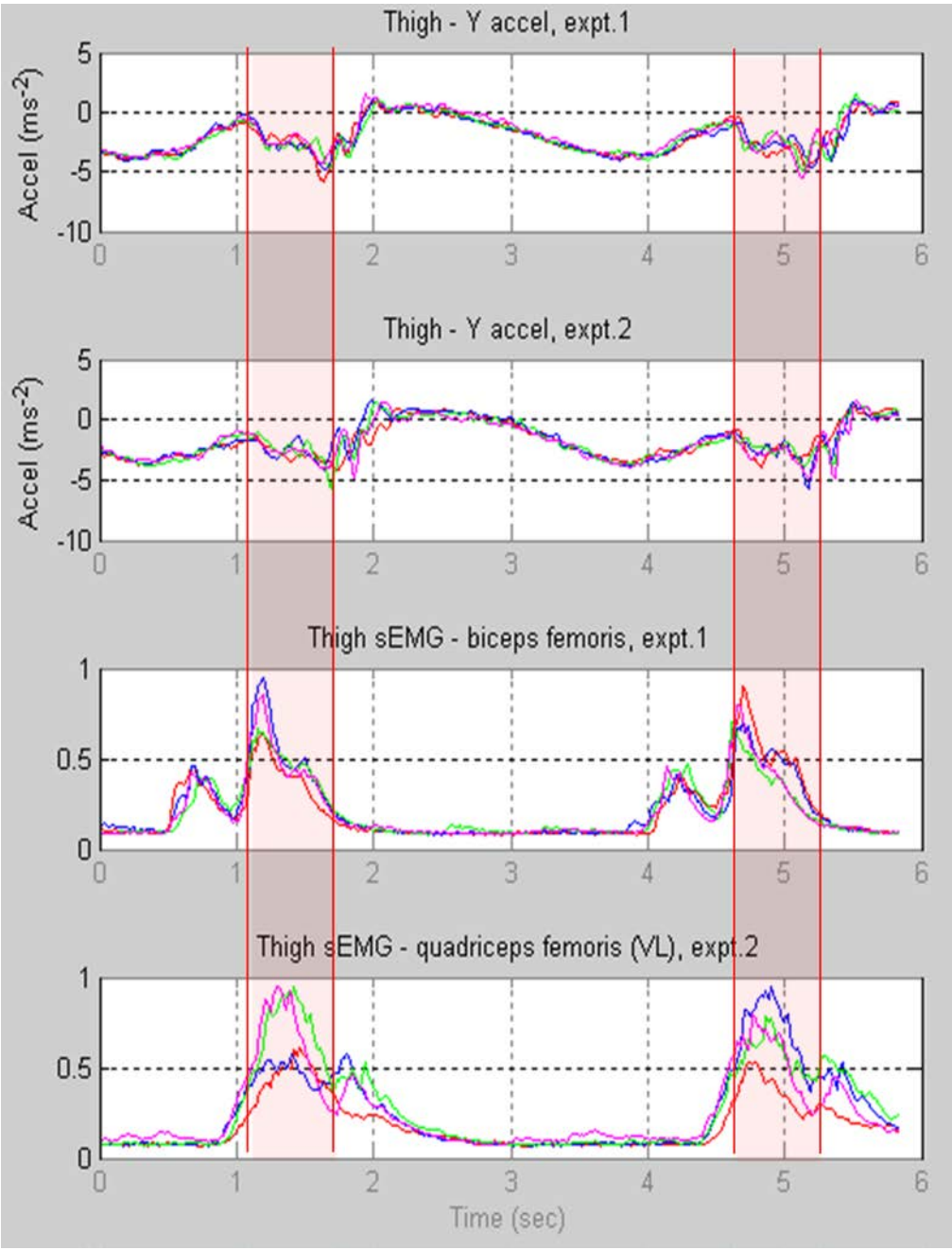

Figure 5-13: Thigh acceleration and muscle activity data over two experiments

Experiments aligned by thigh acceleration data to allow analysis of sEMG data from multiple experiments

Variance Ratio VR = 0.10, 0.03 and 0.07 for thigh acceleration, biceps femoris and quadriceps femoris (VL) muscles

Figure 5-13 shows thigh data for four strokes from each experiment aligned and overlaid (the drive phase is also highlighted). Muscle activity was again normalised to the maximum signal in the data window displayed. Good stroke

alignment allows the activation time of posterior and anterior muscles from the same limb segment to be compared. Similar graphs of shank, upper-arm, upper-back, abdomen and gluts can be found in appendix C.2.

The Variance Ratio (VR) optimality criterion developed by Hershler and Milner (Hershler and Milner 1978) to measure repeatability of a signal over a given number of identical footsteps in gait analysis was used to analyse stroke repeatability, as Hershler and Milner stress its suitability for determination of repeatability of any repetitive signal (VR=0 for completely reproducible signals, and VR=1 for completely irreproducible signals).

Excellent VR values were calculated for accelerations and sEMG signals at all nodes, varying from best 0.03 to worst 0.21. Since data from multiple experiments were aligned using back and thigh acceleration data, it is noted that VR values of back and thigh acceleration in the main axes of interest were 0.06 and 0.10 respectively. All other values are noted in the figure captions in Figure 5-13 and in appendix C.2.

With confidence that strokes from the two experiments could be aligned and compared, the muscle data for all nodes was overlaid in Figure 5-14. Also displayed are the thigh and upper-back acceleration to allow the drive and recovery phases of the stroke to be better understood, and to demonstrate the good correlation of the strokes overlaid. A third experiment, conducted at a later time to increase the muscles observed also displays the latissimus dorsi and deltoid muscles (thigh and upper-back acceleration was also monitored during this additional experiment so that the strokes could be properly aligned as before).

It can be seen from the overlaid data that the posterior leg muscles – the biceps femoris and gastrocnemius muscles are contracting to aid deceleration towards the catch to slow the slide in preparation for the next stroke, and in the flexion of the knee. The trapezius muscle is employed during the lock-on to the ergometer handle at the catch, followed by strong recruitment of both anterior and posterior thigh muscles – the quadriceps femoris (VL) and biceps femoris - and plantar flexion of the foot by the gastrocnemius of the posterior calf for the drive phase of the stroke. Partway through the drive phase the biceps and particularly triceps brachii are active to flex the elbow for the pull-through of the ergometer handle back to its finish position at the chest. The rectus abdominus muscles and latissimus dorsi muscles likewise play a strong role in the drive phase, maintaining the trunk stability to transfer the power of the legs to the ergometer handle. The biceps brachii, the deltoid and the trapezius muscles are active for the hands-away, and the rectus abdominus, the gluteus maximus and anterior leg muscles – the quadriceps femoris (VL) and tibias anterior – recruited during the rock-over and commencement of the recovery. As the rower progresses up the slide during the recovery, the tibias anterior of the lower leg is active due to the dorsiflexion of the ankle, and the deltoid muscles of the shoulder are contracting, along with low level activity of the trapezius and latissimus dorsi. These results agree with the descriptions given by Mazzone (Mazzone 1988) of the kinesiology of the rowing stroke.

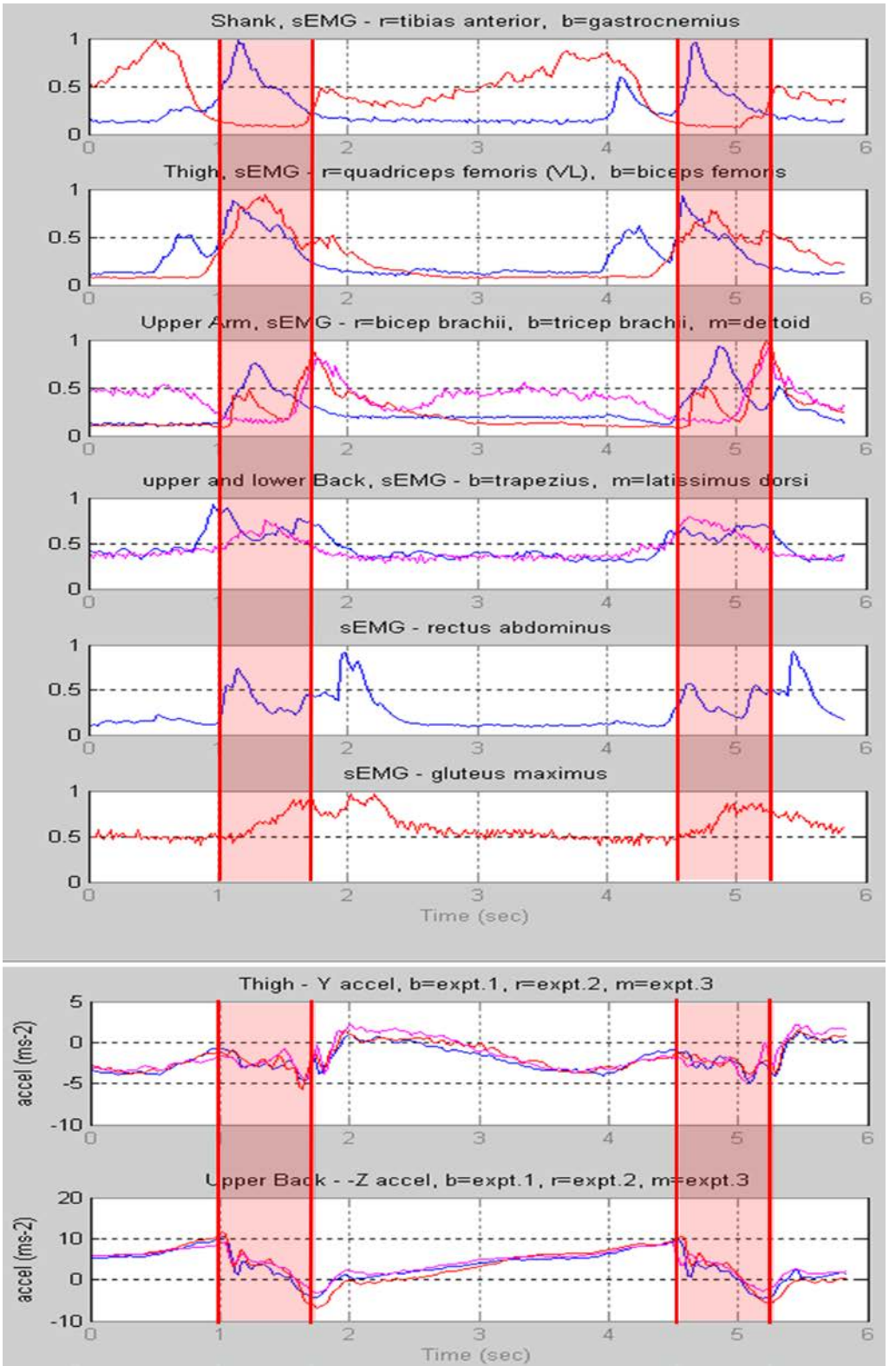

Figure 5-14: Overlaid muscle activity measurements and acceleration measurements for comparison.

The 3 experiments aligned by thigh and upper back acceleration data to allow analysis of sEMG data from multiple muscles during the rowing stroke

There are several common errors that rowers can make in the rowing stroke. Errors in the arms include breaking (bending) of arms at the catch, and “chicken wing” arms at the finish, back errors include excessive “lay-back” at the finish, lunging and overreaching at the catch, and errors of the legs include bending the knees too early in the commencement of the recovery, rushing the slide in the recovery, over-compressing at the catch, and “bum-shoving” (shooting the slide). The rower was asked to simulate the common rowing fault of “bum-shoving” for several strokes to determine if this could be detected from the measured data. This error consists of driving with the legs such that the seat leads the back in the drive phase rather leg and back drive acting as one phase. Figure 5-15 compares a normal rowing stroke with the rower simulating bum-shoving.

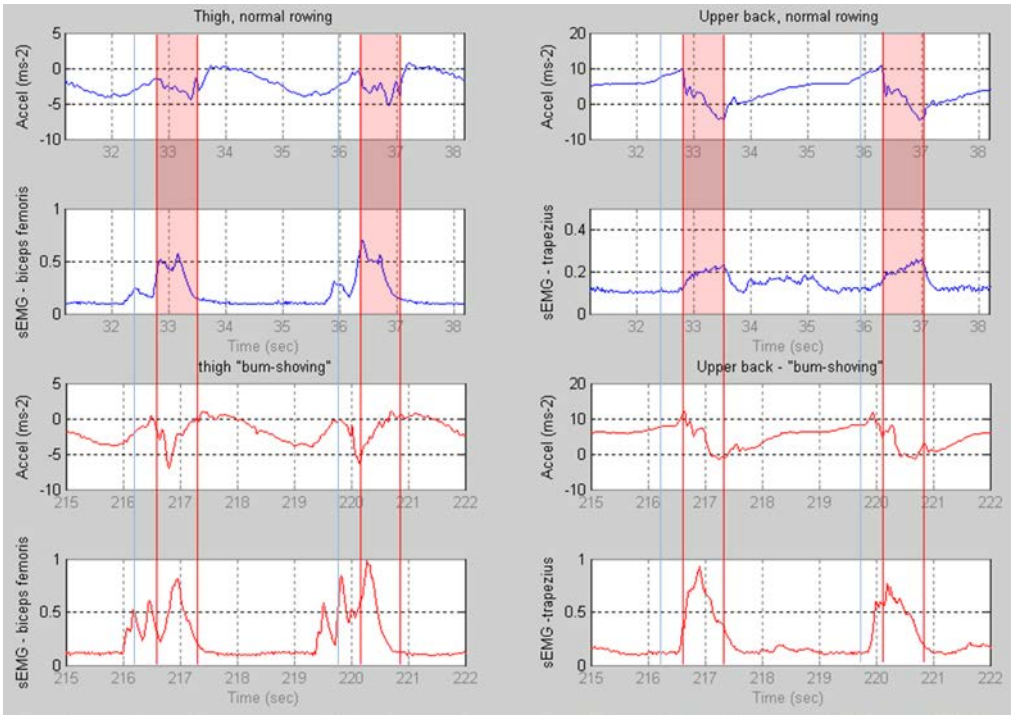

Figure 5-15: Comparison of normal rowing v “bum-shoving”

Both acceleration and sEMG data shows marked differences between normal and back-technique rowing

Analysis of the thigh and upper-back data clearly shows the difference in the thigh data, with a dramatic but short duration deviation of acceleration from the underlying gravitational base value, rather than the longer shallower deviation. This is due to the two-phase nature of the bum-shoving movement (legs, then back) such that the legs are driven flat over a shorter portion of the drive phase. The sEMG signal of the biceps femoris demonstrates a peak at the lock-on which was not evident during the normal rowing, and then a narrower peak over the drive as the full force of the leg-drive is expended in a shorter time. The acceleration data of the upper-back is missing the sharp decrease at the catch because the leading drive of the legs causes increased forward body lean, increasing the gravitational component at this point. The back is not recruited into the drive phase until later, after the initial leg drive. However, the sEMG signal from the trapezius muscle is greater and activates earlier during the erroneous stroke. It is hypothesised that this is because the back is in extension due to the legs driving early and the upper back being left at the catch.

Kleshnev (Kleshnev and Kleshneva 1992) quoted the percentage contributions of the different parts of the body in ergometer rowing: leg:trunk:arm as 44%:36%:20% respectively. It would be interesting to be able to see if a similar force curve to that generated by flywheel speed measurements of the ergometer on-board computer could be generated by weighted summing of the muscle data. To this end, the individually measured leg muscle, arm muscles and trunk muscles were summed to give an overall value for each body segment, then weighted and summed to give an overall time-varying metric proportional to power. The results are shown in Figure 5-16 for two strokes. It is interesting to note that a force pattern is generated that is not dissimilar to that measured on the ergometer computer, and that effort exerted during the recovery is also

visible. The recovery effort cannot be measured by the ergometer. Caution should also be noted however, as several assumptions were made: the sEMG signals were normalised due to the variation in signal level due to subcutaneous tissue between muscle and measurement site, muscles in a body segment were equally summed (e.g. it was assumed that equal contribution was made by thigh and shank), and the weightings were applied over the entire stroke (the legs for example might contribute much greater than Kleshnev's quoted 44% at the beginning of the drive phase, and significantly less later. It is also acknowledged that whilst many muscles were measured, these constitute only a fraction of the muscles actually recruited over the rowing stroke. Nevertheless, it remains an interesting exercise to give a qualitative measure of force worthy of further consideration.

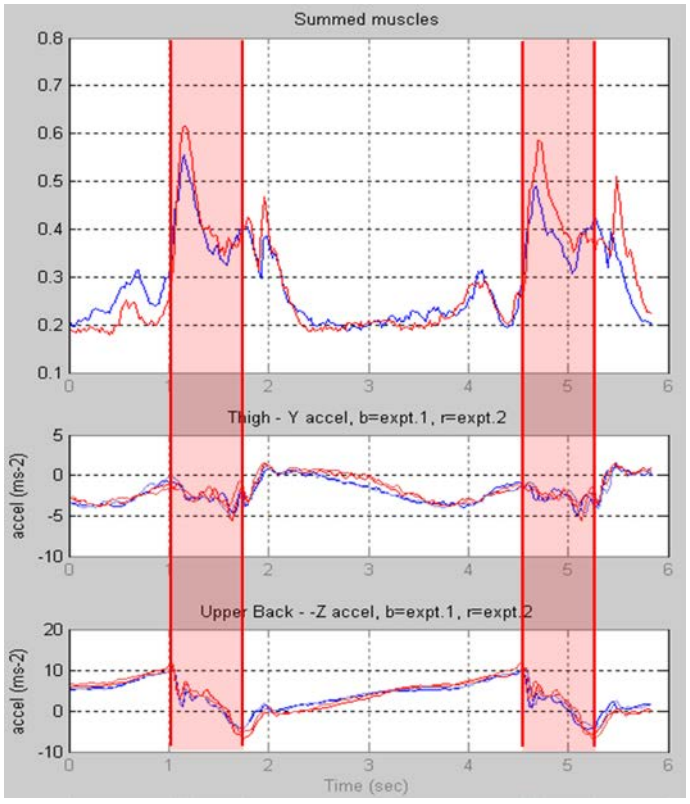

Figure 5-16: Weighting and Summing of muscle data

Allows effort during the recovery to be monitored in addition to drive phase

5.2.4 In-boat measurement of muscle activity.

The ergometer muscle experiment was followed up with measurements at similar node sites upon a rower in a single scull boat. As one node needed to be used to monitor the boat acceleration (placed towards the bow behind the back-stops position of the rower), the remaining four nodes were cited at the points of most interest: the shank, thigh, upper-arm and upper-back. Two experiments were performed, one with posterior muscles of the body segments monitored, and a second where the anterior muscles were monitored. Again, these were overlaid after it was determined that good correlation of the rowing strokes could be achieved through aligning the acceleration. Additionally, upstream and downstream strokes were analysed separately; rowers report a much stronger catch in upstream rowing than downstream, and in the case of the experiment undertaken, the river was high and fast after prolonged rain making upstream and downstream conditions especially different.

Figure 5-17: In-boat measurement of muscle activity with Wireless BSN

Comparison between boat and ergometer data is shown in Figure 5-18. Note that because of the difference in stroke-rate between the ergometer experiment and the boat experiment (erg: 17spm, river: 20spm) the ergometer data was re-sampled in MATLAB at a higher rate in the conversion from samples to time such that the duration of the strokes matched. Because the lock-on at the catch plays an important part in the overall acceleration of the boat, this phase of the stroke has been highlighted in the figure along with the drive. It can be seen for example that the boat decelerates at the lock-on, as the blades enter the water but have not yet contributed to accelerating the boat forward.

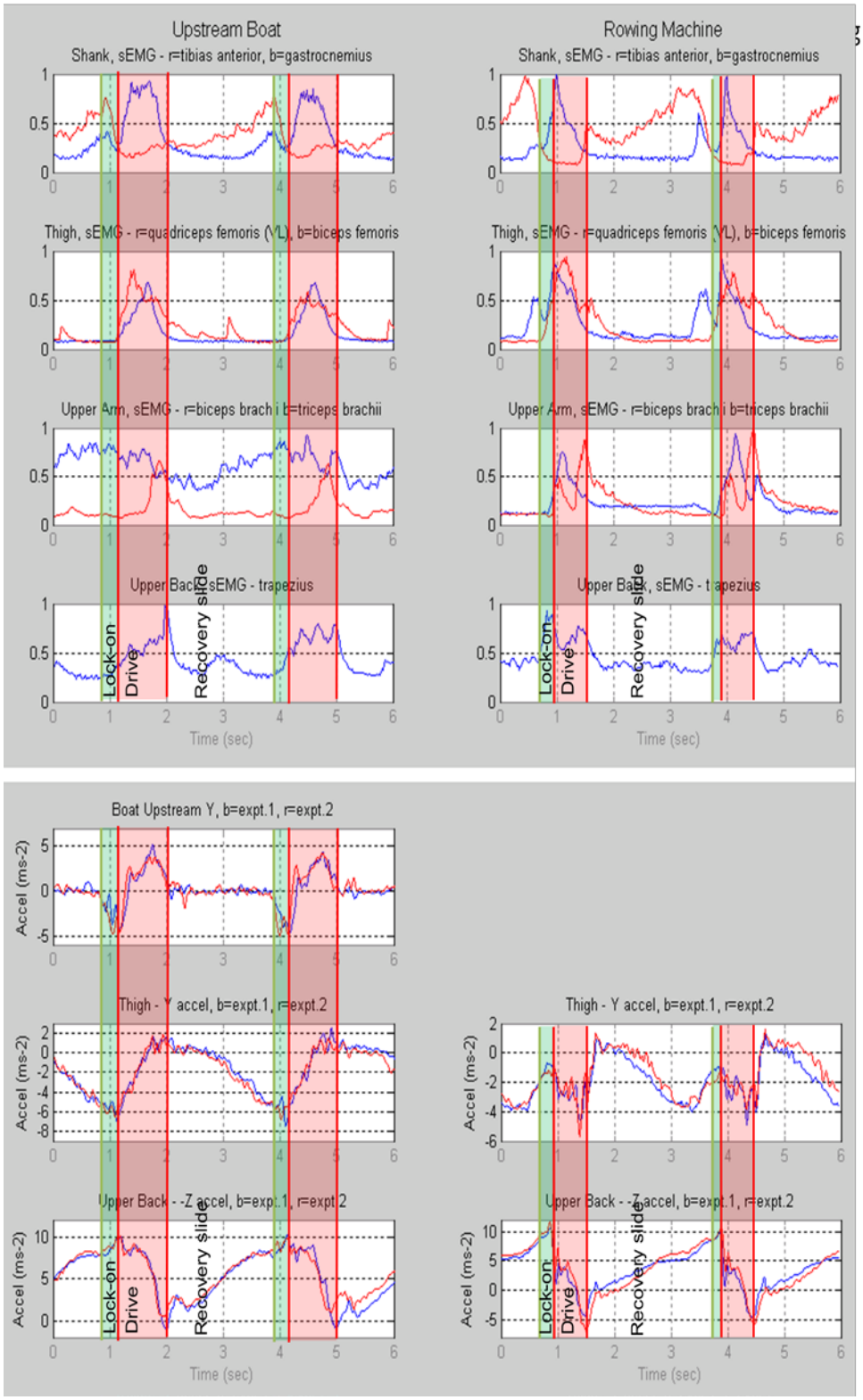

Figure 5-18: Comparison of river and ergometer rowing data

Acceleration data in-boat demonstrates the effect of acceleration measurements in an accelerated system (the boat), sEMG measurements exhibit differences in muscle recruitment over the stroke in-boat compared to ergometer rowing

Analysing first the acceleration data of the thigh and upper-back, it is clear that the accelerations measured in the boat differ markedly from the accelerations measured upon the ergometer. This is to be expected, as the accelerometers upon the rower in the boat are operating in an accelerated system: the boat itself. It is not possible to simply subtract the acceleration of the boat from that of the body-segments because the axes of the accelerometers upon the rower are rotating relative to the fixed axis of the accelerometer in the boat. However, it can be seen that the acceleration of the boat largely cancels the step change in acceleration value observed by the thigh accelerometer during the drive phase. As such, the thigh accelerometer displays a saw-tooth style signature, with a sharp positive gradient over the drive, and a gradually changing negative gradient over the recovery, this latter remaining similar to the ergometer thigh signature as the acceleration in the boat is near zero. The back accelerometer data in the boat more closely resembles that of its equivalent ergometer data, but again displays a change in signature over the drive phase due to the underlying influence of the boat acceleration.

A number of differences are evident in the muscle activity. The most notable difference in the shank data is the more sustained input to the drive phase of the gastrocnemius than upon the ergometer. The activity of the quadriceps femoris (VL) and biceps femoris is similar over the drive phase, though the input of the biceps femoris to the deceleration of the slide to the catch is missing. This might in part be because of the differences between the recovery stages of boat compared to ergometer. The boat is effectively allowed (through breaking the knees at the start of the recovery) to move under the rower's seat such that the seat appears, from within the boat, to travel up the slide to front-stops. This is different from a stationary ergometer, where, although the ergometer handle is in

tension and aiding a return of the rower up the slide, the seat itself has no direct assistance to do so, other than through rower input.

The biceps brachii makes no contribution at the catch, but similar input at the finish. Again there are clear differences in the requirements of the arm in the boat, as they have to control the oar (including feathering and squaring of the blade). The triceps brachii signal is poor, probably through badly sited, or disturbed electrodes. The trapezius muscle activity is similar to the ergometer data.

An interesting feature in the quadriceps femoris (VL) thigh data is a short peak mid-recovery. This is accompanied by a small dip in the net decreasing acceleration of the thigh acceleration data. It is hypothesised that this might be due to lateral rotation of the thigh in the approach to the catch that is much less apparent in ergometer rowing. Figure C-13 in appendix C.2 allows analysis of the lateral acceleration (Z axis) of the thigh compared to muscle activity. There does appear to be a dip in the net acceleration corresponding to the muscle activity, but it is unclear precisely what might be the cause.

Guevel et al (Guevel et al. 2011), concentrating upon the thigh muscles, averaged the normalised signals of sEMG measurements upon 9 oarsmen, and plotted these results as a percentage of the recovery and drive phases. A similar approach was taken with the results of the measurements of the rower in the single scull. Averaging over 10 strokes, results were calculated and plotted for normalised biceps femoris and quadriceps femoris (VL) sEMG data, and compared to the same muscles from the results by Guevel (Figure 5-19).

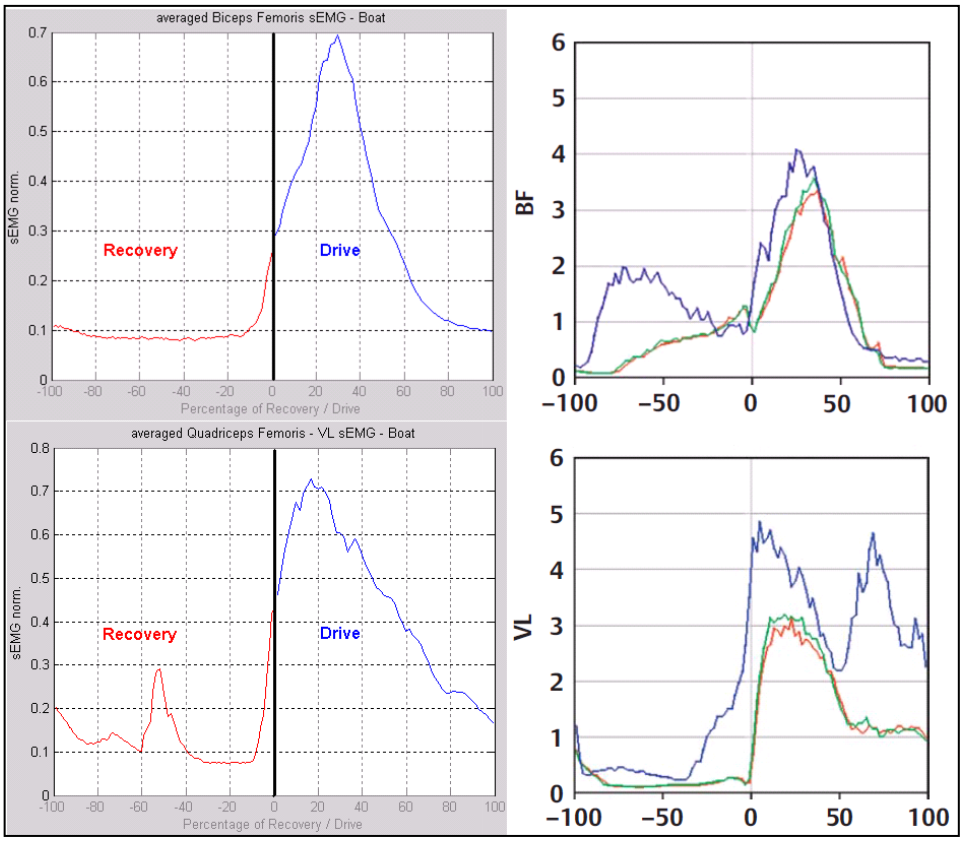

Figure 5-19: Normalised and averaged sEMG data for biceps femoris and quadriceps femoris (VL)

Presented as a percentage of recovery and drive phases, with comparison to results obtained by Guevel et al.

Note: In Guevel graphs, the red and green traces are for steady state rowing, and thus comparable to the results here. The blue trace is for race-start rating and non-representative.

It can be seen that the results show a good match for the steady state rowing in Guevel's results (red/green). Differences in the recovery phase (in particular the feature mid-recovery in the quadriceps femoris previously mentioned) would likely reduce if averaged over several subjects.

Additionally, this same process was performed upon the ergometer data to further analyse differences between the two. Results are shown in Figure 5-20. The differences previously highlighted in Figure 5-18 are even more clearly presented using this approach.

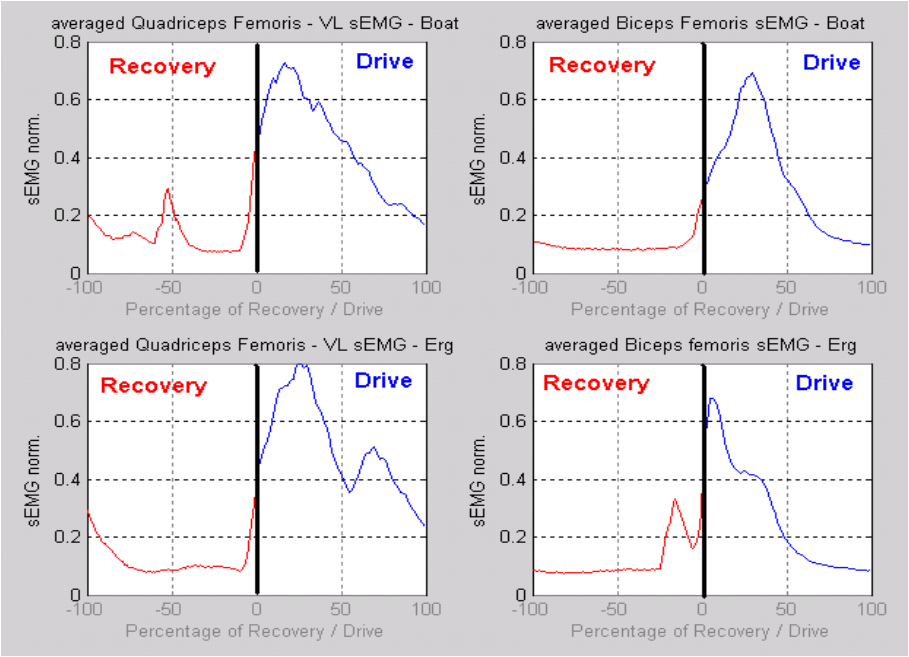

Figure 5-20: Comparison of Boat and Rowing machine sEMG Quadriceps femoris and biceps femoris muscle data

Presented as a percentage of recovery and drive phases

Finally, Figure 5-18 also allows the acceleration of the boat to be analysed relative to the phases of the stroke. A sharp deceleration is evident at the catch, translating sharply to an acceleration early in the drive phase that is sustained throughout the drive. Over the recovery when the blades are not in the water to propel the boat, the net acceleration is zero. This shows close correlation to the literature (Kleshnev et al. 1996) shown in Figure 5-21. In his graph, he has plotted acceleration over increasing stroke-rates. The experiment conducted here was performed at low stroke-rate and agrees closely with the lower stroke-rate trace of Kleshnev's results (the thick dotted line with deceleration at the catch reaching a minimum of -5ms^{-2}).

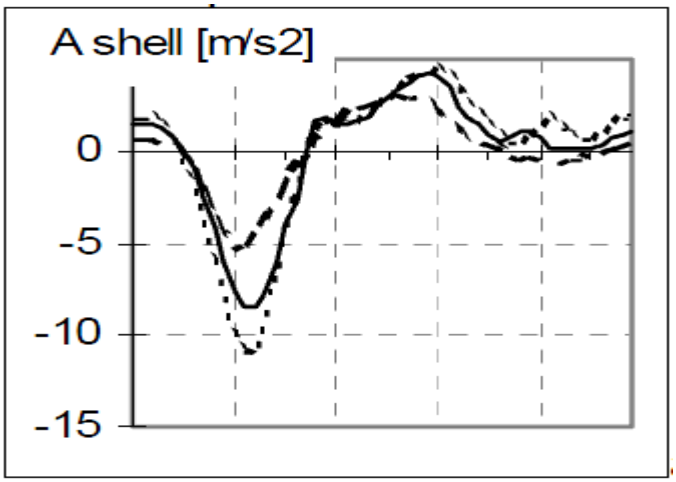

Figure 5-21: Boat acceleration curve over the stroke cycle
At stroke-rates averaging 26, 32, and 36spm (Kleshnev et al. 1996)

Analysing upstream and downstream rowing, acceleration and muscle recruitment is similar as you would expect. Figure 5-22 possibly gives an indication of the increased effort to row the boat upstream during the fast-flow conditions under which the experiment was conducted. The muscle data for each experiment was normalised as previously, and it would appear that the gastrocnemius and the trapezius muscles of the shank and back respectively are exerting increased effort upstream compared to downstream.

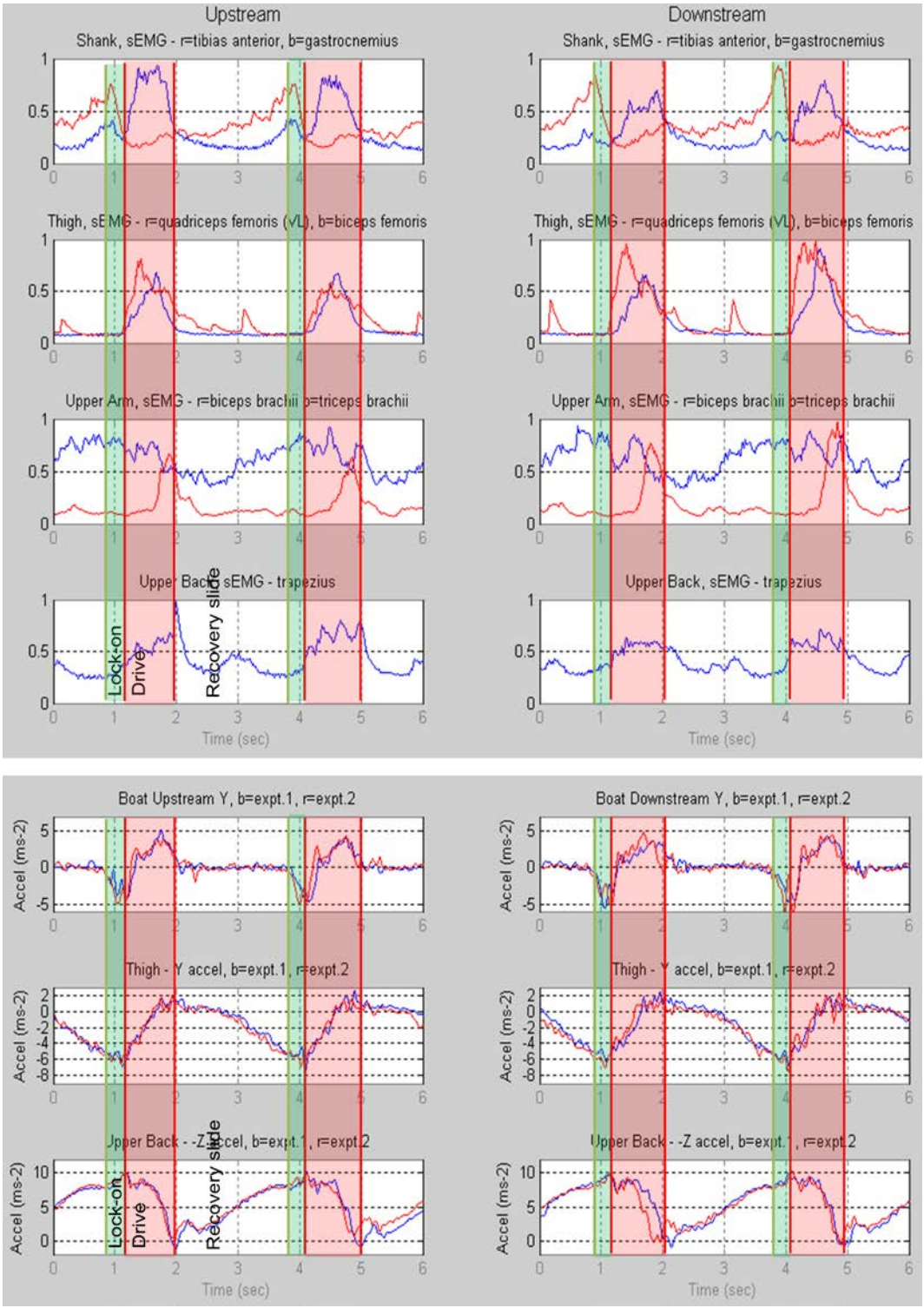

Figure 5-22: Upstream and downstream rowing

Acceleration and sEMG data measured during two experiments (blue and red) to allow comparison of rowing with or against the water flow.

5.2.5 Simultaneous measurement upon two rowers

An experiment was conducted upon two club rowers, of similar height, build, and rowing skill, in a double scull to demonstrate the use of a wireless BSN to monitor crew rowing. One node was placed in the boat to monitor boat acceleration, and two nodes were placed upon each rower at thigh and upper-back. The muscles measured were the biceps femoris of the thigh, and the trapezius of the upper back. Figure 5-23 shows two strokes, with the data from the two rowers overlaid. Row_S indicates the stroke rower, Row_B indicates the rower in bow. As such, Row_S is dictating the stroke-rate and timing of the boat.

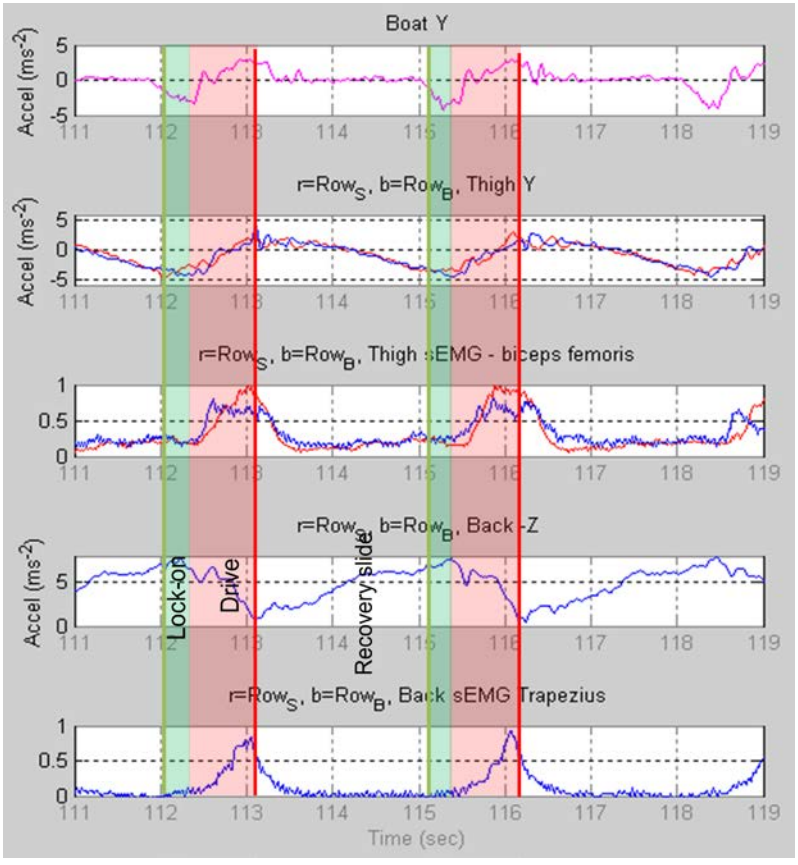

Figure 5-23: Data collected upon two rowers in a double scull boat

Red – stroke, blue – bow, magenta – boat acceleration. Back and thigh acceleration, trapezius and biceps femoris sEMG data.

Stroke back data missing owing to data upload failure.

Unfortunately extremely cold weather conditions were such that a heavy condensation was accumulating upon the central coordinator node (this is housed in an open protective Perspex cage (to facilitate access to the connectors used during development). A similar effect was likely upon the sensor nodes, particularly those attached to the upper back which would be subjected to both the heat of the rower's core body and the cold of the ambient air. As such, the range of the Zigbee radios was affected. Whilst the distance over which the data needed to be transmitted was small (within a boat), the patch antennas employed by the radios (essentially a small rectangle of metallised circuit board) was greatly affected. Thus, whilst all nodes did upload data, the back node of Row_{S} only uploaded about 30seconds of data in its upload interval, insufficient to monitor open water rowing, only recording manoeuvring from the landing stage.

However, the results show that simultaneous collection of data from a crew is facilitated through the use of a wireless BSN, and good correlation can be seen between the thigh acceleration data of the two rowers, though whilst Row_{B} sustains a steady muscle input over the drive phase, the muscle data of Row_{S} would appear to show an increase to a peak over the drive. Additionally, it can be seen that their thigh muscles are active over a similar period. It can also be seen, that by comparing Row_{B} acceleration back data to the single scull data (which was conducted using Row_{S}), the acceleration signature shape shows close correlation. The boat acceleration again matches that previously described in the literature.

This experiment was repeated immediately afterwards upon land ergometers. The condensation upon the nodes quickly cleared within gymnasium conditions and data uploading to the central node was successful for all sensor nodes.

Figure 5-24 shows acceleration and muscle results for the two rowers: again Row_S dictated the stroke-rate and timing, with Row_B following.

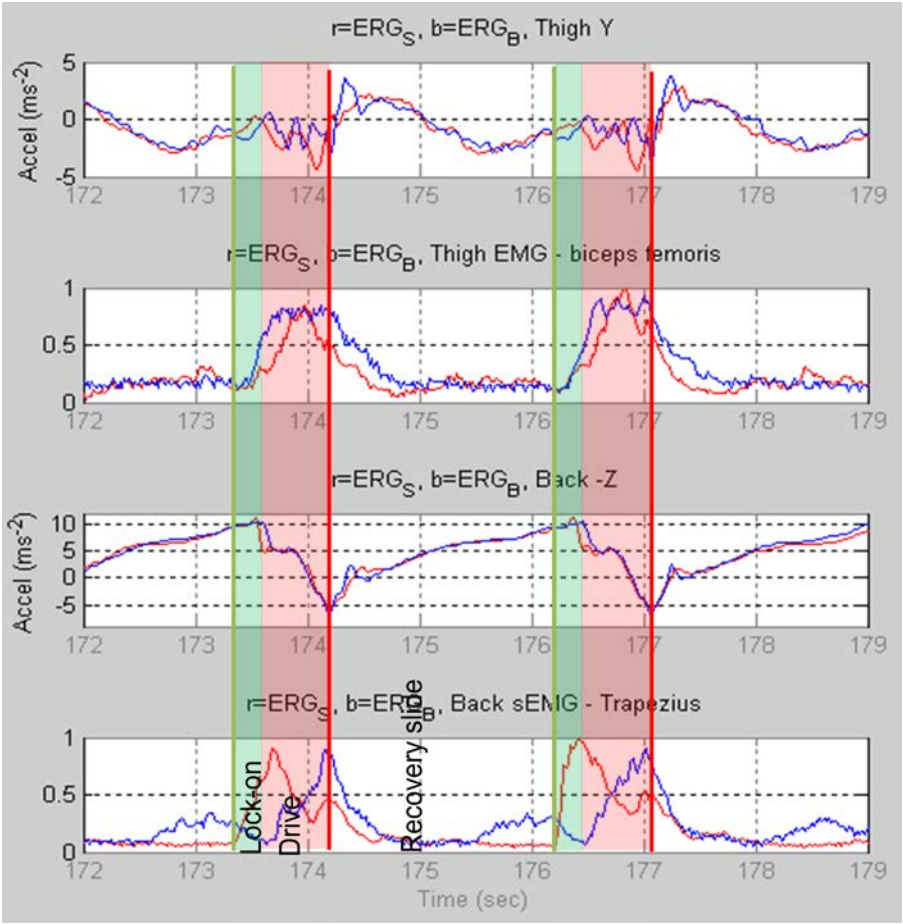

Figure 5-24: Two rowers measured simultaneously upon ergometers

Red – stroke, blue – bow. Back and thigh acceleration, trapezius and biceps femoris sEMG data.

Good correlation is evident in the acceleration data of both thigh and upper-back. However, it can be seen that Row_B, who follows Row_S, is slightly late at the catch – about 0.05sec – (particularly evident in the back acceleration data) but their finishes are matched perfectly. As previously indicated in the river experiment, the muscle data of Row_S indicates a peak thigh value compared to the wider, flatter peak of Row_B. Most interesting is the data of the trapezius muscle. It would

seem that the two rowers, whilst exhibiting largely well-matched timing, exhibit rather different recruitment of their back muscles. Row_S recruits back muscles at lock-on, peaking at the catch, then sustained throughout the drive, peaking again at the finish and during hands-away. Row_B in contrast, has minimal activity of the trapezius at the catch, building over the drive phase to a maximum at the finish. He also appears to recruit the trapezius in the final stages of the recovery in the approach to the catch. This could be explained through a difference in technique, different physiology, or a combination of both. As only one muscle of the back was monitored during this experiment it is difficult to determine whether Row_B is in fact recruiting other back muscles in the early part of the drive. It would be interesting to monitor multiple back muscles of the two rowers and to repeat the experiment.

5.2.6 Signal strength measurements

Received Signal strength (RSSI) at a receiving Zigbee radio upon reception of data packets from nodes placed upon a rower was monitored (using the Zena Network analyser and Zena Network traffic monitoring, previously mentioned in chapter 4) to gauge the attenuation of the signal through occlusion by the body. The greater the negative value of the RSSI signal, the weaker the received signal at the receiver. These measurements were not undertaken with a view to determine accurate signal strength data, only to determine if nodes placed upon the body might experience high attenuation of their signal. With the receiving radio placed directly behind the ergometer, RSSI values varied from -10 to -19dBm upon packets received from a node placed upon the upper back depending upon the position of the rower upon the slide (front-stops, half-slide

and back-stops measurements were taken). Nodes placed upon the thigh had RSSI values of -19 to -23dBm depending upon slide position. To simulate the alternative scenario of data collected by a coach in a launch boat, measurements were taken off to one side of the ergometer at a distance of 3m. A node placed upon the upper back produced RSSI values of -23 to -33dBm depending upon slide position. A node placed upon the nearside thigh (relative to the receiver) measured -18 to -21dBm, and a node placed upon the far-side thigh measured between -30 and -32dBm. A table of RSSI results at each node position can be found in appendix C.3. Such values should cause no reception problems, but does not take into account materials of the boat, or effects of signal reflection on water or weather conditions.

5.3 Chapter Summary

The thigh and upper-back were determined through experimentation to yield accelerometer information most useful to enhance the analysis of muscle activity during the rowing stroke. Good correlation was made between data collected using the wireless BSN and Qualsys landmark measurement motion capture and Delsys sEMG. Ergometer and on-water experiments were conducted and compared, noting good correlation between ergometer and in-boat rowing with some notable differences due to differences in required technique. Data from in-boat rowing was analysed in conjunction with the boat acceleration. Simultaneous measurement of acceleration and muscle activity was demonstrated upon a rowing crew both on-river and on land ergometers allowing their timing and muscle activity to be compared. Small timing differences at the catch were noted, along with differences in their upper-back muscle recruitment.

6 Conclusions and Further Work

6.1 Conclusions

The experiments undertaken and discussed in chapter 5 demonstrated the feasibility and benefits of a wireless BSN for the purpose of the measurement and collection of synchronous sensor data upon single or multiple rowers on land-based ergometers or in-boat. Data was collected with minimum disruption to the rower, and did not require lengthy setting up procedures, alignment or calibration.

The optimisation of the system, notably the linear envelope extraction of the sEMG signal prior to sampling and digitisation, greatly reduces the amount of data collected and transmitted. This differs from other recent sEMG measurement systems available (Delsys, Shimmer). Such optimisation allows transmit time to be reduced, both reducing the power requirements of a sensor node, increasing node power longevity, and allowing expansion of the wireless network to a greater number of nodes sharing a radio channel.

Previous studies in rowing have employed either wired (or only partially wireless) measurement systems (Kleshnev 2011; Tessendorf et al. 2011) or personal data-loggers upon the rower (Sommer et al. 2008; Guevel et al. 2011; Fleming and Donne 2012) where increased measurement points increases the required connections to the data-logging unit. The wireless BSN requires no additional infrastructure for each additional node.

In-laboratory testing and rowing experimentation, validated using Motion Capture measurement, has proven that synchronous measurement can be achieved across the wireless network of nodes. Data collected synchronously with Motion Capture data was analysed and the two datasets concurred in their findings.

The wireless BSN allowed acceleration data of body segments and of a rowing boat to be monitored and analysed, and used to facilitate identification of the phases of the rowing stroke. This data was additionally used to correlate the muscle activity data measured of several muscles during rowing activity to the different stages of the rowing stroke. Deviation in rowing style could be identified from the collected data.

Weighting and summing of the muscle data was proposed as a method for developing a qualitative force-time profile over both the drive and recovery phases of the rowing stroke.

Comparisons made between ergometer rowing and on-water rowing showed that muscles are recruited in a similar manner in the two environments, but allowed for differences (for example in the activity profile of the gastrocnemius muscle during the drive phase) to be highlighted. Further prolonged studies should allow further analysis and correlation to the performance of the boat.

Finally, the measurement of acceleration and muscle activity upon two rowers demonstrated the ease with which data could be synchronously collected from two moving athletes by wireless means. This technique could easily be expanded to larger crews, and allow differences in muscle recruitment and particularly timing issues to be brought to the attention of coaches.

In conclusion, a novel wireless BSN, monitoring acceleration and sEMG, with optimisation benefitting power and processing requirements, and future expandability, has been demonstrated to benefit the analysis of the rowing stroke and inter-crew cohesion on-water.

There are however many areas requiring, or worthy of further work. The next section is divided into two sections: further technical development, and future research study.

6.2 Further work

6.2.1 Technical development

Several relatively simple technical improvements would greatly enhance the performance of the wireless BSN.

The reduction in size of Zigbee radios since the initial design phase of the project means that it should be possible to greatly reduce the size of the sensor nodes. It should be possible to reduce the nodes to less than 40mm^2, thus expanding the possibilities for node placement.

Short cables were used between the nodes and the EMG electrodes. These were short enough that cable artefacts and ambient noise pick-up of the cables was minimised, and facilitated experimentation with a limited number of sensor nodes, but it would be beneficial to eliminate the electrode wires altogether. Active electrodes (where the measurement electronics and electrodes are integrated) further improve the signal fidelity, and would further reduce the set-up time of the nodes upon the body. Recent commercial sEMG measurement systems (Delsys) have employed this technique.

It was found that the EMG circuitry lacked gain due in part to the reduction in signal amplitude in the RMS-to-dc conversion of the high frequency signal to low frequency envelope, and due to the wide range of signal values measured at the electrode due to attenuation by subcutaneous tissue at some sites. A gain stage

post envelope detection, possibly variable, would greatly enhance sensitivity of the EMG circuitry.

Microcontroller technology has improved since initial circuit design. Porting the control code to a more powerful processor would allow increased (and faster) processing to be performed upon the sensor nodes themselves. This is discussed further in the next section.

6.2.2 Future research study

The current system transmits raw data from the three accelerometer axes, as well as muscle activity data, to the central coordinating node. The experiments conducted largely relied upon a single axis of accelerometer data (though multiple axes were studied). It was found that a single accelerometer axis yielded a signature shape that could be used to determine the phases of the rowing stroke. As such, the system could be optimised by only sampling and transmitting one chosen axis of accelerometer data. This would reduce by 2/3 the amount of raw acceleration data transmitted. This saving could be exploited by adding further sensors to the wireless node. Whilst maintaining minimum node size is still of paramount importance, the addition of a gyroscope IC would add little to the size and weight of the node, and would allow the challenge of the combined inertial and gravity accelerations to be targeted (King et al. 2009). This would open opportunities to generate angle, velocity and positional information from the collected data.

Further study needs to be made into the existing accelerometer data, to determine what further processing could be undertaken to enhance the features of the signature shape.

The clear advantages of a wireless BSN can be further enhanced if real-time feedback could be demonstrated (both Hume (Hume 2005) and Fothergill (Fothergill 2009) present evidence to suggest the benefits of visual feedback to develop coordination skills and maintain consistent good technique). A major piece of further work should therefore be to progress this, employing further feature extraction (both at the sensor node to transmit reduced data, and at the coordinating node or laptop), and to investigate the best form of immediate feedback. The simplest form of feedback would be to employ the acceleration data to determine the phases of the rowing stroke and to use this to aid ta dynamic visual display of the muscle activity.

Finally, further ergometer and boat-based experimentation should be undertaken to further investigate the ways in which a Wireless BSN can facilitate rowing biomechanics analysis. In particular, further study of longer boat trials at different intensities and stroke rating would allow analysis of boat performance related to the measured signal data.

7 References

ADInstruments. Goniometer. http://www.adinstruments.com/products/mlts700#overview [accessed 01/11/12].

Akay, M. et al. 2003. Unconstrained Monitoring of Body Motion During Walking. *IEEE Engineering in Medicine and Biology Magazine* 22(3), pp. 104-109.

Analog Devices. 2008. *Linear Circuit Design Handbook*.

Arcom Control Systems. 2005. *Using ZigBee for the last few hundred feet of connectivity in telemetry.*

Aziz, O. et al. 2006. Introduction: Wireless Sensor Networks. In: Yang, G.-Z. ed. *Body Sensor Networks*. Springer.

Baird, E. D. and Soroka, W. W. 1951. Measurement of Force-time relations in racing sculls. *American Society of Mechanical Engineers*.

Baker, N. 2005. ZigBee [trademark] and bluetooth [trademark] - Strengths and weaknesses for industrial applications. *IEE Conference Publication* (2005-10868), pp. 135-147.

Baudouin, A. and Hawkins, D. 2004. Investigation of biomechanical factors affecting rowing performance. *J Biomech* 37(7), pp. 969-976.

BBC News. 2006. *Bluetooth Rival unveiled by Nokia.* BBC News,.

Benson, A. et al. 2011. Comparison of rowing on a Concept 2 stationary and dynamic ergometer. *Journal of Sports Science and Medicine* 10(2), pp. 267-273.

Bernstein, I. et al. 2002. An ergonomic comparison of rowing machine designs: possible implications for safety. *Br J Sports Med* 36(2), pp. 108-112.

Bernstein, J. Feb 2003. *An overview of MEMs inertial sensing technology.* Sensors Magazine.

Bible, S. 2008. PICDEM Z Demonstration Kit User Guide. In: inc, M.T. ed. *DS51524C*.

Bluetooth Special Interest Group. 2010. 802.15.1 Standard Version 4.0. Bluetooth SIG.

Briiysy, V. et al. eds. 2010. *Movement Tracking of Sports Team Players with Wireless Sensor Network*. Ubiquitous Positioning Indoor Navigation and Location Based Service (UPINLBS), 2010.

Buckeridge, E. et al. 2012. Kinematic Asymmetries of the Lower Limbs during Ergometer Rowing. *Medicine and Science in Sports and Exercise* 44(11), pp. 2147-2153.

Bull, A. M. J. and McGregor, A. H. 2000. Measuring spinal motion in rowers: The use of an electromagnetic device. *Clinical Biomechanics* 15(10), pp. 772-776.

Byford, M. D. 1992. EMG Analysis - Some Implications For Rowing Stroke Kinesiology. *Measurement in Sport and Exercise, IEE Colloquium on*, pp. 11-13.

Cairns, S. P. 2006. Lactic Acid and Exercise Performance: Culprit or Friend? *Sports Medicine* 36(4).

Carney, W. 2002. IEEE 802.11g: New Draft Standard Clarifies Future of Wireless LAN. Texas Instruments.

Chelius, G. et al. 2011. A Wearable Sensor Network for Gait Analysis: A Six-Day Experiment of Running Through the Desert. *Ieee-Asme Transactions on Mechatronics* 16(5), pp. 878-883.

Colloud, F. et al. 2006. Fixed versus free-floating stretcher mechanism in rowing ergometers: mechanical aspects. *J Sports Sci* 24(5), pp. 479-493.

Colloud, F. et al. 2002. Kinematic symmetry in rowing: comparison of fixed versus free-floating ergometers. In: *Scientific Proceedings of the XXth International Symposium on Biomechanics in Sports.*

Constable, R. et al. 1994. Time-frequency analysis of the surface EMG during maximum height jumps under altered-G conditions. *Biomedical Sciences Instrumentation* 30, pp. 69-74.

Cooper, G. et al. 2010. Inertial sensor-based knee flexion/extension angle estimation (vol 42, pg 2678, 2009). *Journal of Biomechanics* 43(3), pp. 598-598.

Cornett, J. et al. 2008. An 8-factor model for evaluating crew race performance. *International Journal of Sports Science and Engineering* 2(3).

Coyle, S. et al. 2009. Textile-based wearable sensors for assisting sports performance. *Sixth International Workshop on Wearable and Implantable Body Sensor Networks, Proceedings*, pp. 307-311.

Daintree Networks inc. 2006. Understanding the Zigbee Applications Framework.

Dawson, R. et al. 1998. The rowing cycle: Sources of variance and invariance in ergometer and on-the-water performance. *Journal of Motor Behavior* 30(1), pp. 33-43.

de Brouwer, A. J. et al. 2013. Don't Rock the Boat: How Antiphase Crew Coordination Affects Rowing. *PLOS One* 8(1).

De Luca, C. J. 1997. The use of surface electromyography in biomechanics. *Journal of Applied Biomechanics* 13(2).

De Luca, C. J. 2002. Surface Electromyography: Detection and recording. In: Inc, D. ed.

De Luca, C. J. 2006. Electromyography. Encyclopaedia of Medical devices and instrumentation. John Wiley.

De Luca, G. 2001. Fundamental concepts in EMG Signal Acquisition. In: Delsys ed.

Deffree, S. January 2006. *No Standard for UWB.* Electronic News.

Descleves, C. March 2006. *Understanding ZigBee transmission.* RF Design.

Di Prampero, P. et al. 1971. Physiological aspects of rowing. *J Appl Physiol* 31(6), pp. 853-857.

Doscher, J. 1999. Accelerometer Design and Applications. In: Devices, A. ed.

Dynastream. 2012. This is ANT: Q&A.

Elliot, B. et al. 2003. The Rowperfect Ergometer: A training aid for on-water single scull rowing. *Sports Biomechanics*.

Elson, J. et al. 2002. Fine-grained network time synchronization using reference broadcasts. *Usenix Association Proceedings of the Fifth Symposium on Operating Systems Design and Implementation*, pp. 147-163.

Favre, J. et al. 2008. Ambulatory measurement of 3D knee joint angle. *Journal of Biomechanics* 41(5), pp. 1029-1035.

Favre, J. et al. 2006. Quaternion-based fusion of gyroscopes and accelerometers to improve 3D angle measurement. *Electronics Letters* 42(11), pp. 612-614.

Ferrari, P. et al. 2006. IEEE802.11 sensor networking. *Instrumentation and Measurement, IEEE Transactions on* 55(2), pp. 615-619.

Fleming, N. and Donne, B. 2012. Comparison of recruitment patterns during on-water and on-ergometer rowing. In: *17th Annual congress of European College of Sports Science.* Bruges.

Fleming, N. et al. 2012. A biomechanical assessment of ergometer task specificity in elite flatwater kayakers. *Journal of Sports Science and Medicine* 11(1), pp. 16-25.

Florimond, V. 2010. Basics of Surface Electromyography, Applied to Physical Rehabilitation and Biomechanics. Though Technology Ltd.

Flowers, D. and Yang, Y. 2010. MiWi Wireless Networking Protocol Stack. In: Microchip ed. *AN1066*.

Fok, C. L. et al. 2004. TinyCoxswain: Using a Sensor Network to Enhance Crew Performance. http://www.cse.wustl.edu/~liang/cse521fl06/tinycoxwain.pdf [accessed 31/10/2007].

Fothergill, S. 2009. Examining the effect of real-time visial feedback on the quality of rowing technique. In: *8th Conference of the International Sports Engineering Association (ISEA).*

Frank, R. March 2004. *Move Over, Bluetooth; ZigBee is here.* Design News.

Frenzel, L. 2012. *Understanding modern digital modulation techniques.* Electronics Design.

Fuhr, P. L. March 2002. *A review of frequencies available for wireless sensing applications.* Sensors Magazine.

Gang, D. et al. 2005. Reliable broadcast in ZigBee networks. *Sensor and Ad Hoc Communications and Networks, 2005. IEEE SECON 2005. 2005 Second Annual IEEE Communications Society Conference on*, pp. 510-520.

Geer, D. 2005. Users make a beeline for ZigBee sensor technology. *Computer* 38(12), pp. 16-19.

Geier, J. August 2002. 802.11 Alphabet Soup. Wi-Fi Planet.

Gerber, H. et al. 1987. Biomechanical performance analysis in rowing with a new measurement system. *Biomechanics*.

Gold, S. Jan/Feb 2005. Bluetooth bares its teeth. Infosecurity today.

Gray, H. 1998. Gray's Anatomy. Parragon Plus.

Guevel, A. et al. 2011. Thigh muscle activities in elite rowers during on-water rowing. *Int J Sports Med*.

Haartsen, J. C. and Mattisson, S. 2000. Bluetooth-a new low-power radio interface providing short-range connectivity. *Proceedings of the IEEE* 88(10), pp. 1651-1661.

Hagerman, F. C. et al. 1978. Energy Expenditure during simulated rowing. *Journal of Applied Physiology* 45.

Haglin, P. J. and Sztul, H. 2000. Video Analysis of rowing and weightlifting. Colgate University.

Hartmann, U. and Mader, A. 2005. Rowing Physiology. In: Nolte, V. ed. *Rowing Faster*. Human Kinetics, pp. 9-23.

Hawkins, D. 2000. A new instrumentation system for training rowers. *Journal of Biomechanics* 33(2), pp. 241-245.

Hershler, C. and Milner, M. 1978. An Optimality Criterion for Processing Electromyographic (EMG) Signals Relating to Human Locomotion. *IEEE Transactions on Biomedical Engineering* 25(5).

Heydon, R. and Hunn, N. 2011. Bluetooth Low Energy. In: CSR ed. Bluetooth SIG.

Hilding, T. 2012. *WSU researchers create super lithium-ion battery.* Washington State University News.

Hill, H. 2002. Dynamics of coordination within elite rowing crews: evidence from force pattern analysis. *J Sports Sci* 20(2), pp. 101-117.

Hirt, W. 2003. Ultra-wideband radio technology: Overview and future research. *Computer Communications* 26(1), pp. 46-52.

Holt, P. et al. 2003. Kinematics of spinal motion during prolonged rowing. *Int J Sports Med* 24(8), pp. 597-602.

Hume, P. 2005. *Visual feedback to change rowing technique.* Brian Mackenzie's Successful Coaching.

IEEE. 1997. 802.11 WLAN-1997. IEEE Standards.

IEEE. 2002. IEEE Bluetooth Standard 802.15.1-2002. IEEE Standards.

IEEE. 2012a. 802.11 WLAN Standard. IEEE Standards.

IEEE. 2012b. 802.15.6-2012 BAN Standard. IEEE Standards.

IEEE TG6. 2007. IEEE 802.15 WPAN Task Group 6 (TG6)Body Area Networks.

Janshen, L. et al. 2009. Muscular coordination of the lower extremities of oarsmen during ergometer rowing. *Journal of Applied Biomechanics* 29(2).

Joe F Jabre, J. F., Hackett, Earl. R. 1983. *EMG Manual*. Charles C Thomas Pub Ltd.

Jovanov, E. et al. 2009. Avatar - a Multi-sensory System for Real Time Body Position Monitoring. *Embc: 2009 Annual International Conference of the Ieee Engineering in Medicine and Biology Society, Vols 1-20*, pp. 2462-2465.

Jovanov, E. et al. 2005. A WBAN System for Ambulatory Monitoring of Physical Activity and Health Status: Applications and Challenges. *Conf Proc IEEE Eng Med Biol Soc* 4, pp. 3810-3813.

Kamen, G. and Gabriel, D. 2009. *Essentials of Electromyography*. Human Kinetics.

Kapp, S. 2002. 802.11: Leaving the wire behind. *IEEE Internet Computing* 6(1), pp. 82-85.

Kaya, M. et al. 1995. Motion analysis of optimal rowing form by using biomechanical model. *Annual International Conference of the IEEE Engineering in Medicine and Biology - Proceedings* 17(2), pp. 1281-1282.

Kester, W. 1999. Bridge Circuits. In: Devices, A. ed. *Practical Design Techniques for Sensor Signal Conditioning*.

Khanh Tuan, L. 2004. Designing a ZigBee-ready IEEE 802.15.4-compliant radio transceiver. *R.F. Design* 27(11), p. 42.

King, R. et al. 2009. Body Sensor Networks for Monitoring Rowing Technique. *Sixth International Workshop on Wearable and Implantable Body Sensor Networks, Proceedings*, pp. 251-255.

Kleshnev, V. 1998. *Estimation of Biomechanical parameters and Propulsive Efficiency of Rowing*. Australian Institute of Sport:

Kleshnev, V. ed. 1999. *Propulsive efficiency of rowing*. XVII International Symposium on Biomechanics in Sports. Perth, Western Australia.

Kleshnev, V. 2000. *Power in Rowing*. Australian Institute of Sport.

Kleshnev, V. ed. 2005a. *Comparison of on-water rowing with its simulation on Concept 2 and Rowperfect machines*. *Proceedings of XXIII International Symposium on Biomechanics in Sports.*

Kleshnev, V. 2005b. Technology for Technique Improvement. In: Nolte, V. ed. *Rowing Faster*. Human Kinetics, pp. 209-225.

Kleshnev, V. 2006. *Rowing Biomechanics*. Rowing Biomechanics Newsletter:

Kleshnev, V. 2010. *Rowing Biomechanics 2010*. Rowing Biomechanics Newsletter:

Kleshnev, V. 2011. Biomechanics for effective rowing technique. In: *World Rowing Coaches Conference.* Varese, Italy.

Kleshnev, V. and Kleshneva, E. 1992. Work performance of different body segments in rowing. *Biology of Sport*.

Kleshnev, V. et al. 1996. The application of computer technologies to the management of sport specific training in rhythmic sports. *Current Research in Sports Sciences*, pp. 137-145.

Kulwanoski, G. and Schnellinger, J. 2004. *The Principles of Piezoelectric Accelerometers.* Sensors.

Kusy, B. et al. 2006. Elapsed time on arrival: a simple and versatile primitive for canonical time synchronisation services. *International Journal for Ad Hoc and Ubiquitous computing*.

Kwak, K. S. et al. eds. 2010. *An overview of IEEE 802.15.6 Standard*. The 3rd International Symposium on Applied Sciences in Biomedical and Communication Technologies.

Lamb, D. 1989. A kinematic comparison of ergometer and on-water rowing. *Am J Sports Med* 17(3), pp. 367-373.

Le Sage, T. et al. eds. 2010. *Development of a real time system for monitoring of swimming performance*. 8th Conference of the International Sports Engineering Association (ISEA).

Le Sage, T. et al. eds. 2011. *Development of a Wireless Sensor Network for Embedded Monitoring of Human Motion in a Harsh Environment*. 2011 IEEE 3rd International Conference on Communication Software and Networks (ICCSN),.

Liu, C. 2006. Piezoresistive sensors.*Foundations of MEMS*. Prentice Hall.

Liu, K. et al. 2009. Ambulatory Measurement and Analysis of the Lower Limb 3D Posture Using Wearable Sensor System. *2009 Ieee International Conference on Mechatronics and Automation, Vols 1-7, Conference Proceedings*, pp. 3065-3069.

Llosa, J. et al. 2009. REMOTE, a Wireless Sensor Network Based System to Monitor Rowing Performance. *Sensors* 9(9), pp. 7069-7082.

Loschner, C. and Smith, R. eds. 1999. *The relationship between seat movement and boat acceleration during sculling*. XVII International Symposium on Biomechanics in Sports.

Loschner, C. et al. 2000. Boat orientation and skill level in sculling boats. In: Infoservice, A.I.o.S.C. ed. *XVIII International Symposium on Biomechanics in Sports*. Hong Kong.

Luinge, H. and Veltink, P. 2005. Measuring orientation of human body segments using miniature gyroscopes and accelerometers. *Medical & Biological Engineering & Computing* 43(2), pp. 273-282.

Luinge, H. J. et al. 1999. Estimating orientation with gyroscopes and accelerometers. *Technology and health care*.

Mantyjarvi, J. et al. 2002. Recognizing human motion with multiple acceleration sensors. *2001 Ieee International Conference on Systems, Man, and Cybernetics, Vols 1-5*, pp. 747-752.

Maroti, M. et al. 2004. The flooding time synchronization protocol. In: *Proceedings of the 2nd international conference on embedded network sensor systems.*

Martin, H. et al. eds. 2011. *Enhancing activity recognition by fusing inertial and biometric information*. 14th International Conference on Information Fusion.

Martin, T. P. and Bernfield, J. S. 1980. Effect of stroke rate on velocity of a rowing shell. *Medicine and Science in Sports and Exercise* 12(4), pp. 250-256.

Mazzone, T. 1988. Kinesiology of the rowing stroke. *National Strength and conditioning journal* 10(2).

McArthur, J. 2002. *High performance rowing*. The Crowood press ltd.

McBride, M. 2005. Rowing Biomechanics. In: Nolte, V. ed. *Rowing Faster*. Human Kinetics, pp. 111-123.

McGregor, A. 2003. *Technology in motion – spinal motion project.* Performance Magazine, Sports Science.

Microchip Technology inc. 2010. MRF24J40 IEEE 802.15.4 2.4GHz RF Transceiver Datasheet.

Mlinarsky, F. 2008. *Wireless HD video: Raising the UWB throughput bar again.* EE TImes.

MuRata. 2012a. CC3000 Wireless LAN module data sheet. In: Instruments, T. ed.

MuRata. 2012b. SN2100 / CC2560 Bluetooth Class 1 module. In: Instruments, T. ed.

Murphy, A. et al. 2010. The calibration and application of a force-measuring apparatus on the seat of a rowing ergometer. *Proceedings of the Institution of Mechanical Engineers Part P-Journal of Sports Engineering and Technology* 224(P1), pp. 109-116.

Nekoogar, F. 2005. *Introduction to Ultra-Wideband Communications*. Prentice Hall PTR.

Nolte, V. 1991. Introduction to the biomechanics of rowing. *FISA Coach* 2(1).

Nolte, V. 2005. *Rowing faster*. Champaign, IL: Human Kinetics, pp. viii, 294 p.

Nordic Semiconductor. 2010. *nRF24AP2-8CH ANT Connectivity IC)* [Online]. Available at: [Accessed.

Nordic Semiconductor. 2011. *Bluetooth low energy wireless technology backgrounder*. In: Nordic Semiconductor ed. Nordic Semiconductor.

Nowicky, A. et al. 2005. The impact of ergometer design on hip and trunk muscle activity patterns in elite rowers: An electromyographic assessment. *Journal of Sports Science and Medicine* 4(1), pp. 18-28.

Oartec. 2011. *Repetitive Overloading - Dynamic vs Stationary* [Online]. http://www.oartec.co.uk/slider_whyslider.php [accessed 01/11/12]: Available at: [Accessed: June 2012].

Paradiso, R. and De Rossi, D. 2006. Advances in textile technologies for unobtrusive monitoring of vital parameters and movements. *Annual International Conference of the IEEE Engineering in Medicine and Biology - Proceedings*, pp. 392-395.

Paradiso, R. et al. 2005. WEALTHY - a wearable healthcare system: new fronteer on e-textile. *Journal of Telecommunications and Information Technology*.

Parkin, S. et al. 2001. Do oarsmen have asymmetries in the strength of their back and leg muscles? *J Sports Sci* 19(7), pp. 521-526.

Patel, M. and Wang, J. 2010. APPLICATIONS, CHALLENGES, AND PROSPECTIVE IN EMERGING BODY AREA NETWORKING TECHNOLOGIES. *Ieee Wireless Communications* 17(1), pp. 80-88.

Poole, I. 2004. What exactly is ZigBee? *Communications Engineer* 2(4), pp. 44-45.

Pulman, C. 2005. The Physics of Rowing. University of Cambridge: Ithaca.

Rabaey, J. ed. 2011. *BWRC Wireless Sensor Workshop*. 2011 BWRC Sensor Workshop.

Redgrave, S. 1995. *Complete book of rowing*. 2nd ed. Partridge Press.

Rodgers, J. L. and Nicewander, W. A. 1988. Thirteen Ways to Look at the Correlation Coefficient. *The American Statistician* 42(1).

Roth, W. 1991. Physiological - Biomechanical Aspects of the Load Development and Force Implementation in Rowing. *FISA Coach* 2(1).

Roth, W. et al. 1993. Force-time characteristics of the rowing stroke and corresponding physiological muscle adaptations. *Int J Sports Med* 14 Suppl 1, pp. S32-34.

Rothmaier, M. et al. 2008. Photonic textiles for pulse oximetry. *Optics Express* 16(17), pp. 12973-12986.

Schneider, E. et al. 1978. Biomechanics in Rowing. *Biomechanics*.

Schwanitz, P. 1991. Applying Biomechanics to Improve Rowing Performance. *FISA Coach* 2(1).

Seifert, K. and Camacho, O. 2007. Implementing positioning algorithms using accelerometers. In: semiconductor, F. ed.

SENIAM Project. SENIAM Project: Surface EMG for Non-Invasive Assessment of Muscles-Project. www.seniam.org [accessed 18/12/12].

Smith, R. and Draper, C. eds. 2002. *Quantitative Characteristics of Coxless pair-oar rowing*. XXth International Symposium on Biomechanics in Sports.

Smith, R. and Draper, C. eds. 2006. *Skill Variables Discriminate between the elite and sub-elite in coxless pair-oared rowing*. *Proceedings of the XXIV International Symposium on Biomechanics in Sports.*

Smith, R. and Spinks, W. 1995. Discriminant analysis of biomechanical differences between novice, good and elite rowers. *J Sports Sci.* 13(5).

Smith, R. M. and Loschner, C. 2002. Biomechanics feedback for rowing. *Journal of Sports Sciences* 20(10), pp. 783-791.

Smith, R. M. et al. 1988. *ROWSYS: An on-water biomechanical analysis system for rowing*. National Sports Research Centre: Australian Sports Commission.

Sommer, M. et al. 2008. The effect of stroke rate on activation patterns of rowing in boat and ergometer trials: an EMG analysis. In: *World Congress of Performance Analysis of Sport, 2008.* Hamburg.

Song, P. et al. 2009. Highly Precise Time Synchronization Protocol for ZigBee Networks. *2009 Ieee/asme International Conference on Advanced Intelligent Mechatronics, Vols 1-3*, pp. 1247-1251.

Soper, C. and Hume, P. 2004a. Reliability of power output during rowing changes with ergometer type and race distance. *Sports Biomech* 3(2), pp. 237-248.

Soper, C. and Hume, P. 2004b. Towards an ideal rowing technique for performance : the contributions from biomechanics. *Sports Med* 34(12), pp. 825-848.

Spracklen, M. 2005. Bladework. In: Nolte, V. ed. *Rowing Faster*. Human Kinetics, pp. 141-154.

Streeton, M. and Stanfield, C. 2005. ZigBee: The telemetry solution? *IEE Conference Publication* (2005-11009), pp. 55-60.

Takahashi, D. 2009. *Tzero Technologies shuts down; that's the end of ultrawideband.* Venturebeat.

Tesconi, M. et al. 2007. Wearable sensorized system for analyzing the lower limb movement during rowing activity. *2007 Ieee International Symposium on Industrial Electronics, Proceedings, Vols 1-8*, pp. 2793-2796.

Tessendorf, B. et al. eds. 2011. *An IMU-based sensor network to continuously monitor rowing technique on the water*. Seventh international Conference on Intelligent Sensors, Sensor Networks and Information Processing.

Texas Instruments. 2010. CC2531: A USB-enabled Syatem-on-chip solution for 2.4GHz IEEE 802.15.4 and Zigbee Applications.

Tonks, R. 2005. Leg Drive. In: Nolte, V. ed. *Rowing Faster*. Human Kinetics, pp. 165-176.

Tuck, K. 2007a. Implementing auto zero calibration technique for accelerometers. In: Freescale ed. Freescale semiconductor application note.

Tuck, K. 2007b. Tilt Sensing using linear accelerometers. In: Semiconductor, F. ed. *AN3461*.

Veltink, P. H. et al. 1993. Feasibility of posture and movement detection by accelerometry. *Proceedings of the Annual Conference on Engineering in Medicine and Biology* 15(pt 3), pp. 1230-1231.

Vlasic, D. et al. 2007. Practical motion capture in everyday surroundings. *Acm Transactions on Graphics* 26(3).

Wang, Z. et al. eds. 2010. *A Pilot Study on Evaluating Recovery of the Post-Operative Based on Acceleration and sEMG*. 2010 International Conference on Body Sensor Networks.

Wilson, J. M. 2002. Ultra-Wideband/a Disruptive RF Technology? In: Development, I.R. ed.

Winter, M. and Brodd, R. 2004. What are batteries, fuel cells, and supercapacitors? *Chemical Reviews* 104(10), pp. 4245-4269.

Yang, G.-Z. 2006. *Body Sensor Networks*. Springer.

Yang, G.-Z. and Hu, X. 2006. Multi-Sensor Fusion. In: Yang, G.-Z. ed. *Body Sensor Networks*. Springer.

Yarovoy, A. G. and Ligthart, L. P. 2004. Ultra-wideband technology today. *15th International Conference on Microwaves, Radar and Wireless Communications, MIKON - 2004* 2, pp. 456-460.

Yeatman, E. and Mitcheson, P. 2006. Energy Scavenging. In: Yang, G.-Z. ed. *Body Sensor Networks*. Springer.

Young, K. and Muirhead, R. 1991. On-Board-Shell Measurements of Acceleration. *Centre for Rowing Science* 91(5).

Yourdon, E. 1989. *Modern Structured Analysis*. Prentice Hall.

Zhang, Z. Q. et al. 2011. Human back movement analysis using BSN. In: *2011 International Conference on Body Sensor Networks.*

Zigbee Alliance. 2006. Zigbee Specification.

Zijlstra, W. et al. 2010. A body-fixed-sensor-based analysis of power during sit-to-stand movements. *Gait & Posture* 31(2), pp. 272-278.

A. Appendix

A.1 Modulation Techniques Summary

A.1.1 Frequency Hopping Spread Spectrum (FHSS)

Frequency Hopping Spread Spectrum (FHSS) instantaneously occupies a narrow bandwidth, but averaged over time, its signal is spread over a broad bandwidth.

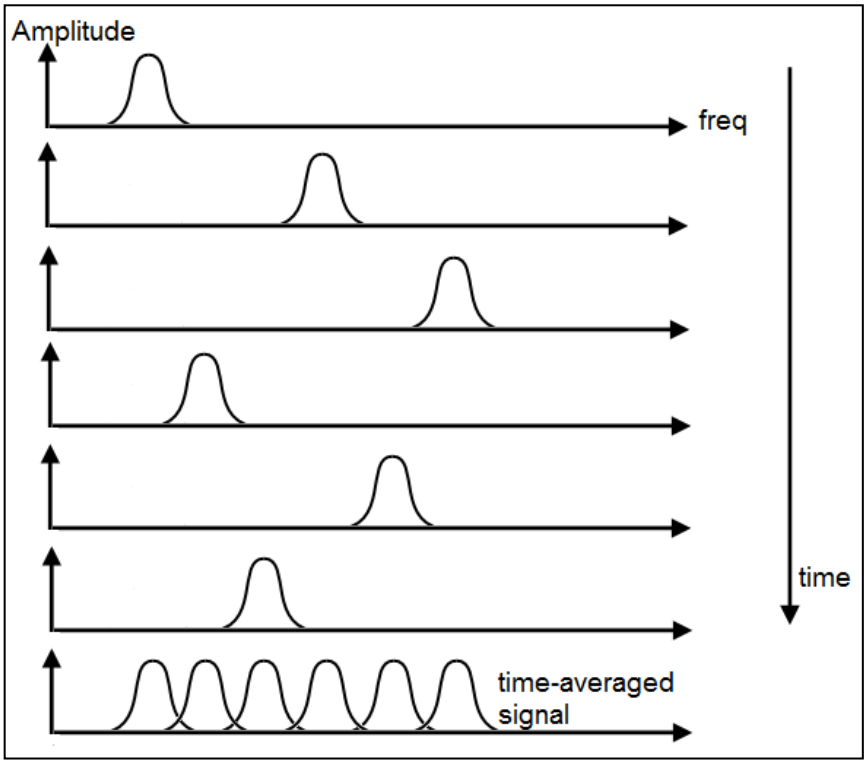

Figure A-1: Time-averaged spreading of FHSS signal

A.1.2 Direct System Spread Spectrum (DSSS)

In Direct System Spread Spectrum (DSSS), the data is spread over a wide bandwidth (for Zigbee 5MHz). Each 4-bit nibble of raw data is substituted with one of 16 different symbols, where a symbol is a 32-bit sequence called a chipping code. Each bit of the sequence is a chip, and a chip interval is thus much shorter, spreading the energy of the signal in the frequency domain.

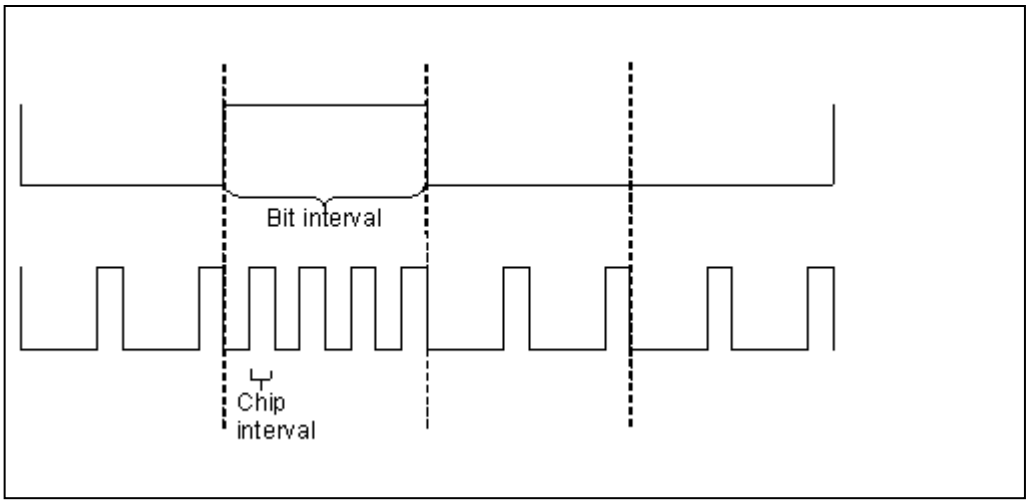

Figure A-2: Code-spreading of DSSS

A.1.3 Orthogonal Frequency Division Multiplexing (OFDM)

Orthogonal Frequency Division Multiplexing (OFDM): Many signals are transmitted at the same time at different frequencies (each signal is modulated with a different sub-carrier. The signals are carefully chosen to be orthogonal (mathematically perpendicular) to avoid interference, meaning that they can be closer in frequency (even overlapping). These closely packed frequencies are therefore more spectrally efficient.

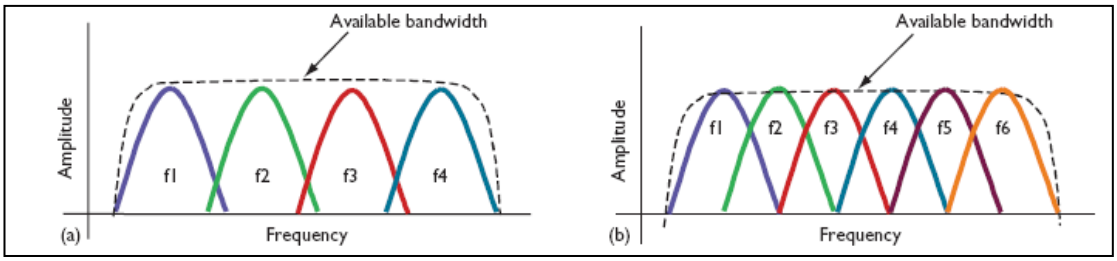

Figure A-3: Overlapping Orthogonal frequencies of OFDM

(Kapp 2002)

A.1.4 Phase Shift Keying (PSK)

A modulating technique. The information contained in a stream of data is coded into the changes of phase of the transmitted signal. The simplest, Binary Phase shift keying (BPSK) has 180^{o} phase shifts in the signal when there is a transition from 1 to 0 or 0 to 1 of the data.

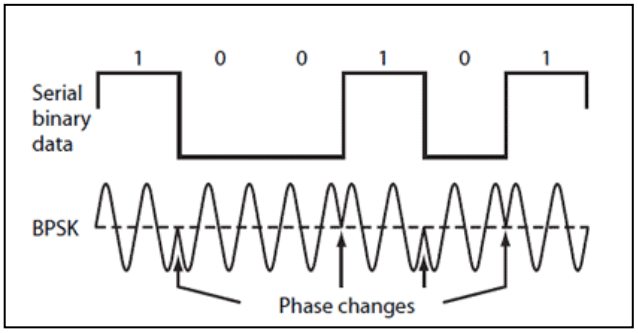

Figure A-4: Binary Phase Shift Keying (BPSK)

(Frenzel 2012)

Variations are Quadrature Phase Shift Keying (QPSK) which has 4 different phases meaning that 2-bits can be coded by each phase. Offset QPSK is a further variation on this (By offsetting the timing of the bit changes of the two coding bits, the in-phase and quadrature components will never change at the same time.

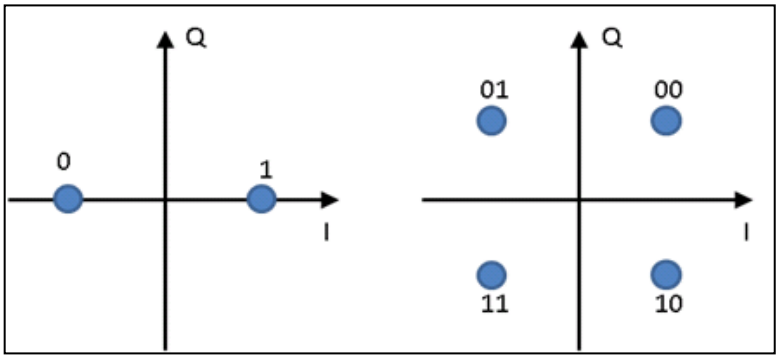

Figure A-5: Phasor diagrams for BPSK and QPSK

A.1.5 Frequency Shift Keying (FSK)

Frequency shift keying shifts the carrier between two different frequencies to modulate it with the information signal (Figure A-6a).

A.1.6 On-Off Keying (OOK)

This is the simplest form of amplitude shift keying, where the digital signal is coded through the presence or absence of a carrier signal Figure A-6b.

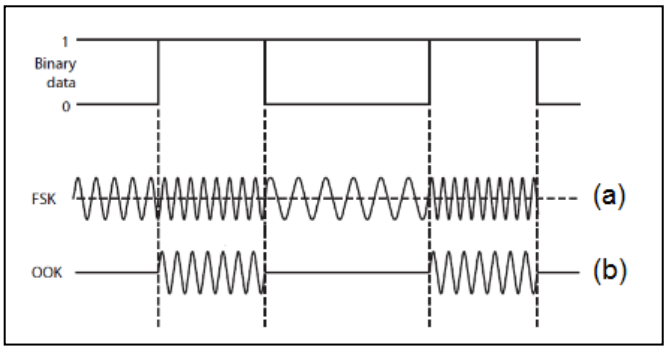

Figure A-6: Examples of On-Off Keying and Frequency Shift Keying

A.1.7 Time Division Multiple Access (TDMA)

TDMA allows several users to share the same frequency channel by dividing the signal into different time slots.

A.1.8 Wideband Frequency Modulation

Frequency modulation involves the encoding of a carrier wave by variation of its frequency according to the information signal. Wideband frequency modulation has a modulation index (ratio of the maximum deviation frequency to the frequency of modulation) >1 such that the frequency is spread over a wider spectrum.

Further information on many modulation schemes can be found at the following link:

http://electronicdesign.com/communications/understanding-modern-digital-modulation-techniques [accessed 18/01/13]

A.2 Power consumption comparison of WLAN, Bluetooth and Zigbee ICs

Comparison of:

- TI/MuRata CC3000 WLAN Module (MuRata 2012a)
- TI/MuRata CC2560 Bluetooth Module (MuRata 2012b)
- TI CC2531 802.15.4/Zigbee Module (Texas Instruments 2010)

	CC3000 WLAN 802.11b	CC3000 WLAN 802.11g	CC2560 Bluetooth	CC2531 802.15.4 /Zigbee
Supply Voltage	3.6V	3.6V	3V	3V
Typical Current (mA) Tx	292 (≡1.05W)	180 (≡0.65W)	165 (≡0.50W)	29 (≡87m W)
Typical Current (mA) Rx	92 (≡0.33W)	92 (≡0.33W)	50 (≡0.15W)	24 (≡72m W)
Typical Current (mA) standby/sleep – where given			3.5 (≡10.5mW)	<0.2 (≡0.6m W)

Table A-1: Comparison of WLAN, Bluetooth and Zigbee module power consumptions

A.3 BAN Frequency bands

Frequency Band	Packet Component	Modulation	Symbol Rate (Kbps)	Code Rate BCH (n,k)	Information Data Rate (Kbps)
402 - 405 MHz	PLCP Header	π/2-DBPSK	187.5	(31,19)	57.5
	PSDU	π/2-DBPSK	187.5	(63,51)	75.9
	PSDU	π/4-DQPSK	187.5	(63,51)	303.6
420 - 450 MHz	PLCP Header	GMSK	187.5	(31,19)	57.5
	PSDU	GMSK	187.5	(63,51)	75.9
	PSDU	GMSK	187.5	(63,51)	151.8
863 - 870 MHz	PLCP Header	π/2-DBPSK	250	(31,19)	76.6
	PSDU	π/2-DBPSK	250	(63,51)	101.2
	PSDU	π/4-DQPSK	250	(63,51)	404.8
902 - 928 MHz	PLCP Header	π/2-DBPSK	300	(31,19)	91.9
	PSDU	π/2-DBPSK	300	(63,51)	121.4
	PSDU	π/4-DQPSK	300	(63,51)	485.7
950 - 956 MHz	PLCP Header	π/2-DBPSK	250	(31,19)	76.6
	PSDU	π/2-DBPSK	250	(63,51)	101.2
	PSDU	π/4-DQPSK	250	(63,51)	404.8
2360-2400 MHz 2400-2483.5 MHz	PLCP Header	π/2-DBPSK	600	(31,19)	91.9
	PSDU	π/2-DBPSK	600	(63,51)	121.4
	PSDU	π/2-DBPSK	600	(63,51)	485.7

Table A-2: BAN: Frequency bands, Modulation schemes and data rates for BAN Narrowband PHY

(Kwak et al. 2010)

A.4 Acceleration Sensitivity related to Axis orientation

It can be seen in Figure A-7 that the gradient of the acceleration output is at its maximum as it passes through 0g, and at a minimum as it passes through +1g or -1g. The inset graph shows that a 1^{o} tilt around the 0g is equivalent to 11^{o} of tilt around the 1g axis.

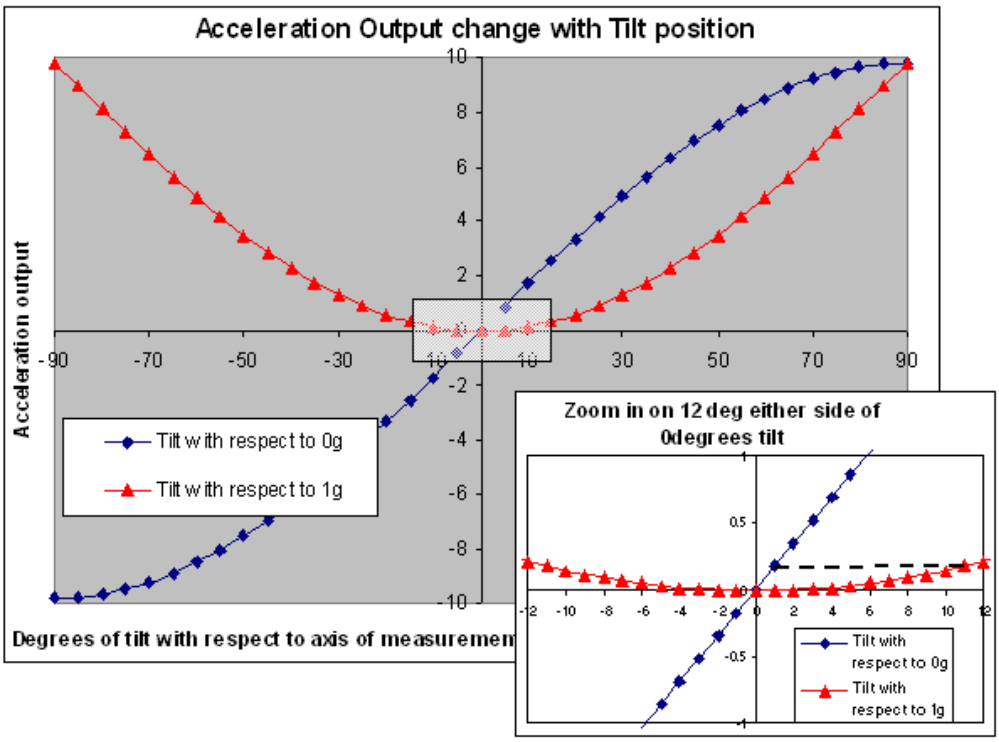

Figure A-7: Graphical explanation of Sensitivity of an accelerometer depending upon axis orientation

B. Appendix

B.1 Hardware details and circuit schematics

Features	PIC18F4620
Operating Frequency	DC – 40 MHz
Program Memory (Bytes)	65536
Program Memory (Instructions)	32768
Data Memory (Bytes)	3968
Data EEPROM Memory (Bytes)	1024
Interrupt Sources	20
I/O Ports	Ports A, B, C, D, E
Timers	4
Capture/Compare/PWM Modules	1
Enhanced Capture/Compare/ PWM Modules	1
Serial Communications	MSSP, Enhanced USART
Parallel Communications (PSP)	Yes
10-bit Analog-to-Digital Module	13 Input Channels
Resets (and Delays)	POR, BOR, RESET Instruction, Stack Full, Stack Underflow (PWRT, OST), MCLR (optional), WDT
Programmable Low-Voltage Detect	Yes
Programmable Brown-out Reset	Yes
Instruction Set	75 Instructions; 83 with Extended Instruction Set enabled
Packages	40-pin PDIP 44-pin QFN 44-pin TQFP

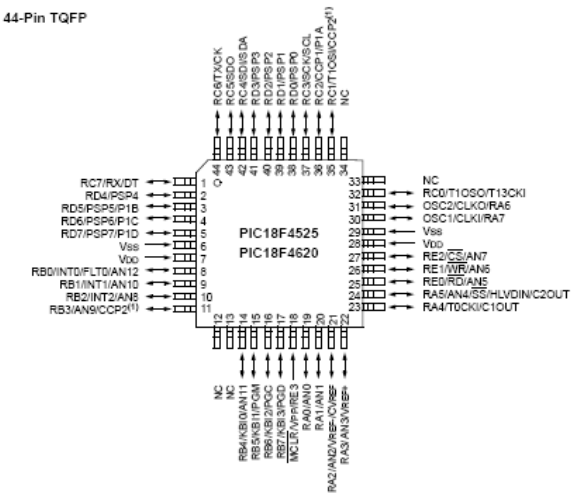

Figure B-1: Microchip PIC18F4620 Features summary and pin-out diagram

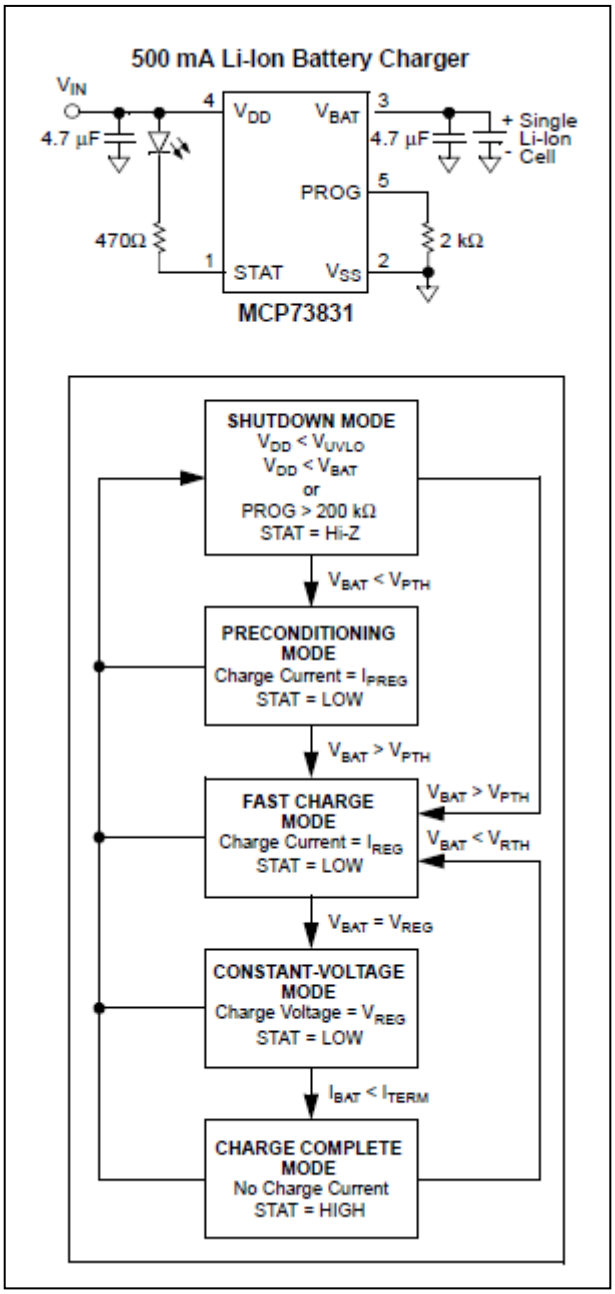

Figure B-2: Charge management for Li-ion batteries

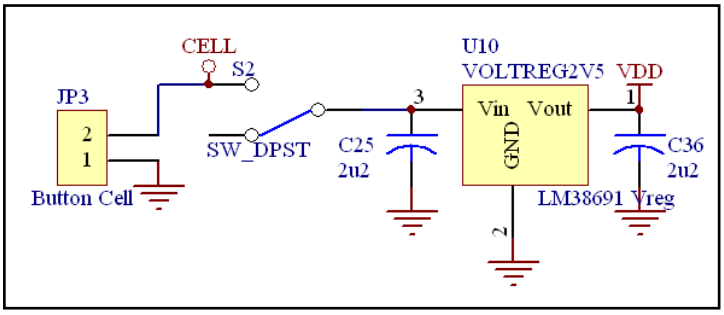

Figure B-3: Voltage regulation sub-circuit

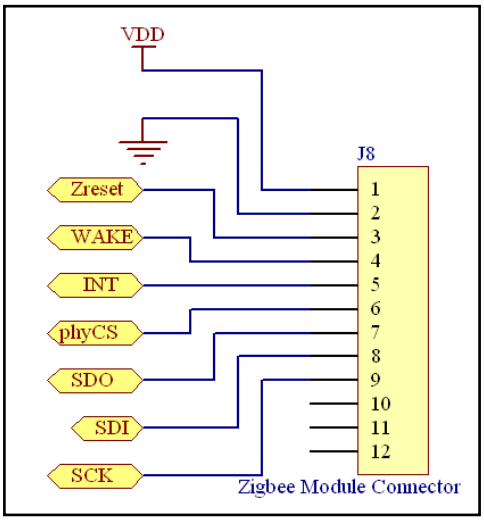

Figure B-4: Zigbee radio module sub-circuit - connection

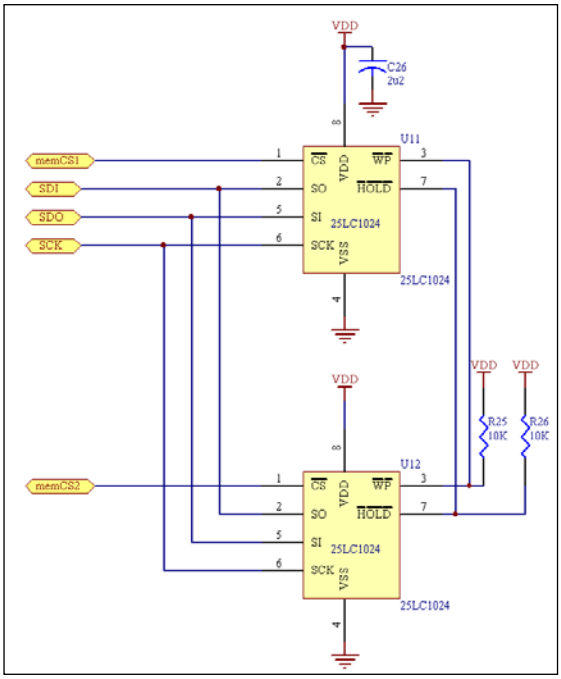

Figure B-5: Local memory sub-circuit

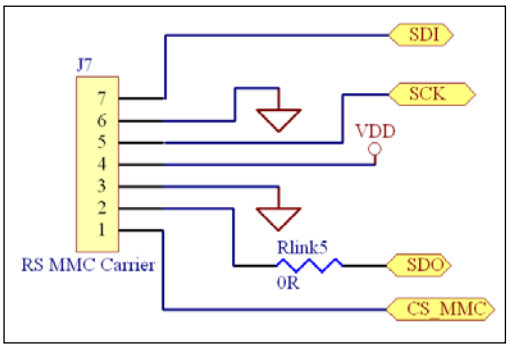

Figure B-6: Central Data Storage sub-circuit – RS MMC Card Carrier

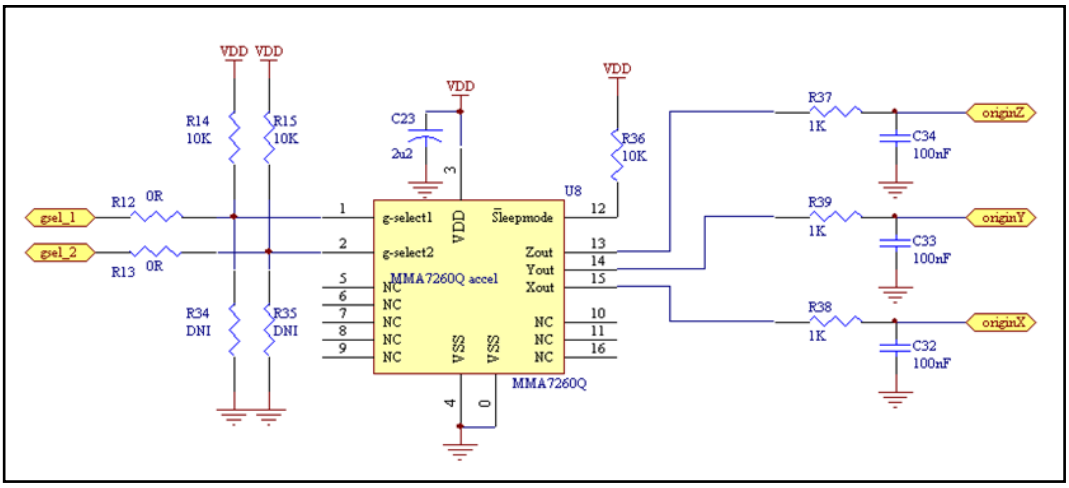

Figure B-7: Accelerometer sub-circuit schematic

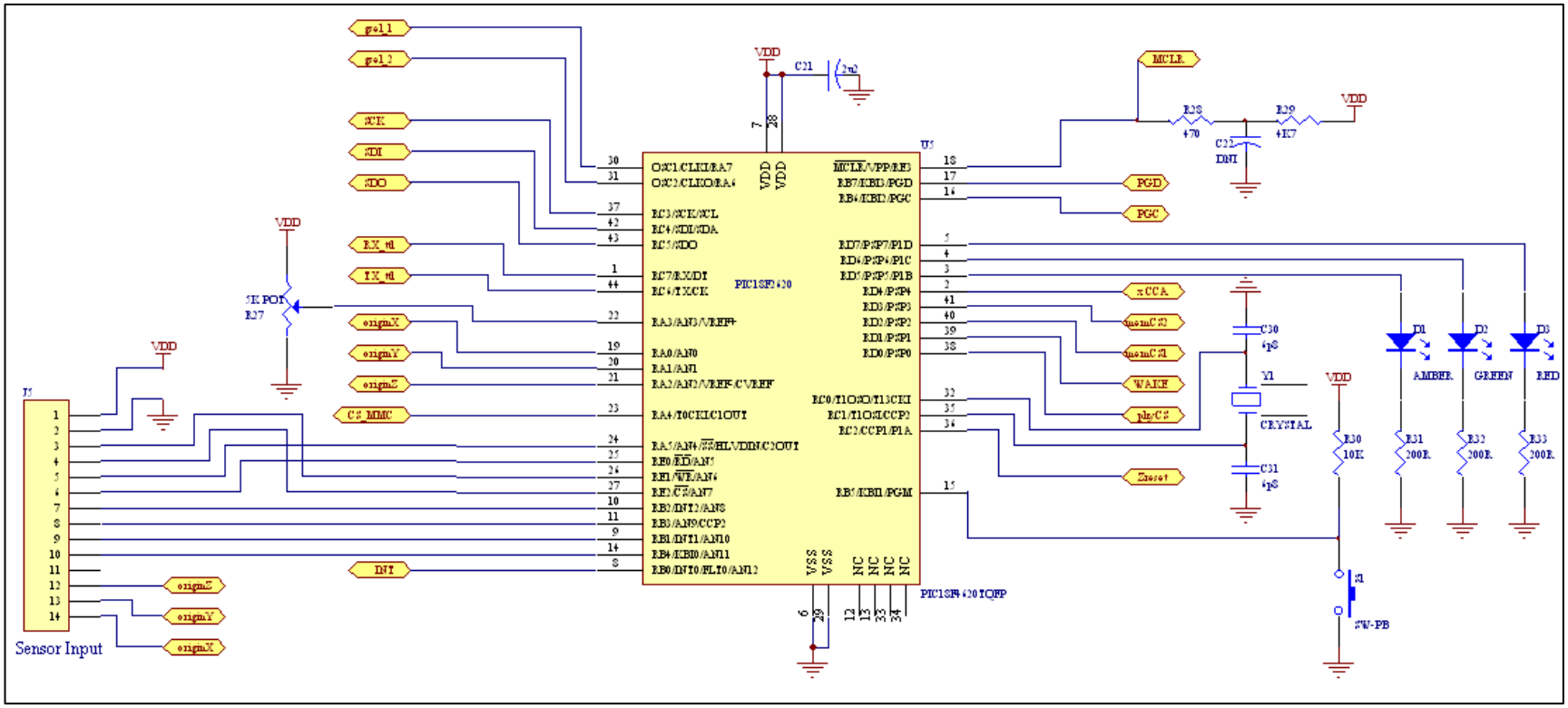

Figure B-8: Microcontroller and peripheral circuitry

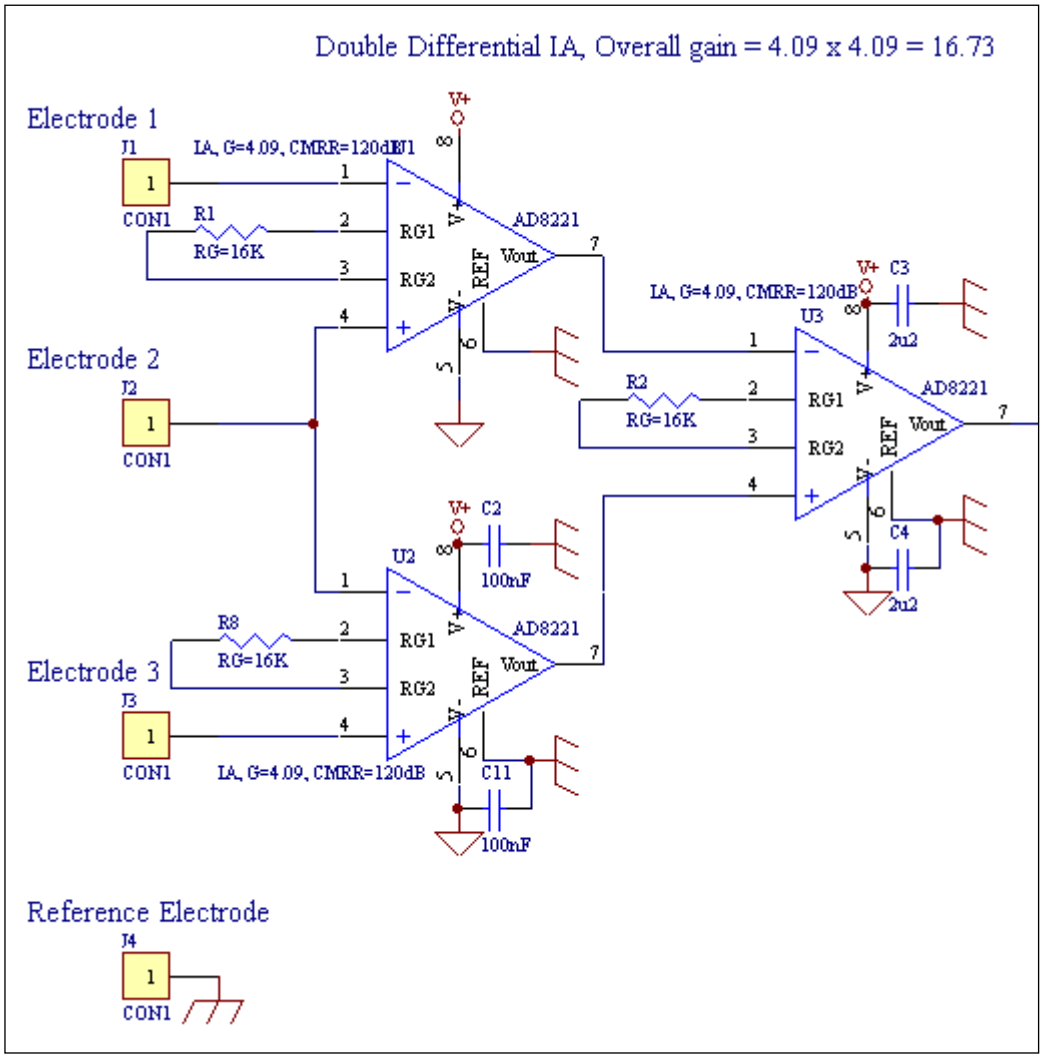

Figure B-9: sEMG Double Differencing stage sub-circuit schematic

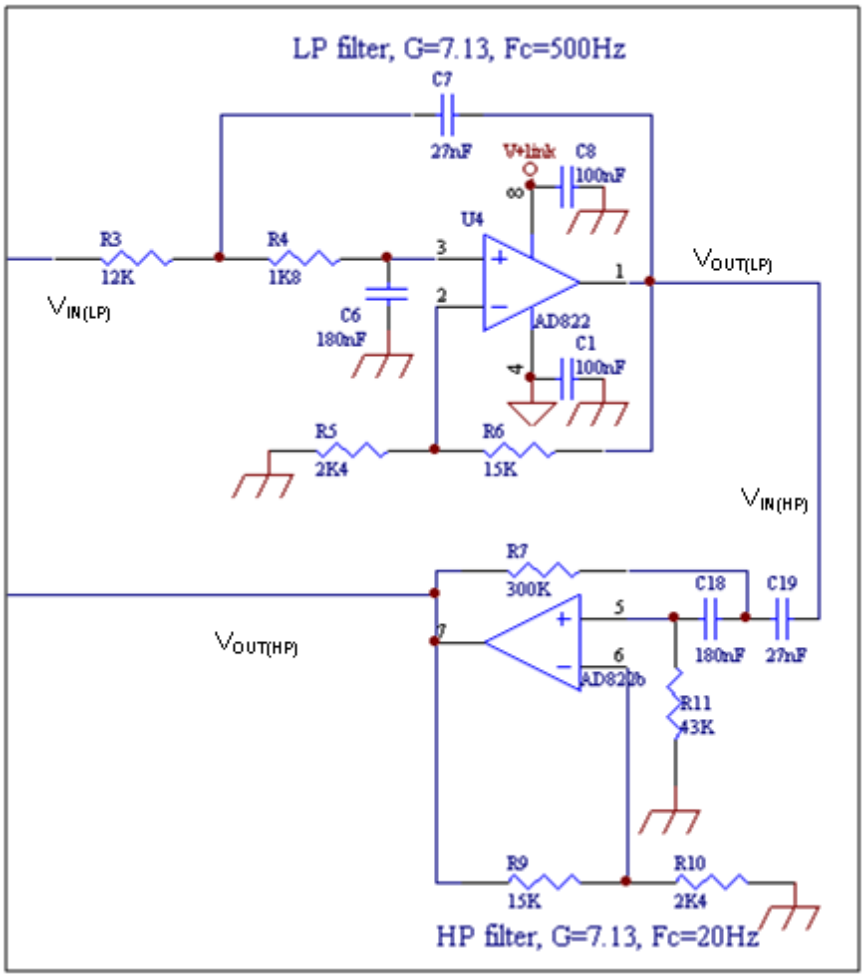

Figure B-10: sEMG Low pass and high pass filters sub-circuit schematic

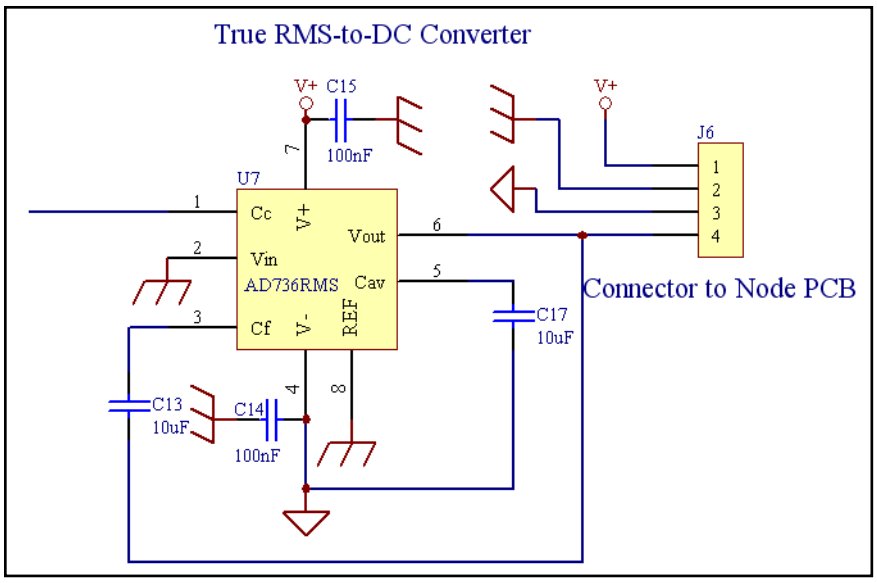

Figure B-11: sEMG RMS to DC conversion sub-circuit schematic

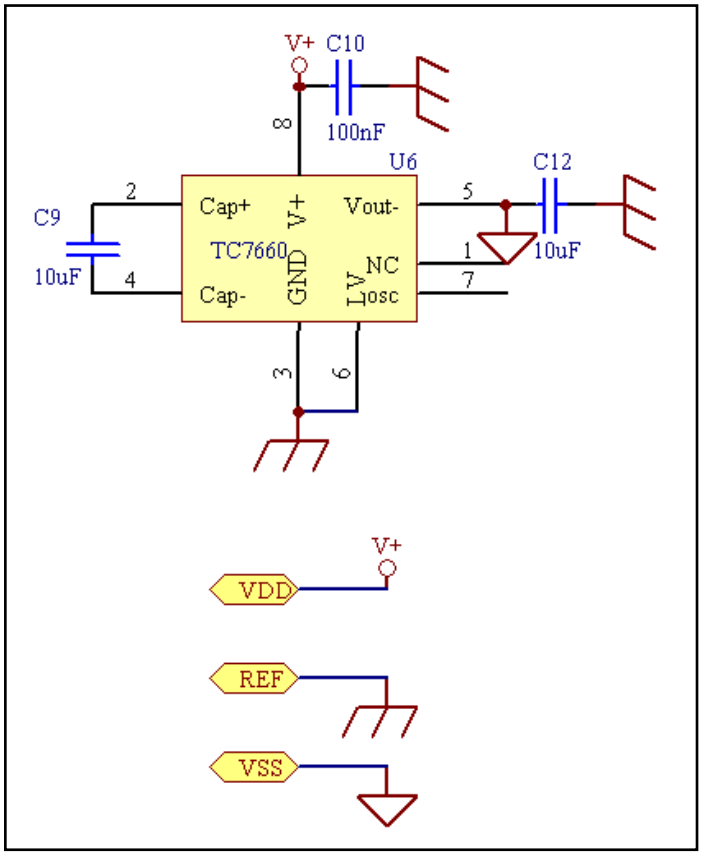

Figure B-12: sEMG Negative voltage converter sub-circuit schematic

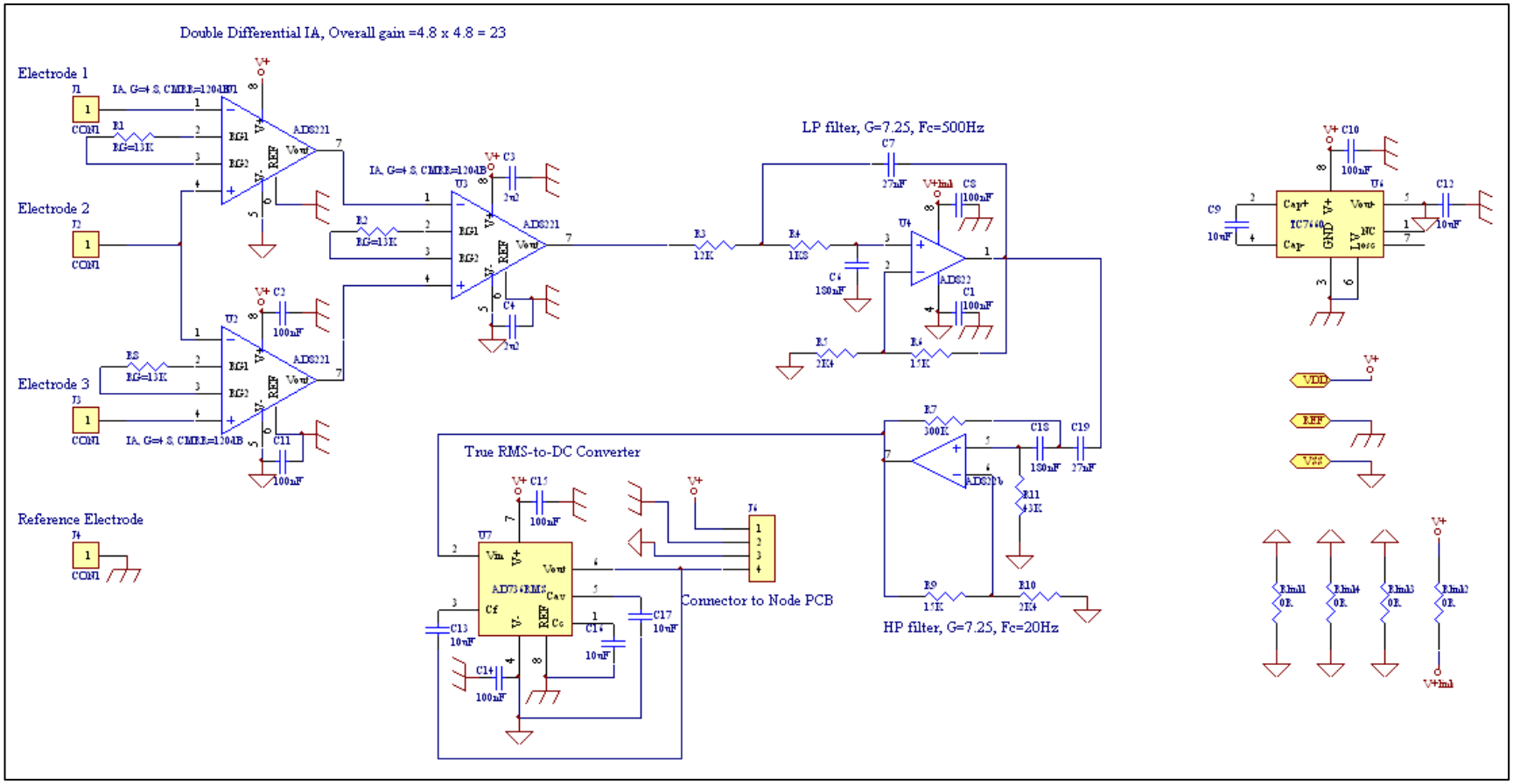

Figure B-13: Complete sEMG circuit schematic

B.2 Individual Accelerometer calibration values

Node	Axis	Min ADC value	Max ADC Value	2g range (units)	Sensitivity (mV/g)	Zero g (units[V])
#S1	X	270	640	370	451	455 [1.11]
	Y	275	645	370	451	460 [1.12]
	Z	335	700	365	445	518 [1.26]
#S2	X	265	635	370	451	450 [1.10]
	Y	295	665	370	451	480 [1.17]
	Z	335	700	365	445	518 [1.26]
#S3	X	265	645	380	464	455 [1.11]
	Y	305	680	375	458	493 [1.20]
	Z	345	705	360	439	525 [1.28]
#S4	X	300	660	360	439	480 [1.17]
	Y	275	650	375	458	463 [1.13]
	Z	360	710	350	427	535 [1.31]
#S5	X	260	630	370	451	445 [1.09]
	Y	290	655	365	445	473 [1.15]
	Z	335	695	360	439	515 [1.26]

Table B-1: Accelerometer sensitivity and zero-g calibration

2.5V supply ≡ 2.44mV/unit

B.3 sEMG filter design, simulation and measurement

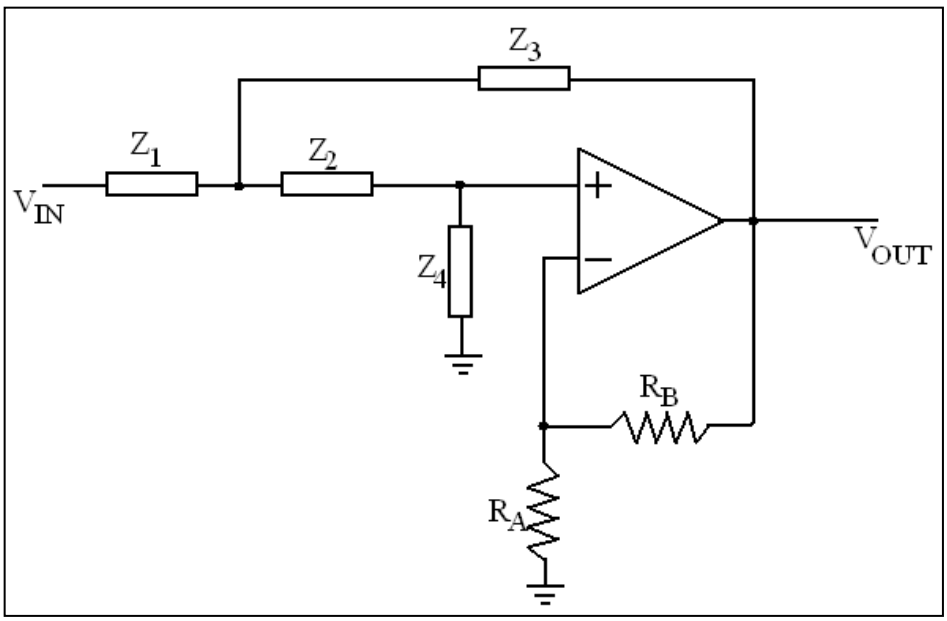

Figure B-14: Sallen and Key filter topology

Nodal (KCL) analysis of Figure B-14 yields the following transfer function:

$$T(s) = \frac{G.Z_3.Z_4}{Z_3(Z_1 + Z_2 + Z_4) + Z_1.Z_2 + Z_1.Z_4(1-G)}$$

where

$$G = 1 + \frac{R_B}{R_A}$$

This generic topology can be transformed into a low pass filter by replacing Z_1 and Z_2 with resistors (which allow low frequency signals to pass through into the amplifier) and Z_3 and Z_4 with capacitors (which will cause the output to roll off at higher frequencies). Switching the position of the resistors and capacitors achieves high pass behaviour. Thus the transfer function becomes:

$$T(s) = \frac{G.\dfrac{1}{R_1.R_2.C_1.C_2}}{s^2 + s\left(\dfrac{1}{C_1}\left[\dfrac{1}{R_1}+\dfrac{1}{R_2}\right]+\dfrac{1}{R_2C_2}\left[1-G\right]\right)+\dfrac{1}{R_1.R_2.C_1.C_2}}$$

The polynomial of a two pole Butterworth filter (chosen for its flatness in the pass-band) is:

$$T(s) = \frac{G}{s^2+1.41425s+1} \Rightarrow \frac{G}{\left(\dfrac{s}{2.\pi.f}\right)^2+1.41425.\left(\dfrac{s}{2.\pi.f}\right)+1}$$

The left hand transfer function describes a normalised filter with f=1rad/sec and a gain of G, whilst applying frequency scaling results in the right hand function. Through equating these equations, the Salen key circuit topology can be made to fit the Butterworth polynomial, and the components calculated.

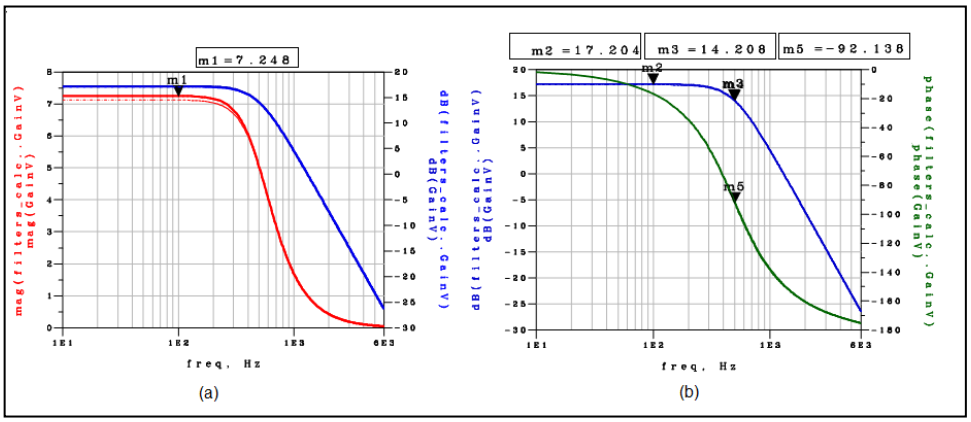

Figure B-15: Low Pass filter simulation

(a): Gain and gain in dB calculated values v available, (b) Gain and Phase

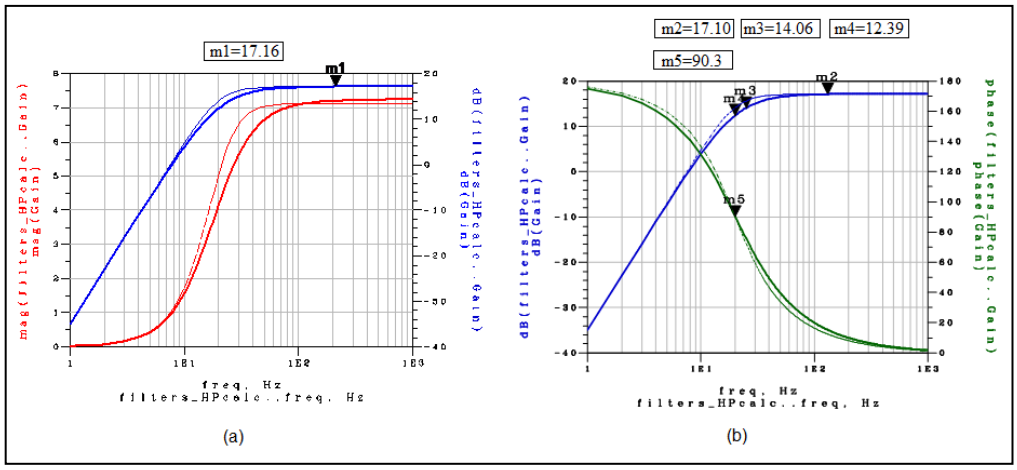

Figure B-16: High Pass filter simulation

(a): Gain and gain in dB calculated values v available, (b) Gain and Phase

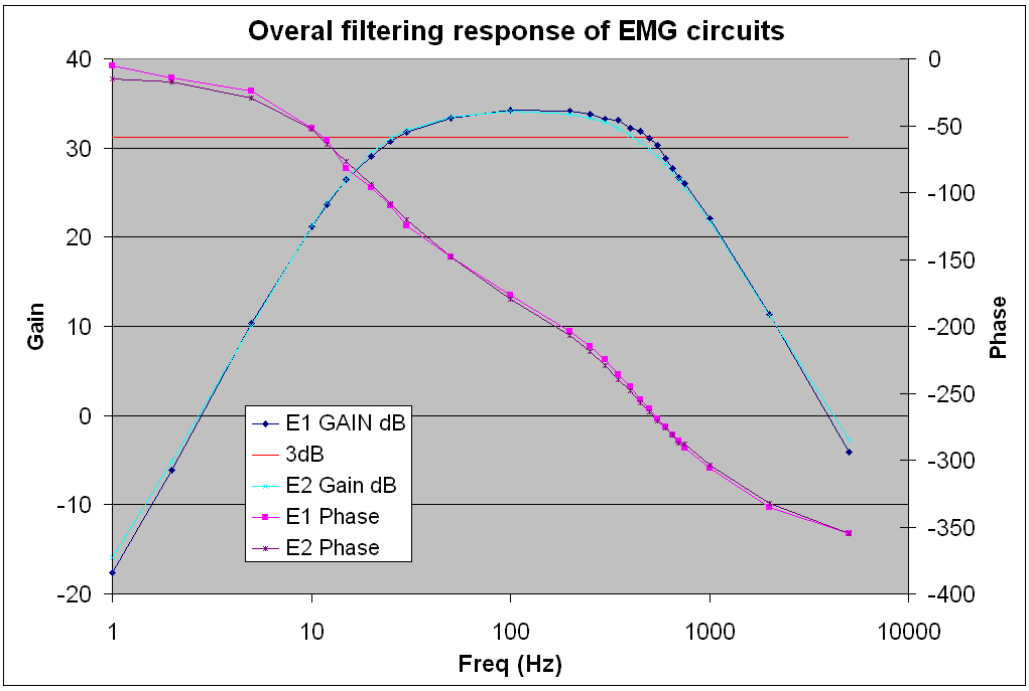

Figure B-17: Overall measured filtering response of EMG circuits, PCBs E1 and E2.

B.4 State Transition diagram of user-controlled program flow:

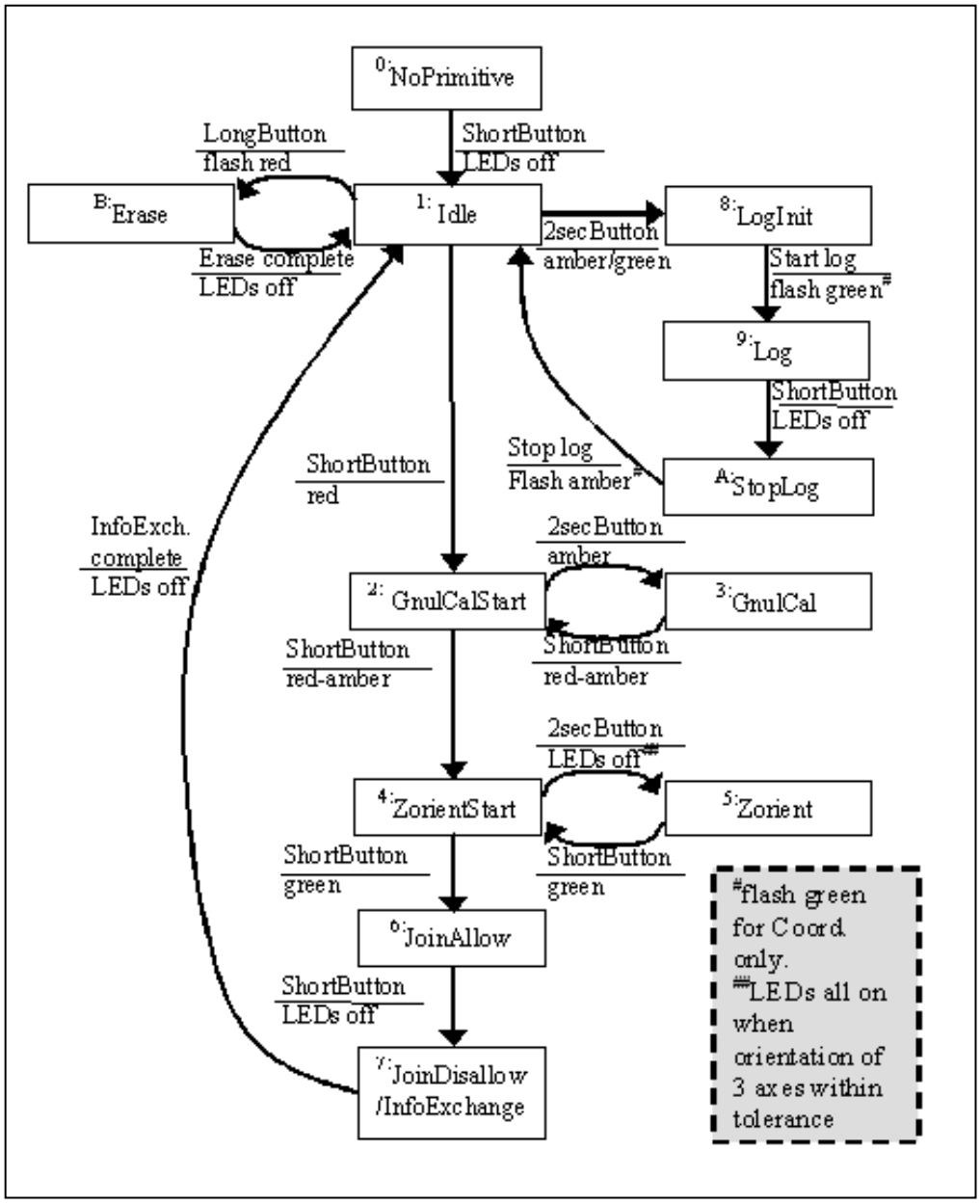

Figure B-18: User-controlled system flow of Wireless BSN function

C. Appendix

C.1 Additional graphs from Validation of measurements through Motion Capture

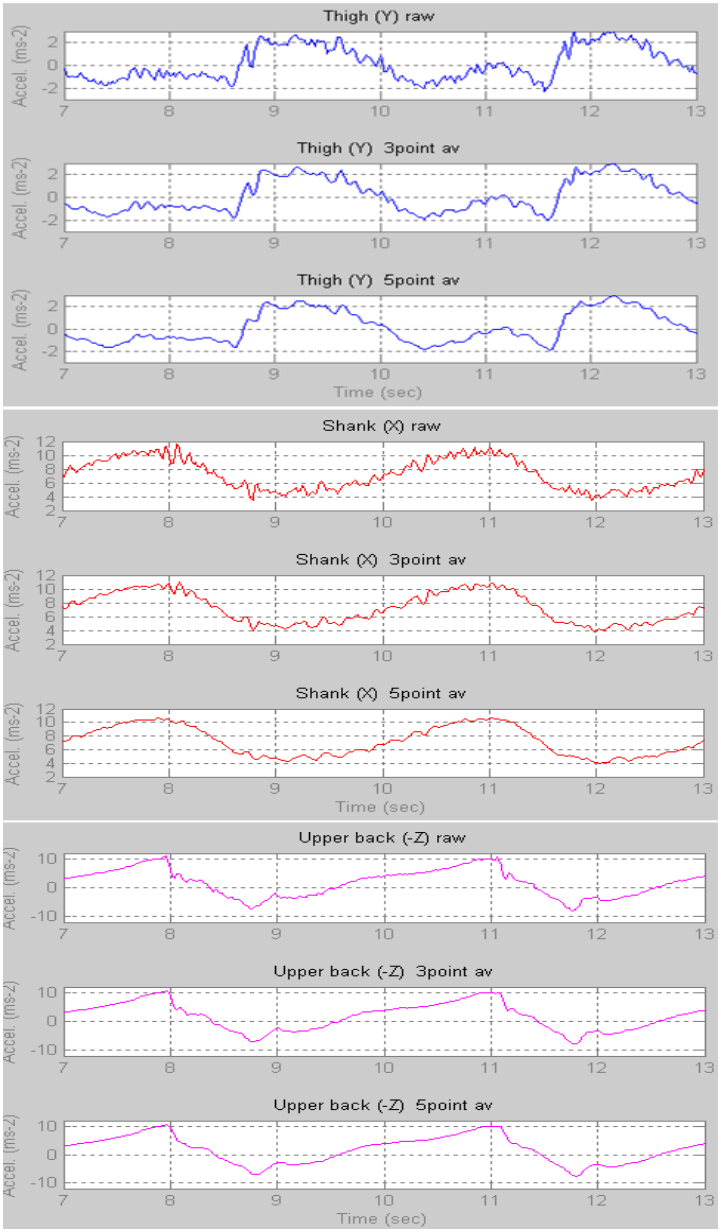

Figure C-1: Examples of 3-and 5-point moving window averaging of acceleration data on dominant axes of measurement

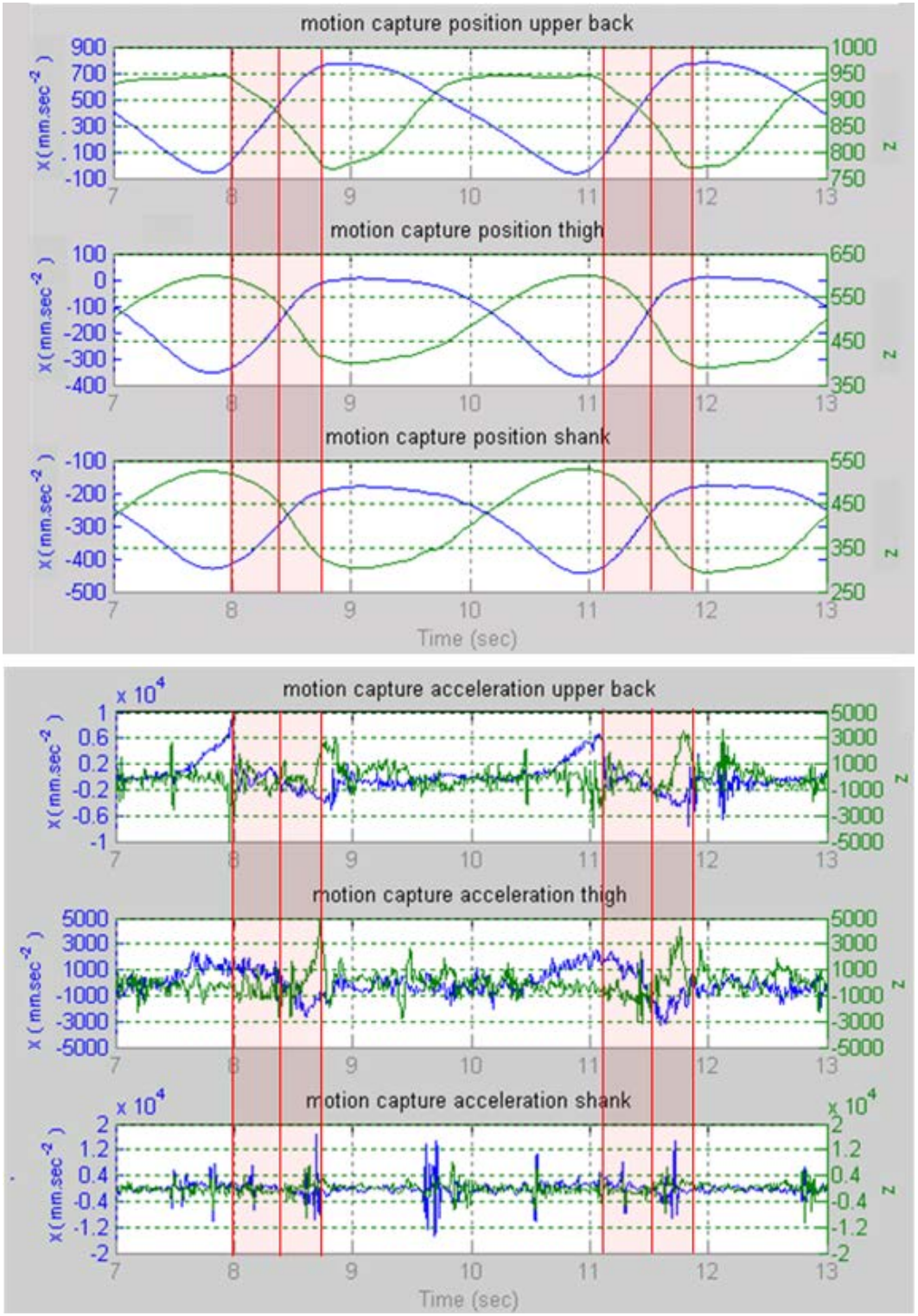

Figure C-2: Positional (top) and Acceleration (bottom) motion capture data for x and z axes: upper back, thigh, and shank

Traces from top to bottom: motion capture position of back, thigh and shank nodes in x—z plane, motion capture acceleration of back thigh and shank nodes

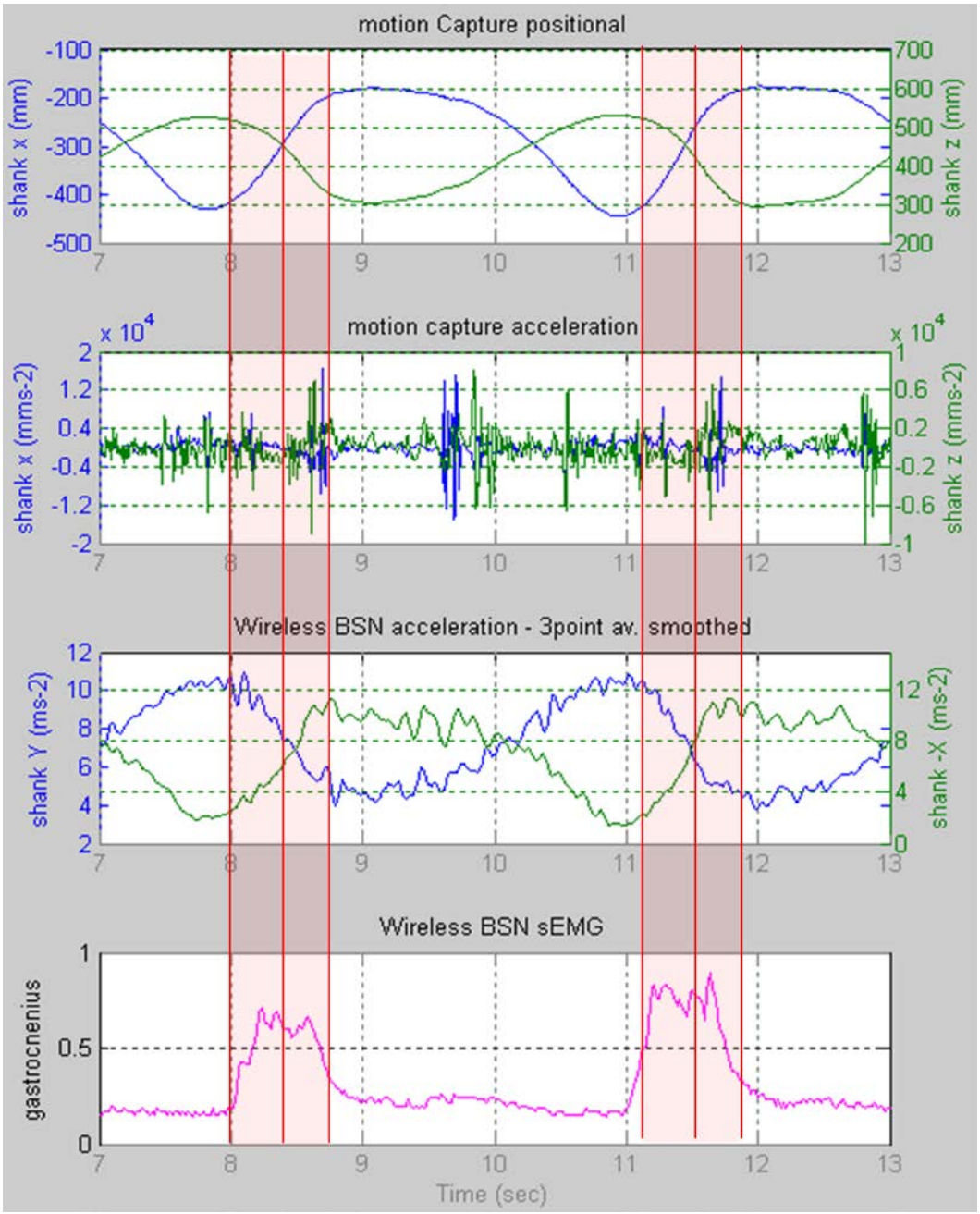

Figure C-3: Shank motion capture and wireless BSN data comparison

Traces from top to bottom: motion capture position of shank node in x—z plane, motion capture acceleration of shank node, Wireless BSN acceleration of shank node (Y—-X plane), gastrocnemius sEMG

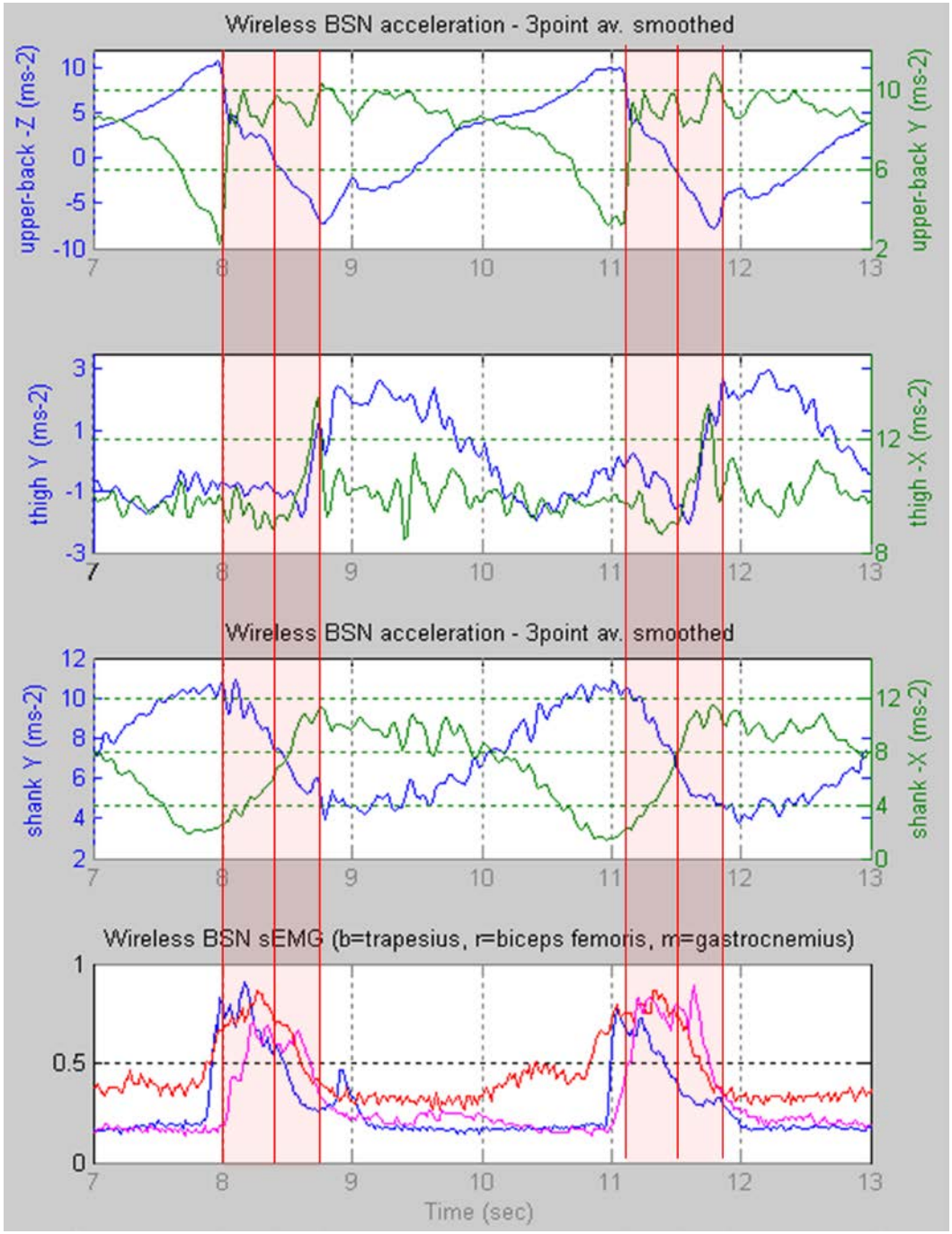

Figure C-4: Wireless BSN data: acceleration (relevant axes) and sEMG muscle data

Traces from top to bottom: Wireless BSN acceleration of back node (-Z—Y plane), thigh node (Y—-X plane), shank (Y—-X plane), blue – trapezius, red – biceps femoris, magenta - gastrocnemius sEMG

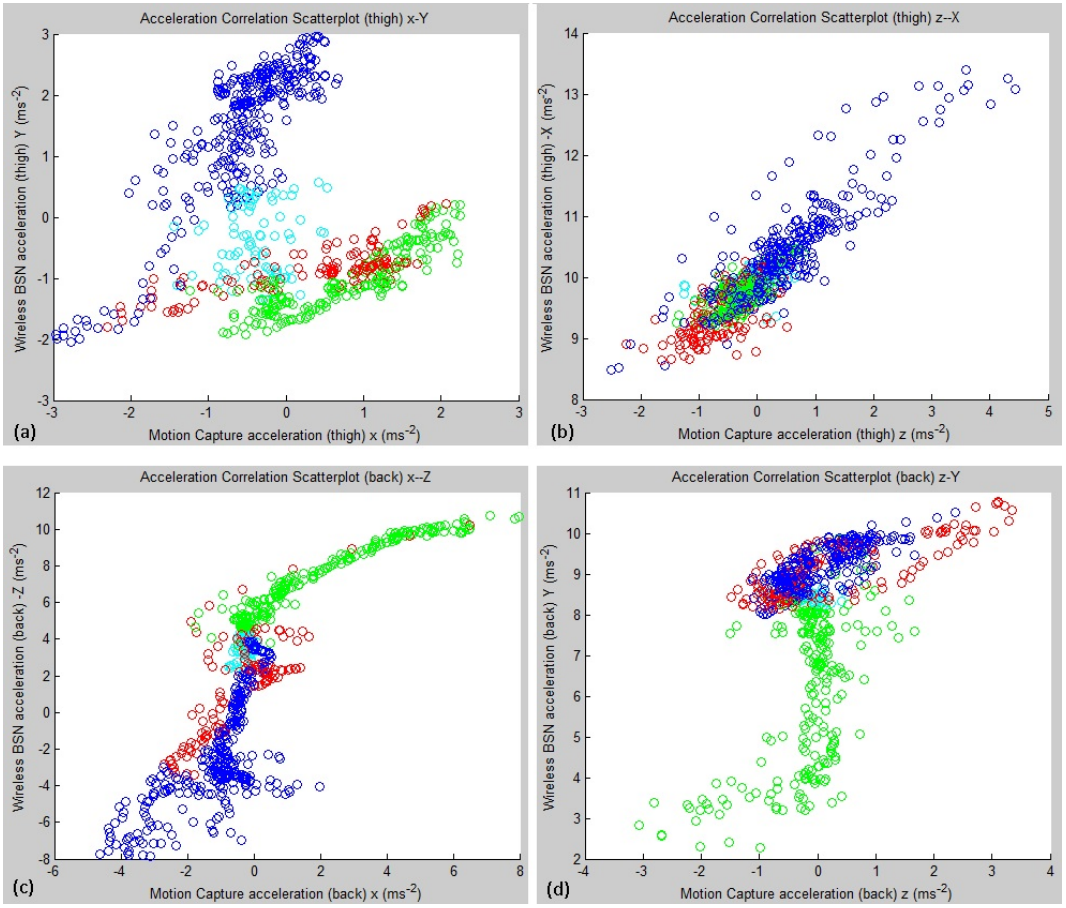

Figure C-5: Scatterplots to analyse correlation between Motion Capture and Wireless BSN acceleration measurements

(a) and (b) are thigh node measurements, (c) and (d) back measurements. Colours indicate stroke phases; red: drive phase, blue: hands-way/rock-over, green: recovery, cyan indicates transition between phases.

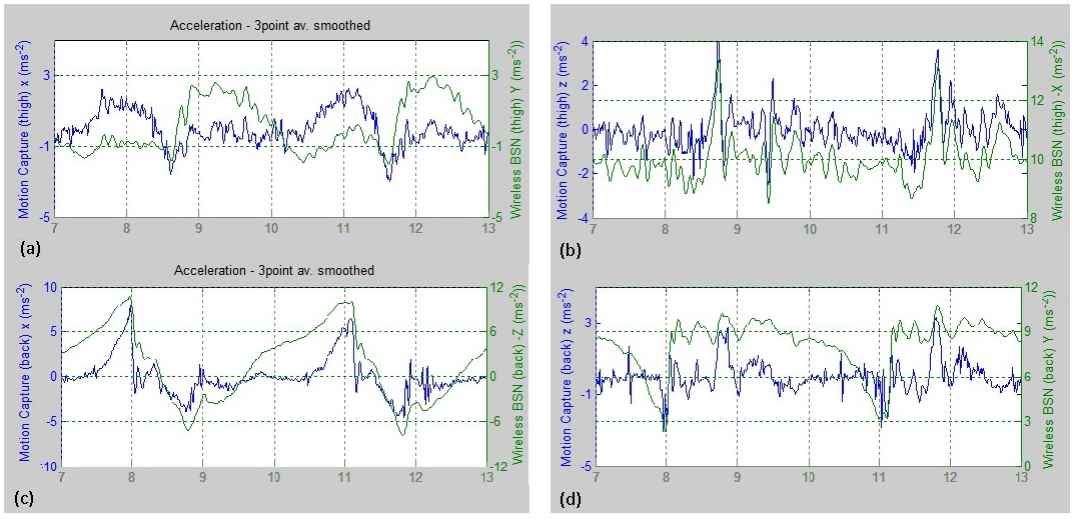

Figure C-6: Overlaying equivalent acceleration axes from Motion Capture and Wireless BSN systems for correlation analysis

C.2 Additional graphs from Synchronous measurement of muscle activity

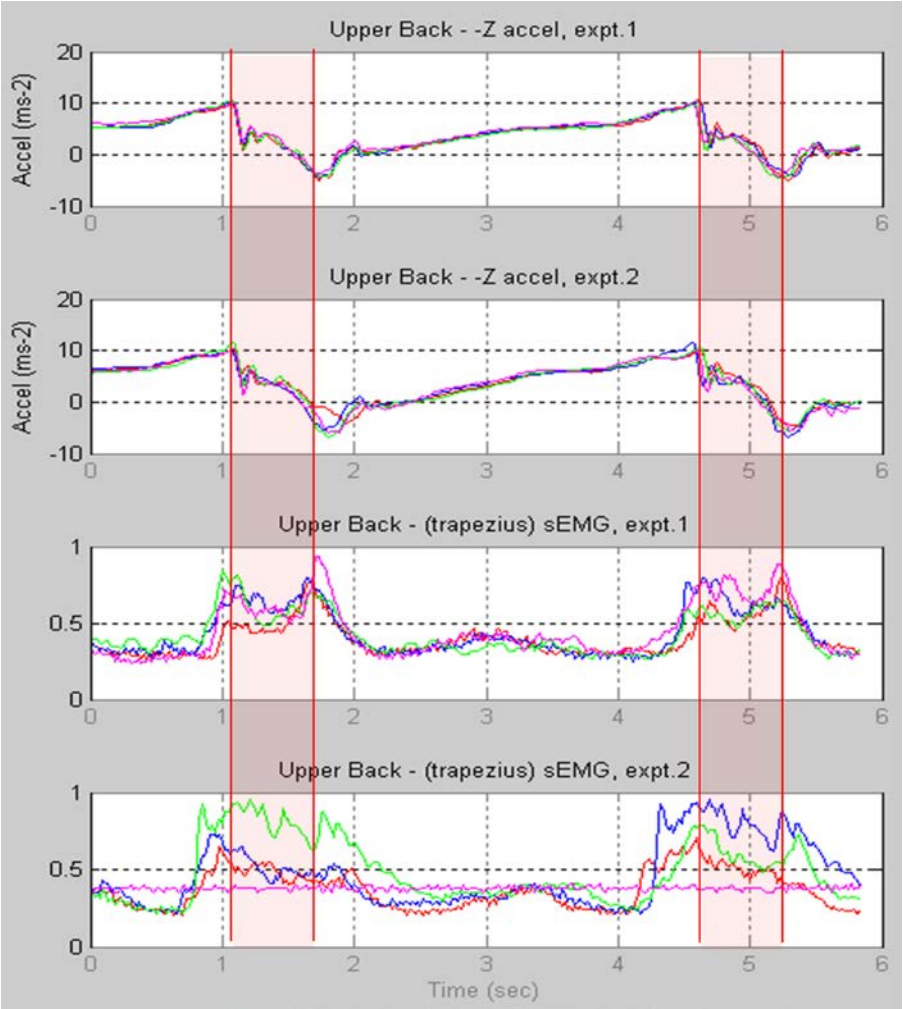

Figure C-7: Correlation of trapezius muscle measurements (and corresponding upper back acceleration of dominant axis) over 2 experiments, 4 strokes correlated per experiment

Note1: Upper back electrodes remained in the same position for both expt1 and expt2.

Note2: An electrode measuring the trapezius muscle became displaced in latter stages of expt 2 (magenta)

Acceleration VR= is 0.06, Trapezius sEMG VR=0.06

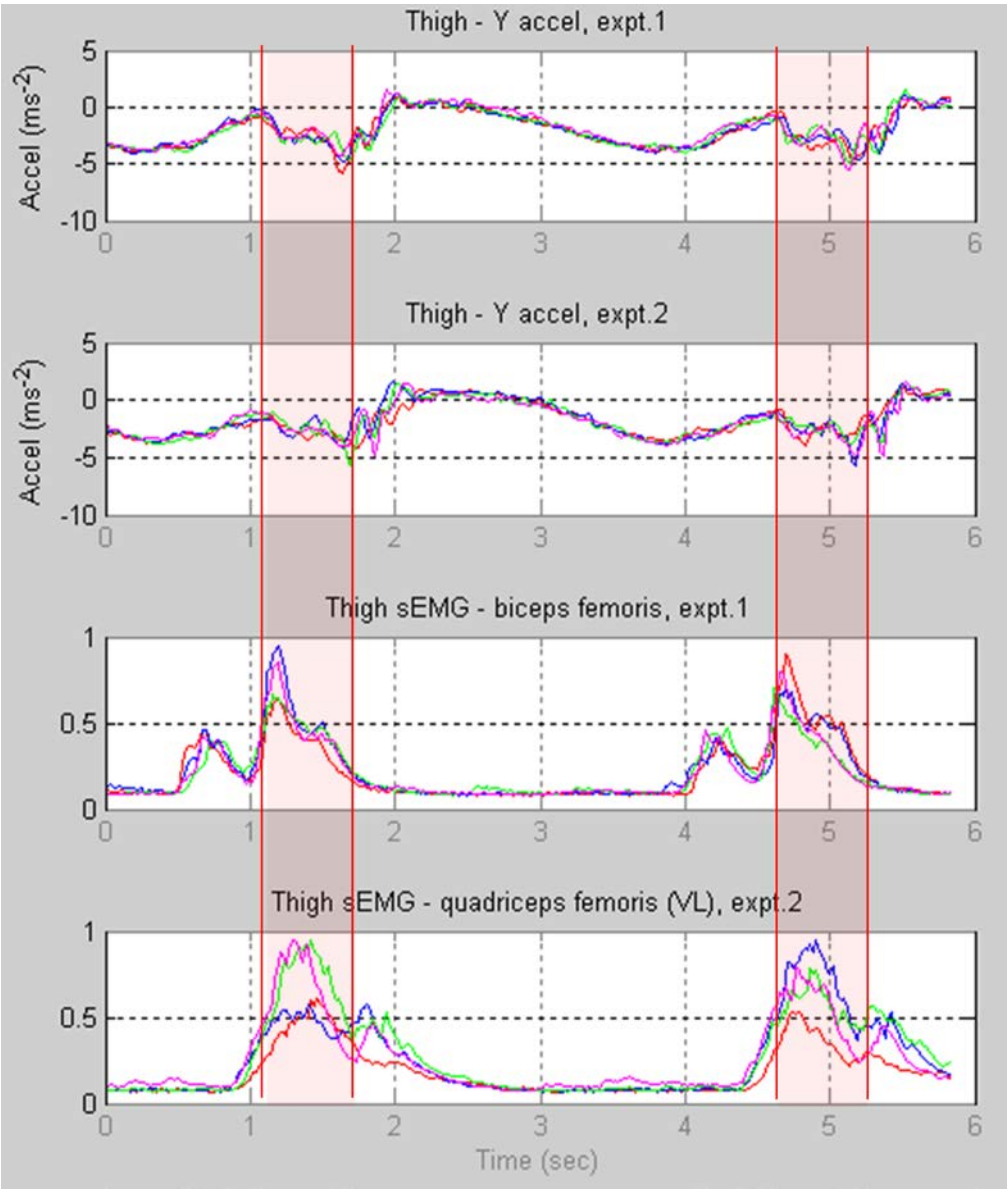

Figure C-8: Correlation of thigh muscle measurements (and corresponding acceleration of dominant axis) over 2 experiments

Aligned by thigh acceleration data, 4 strokes aligned per experiment

Acceleration VR= is 0.10, Biceps Femoris sEMG VR=0.03,Quadriceps Femoris (VL) sEMG VR=0.07

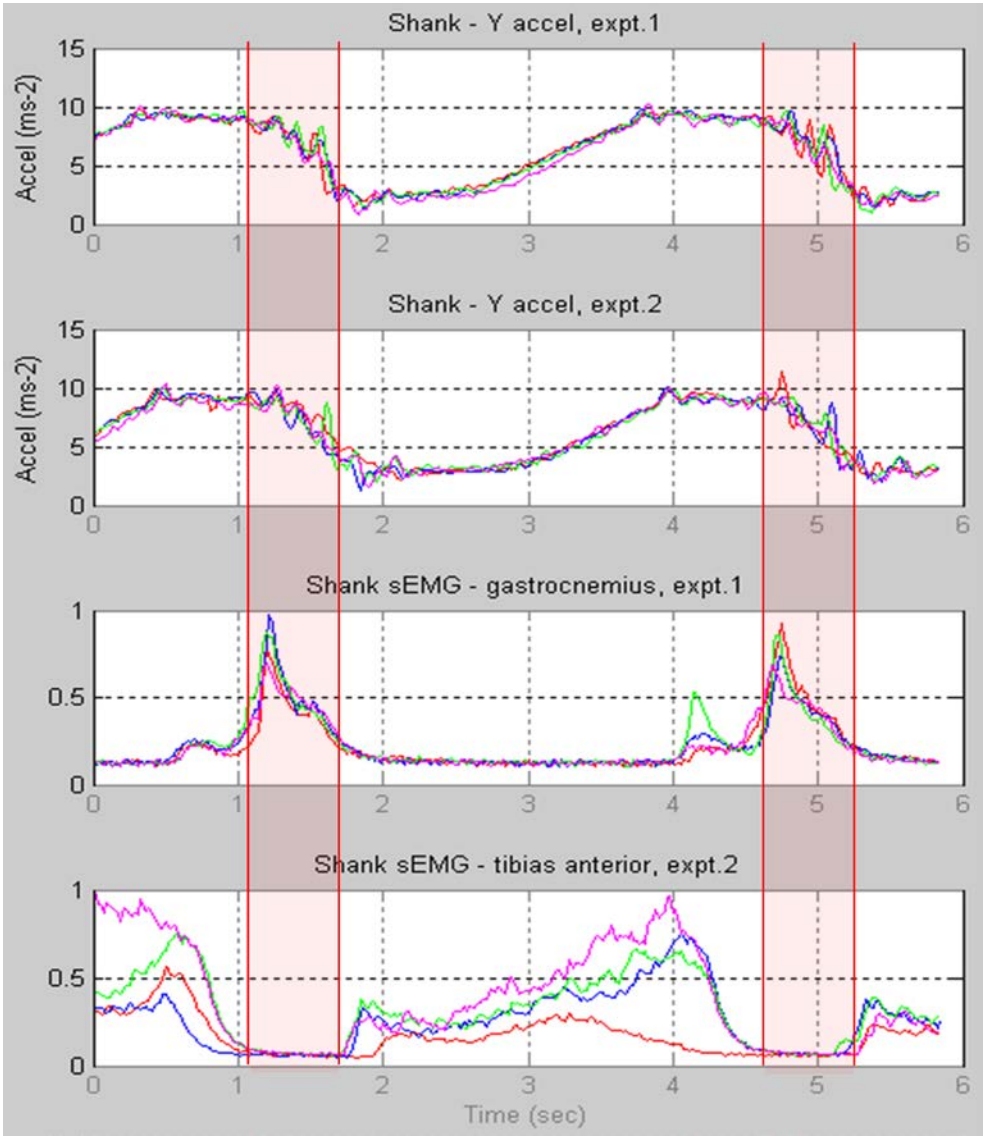

Figure C-9: Correlation of shank muscle measurements (and corresponding acceleration of dominant axis) over 2 experiments,

Aligned by thigh acceleration data, 4 strokes aligned per experiment

Acceleration VR= is 0.05, Gastrocnemius sEMG VR=0.02,Tibias Anterior sEMG VR=0.21

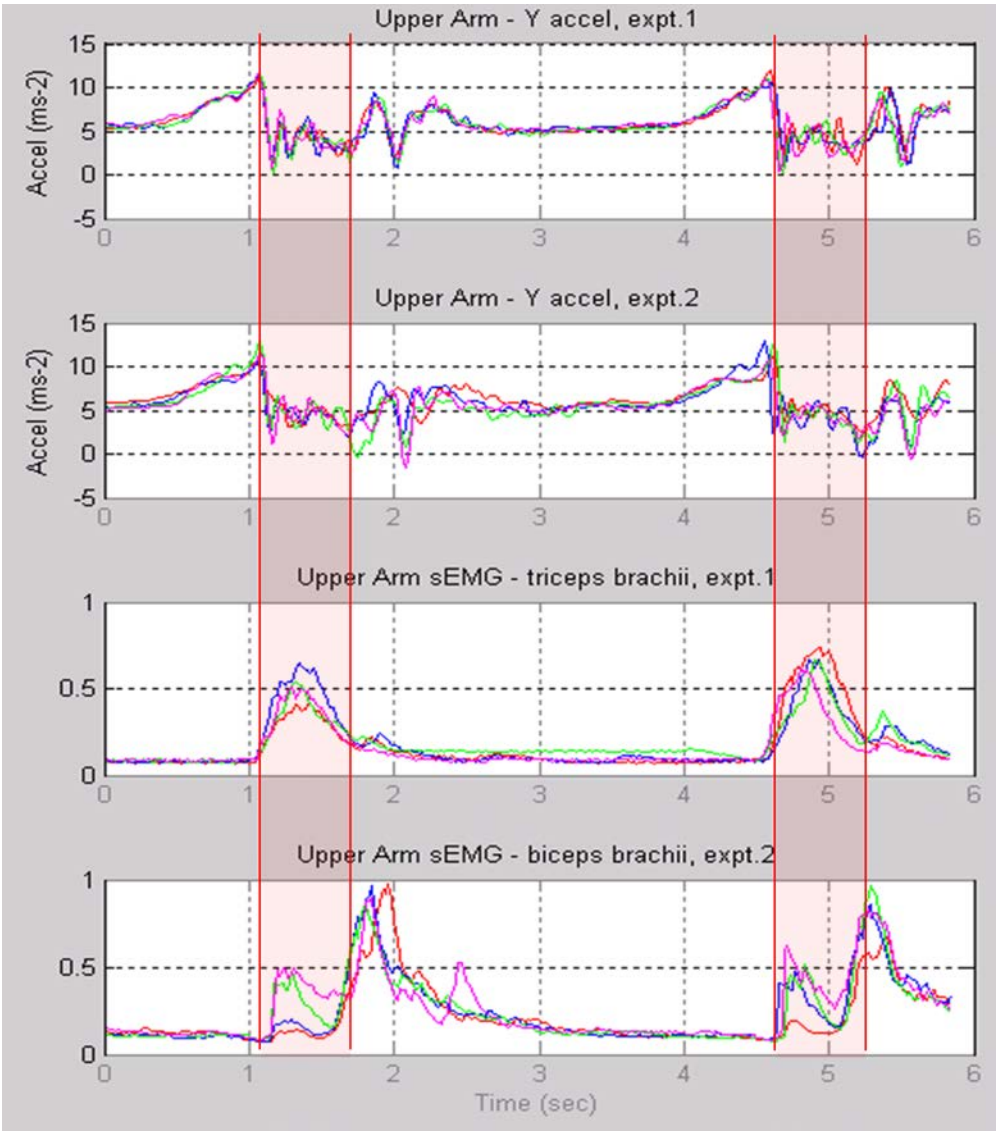

Figure C-10: Correlation of upper arm muscle measurements (and corresponding acceleration of dominant axis) over 2 experiments

Aligned by thigh acceleration data, 4 strokes aligned per experiment

Acceleration VR= is 0.03, Triceps Brachii sEMG VR=0.03,Biceps Brachii sEMG VR=0.06

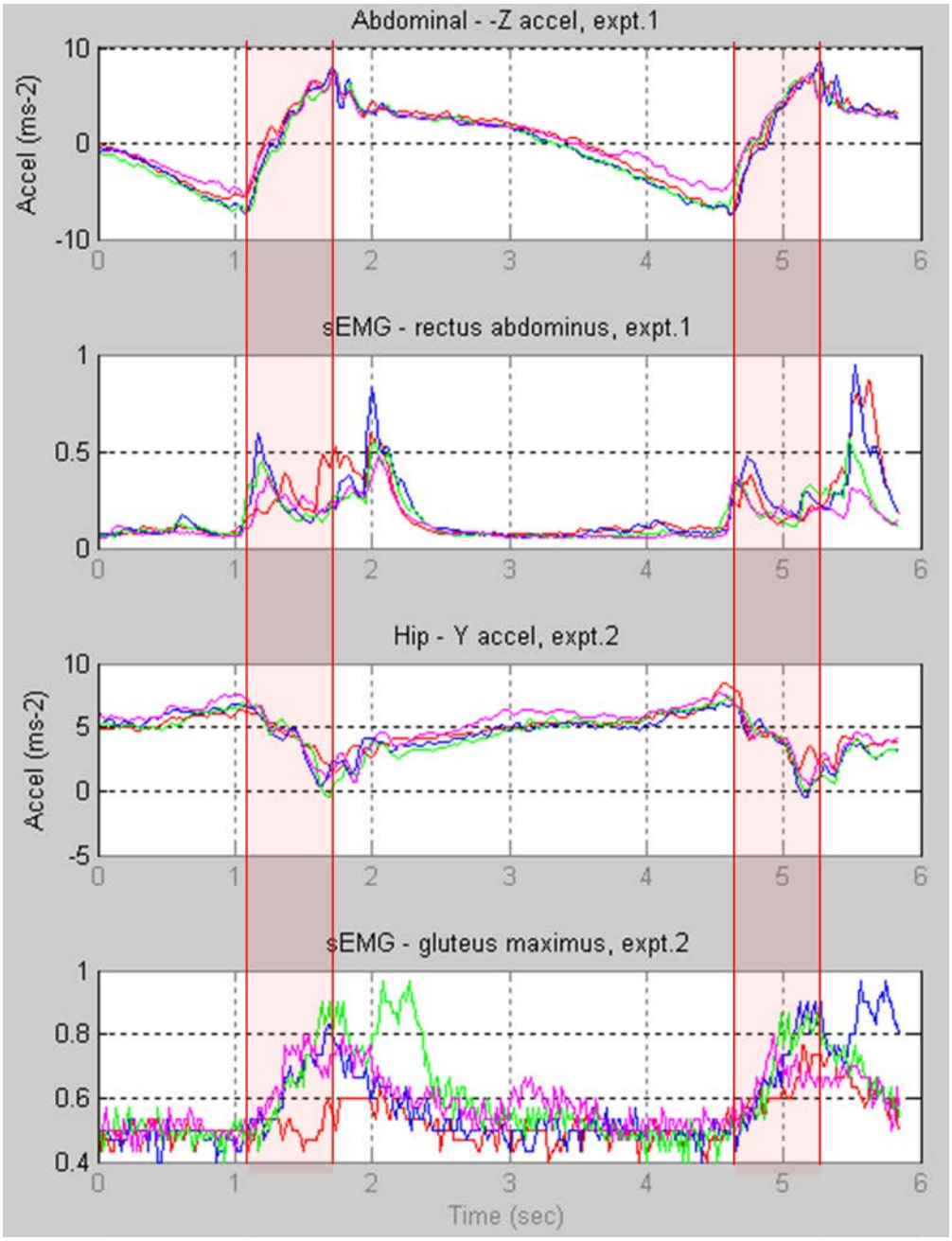

Figure C-11: Correlation of rectus abdominus measurements (top 2 traces) , and gluteus maximus measurements (bottom 2 traces) over 2 experiments

Aligned by thigh acceleration data, 4 strokes aligned per experiment

Note: The gluteus maximus muscle measurement was of very low level, resulting in evident ADC quantisation noise

Abdominal Acceleration VR= is 0.03, Rectus Abdominus sEMG VR=0.07

Hip Acceleration VR= is 0.12, Gluteus Maximus sEMG VR=0.09

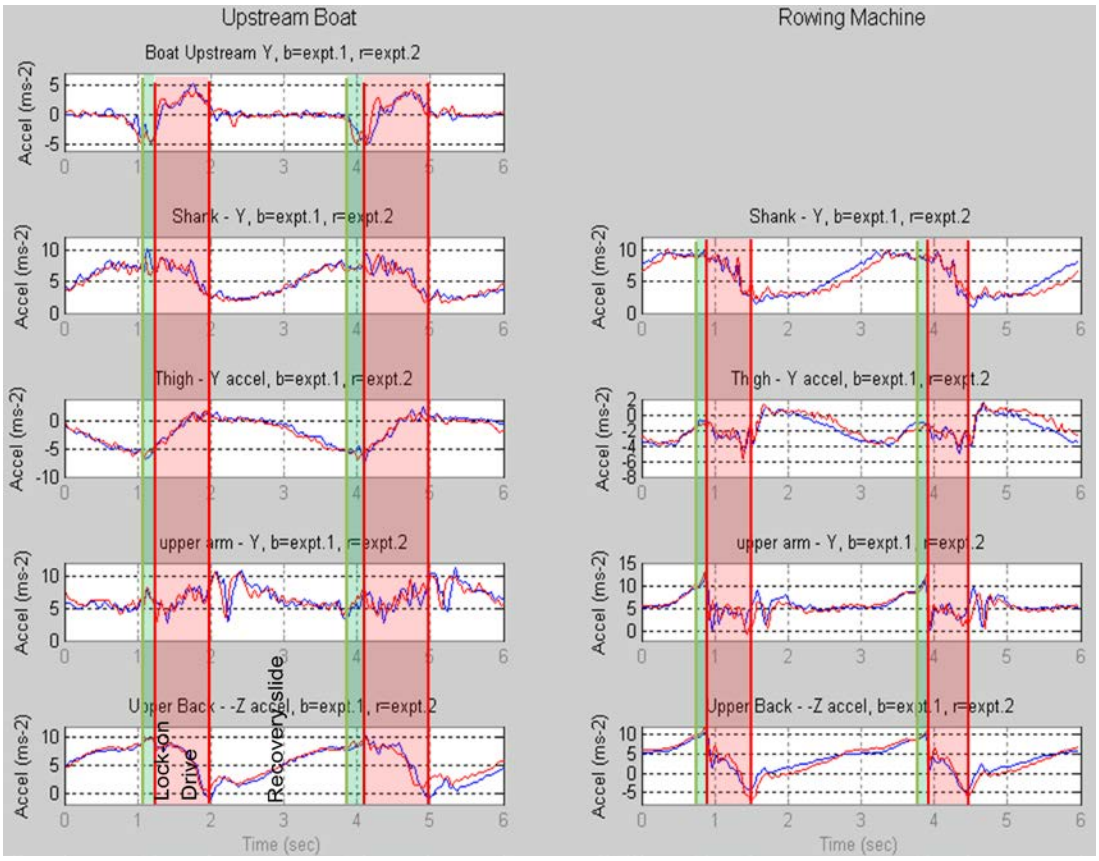

Figure C-12: Comparison of acceleration data measured in-boat and on ergometer over 2 experiments (blue, red)

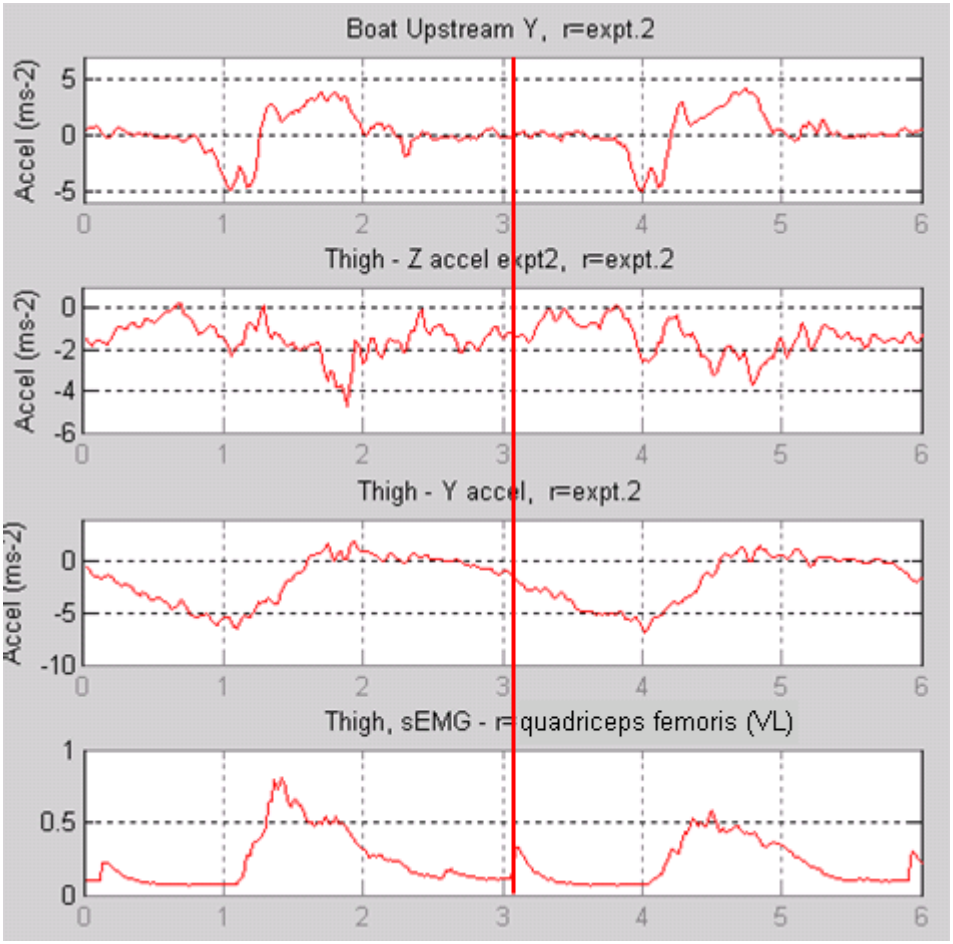

Figure C-13: Muscle activity compared to lateral movement (Z axis) of the thigh

Dominant thigh acceleration axis, and boat acceleration also given

C.3 RSSI measurement data

RSSI data received directly behind the ergometer, and 3m to one side; node placements at upper back, thigh (and for measurements to side, offside thigh). Measurements given for three stroke positions: front-stops, half-slide, back-stops.

Receiver directly behind ergometer			
Rower slide position	Front-stops	Half-slide	Back-stops
Upper back node	-18 dBm	-19 dBm	-10 dBm
Thigh node	-23 dBm	-19 dBm	-23 dBm
Receiver 3m to one side of erg			
Rower slide position	Front-stops	Half-slide	Back-stops
Upper back node	-23 dBm	-26 dBm	-33 dBm
Nearside thigh node	-18 dBm	-18 dBm	-21 dBm
Far-side thigh node	-30 dBm	-32 dBm	-31 dBm

Table C-1: RSSI data for nodes at upper back and thigh, measured behind and 3m to one side of ergometer.